chool of Chemical and Petroleum Engineering

Department of Chemical Engineering

Capture of Carbon Dioxide in Metal Organic Frameworks

Hussein Rasool Abid

This thesis is presented for the degree of

Doctor of philosophy

of

Curtin University

May 2012

Declaration

To the best of my knowledge and belief this thesis contains no material previously published by any other person except where due acknowledgment has been made.

This thesis contains no material which has been accepted for the award of any other degree or diploma in any university.

Signature: …….

Date: ……...

To my Mother and Father

ACKNOWLEDGEMENTS

First of all, I must thank Allah and his guardians for giving me the patience and the ability to complete this work. Then, I would like to express my deep thanks to Associate Professor Shaobin Wang for his perfect supervision and guidance during my PhD study. He has been always helpful, friendly and ready to support me by his prime instructions and encouragement. A big thank and gratitude to Prof. Ming Ang for his co-supervision. Also, I would like to introduce my grateful to Prof. Moses Tade who has been my thesis chairperson.

My great thank must be introduced to Iraqi ministry of higher education to award me PhD scholarship and financial support(Tuition fees, living cost, health insurance and others). Also, I would like to acknowledge the financial support of the Australian Research Council for ARC LIEF Grants LE0775551 and LE0989180.

I am also thankful to Dr. Hung Pham, Dr. Hongqi , Dr. Firas Ridha , Dr. Pradeep and Dr. Hussein Znad for their helps. My thanks are owed to my colleagues, Saad Al-saadi, Ruh ulllah, Yanwu Yang, Jin Shang, Eddy, Shahin, and Syaifullah for their helps in different situations. I would like to extend my thanks to technical staff members, Karen Haynes, Jason Wright, Jimmy Xiao Hua, and Roshanak Doroushi in Chemical Engineering Department at Curtin University for their helps to provide the facilities and chemicals. Also, I have to introduce my gratitude to Imaging and Applied Physics at Curtin University to help me by providing training course on XRD and SEM instruments, especially to Ms Elain Millar. In addition, I have to introduce my grateful to Chemical Engineering Department at Monash University for using their labs, particularly Dr. Ranjeet Singh.

I must express my gratitude to my original family, my parents who always have been praying for me. Also, I would like to thank my brothers and sisters, particularly, my younger brother, Fawzi. Finally, I must give my special thank for my respected wife and my sons, Ali and Ahmed who have emotionally supported me and been enduring with me throughout the period of my PhD.

Abstract

This scholarly research investigates synthesis of different Zr-MOFs and some of Al-MOFs and studies their charcateristics and applications in capture or separation of carbon dioxide. CO_2 is consdered as a main gas in greenhouse gases which have caused global warming.

This thesis takes into account of using modified synthesis and activation procedures toward improving MOF affinity to adsorb CO_2 and reducing its heat of adsorption. Also, the dynamic adsorption capacities were calculated for some Zr-MOFs and Al-MOFs from breakthrough experiments.

Zr-MOF, Zr-MOF-NH_4, Zr-MOF-NH_2, Zr-MOF-NO_3, and Zr-MOF-NO_2 were obtained during direct synthesis process while MIL-53, and amino-MIL-53 were synthesized according to previous procedures with some modifications in activation process and MIL-96 was synthesized and activated by a new procedure.

A fine crystalline powder of Zr-MOF was solvothermally synthesized and activated by chloroform and methanol separately. Chloroform activation was more vigorous to enhance surface area; the BET surface area was 1434 $m^2 g^{-1}$ which is higher than that of samples in methanol activation and previously reported. The Zr-MOF was stable up to 753 K. Chloroform activated Zr-MOF presented CO_2 adsorption capacity of 79 and 45 cc g^{-1} at 1 atm, 273 and 302 K, respectively. Also, the heat of CO_2 adsorption was around 28 kJ mol^{-1}. However, the separating factor of CO_2/CH_4 was higher for methanol activated Zr-MOF although the adsorption capacity was lower.

Ammonium hydroxide was used as an additive in the synthesis process to modify the pore size. Zr-MOF-NH_4-2 showed the largest pore size; it was 2.3 nm. It was found that this modification has a negative impact on the CO_2 adsorption capacity at STP. However, the adsorption capacity increased at increasing pressure over 5 atm(8.63 mmol g^{-1} at 987 kPa) while the heat of adsorption was 22 kJ/mol (which was calculated at 1 atm at the coverage of 5- 29 cc/g). In addition, Zr-MOF-NH_4-1 and Zr-MOF-NH_4-3 were more selective to separate CO_2 from CO_2-CH_4.

Amino-Zr-MOF was thermally stable up to 623K. In addition, its surface area was lower than Zr-MOF-(Parent). On the other hand, CO_2 adsorption capacity was higher, giving 100 cc g^{-1} (4.46 mmol) at 273K and 1 atm. Also, it showed 9 mmol g^{-1} at 273K and 988 kPa.

Another modification in direct synthesis process was achieved using nitric acid as an additive or using NO_2-functionalised linker. NO_3-modified samples exposed thermal stability the same as Zr-MOF (Parent), they may be decomposed at 773K. However, Zr-MOF-NO_2 decomposed at 623K. Nitric acid additives played a main role in enlarging the pore size and reducing crystal size. Zr-MOF-NO_3 exposed lower CO_2 adsorption at STP with increasing amount of the additives. Zr-MOF-NO_3-1 and Zr-MOF-NO_3-2 presented adsorption capacities of 61.4 and 57.9 cc g^{-1} respectively, while Zr-MOF-NO_3-2 had the lowest heat of adsorption of 17.8 kJ/mol. Conversely, Zr-MOF-NO_2 revealed an adsorption capacity of 74.7 cc g^{-1} and the heat of adsorption was 37 kJ/mol. However, Zr-MOF-NO_3 samples exposed higher CO_2 adsorption capacity at high pressure. Also, the selectivity of CO_2/CH_4 was the highest on Zr-MOF-NO_3-2.

Al-MOF exposed different thermal stability. MIL-53, MIL-96 and amino-MIL-53 were stable up to 773, 570, and 650K respectively. MIL-96 exposed higher CO_2 adsorption as 124 cc g^{-1} at STP while amino-MIL-53 has lower value at 48 cc g^{-1}. However, amino-MIL-53 demonstrated heat of adsorption of 28 kJ/mol. Also, MIL-53 displayed the highest dynamic adsorption (169 cc g^{-1} at 1 bar and 304K).

Publications from this work

1. Abid H. R. , G. H. Pham, H. M. Ang, M. O. Tade, and S. Wang , *Adsorption of CH4 and CO2 on Zr-metal organic frameworks.* Journal of Colloid and Interface Science, 2012. **366**(1): p. 120-124.

2- Abid H. R. , H. Tian,H. M. Ang, M.O. Tade, C.E. Buckley, and S.Wang , *Nanosize Zr-metal organic framework (UiO-66) for hydrogen and carbon dioxide storage.* Chemical Engineering Journal, 2012. **187**(0): p. 415-420.

3- Abid, H.R., H.M. Ang, and S. Wang, *Effects of ammonium hydroxide on the structure and gas adsorption of nanosized Zr-MOFs (UiO-66).* Nanoscale, 2012. **4**(10): p. 3089-3094.

4- Abid H. R., J. Shang, H. M. Ang, and S. Wang, *Amino-Functionalised Zr-MOF Nanoparticle for Adsorption of CO_2 and CH_4.* IJSNM, 2012, in Press.

Table of contents

4- Chapter 4: Effects of ammonium hydroxide additives in synthesis process of Zr-MOF on the characteristics and CO_2 adsorption

6- Chapter6: Effect of HNO_3 additives in the synthesis of Zr-MOFs on their structure and capacities of carbon dioxide adsorption

List of Figures

Figure Title……..Page

Figure Title……..Page

Figure Title……..Page

Figure Title……..Page

Figure Title……..Page

List of Tables

Table Title……Page

NOMENCLATURE

UiO	University of Oslo (in Norway)
MOF	Metal Organic Frameworks
MIL	Materials of the Institut Lavoisier
M-O-C	Metal- Oxygen-Carbon
ϵ_r	Dipole moment
SBUs	Secondary Building Units
ZIF	Zeolitic Imidazolate Frameworks
IRMOF	Isoreticular
HKUST	Hong Kong University of Science and Technology
DUT	Dresden University of Technology
UMCM	University of Michigan Crystalline Material
NU	Northwestern University
NOTT	Nottingham University
PSM	Post-Synthesis Modification
SNU	Southern Nazarene University
MMOF	Micropore Metal Organic Frameworks
ZnPO-MOF	MOF with Lewis acidic (porphyrin)Zn struts
UTSA	University of Texas at San Antonio
COF	Covalent Organic Frameworks
PCN	porous coordination network
Cd-4TP-1	Nitrogen Rich Cadmium-Tetrazolate Based-MOF
CD-MOF-2	Cyclodextrin-Metal Organic Framework

DOBDC	2, 5-dioxido-1, 4-benzene-dicarboxylates
BDC	1, 4-Benzene dicarboxylic acid
BTC	1, 3, 5 Benzene tricarboxylic acid
DMF	N, N'-Dimethylformamide
XRD	X-Ray Diffraction
FTIR	Fourier Transform Infrared Spectroscopy
TGA	Thermogravimetric Analysis
SEM	Scanning Electron Microscopoy
BET	Brunauer, Emmett and Teller
STP	Standard Temperature and Pressure
V_{CO2}	Adsorbed amount of pure CO_2 in mmol g^{-1}
V_{CH4}	Adsorbed amount of pure CH_4 in mmol g^{-1}
Zr-MOF-(Parent)	Chloroform activated Zr-NOF
Zr-MOF-NH_2	amino functionalized Zr-MOF
Zr-MOF-NH_3	Ammonium hydroxide in the synthesis of Zr-MOF
Zr-MOF-NO_2	Nitro functionalized Zr-MOF
Zr-MOF-NO_3	Nitric Acid in the synthesis of Zr-MOF
PTFE	polytetrafluoroethylene
GC	Gas Chromatography
TCD	Thermal Conductivity Detector
GFC	Gas Flow Controller
MP	Micropore
t_t	Total Breakthrough time

C	The concentration of CO_2 at time t
C_o	Concentration of CO_2 in inlet
y_{CO2}	mole fraction of CO_2 in inlet
Q_f	the total volumetric flow rate at STP
P_s	Standard pressure
V_b	packed volume of material
P_b	pressure inside the bed
T_b	Temperature inside the bed
T_s	Temperature at standard condition
R	Universal gas constant (8.314 Joules/gram-mole)
ϵ_T	Total porosity of packed material

1

Chapter One: Introduction

1.1 Motivation

Climate change has been considered as a main global problem since the last decade of twentieth century. Power plants have been considered as main sources for carbon dioxide emission(1). The global warming over the past century is unprecedented in the past 1000 years (2).

One of the main negative impacts of global warming is slow growth of economy(3). Researchers have focused on the separation of carbon dioxide from gaseous mixture such as CH_4, N_2, H_2 by chemical solvents, activated carbon (4, 5) and zeolitic adsorbents(6), which have been commonly used in different industrial applications.

In general, chemical solvent for CO_2 absorption has been considered in industry. This technology is depended on the amine fuctionality of alkanoamine which has a good attraction toward carbon dioxide gas interaction. Despite enhancement in this technique (7), it has many problems related to the cost because regeneration of solvents requires high energy (8).

Activated carbon is a highly microporous material with a large surface area (9). This material is always applied for modifications by functionalising the surface of the pores to increase the adsorption capacity (10). Also some carbon-based sorbents are more reliable than zeolites because they are cheaper and CO_2 adsorption may not be affected by moisture.

It was discovered that the selectivity for CO_2 over N_2 at pressure less than 1 atm is moderate and it reduced at high pressure (11). In general, the selectivity and capacity of carbonaceous adsorbents for CO_2 have been much reduced in post-combustion applications and it can be more suitable for pre-combustion process (12). In general, large amount of CO_2 has been emitted from conventional power plants which could be removed by post-combustion capture (13)

Different types of zeolite, such as natural zeolite (14), zeolite 13X (15), zeolite ZSM -5 (16), MCM-41 (17) and others (18, 19), have been used to control carbon dioxide emission. Zeolites have a high affinity to be functionalised with active functional groups such as amine groups and that can enhance their capacity for carbon dioxide

adsorption (20). However, zeolites may be affected by the presence of water in flue gases. The presence of water can block the cages in some types of zeolite as the molecules of water interact strongly by hydrogen bonding with the frameworks (21) while this interaction affinity may enhance the adsorption capacity of some materials (22) or decrease the adsorption capacity of zeolites depending on the polarity of adsorbates. The interaction of water can cause reduction in the strength and heterogeneity of the electric field (23). However, most zeolites need high energy for regeneration in reuse and that takes them away from promising adsorbents for capture of carbon dioxide (20, 24).

Although most of the above materials have huge capacity and high thermal stability to adsorb carbon dioxide (19, 25, 26). Metal organic frameworks (27, 28) have attracted much interests of researchers to be alternative adsorbents for carbon dioxide capture (29) .

1.1.1 Metal Organic Frameworks (MOFs)

Many scientific terms such as hybrid inorganic and organic framework, coordination polymers, and metal organic frameworks can be used to describe extended solid state frameworks which usually have structures by connecting metal ions and organic spacer ligands (30). In general, coordination polymers are consisted of metal−organic units coupled together in one-, two- or three-dimension to build an infinite array by extended coordinate or covalent connections (31). There are a huge number of MOFs which have been synthesized and they are increasingly growing up depending on type of functionalized organic linkers that can be joined with the inorganic parts containing O or N donors which represents a promising linkage with the inorganic cations (32). Originally, three dimensional frameworks with high surface area and pore volume have the greatest interest in many applications because the pores and voids can contain guest molecules and the pore walls can be easily functionalized for particular applications (33) including catalysis, separation, purification, optoelectronics, gas storage (34) and others.

1.1.2 Capture of CO_2 on Metal Organic Frameworks

Carbon dioxide has taken the priority amongst the gases that are causing global warming. Based on the energy consumption for regeneration process in recent separation technologies, physical sorption technologies are greatly used to capture carbon dioxide on porous materials at high capacity and low energy for regeneration. The metal organic frameworks with high surface area and effective functional groups have exposed unprecedentedly ability to adsorb and separate carbon dioxide gas from flue gases (35). Activation process is very important before testing these materials for carbon dioxide adsorption; it can increase the number of open metal sites which are considered the main sites for interaction with carbon dioxide gas as well as methane gas (36).

Most adsorption studies on metal organic frameworks were confined at equilibrium adsorption measurements which may have a poor indicator to predict their separation ability at industrial applications. It was observed that dynamic capacity should be measured to assess the reliability of using these materials as adsorbents under industrial conditions (37). Carbon dioxide molecules have quadrapolar moment , it is selectively adsorbed over methane on MOFs (36). These materials with their interesting application in gas storage and gas separation are seriously taken by many researchers toward modifications and applications.

1.2 Scope and Objectives of the Thesis

The objective of this thesis is to investigate the sorption properties of carbon dioxide on some metal organic frameworks to determine which MOF can have a significant capacity of gas storage. The aims are to

- Prepare several samples of zirconium-Metal Organic Frameworks by modified procedure in synthesis and activation.
- Use functionalised linker such as NH_2-BDC and NO_2-BDC or using HNO3 and NH4OH as chemical additives in the synthesis procedure.

- Quantify the structural and thermal stability as well as other characteristics.
- Measure adsorption isotherms of carbon dioxide at low pressure and different temperatures and adsorption isotherms of carbon dioxide and methane at high pressure and 273K.
- Evaluate the dynamic adsorption of carbon dioxide on different types of metal organic frameworks by column experiments.

1.3 Organization of the Thesis

Chapter one: This chapter includes a briefly historical review for traditional methods and adsorbents which have been used to capture carbon dioxide. Also, it explains a general concept about metal organic frameworks and their applications. Scope and objective as well as chapter wise summary of this thesis are also presented in this chapter.

Chapter two: This chapter displays the detailed literature review for metal organic frameworks from synthesis to applications including introduction, hydrothermal and solvothermal synthesis, interpenetration problem, flexibility and stability, functionalization and various applications.

Chapter three: This chapter are specified for study of CO_2 adsorption on modified Zr-MOF at 1 atm and different temperatures as well as CO_2 and CH_4 adsorption at high pressure. More specifically, it includes modified procedures for synthesis and activation; characterizations for Zr-MOF are measured. Furthermore, it contains comparative view between methanol and chloroform activations.

Chapter four: This chapter contains modification of Zr-MOF by adding NH_4OH as an additive in the synthesis procedure. It discusses carbon dioxide adsorption at low pressure and high pressure; also, it discusses the changes which may happen to this material with NH_4OH additives including the changes in pore size and crystal size and the effects on the adsorption capacity at high pressure and heat of adsorption.

Chapter five: This chapter includes synthesis of NH_2-Zr-MOF by a modified procedure and using methanol in activation process at different temperatures. Also,

all characterizations are determined in this chapter. CO_2 and CH_4 adsorption is discussed including determination of selectivity.

Chapter six: This chapter refers to the effects of HNO_3 additives in the synthesis of Zr-MOF on the properties and CO_2 adsorption capacity of Zr-MOF as well as on the heat of adsorption. Also, it includes synthesis of NO_2-ZrMOF in modified procedure and activation process by methanol which is compared with NO_3-modified-Zr-MOF in characteristics and adsorption capacities.

Chapter seven: This chapter studies the characterizations of different MOFs including MIL-53(Al), MIL-96, and amino-MIL-53. Also, static adsorption is measured at standard pressure and different temperatures. Breakthrough experiments are done for above Al-MOFs and some Zr-MOFs. The dynamic adsorption is compared.

Chapter eight: It refers to overall summary of the thesis including modification synthesis procedure and the main changes in the modified samples as well as the isotherm and dynamic adsorption for carbon dioxide on different MOFs. Also, some major points are recommended for future works.

1.4 References

1. Pacala S, Socolow R. Stabilization Wedges: Solving the Climate Problem for the Next 50 Years with Current Technologies. Science. 2004 August 13, 2004;305(5686):968-72.

2. Crowley TJ. Causes of Climate Change Over the Past 1000 Years. Science. 2000 July 14, 2000;289(5477):270-7.

3. Tol RSJ. How much damage will climate change do? Recent estimates. World economics. 2000;1(4):179.

4. Kikkinides ES. Concentration and recovery of carbon dioxide from flue gas by pressure swing adsorption. Industrial & Engineering Chemistry Research. 1993;32(11):2714.

5. Heuchel M. Adsorption of carbon dioxide and methane and their mixtures on an activated carbon: simulation and experiment. Langmuir. 1999;15(25):8695.

6. Golden TC, Sircar S. Gas Adsorption on Silicalite. Journal of Colloid and Interface Science. 1994;162(1):182-8.

7. Maliz C. Carbon dioxide recovery: large scale design trends
Proceedings of Technical Meeting / Petroleum Conference of The South Saskatchewan Section1995.

8. Wolsky AM, Daniels EJ, Jody BJ. CO_2 Capture from the flue gas of conventional fossil-fuel-fired power plants. Environmental Progress. 1994;13(3):214-9.

9. Guo B, Chang L, Xie K. Adsorption of Carbon Dioxide on Activated Carbon. Journal of Natural Gas Chemistry. 2006;15(3):223-9.

10. Dantas TLP, Amorim SlM, Luna FMT, Silva IJ, de Azevedo DCS, Rodrigues ArE, et al. Adsorption of Carbon Dioxide onto Activated Carbon and Nitrogen-Enriched Activated Carbon: Surface Changes, Equilibrium, and Modeling of Fixed-Bed Adsorption. Separation Science and Technology. 2009 2011/12/09;45(1):73-84.

11. Radosz M, Hu X, Krutkramelis K, Shen Y. Flue-Gas Carbon Capture on Carbonaceous Sorbents: Toward a Low-Cost Multifunctional Carbon Filter for "Green" Energy Producers. Industrial & Engineering Chemistry Research. 2008 2011/12/09;47(10):3783-94.

12. D'Alessandro DM, Smit B, Long JR. Carbon Dioxide Capture: Prospects for New Materials. Angewandte Chemie International Edition. 2010;49(35):6058-82.

13. Klara SM, Srivastava RD. U.S. DOE integrated collaborative technology development program for CO_2 separation and capture. Environmental Progress. 2002;21(4):247-53.

14. Siriwardane RV, Shen M-S, Fisher EP. Adsorption of CO_2, N_2, and O_2 on Natural Zeolites. Energy & Fuels. 2003 2011/12/09;17(3):571-6.

15. Mérel J, Clausse M, Meunier F. Carbon dioxide capture by indirect thermal swing adsorption using 13X zeolite. Environmental Progress. 2006;25(4):327-33.

16. Armandi M, Garrone E, Areán CO, Bonelli B. Thermodynamics of Carbon Dioxide Adsorption on the Protonic Zeolite H-ZSM-5. ChemPhysChem. 2009;10(18):3316-9.

17. Kim JM, Kwak JH, Jun S, Ryoo R. Ion Exchange and Thermal Stability of MCM-41. The Journal of Physical Chemistry. 1995 2011/12/09;99(45):16742-7.

18. Delgado JA, Uguina MaA, Sotelo JL, Ruأ-z B, Rosعأrio M. Carbon Dioxide/Methane Separation by Adsorption on Sepiolite. Journal of Natural Gas Chemistry. 2007;16(3):235-43.

19. Lee J-S, Kim J-H, Kim J-T, Suh J-K, Lee J-M, Lee C-H. Adsorption Equilibria of CO2 on Zeolite 13X and Zeolite X/Activated Carbon Composite. Journal of Chemical & Engineering Data. 2002 2011/12/09;47(5):1237-42.

20. Zhao H, Hu J, Wang J, Zhou L, Liu H. CO2 Capture by the Amine-modified Mesoporous Materials. Acta Physico-Chimica Sinica. 2007;23(6):801-6.

21. Hutson ND, Zajic SC, Yang RT. Influence of Residual Water on the Adsorption of Atmospheric Gases in Li- X Zeolite: Experiment and Simulation. Industrial & Engineering Chemistry Research. 2000 2011/12/09;39(6):1775-80.

22. Moïse J-C, Bellat J-P. Effect of Preadsorbed Water on the Adsorption of p-xylene and m-xylene Mixtures on BaX and BaY Zeolites. The Journal of Physical Chemistry B. 2005 2011/12/09;109(36):17239-44.

23. Brandani F, Ruthven DM. The Effect of Water on the Adsorption of CO_2 and C_3H_8 on Type X Zeolites. Industrial & Engineering Chemistry Research. 2004 2011/12/09;43(26):8339-44.

24. Harlick PJE, Tezel FH. An experimental adsorbent screening study for CO_2 removal from N2. Microporous and Mesoporous Materials. 2004;76(1-3):71-9.

25. Kokotailo GT, Kokotailo. Structure of synthetic zeolite ZSM-5. Nature. 1978;272(5652):437.

26. Jadhav PD, Chatti RV, Biniwale RB, Labhsetwar NK, Devotta S, Rayalu SS. Monoethanol Amine Modified Zeolite 13X for CO_2 Adsorption at Different Temperatures. Energy & Fuels. 2007 2011/12/09;21(6):3555-9.

27. Férey G. Crystallized frameworks with giant pores: Are there limits to the possible? Accounts of Chemical Research. 2005;38(4):217.

28. Yaghi OM, O'Keeffe M, Ockwig NW, Chae HK, Eddaoudi M, Kim J. Reticular synthesis and the design of new materials. Nature. 2003;423(6941):705-14.

29. Bourrelly S, Llewellyn PL, Serre C, Millange F, Loiseau T, Ferey Gr. Different Adsorption Behaviors of Methane and Carbon Dioxide in the Isotypic Nanoporous Metal Terephthalates MIL-53 and MIL-47. Journal of the American Chemical Society. 2005 2011/12/09;127(39):13519-21.

30. Biradha K, Ramanan A, Vittal JJ. Coordination Polymers Versus Metal-Organic Frameworks. Crystal Growth & Design. 2009 2011/12/28;9(7):2969-70.

31. Janiak C. Engineering coordination polymers towards applications. Dalton Transactions. 2003(14):2781-804.

32. Ferey G. Hybrid porous solids: past, present, future. Chemical Society Reviews. 2008;37(1):191-214.

33. Ma S. Gas adsorption applications of porous metal–organic frameworks. Pure and applied chemistry. 2009;81(12):2235.

34. Fischer RA, Wöll C. Functionalized Coordination Space in Metal–Organic Frameworks. Angewandte Chemie International Edition. 2008;47(43):8164-8.

35. Simmons JM, Wu H, Zhou W, Yildirim T. Carbon capture in metal-organic frameworks-a comparative study. Energy & Environmental Science. 2011;4(6):2177-85.

36. Dietzel PDC, Besikiotis V, Blom R. Application of metal-organic frameworks with coordinatively unsaturated metal sites in storage and separation of methane and carbon dioxide. Journal of Materials Chemistry. 2009;19(39):7362-70.

37. Britt D, Furukawa H, Wang B, Glover TG, Yaghi OM. Highly efficient separation of carbon dioxide by a metal-organic framework replete with open metal sites. Proceedings of the National Academy of Sciences. 2009 December 8, 2009;106(49):20637-40.

2

Chapter 2: Literature Review

2.1 Introduction

Material synthesis is complex and tuning of pore structure is very important for adsorption. Apart from MCM-41S structure, it was noted that zeolite synthesis is also difficult to be logically planned or designed, and the final products mostly depend on the probability, accompanied with unexpected transformation (1). In addition, activated carbon has been limited by deficiency of the controlling on the pore properties because the network of this porous material is mostly amorphous (2). On the other hand, coordination polymers have been rapidly developed (3-6) and largely used in different applications (7-11). They are essentially constructed by coordination bonding between inorganic connecters and organic linkers (12, 13). Metal organic frameworks (MOFs) are one type of coordination polymers with exceptionably structural and textural characteristics (14, 15). The topologies and connectivities of metal organic frameworks have been controlled by selecting the favourable coordinating connections between metal clusters and organic linkers, in addition, a template material has a little role in the direction of their structures in contrast with that in zeolites (16). Also, they can be designed in well-known molecular building blocks which are assembled periodically in extended frameworks (17). Furthermore, these materials could be constructed from two or more transition metals which usually are geometrically connected by organic ligands. To synthesise final products with a sufficient rigidity, it is necessary that organic ligands combine with the metal ions by more than one site, enhancing the crystalinity of the product (18). In addition, M-O-C containing-clusters have the ability to create high rigid networks therefore secondary building units should make all metal ions confined in their sites by multicarboxylate groups. Hence, if these clusters (vertices) are connected with suitable ligands, extended frameworks might be formed (19). In other words, the synthesis of MOFs can result in robust extended framework with permanent porosity which may be fulfilled when the molecular building nets are connected by strong bonds (20)**.** Figure 2.1 shows that MIL-53 structure is based on corner sharing chain of AlO_6 octahedra linked with terephthalate groups via strong coordinating bonds. Most metals, especially, transition metals have been used increasingly in the synthesis of MOFs, but the more interest is only limited to a number of metal ions, such as Cu^{+}, Cu^{+2}, Ag^{+}, Cd^{+2}, Co^{+2}, Ni^{+2} (18, 21, 22), Zn^{+2} (23-

25), Fe^{+3}, Cr^{+3}, Al^{+3}, V^{+3} (26-32), and Zr^{+4} (33). Eventually, the relation between the metal ions and organic ligands can be organised in the synthesis process and rigid products can be produced when the organic linkers are multi-dentate ligands. Many factors can control the creation process of these materials such as the solvent, organic linker, metal salt and solubility of the reactants in the solvent as well as the polarity of the solvents (17).

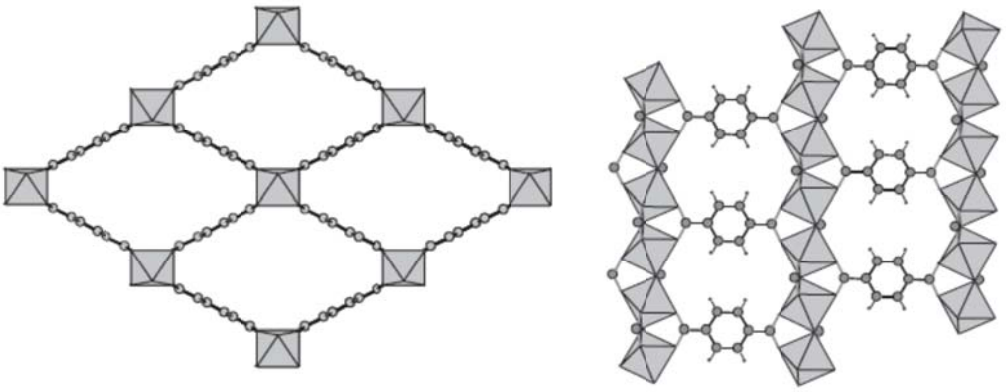

Figure: 2.1 MIL-53 structure including AlO_6 octahedra linked with benzene dicarboxylate groups (1)

2.2 Synthesis of Metal Organic Frameworks

The synthesis of metal organic frameworks can be achieved either by hydro- or solvo-thermal reactions. Solvothermal reaction is known as a chemical reaction that can happen in a closed system in the presence of a solvent which can be polar or non-polar at the temperature higher than the boiling point of the solvent and high pressure (34-37). The choice of the suitable temperature depends on the required reactions for obtaining the targeted material through the involved process (34, 38).

Hydrothermal synthesis is a process involved in using water as a solvent. When the operation contains some other solvents the process is called solvothermal reaction and it can be used to prepare different materials for various applications (34, 39). In general, a chemical reaction under high pressure and mild temperature brings in huge

benefits to chemistry and material sciences. There are two factors that dominate a reaction. The first one is the chemicals and the second one depends on thermodynamical conditions of the reaction. The interaction between reactants and solvent plays an important role in solvothermal reactions (37). Electing a solvent can mainly contribute to produce the required products during the reaction (34). Usually the solvothermal reaction may occur at elevated temperature more than 100 °C and pressure more than few atmospheres inside "autoclaves" or "bombs". Moreover, the requirements for starting materials are known composition, as homogeneous as possible, as pure as possible and as fine as possible (40, 41). There are many properties should be provided by the selectable solvents such as high solubility for the solute, appreciable change of solubility with temperature, rather low melting point, low vapour pressure to avoid changes in the solvent-solute ratio, low dynamic viscosity in the range between 1 and 10 mPa, low reactivity with material of the growth vessel, the easy of separation of the growth crystal from the solvent by chemical or physical means, appropriate physical density, availability in high purity at reasonable cost and finally low toxicity.

For some cases, hydrothermal may include mineralisers under elevated temperature and pressure when the solute is difficult to dissolve in a solvent under ordinary conditions (40, 42) .

The thermodynamical conditions such as temperature and pressure as well as reaction time could be controlled and managed by a suitable autoclave size with specified properties. Actually, the temperature should be below than 400 °C. Increasing the temperature and pressure will improve the solubility of solutes in solvents, enhancing the precursor concentration in the solvent and contributing to increase the rate of crystal growing (34).

So far the most widely used solvent is water, which has a suitably high dipole moment (ϵ_r=78) to permit dissolution of ionic and partially ionic solids and acceptably low vapour pressures at the temperature (usually 100-200 °C). For this purpose, typically, Teflon-lined stainless steel autoclaves are used with recommended maximum fill levels of around 75% to avoid problems associated with thermal expansion and excessive pressure build up (1).

It is important in synthesis of metal organic frameworks to make solutions including solvent, metal ions and multidentate organic ligand as a linker. Further specifically, frameworks should have ligand or other chemical portions which can be discarded from a metal centres to create uncoordinated metal sites (43). Moreover, these ligands may be water, solvent molecules, metal clusters, and other chemical species with high electronegative density to connect to the metal centres. Selectively, using counterions in the solutions is essential to balance the charged framework (44) including "sulphate, nitrate, halogen, phosphate, ammonium, and mixtures" (45). It is compulsory in synthesis of MOFs in the selection of linkers and their functional groups which are usually joined with the linker terminally. Additionally, the linker integrity in a final framework should be kept through a full path of synthesis (20). Metal - containing nodes have been successfully exploited to determine the properties of final product and these vertices also have specific ability to control a suitable directional degree (angle) of interaction between the metal centre and organic ligand (1) in a way preventing the collapse of framework upon discarding the guest materials from pores (20). Contribution of anion elements in the building of metal-organic frameworks is preferred sharing to predicting the coordination polymer (43). It means that the electronegative properties of anions and their ability to correlate metal ions are important (18). Generally, the majority of metal organic frameworks are neutralized by solvent molecules which can be removed easily, when the interaction is hydrogen bonding between the guest molecules and MOF structures (46). Coordination polymers have successfully been synthesized by solvothermal reaction with high rigidity or flexibility. However, the removal of the guest molecules and non-interacted reactants may not be always easy.

2.3 Interpenetrating impediment

In early stage, metal organic frameworks suffered from interpenetrating impediment problem that leads to hugely reduction in surface area (Figure 2.2). This problem can be overcome in the following ways;

- The hydrogen bond-interaction of template materials within MOF structure should be dominated to prevent interpenetration formation (22).

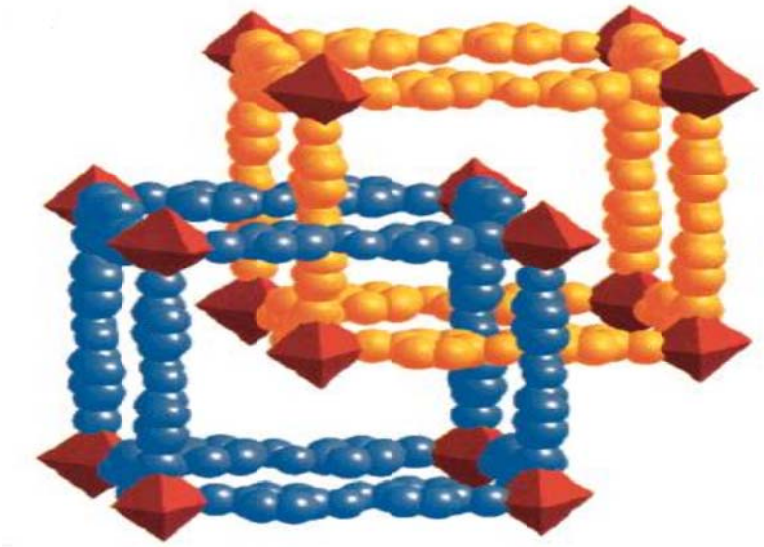

Figure: 2.2 sample of interpenetrating formation(19)

- It was recommended that the clusters of metal centres in metal organic frameworks have been preferred to possess SBUs with M-O-C bond to avoid any interpenetration and produce sufficiently rigid frameworks (19).
- Design of MOFs can be achieved without owing interpenetrating problem and that depend on the ratio of size of vertex to the size of cavity, which has to be less than one (13). However, the cavity sizes sometimes may be increased by increasing the length of linking ligand, and that may be accompanied also by interpenetrating between adjacent networks (12).
- The interpenetration formation can be restricted by controlling the concentration of synthesis solution so that the interpenetration might disappear if the synthesis process has been accomplished under soft conditions (12).

- Finally, there is another possibility to obviate the interpenetration problem when a structure has the ability to self-fill by deviating framework layers from planarity (18).

2.4 Flexibility and Stability of Metal Organic Frameworks

Metal organic frameworks have been experiencing in three generations according to their stability and flexibility as described below;

a- First generation can be synthesized by using weak linkers such as 4, 4'-bipyridine therefore the crystalline product may be transferred to amorphous product at increasing temperature (22, 47-49).

b- Second generation is more rigid by using a strong functional group in the linker materials such as benzene-dicarboxylic acid and the crystalline products may maintain their structure upon the removal of guest material with high surface area and pore volume (49-53).

c- Third generation can get flexibility as well as structure integrity (16, 54). Crystalline products are more dynamic, which comes from hydrogen bonds in their structure, therefore the structural transformation of crystalline material may be reversible (55). As a result, the structures can rearrange leading to change of pore from close to open under the guest molecules (56). Furthermore, dynamic structural transformation based on flexible frameworks is one of the most interesting behaviours in MOFs upon removing or adsorbing guest molecules (49). It was mentioned that when the guest material is charged to balance the framework, it will be difficult to remove without shrinkage of the framework (45) but this phenomenon was eliminated to exchange the guest materials (due to their mobility) with other materials which can be facilely discarded from frameworks (57), though the structure may be contracted or expanded (breathing). The nature of guest materials affected a breathing behaviour of MOFs (58). MIL (Material Institute Lavoisier) - family structures intensively comply with breathing behaviour to the degree, the pore volumes having expansion or contraction change by hundreds of A^3 (59). More specifically,

volume of MIL-53 and MIL-69, -82 can grow up 50% or 85% and these materials are more reliable in various applications. Moreover, as shown in Figure 2.3, the hydration process in the frameworks has caused some disfigurations in a geometrical pore shape because hydrogen bonds may be formed between the hydrogen of water molecules, oxygen atoms of carboxylate groups, and hydroxyl groups of metal centres (58).

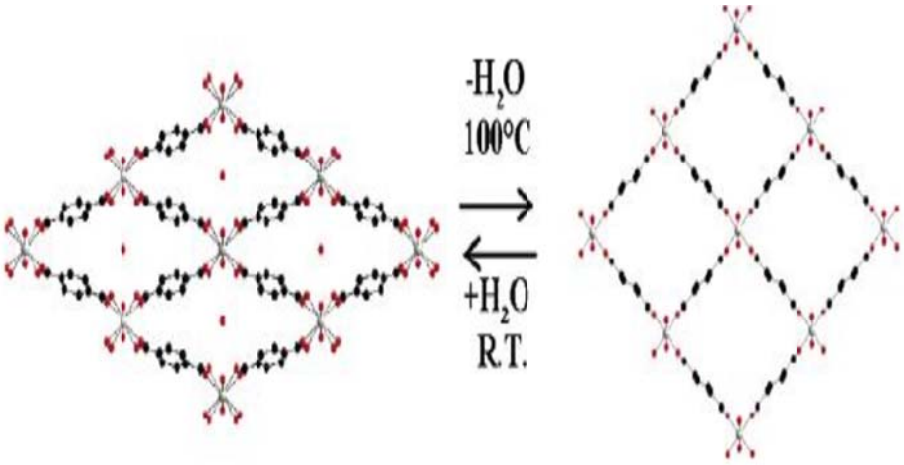

Figure: 2.3 Hydration and dehydration process occurring in MIL-53(Al, Cr). (60)

It is noted that the altering of metal in metal organic frameworks can change the breathing behaviour of the frameworks. For instance, Cr^{+3} and Fe^{+3} have similar radii and electro-negativities; they have different behaviour when each of them interacts with a simple template material such as H_2O. This effect can be taken to make huge modifications in properties of frameworks and extending their applications (59, 61). In addition, the size of structural pores completely depends on the type of guest material which is prime reason for breathing (16). It was known, guest molecules can play a prime role in controlling bond direction although the common interaction of the guest molecules inside the pores is almost controlled by hydrogen bond. Moreover, this effect can influence all molecules throughout the pores. Therefore, the pores may suffer expansion and shrinkage depending on the affinity of the guest molecules with the surface of the pores (49).

It was essential to remove the guest material prior using MOFs to adsorb gas molecules. Removal of guest material from the pores can be achieved by activation process including heating procedure (60). However, after heating, huge negative expansion was observed in many isoreticular metal organic frameworks (IRMOFs) (61-63). The main reason for contraction in crystal lattice with heating may be related to decreasing vibrational energy at increased temperature as the benzene rings and the ZnO_4 nodes move as stiff units and the carboxyl groups as linkages (64).

Most coordination polymers do not have sufficient thermal and chemical stability (65) and that may be due to some weakness in a linker (66). Therefore it is necessary to use a multidentate organic linker to enhance the thermal stability such as 1, 4-benzene dicarboxylic acid (57, 67-69) and 1, 3, 5- benzene tricarboxylic acid or their derivatives. For example, using 1, 3, 5-benzene tricarboxylic acid, it is possible to synthesize non-interpenetrating MOFs with enhanced thermal stability and rigidity (70). MIL-53(Al) framework has a very high stability at high temperature. This framework has ability to adsorb and desorb water molecules at ambient temperature, and the dehydrated structure could be stable at temperature up to 500˚C (71). In addition UiO-66, -68, -69 have high thermal stability and high chemical stability in different solvents. It was observed that these structures have one weakened position in the interaction point between the benzene ring and its terminal functional groups (carboxyl groups) while the connection with metal centre can be retained. As a result, with changing of organic ligand groups, there is no change in the rigidity of the structures but one can enhance the stability of these metal organic frameworks by increasing stability of their linkers (33).

On the other hand, the frameworks (MIL-53-NH_2 and MIL-53-NHCHO) are thermally stable up to 400 ºC (72). NO_2 or NH_2–UiO-66 may maintain as crystalline structure in a temperature lower than 350 ºC (73). That means the functional groups on the benzene rings of organic linker in MOFs might affect negatively on their thermal stability.

It was claimed, imidazolate-metal organic frameworks (ZIFs) demonstrated high thermal stability up to 550 ºC (in nitrogen atmosphere) as well as high chemical stability in different chemical solvents (74).

Metal organic frameworks presented different behaviours against the moisture content. Some of them decomposed quickly after exposing in air with trace content of moisture such as MOF-177, MOF-5, IRMOFs (75-78), while some materials can withstand the trace moisture content but they may decompose in liquid water such as HKUST-1 (79). But, Zr-MOFs are very stable in the presence of water (33, 80). Material Institute Lavoisier (MIL) type of materials were also good to adsorb water molecules (78) without changing their structure, which can have a breathing phenomenon as a result of water inside the pores (28). Moreover, ZIF-8 and DUT-4 were tended to be inert at ambient conditions (79). Both of flexibility and stability are important in design of MOFs to be reliable in different applications.

2.5 Functionalization of Metal Organic Frameworks

Functionalization can produce extra functional groups on the surface of the pores to meet a suitable application (81). There are two strategies for functionalization. The first may be directly achieved in the synthesis process, and the second can be done after synthesis of a porous material as post-synthesis modification(PSM) (82). Porous carbon can be functionalised through a direct participation of various atoms in the carbon synthesis, oxidation of the surface and activation, grafting, sulfonation, halogenations, adhesive of nanoparticles on the surface and covering the surface by polymers (81, 83, 84).

Mesoporous inorganic silica and zeolite materials with their organized pore structures have attracted great awareness for different applications (85). These materials can be modified by surface functionalization toward improving their characteristics, such as reactivity, hyrophobicity and adsorption characteristics (86). Post-synthesis modification (PSM) can make beneficial modifications in their structures and their applications (87). The functional groups can be attached covalently to the internal silanol defect positions (87, 88).

In MOFs with carboxylates, it becomes possible to functionalize a linear bridge of metal carboxylate with chiral groups to produce a chiral MOF that may lead to minimize the void space. The functionalization in first generation of MOFs which

used pyrazines as linear bridge and single metal as node faced many problems (82); with adding functional group on the linear bridge, both of the metal coordinated geometry and framework topologies were very sensitive. That may alter the metal geometry and framework topologies (89) or the coordination geometry of a metal may maintain even the framework topology was changed (90). In the second and third generations of metal organic frameworks, besides, using the different linkers (isoreticular chemistry) with different lengthes to synthesize large pore frameworks (91), the functionalization process has been used to modify the pores and increase diversity of applications (72). The functionalization in direct synthesis may be more common by using functionalized organic linkers in the synthesis process, but some of them had the problems of guest molecules removal from the pores (73). Also, the functional groups in narrow pores may lead to increase the average of differential adsorption energy due to finding sufficiently strong Van der-Waals interactions with the functional group in the structure (72). However, it is difficult to build a new functional group during the direct synthesis of MOFs by some additives for several reasons. Some may due to solvothermal reaction conditions (92) and others may be related to sensitivity of mechanism of coordination process (93). Hence, post-synthesis modification(PSM) is very essential to make huge modification on the linkers of frameworks and that is possible when these coordinated linkers already contain during direct synthesis free functional groups such as amines (94-96). MOFs, which normally have hydrophilic properties, were possible to be functionalized toward hydrophobic or super-hydrophobic materials by using alkyl substituent to increase the resistivity of these material against moisture (78).

Recently, a new method was discovered to functionalise MOFs in direct synthesis by including nanoparticles as functional (inorganic, organic or semiconductor) into nucleating seeds of synthesis process. This method can provide good characteristics for selective applications (97). MOFs can be widely used in different fields in industry when they are successfully functionalised by post-synthesis modifications (PSM) or direct synthesis with suitable functional groups.

2.6 Applications of Metal Organic Frameworks

2.6.1 Catalysts:

Catalysts based on MOF can be classified into three classes;

- Presence of active sites on the framework: Catalytic activity of metal organic frameworks relied on their structures for heterogeneous asymmetric catalysis as it was proved after testing of two homochiral MOFs having the same building units (98, 99). Some MOFs such as vanadium-containing metal–organic frameworks, MIL-47 and MOF-48, have been used to convert methane gas to acetic acid with high activity for both homogenous and heterogeneous systems (100). Moreover, a MOF was synthesized with mixed linkers as a promising catalyst to synthesize propylene carbonate (PC) from carbon dioxide and propylene oxide (101).
- Presence of encapsulated active moieties: Encapsulation was a very good method to include a catalyst in supramolecular porous frameworks as a metal complex in three dimensions by the hydrogen bonding and π- π interactions (102-104).
- Attaching active sites by post-synthesis modification: PSM has opened huge space for different applications, such as heterogeneous and homogenous catalysis but with limited success (105). PSM can be used to form chelating sites into a MOF, and these sites can be connected with divalent or trivalent transition metals. As a result, these materials may be exploited as stout catalysts for C–C bond forming interactions (106). Recently, different metal organic frameworks were used as catalysts with high chemo-selectivity towards reduction of nitro-aromatic (107) or as electro-catalysts in fuel cells (108). MOFs with a variety of mechanisms have a great chance to be as a catalyst to synthesize and decompose many chemical compounds.

2.6.2 Sensors

Metal organic frameworks (MOFs) demonstrate an extensive range of luminescent behaviours as a consequence from the makeup of their structures in multifacets

(109). Luminescent MOFs may be easily modified toward adjusting their sensing utility with explicit anions through diversity of terminal solvents and pore structures (110). Some luminescent MOFs were utilized as a high responsive sensors for detection of small molecules (111). Furthermore, different metal organic frameworks such as Fe-BTC displayed a very good sensing in impedimetric gas sensors. The sensitivity to hydrophilic contents such as humidity, methanol and ethanol, was very good. Also, it was noted that the doped samples showed acceptable sensitivity for humidity lower than that without doping (112). Some discernible sensors were manufactured for sensing some chemical vapours and gases by using a ZIF-8 thin film-based Fabry-Pe rot device (113). Sensing applications may have a huge development using MOFs due to their fascinating characteristics.

2.6.3 Drug Delivery

Metal organic frameworks have been used specifically for drug delivery as promising nanotherapeutics but they need further improvements and modifications to be suitable in clinical applications (114). Also, some metal organic frameworks were used for magnetic resonance imaging and as theranostic agents (115). Although these porous materials reflected high drug loading capacity, biodegradable ability and flexible functionality, this field is still in beginning. Using MOFs in biomedical applications may be bright for this field (116). This area is very important in human life, therefore MOF can make a big enhancement in drug delivery usage.

2.6.4 Gas Storage

Metal organic frameworks with significant characteristics, high surface area, and high pore volume, flexibility, acceptable thermal stability and chemical functionalities, become the most attractive materials in gas storage and separation. These types of porous material can be easily controlled to get the desired pore size by changing the length of organic linkers (25). Many researchers concerted their efforts in this application.

2.6.4.1Carbon Dioxide Storage

With huge growing technologies and populations, the amount of emitting gases into atmosphere has been increased, and consequently global warming threats the earth future. The main source of greenhouse gases is fossil fuel such as coal, oil and natural gas; the main gases are carbon dioxide, methane, and nitrogen oxide (117-119). Different traditional methods have been used to reduce emitted gases.

Monoethanolamine was used for capture of carbon dioxide in practical applications but this process has many problems such as degradation of amine groups by some gases like SO_2 and O_2 which are usually presented in flue gases. In addition, this process was accompanied by damaging the equipment with corrosion and needs high energy for regeneration. Furthermore, ammonia solution was used as novel absorbent to remove the acidic gases such as CO_2, SO_2, NO_x from exhaust gases of power plant with removal efficiency 95-99% (120-122). As it was shown that most studies focused on capture of carbon dioxide because the 2/3 of potential global warming is caused by carbon dioxide (117).

Porous solid materials are easy to handle in avoiding equipment damaging problems (123). Activated carbon (124) and zeolites have been widely used in different industrial activities as adsorbents to purify the flue gases before emitting into surroundings. Some studies focused on using molecular sieves and activated carbon for trap CO_2 from gas mixtures (125). Furthermore, activated carbon was modified toward fibrous adsorbents to improve the adsorption process performance when compared with milled adsorbents and grainy adsorbents (126-128). Recently, novel activated carbon beads have been used successfully as an adsorbent with high selectivity for CO_2 over other gases (129).

Different types of zeolites with high polarity, surface area and pore volume in cationic frameworks (130) displayed very good affinity for adsorption and selectivity of CO_2 from various gases in industrial applications (131). It was claimed that adsorption of carbon dioxide on zeolites was preferred at low pressure but the capacity of adsorption dropped down with further increasing pressure (132). Zeolites are strong for CO_2 adsorption (133). Natural zeolites demonstrated superior adsorption of CO_2 and the major reason may be related to cations in the zeolites which play as a prime factor to adsorb CO_2 (134). Besides, the pressure and

temperature, presence of moisture in flue gases affected the adsorption capacity of carbon dioxide on the amino-functionalized zeolites because the zeolites are hydrophilic and water molecules can easily occupy the adsorption sites in zeolites (135). Water inside the cavities may lead to form bicarbonates, then reduce the electric field heterogeneity (136). All types of zeolites have a common problem in industrial applications which is related to high heat of adsorption for carbon dioxides on zeolites (137-139). Many researchers concentrated their efforts to synthesize and modify hundreds of metal organic frameworks to be effective adsorbents for carbon dioxide storage.

Yaghi and his co-workers have synthesized many MOFs, MOF-210, MOF-200 (140), MOF-177 (141, 142), MOF-5, IRMOF-6 and IRMOF-3 (143). Farah and his co-worker at Northwestern University synthesized a new material(NU-100) with high BET surface area of 6143 m^2/g (144). Also, a UMCM-2(University of Michigan Crystalline Material) has a large BET surface area of 5200 m^2/g (145). Ferey and his co-workers have synthesized and improved porous metal organic framework (MIL-101) to have BET and Langmuir surface area of 4,100 and 5900 m^2/g respectively (146). Furthermore, a desolvated polyhedral framework material (NOTT-112) has a BET surface area of 3800 m^2/g (147, 148).

It was expected that the material may be good for CO_2 storage with low energy for regeneration and very high surface areas (149). According to the adsorption studies of carbon dioxide on metal organic frameworks, it was found that paramount of carbon dioxide can adsorb on these materials at high pressure up to saturated pressure of carbon dioxide without any change in their structures (150). Table 2.1 shows different metal organic frameworks with different surface areas and carbon dioxide capacities at high pressure.

On the other hand, many MOFs demonstrated acceptable capacity to store CO_2 at standard pressure (1 atm). For instance, Mg-MOF-74 presented the highest capacity for CO_2 adsorption at standard conditions although this material displayed absolute adsorption capacity of 15 mmol/g at 313 K and pressure up to 35 bars. MOF-177 and MOF-5 had high adsorption capacity for CO_2 at high pressure but displayed much lower adsorption uptake than Mg-MOF-74 at 1 atm. Table 2.2 shows different metal organic frameworks for carbon dioxide uptake at 1 atm.

Table 2.1: Carbon dioxide adsorption on MOFs at high pressure

MOF	BET-surface area(Langmuir)m^2/g	Excess-gravimetric CO_2 uptake (mmol/g)	Pressure bar	Temperature K	References
MOF-210	6240(10400)	59.98	37	298	(140)
MOF-200	4530(10400)	59.98	50	298	(140)
NU-100	6143	46.4	40	298	(144)
NH_4F-MIL-101	4100(5900)	40	50	303	(146, 150)
UMCM-2	5200(6060)	36.04	45	298	(145, 151)
MOF-177	4310(5460)	33.5	42	298	(141-143)
UMCM-1	4100(6500)	23.5	24	298	(152)
MOF-5	2833(2900)	21.7	35	298	(143, 153)
IRMOF-6	2476(2630)	19.8	40	298	(25, 143, 154)
IRMOF-3	2440(3400)	19	42	298	(143, 155, 156)
MIL-53-Al	950 (1500)	10	25	303	(60, 157)
MIL- 102(Cr)	(42.1)	3.1	50	304	(158)

Table 2.2: Carbon dioxide uptake on different types of metal organic frameworks at 1 atm

MOF	BET surface area (Langmiur)m^2/g	Excess-volumetric CO2 uptake(cc/g)	Temperature K	References
Mg-MOF-74	1174(1733)	225	273	(159, 160)
Mg/DOBDC	1495(1905)	180	296	(161)
Co/DOBDC	1080	156	296	(161)
Bio-MOF-11	1040	134	273	(162)
Ni/DOBDC	(1083)	126	296	(161, 163)
ZTF-1	355.3(443.8)	118.72	273	(164)
IMOF3	802	110	253	(165)
Bio-MOF-1	1680	76.38	273	(166)
CD-MOF-2	1030(1110)	75	273	(167, 168)
Cd-4TP-1	472.2(728.6)	60.48	273	(169)
ZIF-78	620	60	298	(170)
SNU-21S	(905)	58	298	(171)
MIL-53(Al)	1235(1627)	52	303	(172)
ZnPO-MOF	500	48	273	(173)
MOF-5(DMF)	2304(2517)	47.04	295	(174)
MOF-1	1450	45	296	(175, 176)
MMOF	88.4(137.8)	40	273	(177)
MOF-177	3275(5994)	35.7(7wt %)	298	(178, 179)
$C_{94}H_{81}.50N_7O_{30}Zn_4$	1150	22.5	298	(180)
Cu-SNU-6	2590(2910)	15.5	273	(181)

It was observed that the affinity of CO_2 adsorption on metal organic frameworks was various and it cannot be depended on surface area only. Many factors may be taken into account.

1- The polarity of organic ligands: Using ligands with different polar functionalities such as NO_2, NH_3, OH, SO_3H and COOH can enhance the intermolecular interactions of carbon dioxide. These interactions may be obtained between isolated pair donated atoms (N, O) on side groups and C of CO_2 and also may be achieved by hydrogen bonding between acidic protons on COOH and SO_3H groups with oxygen atoms of CO_2 (182-184).
2- Number of vacant sites on metal centre; Removal of the non-linking ligand or other chemical species from the metal cluster will make some metal sites exposed to adsorb chemical molecules, and these sites are called open metal sites (45, 185). Open adsorption sites have huge importance in determining the adsorption capacity of metal organic frameworks and these can be distributed on the two parts of a framework. MOF-5 includes eight sites for adsorption of Ar and N_2, five are metal centres and organic ligands, and three ones are on the surface of pores (186). MOFs with sufficient open metal sites and the pore size relative to the sorbate size have the ability to enhance the potential adsorption separations of gas molecules with differing polarities (187). With availability of unsaturated metal sites, the interaction force of carbon dioxide should be high and that may lead to increased enthalpy of adsorption at low loading (188) during the filling process of unsaturated sites in the metal centre, and then the binding energy may decrease with interacting of the gas molecules with other sites on MOFs (150). Any increasing in the amount of adsorbates on the adsorbent material causes new interaction between gas molecules (189). The number of open metal sites can be enhanced by using effective activation procedure (190, 191).
3- Electrostatic field on metal centre: Electrostatic force plays a prime role in changing the adsorption behaviour, the electrostatic interaction between framework atoms and adsorbate molecules may be dominated at low pressure while the molecules of adsorbates themselves are preferred at high pressure (192). Molecular orientation of carbon dioxide depends on various

electronic distributions of atoms which are connected in the metal centres (193). The electrostatic interaction may be enhanced with exchanging the metallic centre as Nd^{+3} in isostructural lanthanide-organic frameworks was exchanged to Gd^{+3} (194) or by doping with metal-like lithium(Li^{+1}) (195).

4- The surface area and pore volume: Surface area has the main character in determining carbon dioxide storage capacity.

2.6.4.2 Methane storage

Methane was known as low carbon emitting fuel (196) and it was used in fuel cell as a light hydrocarbon (197). Both of activated carbon and zeolites were used for methane storage (198) but their abilities to store this gas were limited (199). Many characteristics should be available in typical materials for CH_4 storage such as; large surface area, high free volume, low material density as well as significant energetic interaction to attach methane molecules, which are matched with MOFs (200).

Metal organic frameworks exhibited very good ability to adsorb methane although this gas molecule has no polarity. For instance, IRMOF-6 had methane capacity of 240 cc/g at 36 bar and 298 K (91) and a microporous metal-organic framework, PCN-14, presented a highest methane storage capacity, 264 cc/g at 35bars and 290 K (201). It was reported 200 cc/g at 36 bar and 303K on MIL-101 and 218 cc/g on HKUST-1 at the same conditions (202) as shown in Table 2.3.

Table 2.3: different MOFs with different capacities for methane storage

MOF's Name	BET surface area m^2/g	CH_4 Excess gravimetric uptake(cm^3/g)	CH_4 Excess volumetric uptake(v/v)	Pressure (bar)	Temperature (K)	references
IRMOF-6	2476	240		36	298	(91, 154)
PCN-14	1753	264		35	290	(201)
MIL-101	4100	200		36	303	(202)
HKUST-1	1502	218		36	303	(202)
UTSA-20	1156		178	35	300	(203)
COF-103	5230		260	100	298	(204)

It was found that open metal sites have a great role in interaction of methane molecules with metal organic frameworks although methane is a non-polar and high symmetrical molecule. The adsorption sites are very high attractive during physio-sorption (205). Besides, the open metal sites which can interact with methane by coulomb forces, small cages/channels is important to capture methane by enhancing van der Waals forces (206). This gas may be captured and reused as new source for energy with improving MOF characteristics toward increasing the methane adsorption capacity.

2.6.4.3 Hydrogen storage

Nowadays, hydrogen is considered as alternative fuel for future because it has zero-emission (196). Many methods were used to store hydrogen such as high pressure gas cylinders, liquid hydrogen in cryogenic tanks, absorbed on interstitial, complex compounds, and metals and complexes together with water (207). Porous materials during adsorption process are more suitable for real applications (208).

Activated carbon was considered as a material to adsorb hydrogen (209, 210) because of low density, wide variety of structural forms, broad pore structure, good chemical steadiness and easy to be modified structures by wide range of preparation, carbonization and activation conditions (208).

Zeolites have a limited micropore volume therefore their capacities to store hydrogen were lower than activated carbon (211).

Metal organic frameworks with their attractive characteristics have been more selectable materials to store hydrogen at high pressure (20-80 bar) and at liquid nitrogen temperature (77 K) (212). It was found that the surface area does not affect too much adsorption of hydrogen on MOFs as shown in Table 2.4, for instance, MOF-177 has the excess weight uptake of 7.5 mg/g at 70 bar and 77 K (213), while MOF-5 displayed excess weight 7.1 mg/g at 40 bar and 77 K (75). In addition, NOTT-12 exposed 7mg/g at 40 bar and 77 K (147) and UMCM-2 had 6.8 mg/g at 46 bar and 77 K (145). Furthermore, MIL-101 had 6.1 mg/g at 60 bar and 77 K (214), JUC-48 had 2.8 at 40 bar and 77 K (215), ZIF-8 had 3.01 mg/g at 55 bar and

70 K (74). Hydrogen adsorption is depended on the temperature; a high capacity may be achieved at 77 K at high pressure while that was not obtained at ambient temperature even at very high pressure. It is important to look for a good synthesis strategy to improve characteristics of metal organic framework toward enhancing hydrogen adsorption capacity (208). One of the main observations was that large surface area and pore volume are not responsible for high capacity for hydrogen storage. Some materials with low surface area demonstrated a high hydrogen uptake because their networks had high interpenetration accompanied with developing narrow pores (216). Also, empty metal sites are very important (163). The optimum pore size can be obtained when the pore diameter as the same as hydrogen molecules, which can maximize van der Waal attraction force on gas molecules (217). A large pore may not be effective for hydrogen storage (214). Moreover, MOFs with very small pores seem not as porous because the molecules of nitrogen may be larger than the pore size while molecules of hydrogen may be passing through easily (218). Therefore, high surface area accompanied with open metal sites, and strong surface dipole moment have been important to boost hydrogen adsorption and further studies will be required (212).

Table 2.4: different MOFs with different capacities for hydrogen storage

MOF's name	BET surface area m^2/g	Excess weight uptake mg/g	Pressure bar	References
MOF-177	**4,000**	**75**	**70**	**(213)**
MOF-5	**2900**	**71**	**40**	**(75)**
NOTT-12	**3800**	**70**	**40**	**(147)**
UMCM-2	**5200**	**68**	**46**	**(145)**
MIL-101	**4100**	**61**	**60**	**(214)**
JUC-48	**629**	**28**	**40**	**(215)**
ZIF-8	**1630**	**30.1**	**55**	**(74)**
PCN-10	**1407**	**43.3**	**20**	**(219)**
MOF-210	**6240**	86	**80**	**(220, 221)**

2.6.4.4 Selectivity of carbon dioxide over other gases

Both selectivity and capacity of adsorbents should be considered in performance of gas separation process (222). Although large CO_2 adsorption capacities at atmospheric pressure are very important for industrial applications of MOFs, the priority of importance should be with selectivity to separate CO_2 from gas mixture (223). The selectivity can be described by the following equation;

$$\boldsymbol{Selectivity} = \frac{\mathbf{X1/X2}}{\mathbf{Y1/Y2}}$$

Where X*i* indicates the mole fraction of component *i* in the adsorbed phase and Y*i* indicates the mole fraction of component *i* in the bulk gas phase (224). In spite of synthesizing ten thousands of MOFs, seventy of them were checked in the selective adsorption studies. The selectivity is replied on many factors, size and shape of adsorbates, adsorbate-surface interaction, and flexibility of a structure (structural rearrangement upon adsorbate-surface interaction) (223). Pressure, temperature and bulk gas composition may also affect the adsorbent selectivity and must be taken in design considerations of adsorbents (225). In addition, it was found that metal organic frameworks with vacant sites on metal centres may enhance the selectivity of polar gas such as CO_2 over non-polar gas such as CH_4. However, metal organic frameworks with 3D interconnected pores can inverse the role of unsaturated metal centres to be harmful to adsorption selectivity because van der Waals interaction for non-polar molecules may be increased like the polar molecules (226).

Post synthesis modifications may lead to reduced surface area but the selectivity may be improved. Some materials were modified during the activation procedure by exchanging the solvent molecules with others which have more affinity toward adsorption of carbon dioxide even the surface area may be much dropped. More specifically, when open metal sites are not occupied, they can be ready to attach with high polar molecules(functional group) such as alkylamine (227), 4-(trifluoromethyl) pyridine (96). Therefore, selectivity of carbon dioxide over methane was improved by functionalizing the metal organic framework with high polar functional group such as amines group to get infinite selectivity (156) as shown in Table 2.5.

Table 2.5: Selectivity of CO_2 over CH_4 for different MOFs at 1 atm

MOFs	BET(Langmuir) surface area (m^2/g)	CO_2/CH_4 selectivity	Temperature K	References
NH2-MIL-53-Al	675	infinite selectivity	303	(156, 228)
Mg-MOF-74	1174(1733)	283	298	(229)
MOF-5	3000	15.53	298	(143, 179)
MIL-53-Cr		15	303	(230)
ZIF-78	620	10.6	273	(231)
ZIF-82	1300	9.6	273	(231)
MIL-53-Al	1235(1627)	7	303	(172, 232)
ZIF-100	595	5.9	273	(231)
ZIF-70	1730	5.2	273	(231)
MOF-177	3275(5994)	4.43	298	(178, 179)

2.7 Summary

Global warming has been a major problem to be resolved, therefore most scientific efforts have been concentrated to reduce emissions of greenhouse gases such as CO_2 and CH_4 into the atmosphere. Traditional methods such as chemical solvents, solid adsorbents were widely used in industrial applications. Although some of these used materials such as activated carbon and zeolites possess high sorption capacities and high thermal stability, metal organic frameworks (coordination polymers) and their unique structural and textural characteristics have attracted importance in research and academic institutions to be used as alternative adsorbents in different applications. These materials are usually synthesized from metal oxides and organic ligands which are coordinatively linked via a solvothermal reaction. Rigid metal organic frameworks can be constructed when metal ions and organic ligands are connected by more than one site. First generation of metal organic frameworks faced some problems concerning to their thermal stability and interpenetrating hindrance.

Interpenetration phenomenon may be resolved by hydrogen bonding of template materials inside the pores while thermal stability can be enhanced by multidentate organic linkers such as 1,4-benzene dicarboxylic acid (BDC) and 1,3,5-benzene tricarboxylic acid (BTC) or their derivatives. It was believed that BTC can be used to synthesize non-interpenetrating MOFs with enhanced thermal stability and rigidity due to triple-bidentate functionality.

Many MOFs have dynamic structural transformations based on flexible frameworks which can be considered as one of the most interesting behaviours. Guest material inside pores may play a great role in the flexibilities of some MOFs when they control the bond direction in MOF's structures. This effect can be produced by comprehensive effect of all guest molecules inside the pores therefore structural expansion and contraction may happen relying on the nature of affinity between the guest molecules and surface of the pores.

MOFs demonstrate various behaviours against the moisture content. Some of them were easily decomposed after exposing to air with a little content of moisture such as MOF-177, MOF-5, IRMOFs, while some materials can resist the trace moisture content but they may decompose in liquid water such as HKUST-1, while UiO-66 showed a good stability against moisture as well as MIL-53(Al, Cr).

It is possible to functionalize metal organic frameworks by two paths; the first is direct synthesis and the second is post-synthesis modifications (PSM). The functionalizing of MOFs is important to increase the diversity of applications. PSM can be used to create chelating sites into a MOF, and these sites can be interacted with divalent or trivalent transition metals. As a result, these materials may be exploited as stout catalysts for C–C bond forming interactions. Also, luminescent MOFs may be easily modified toward gaining their sensing utility with explicit anions through diversity of terminal solvents and pore structures.

Recently, MOFs have been used specially for drug delivery as hopeful class of nanotherapeutics but they need further enhancements and modifications to be properly used in clinical applications.

The most application is gas storage and separation. Carbon dioxide storage, methane storage and hydrogen storage have taken the most interest. Regarding carbon dioxide storage, MOF-210 exposed the best adsorption capacity at high pressure while Mg-

MOF-74 demonstrated the highest adsorption capacity at STP. For storing methane gas, IRMOF-6 was the best MOF to capture methane gas at high pressure while for hydrogen gas MOF-177 was selected as the best adsorbent at elevated pressure. To separate each gas from others both of selectivity and capacity of adsorbents should be measured in performance of gas separation process. The surface area was not much important in enhancing the selectivity, whereas the presence of selective functional group on the structure can upsurge the selectivity even with low surface area. For example, NH_2-MIL-53 exposed very high selectivity for carbon dioxide over methane.

2.8 References

1. Wright PA. Microporous framework solids. Cambridge: Royal Society of Chemistry 2008.

2. Britt D, Tranchemontagne D, Yaghi OM. Metal-organic frameworks with high capacity and selectivity for harmful gases. Proceedings of the National Academy of Sciences. 2008;105(33):11623-7.

3. Robin AY, Fromm KM. Coordination polymer networks with O- and N-donors: What they are, why and how they are made. Coordination Chemistry Reviews. 2006;250(15-16):2127-57.

4. Lee, Kim, Jung D-Y. A Coordination Polymer of Cobalt(II)- Glutarate: Two-Dimensional Interlocking Structure by Dicarboxylate Ligands with Two Different Conformations. Inorganic Chemistry. 2002;41(3):501-6.

5. Paulusse JMJ, Sijbesma RP. Reversible Mechanochemistry of a PdII Coordination Polymer. Angewandte Chemie. 2004;116(34):4560-2.

6. Shin DM, Lee IS, Chung YK, Lah MS. Synthesis and Characterization of Novel Grid Coordination Polymer Networks Generated from Unsymmetrically Bridging Ligands. Inorganic Chemistry. 2003;42(18):5459-61.

7. Ma Z, Moulton B. Recent advances of discrete coordination complexes and coordination polymers in drug delivery. Coordination Chemistry Reviews. 2011;255(15-16):1623-41.

8. Hasegawa S, Horike S, Matsuda R, Furukawa S, Mochizuki K, Kinoshita Y, et al. Three-Dimensional Porous Coordination Polymer Functionalized with Amide Groups Based on Tridentate Ligand: Selective Sorption and Catalysis. Journal of the American Chemical Society. 2007;129(9):2607-14.

9. Ghosh SK, Bureekaew S, Kitagawa S. A Dynamic, Isocyanurate-Functionalized Porous Coordination Polymer. Angewandte Chemie. 2008;120(18):3451-4.

10. Noro S-i, Kitagawa S, Kondo M, Seki K. A New, Methane Adsorbent, Porous Coordination Polymer [{CuSiF6(4,4′-bipyridine)2}n]. Angewandte Chemie International Edition. 2000;39(12):2081-4.

11. Chen W, Yuan H-M, Wang J-Y, Liu Z-Y, Xu J-J, Yang M, et al. Synthesis, Structure, and Photoelectronic Effects of a Uranium-Zinc- Organic Coordination Polymer Containing Infinite Metal Oxide Sheets. Journal of the American Chemical Society. 2003;125(31):9266-7.

12. James SL. Metal-organic frameworks. Chemical Society Reviews. 2003;32(5):276-88.

13. Kitagawa S, Kitaura R, Noro S-i. Functional Porous Coordination Polymers. Angewandte Chemie International Edition. 2004;43(18):2334-75.

14. Fajula Fo, Galarneau A, Renzo FD. Advanced porous materials: New developments and emerging trends. Microporous and Mesoporous Materials. 2005;82(3):227-39.

15. Chaplais G, Simon-Masseron A, Porcher F, Lecomte C, Bazer-Bachi D, Bats N, et al. IM-19: a new flexible microporous gallium based-MOF framework with pressure- and temperature-dependent openings. Physical Chemistry Chemical Physics. 2009;11(26):5241-5.

16. Fletcher AJ, Thomas KM, Rosseinsky MJ. Flexibility in metal-organic framework materials: Impact on sorption properties. Journal of Solid State Chemistry. 2005;178(8):2491-510.

17. Rosi NL, Eddaoudi M, Kim J, O'Keeffe M, Yaghi OM. Advances in the chemistry of metal-organic frameworks. CrystEngComm. 2002;4(68):401-4.

18. James SL. Metal-organic frameworks. Chemical Society Reviews. 2003;32(5):276.

19. Eddaoudi M, Moler DB, Li H, Chen B, Reineke TM, O'Keeffe M, et al. Modular Chemistry: Secondary Building Units as a Basis for the Design of Highly Porous and Robust Metal−Organic Carboxylate Frameworks. Accounts of Chemical Research. 2001;34(4):319-30.

20. Snurr RQ, Hupp JT, Nguyen ST. Prospects for nanoporous metal-organic materials in advanced separations processes. AIChE Journal. 2004;50(6):1090-5.

21. Yaghi OM. Metal-organic Frameworks: A tale of two entanglements. Nat Mater. 2007;6(2):92-3.

22. Yaghi OM, Li H, Groy TL. A Molecular Railroad with Large Pores: Synthesis and Structure of Ni(4,4'-bpy)2.5(H_2O)2(ClO_4)$_2$.1.5(4,4'-bpy) .2H_2O Inorganic Chemistry. 1997;36(20):4292-3.

23. Eddaoudi M, Li H, Reineke T, Fehr M, Kelley D, Groy TL, et al. Design and synthesis of metal-carboxylate frameworks with permanent microporosity. Topics in Catalysis. 1999;9(1/2):105-11.

24. Rosi NL, Eckert J, Eddaoudi M, Vodak DT, Kim J, O'Keeffe M, et al. Hydrogen Storage in Microporous Metal-Organic Frameworks. Science. 2003;300(5622):1127-9.

25. Eddaoudi M, Jaheon K, Rosi N, Vodak D, Wachter J, O'Keeffe M, et al. Systematic Design of Pore Size and Functionality in Isoreticular MOFs and Their Application in Methane Storage. Science. 2002;295(5554):469-72.

26. Serre C, Millange F, Thouvenot C, Nogues M, Marsolier Gr, Louer D, et al. Very Large Breathing Effect in the First Nanoporous Chromium(III)-Based Solids: MIL-53 or $Cr^{III}(OH)\cdot\{O_2C\text{-}C_6H_4\text{-}CO_2\}\cdot\{HO_2C\text{-}C_6H_4\text{-}CO_2H\}x\cdot H_2O_y$. Journal of the American Chemical Society. 2002;124(45):13519-26.

27. Horcajada P. Flexible porous metal-organic frameworks for a controlled drug delivery. Journal of the American Chemical Society. 2008;130(21):6774.

28. Loiseau T. A Rationale for the Large Breathing of the Porous Aluminum Terephthalate (MIL-53) Upon Hydration. Chemistry - A European Journal. 2004;10(6):1373.

29. Llewellyn PL, Horcajada P, Maurin G, Devic T, Rosenbach N, Bourrelly S, et al. Complex Adsorption of Short Linear Alkanes in the Flexible Metal-Organic-Framework MIL-53(Fe). Journal of the American Chemical Society. 2009;131(36):13002-8.

30. Hamon L. Comparative Study of Hydrogen Sulfide Adsorption in the MIL-53 (Al, Cr, Fe), MIL-47 (V), MIL-100 (Cr), and MIL-101 (Cr) Metal− Organic Frameworks at Room Temperature. Journal of the American Chemical Society. 2009;131(25):8775.

31. Devautour-Vinot S, Maurin G, Henn F, Serre C, Devic T, Ferey G. Estimation of the breathing energy of flexible MOFs by combining TGA and DSC techniques. Chemical Communications. 2009(19):2733-5.

32. Janiak C. MOFs, MILs and more: concepts, properties and applications for porous coordination networks (PCNs). New journal of chemistry. 2010;34(11):2366.

33. Cavka JH, Jakobsen S, Olsbye U, Guillou N, Lamberti C, Bordiga S, et al. A New Zirconium Inorganic Building Brick Forming Metal Organic Frameworks with Exceptional Stability. Journal of the American Chemical Society. 2008;130(42):13850-1.

34. Demazeau Gr. Solvothermal reactions: an original route for the synthesis of novel materials. Journal of Materials Science. 2008;43(7):2104-14.

35. Chen XM. Solvothermal in situ metal/ligand reactions: A new bridge between coordination chemistry and organic synthetic chemistry. Accounts of Chemical Research. 2007;40(2):162.

36. Demazeau G. Solvothermal processes: a route to the stabilization of new materials. Journal of Materials Chemistry. 1999;9(1):15-8.

37. Tonto P, Mekasuwandumrong O, Phatanasri S, Pavarajarn V, Praserthdam P. Preparation of ZnO nanorod by solvothermal reaction of zinc acetate in various alcohols. Ceramics International. 2008;34(1):57-62.

38. Rajamathi M, Seshadri R. Oxide and chalcogenide nanoparticles from hydrothermal/solvothermal reactions. Current Opinion in Solid State and Materials Science. 2002;6(4):337-45.

39. Feng S, Xu R. New Materials in Hydrothermal Synthesis. Accounts of Chemical Research. 2000;34(3):239-47.

40. Sōmiya S. Hydrothermal synthesis of fine oxide powders. Bulletin of Materials Science. 2000;23(6):453.

41. Wen B, Huang Y, Boland JJ. Controllable Growth of ZnO Nanostructures by a Simple Solvothermal Process. The Journal of Physical Chemistry C. 2007;112(1):106-11.

42. Ehrentraut D. Solvothermal growth of ZnO. Progress in crystal growth and characterization of materials. 2006;52(4):280.

43. Garnovskiĭ AD. Synthetic Co-Ordination and Organometallic Chemistry2003.

44. Zacher D, Schmid R, Wöll C, Fischer RA. Surface Chemistry of Metal–Organic Frameworks at the Liquid–Solid Interface. Angewandte Chemie International Edition. 2011;50(1):176-99.

45. Yaghi OMLA, CA, US), inventor; Metal-organic frameworks with exceptionally high capacity for storage of carbon dioxide at room-temperature. United States2007.

46. Férey G. Hybrid porous solids: past, present, future. Chemical Society Reviews. 2008;37(1):191.

47. Yaghi OM, Li G, Li H. Selective binding and removal of guests in a microporous metal-organic framework. Nature. 1995;378(6558):703-6.

48. Yaghi OM, Li H. T-Shaped Molecular Building Units in the Porous Structure of Ag(4,4'-bpy)Ĩ·NO3. Journal of the American Chemical Society. 1996;118(1):295-6.

49. Uemura K, Matsuda R, Kitagawa S. Flexible microporous coordination polymers. Journal of Solid State Chemistry. 2005;178(8):2420-9.

50. Perry Iv JJ, Perman JA, Zaworotko MJ. Design and synthesis of metal-organic frameworks using metal-organic polyhedra as supermolecular building blocks. Chemical Society Reviews. 2009;38(5):1400-17.

51. Kim J, Chen B, Reineke TM, Li H, Eddaoudi M, Moler DB, et al. Assembly of Metalâ^'Organic Frameworks from Large Organic and Inorganic Secondary Building Units: New Examples and Simplifying Principles for Complex Structures. Journal of the American Chemical Society. 2001;123(34):8239-47.

52. Yaghi OM, Li H, Groy TL. Construction of Porous Solids from Hydrogen-Bonded Metal Complexes of 1,3,5-Benzenetricarboxylic Acid. Journal of the American Chemical Society. 1996;118(38):9096-101.

53. Robson R. A net-based approach to coordination polymers. Journal of the Chemical Society, Dalton Transactions. 2000(21):3735-44.

54. Sareeya B, Satoru S, Susumu K. Chemistry and application of flexible porous coordination polymers. Science and Technology of Advanced Materials. 2008;9(1):014108.

55. Wu C-D, Lin W. Highly Porous, Homochiral Metal–Organic Frameworks: Solvent-Exchange-Induced Single-Crystal to Single-Crystal Transformations. Angewandte Chemie International Edition. 2005;44(13):1958-61.

56. Maji TK, Mostafa G, Matsuda R, Kitagawa S. Guest-Induced Asymmetry in a Metal- Organic Porous Solid with Reversible Single-Crystal-to-Single-Crystal Structural Transformation. Journal of the American Chemical Society. 2005;127(49):17152-3.

57. Eddaoudi M, Li H, Yaghi OM. Highly Porous and Stable Metalâ''Organic Frameworks: Structure Design and Sorption Properties. Journal of the American Chemical Society. 2000;122(7):1391-7.

58. Llewellyn PL, Bourrelly S, Serre C, Filinchuk Y, Férey G. How Hydration Drastically Improves Adsorption Selectivity for CO2 over CH4 in the Flexible Chromium Terephthalate MIL-53. Angewandte Chemie International Edition. 2006;45(46):7751-4.

59. Millange F, Guillou N, Walton RI, Greneche J-M, Margiolaki I, Ferey G. Effect of the nature of the metal on the breathing steps in MOFs with dynamic frameworks. Chemical Communications. 2008(39):4732-4.

60. Bourrelly S, Llewellyn PL, Serre C, Millange F, Loiseau T, Ferey Gr. Different Adsorption Behaviors of Methane and Carbon Dioxide in the Isotypic Nanoporous Metal Terephthalates MIL-53 and MIL-47. Journal of the American Chemical Society. 2005;127(39):13519-21.

61. Furukawa H, Go YB, Ko N, Park YK, Uribe-Romo FJ, Kim J, et al. Isoreticular Expansion of Metal Organic Frameworks with Triangular and Square Building Units and the Lowest Calculated Density for Porous Crystals. Inorganic Chemistry. 2011;50(18):9147-52.

62. Han SS, Goddard WA. Metal Organic Frameworks Provide Large Negative Thermal Expansion Behavior. The Journal of Physical Chemistry C. 2007;111(42):15185-91.

63. Dubbeldam D, Walton KS, Ellis DE, Snurr RQ. Exceptional Negative Thermal Expansion in Isoreticular Metal–Organic Frameworks. Angewandte Chemie International Edition. 2007;46(24):4496-9.

64. Zhou W, Wu H, Yildirim T, Simpson JR, Walker ARH. Origin of the exceptional negative thermal expansion in metal-organic framework-5 Zn_4O(1,4-benzenedicarboxylate)$_3$. Physical Review B. 2008;78(5):054114.

65. Wu C-D, Hu A, Zhang L, Lin W. A Homochiral Porous Metal- Organic Framework for Highly Enantioselective Heterogeneous Asymmetric Catalysis. Journal of the American Chemical Society. 2005;127(25):8940-1.

66. Schlichte K, Kratzke T, Kaskel S. Improved synthesis, thermal stability and catalytic properties of the metal-organic framework compound $Cu_3(BTC)_2$. Microporous and Mesoporous Materials. 2004;73(1-2):81-8.

67. Van Hung N, Ngoc Phuong Thuy N, Thi Tuyet Nhung N, Thi Thanh Thuy L, Van Nghiem L, Quoc Chinh N, et al. Synthesis and characterization of zinc-organic frameworks with 1,4-benzenedicarboxylic acid and azobenzene-4,4'-dicarboxylic acid. Advances in Natural Sciences: Nanoscience and Nanotechnology. 2011;2(2):025008.

68. Braun ME, Steffek CD, Kim J, Rasmussen PG, Yaghi OM. 1,4-Benzenedicarboxylate derivatives as links in the design of paddle-wheel units and metal-organic frameworks. Chemical Communications. 2001(24):2532-3.

69. Li H, Eddaoudi M, Groy TL, Yaghi OM. Establishing Microporosity in Open Metal- Organic Frameworks: Gas Sorption Isotherms for Zn(BDC) (BDC = 1,4-Benzenedicarboxylate). Journal of the American Chemical Society. 1998;120(33):8571-2.

70. Yaghi OM, Davis CE, Li G, Li H. Selective Guest Binding by Tailored Channels in a 3-D Porous Zinc(II)- Benzenetricarboxylate Network. Journal of the American Chemical Society. 1997;119(12):2861-8.

71. Loiseau T, Serre C, Huguenard C, Fink G, Taulelle F, Henry M, et al. A Rationale for the Large Breathing of the Porous Aluminum Terephthalate (MIL-53) Upon Hydration. Chemistry – A European Journal. 2004;10(6):1373-82.

72. Ahnfeldt T, Gunzelmann D, Loiseau T, Hirsemann D, Senker Jr, Ferey G, et al. Synthesis and Modification of a Functionalized 3D Open-Framework Structure with MIL-53 Topology. Inorganic Chemistry. 2009;48(7):3057-64.

73. Kandiah M, Nilsen MH, Usseglio S, Jakobsen Sr, Olsbye U, Tilset M, et al. Synthesis and Stability of Tagged UiO-66 Zr-MOFs. Chemistry of Materials. 2010;22(24):6632-40.

74. Park KS, Ni Z, Cote AP, Choi JY, Huang R, Uribe-Romo FJ, et al. Exceptional chemical and thermal stability of zeolitic imidazolate frameworks. Proceedings of the National Academy of Sciences. 2006;103(27):10186-91.

75. Kaye SS, Dailly A, Yaghi OM, Long JR. Impact of Preparation and Handling on the Hydrogen Storage Properties of Zn4O(1,4-benzenedicarboxylate)3 (MOF-5). Journal of the American Chemical Society. 2007;129(46):14176-7.

76. Li Y, Yang RT. Gas Adsorption and Storage in Metal- Organic Framework MOF-177. Langmuir. 2007;23(26):12937-44.

77. Greathouse JA, Allendorf MD. The Interaction of Water with MOF-5 Simulated by Molecular Dynamics. Journal of the American Chemical Society. 2006;128(33):10678-9.

78. Nguyen JG, Cohen SM. Moisture-Resistant and Superhydrophobic Metalâ˜Organic Frameworks Obtained via Postsynthetic Modification. Journal of the American Chemical Society. 2010;132(13):4560-1.

79. Küsgens P, Rose M, Senkovska I, Frode H, Henschel A, Siegle S, et al. Characterization of metal-organic frameworks by water adsorption. Microporous and Mesoporous Materials. 2009;120(3):325-30.

80. Gomes Silva C, Luz I, Llabrés iXamena FX, Corma A, García H. Water Stable Zr–Benzenedicarboxylate Metal–Organic Frameworks as Photocatalysts for Hydrogen Generation. Chemistry – A European Journal. 2010;16(36):11133-8.

81. Stein A, Wang Z, Fierke MA. Functionalization of Porous Carbon Materials with Designed Pore Architecture. Advanced Materials. 2009;21(3):265-93.

82. Papaefstathiou GS, MacGillivray LR. Inverted metal organic frameworks: solid-state hosts with modular functionality. Coordination Chemistry Reviews. 2003;246(1-2):169-84.

83. Radkevich VZ, Senko TL, Wilson K, Grishenko LM, Zaderko AN, Diyuk VY. The influence of surface functionalization of activated carbon on palladium dispersion and catalytic activity in hydrogen oxidation. Applied Catalysis A: General. 2008;335(2):241-51.

84. Hirsch A, Vostrowsky O, Schluter AD. Functionalization of Carbon Nanotubes. Functional Molecular Nanostructures. Springer Berlin / Heidelberg; 2005. p. 193-237.

85. Auerbach SMC, K. A. ; Dutta, P.K. Zeolite Science and Technology. New York: Marcel Dekker, Inc; 2003.

86. Vassylyev O, Chen J, Hall GS, Khinast JG. Efficient surface functionalization of zeolites via esterification. Microporous and Mesoporous Materials. 2006;92(1-3):101-8.

87. Lee D-H, Choi M, Yu B-W, Ryoo R. Organic functionalization of mesopore walls in hierarchically porous zeolites. Chemical Communications. 2009(1):74-6.

88. Bae TH, Cheng CH, Chance RR, Nair S, Jones CW, editors. Postsynthesis organic functionalization of the internal surface of zeolite MFI. ACS National Meeting Book of Abstracts; 2008.

89. Kitagawa S, Kawata S, Kondo M, Nozaka Y, Munakata M. Synthesis and Structures of Infinite Sheet Copper(I) Complex Polymers with 2,6-Dimethylpyrazine, {[$Cu_2(C_6H_8N_2)3](ClO_4)2(C_3H_6O)2$}∞, and with 2-Chloropyrazine, {[$Cu_2(C_4H_3N_2Cl)4.5](ClO_4)2$}&infin. Bulletin of the Chemical Society of Japan. 1993;66(11):3387-92.

90. Fujita M, Kwon YJ, Sasaki O, Yamaguchi K, Ogura K. Interpenetrating Molecular Ladders and Bricks. Journal of the American Chemical Society. 1995;117(27):7287-8.

91. Eddaoudi M, Kim J, Rosi N, Vodak D, Wachter J, O'Keeffe M, et al. Systematic Design of Pore Size and Functionality in Isoreticular MOFs and Their Application in Methane Storage. Science. 2002;295(5554):469-72.

92. Farha OK, Mulfort KL, Hupp JT. An Example of Node-Based Postassembly Elaboration of a Hydrogen-Sorbing, Metalâ˜Organic Framework Material. Inorganic Chemistry. 2008;47(22):10223-5.

93. Gadzikwa T, Farha OK, Mulfort KL, Hupp JT, Nguyen ST. A Zn-based, pillared paddlewheel MOF containing free carboxylic acids via covalent post-synthesis elaboration. Chemical communications (Cambridge, England). 2009(25):3720-2.

94. Wang Z, Cohen SM. Postsynthetic modification of metal-organic frameworks. Chemical Society Reviews. 2009;38(5):1315-29.

95. Ko N. Enhanced Carbon Dioxide Adsorption on Post-Synthetically Modified Metal-Organic Frameworks. Bulletin of the Korean Chemical Society. 2011;32(8):2705.

96. Bae Y-S, Farha OK, Hupp JT, Snurr RQ. Enhancement of CO_2/N_2 selectivity in a metal-organic framework by cavity modification. Journal of Materials Chemistry. 2009;19(15):2131-4.

97. Falcaro P, Hill AJ, Nairn KM, Jasieniak J, Mardel JI, Bastow TJ, et al. A new method to position and functionalize metal-organic framework crystals. Nat Commun. 2011;2:237.

98. Wu C-D, Lin W. Heterogeneous Asymmetric Catalysis with Homochiral Metal–Organic Frameworks: Network-Structure-Dependent Catalytic Activity. Angewandte Chemie. 2007;119(7):1093-6.

99. Wenbin L. Homochiral porous metal-organic frameworks: Why and how? Journal of Solid State Chemistry. 2005;178(8):2486-90.

100. Phan A, Czaja AU, Gandara F, Knobler CB, Yaghi OM. Metal Organic Frameworks of Vanadium as Catalysts for Conversion of Methane to Acetic Acid. Inorganic Chemistry. 2011;50(16):7388-90.

101. Kleist W, Jutz F, Maciejewski M, Baiker A. Mixed-Linker Metal-Organic Frameworks as Catalysts for the Synthesis of Propylene Carbonate from Propylene Oxide and CO2. European Journal of Inorganic Chemistry. 2009;2009(24):3552-61.

102. Qiu LG, Xie AJ, Zhang LD. Encapsulation of Catalysts in Supramolecular Porous Frameworks: Size- and Shape-Selective Catalytic Oxidation of Phenols. Advanced Materials. 2005;17(6):689-92.

103. Hwang YK, Hong D-Y, Chang J-S, Jhung SH, Seo Y-K, Kim J, et al. Amine Grafting on Coordinatively Unsaturated Metal Centers of MOFs: Consequences for Catalysis and Metal Encapsulation. Angewandte Chemie International Edition. 2008;47(22):4144-8.

104. Duan C, Wei M, Guo D, He C, Meng Q. Crystal Structures and Properties of Large Protonated Water Clusters Encapsulated by Metalâ^'Organic Frameworks. Journal of the American Chemical Society. 2009;132(10):3321-30.

105. Lee J, Farha OK, Roberts J, Scheidt KA, Nguyen ST, Hupp JT. Metal-organic framework materials as catalysts. Chemical Society Reviews. 2009;38(5):1450-9.

106. Tanabe KK, Cohen SM. Engineering a Metal–Organic Framework Catalyst by Using Postsynthetic Modification. Angewandte Chemie. 2009;121(40):7560-3.

107. D'Vries RF, Iglesias M, Snejko N, Alvarez-Garcia S, Gutierrez-Puebla E, Monge MA. Mixed lanthanide succinate-sulfate 3D MOFs: catalysts in nitroaromatic reduction reactions and emitting materials. Journal of Materials Chemistry. 2012;22(3):1191-8.

108. Proietti E, Jaouen Fdr, Lefevre M, Larouche N, Tian J, Herranz J, et al. Iron-based cathode catalyst with enhanced power density in polymer electrolyte membrane fuel cells. Nat Commun. 2011;2:416.

109. Allendorf MD, Bauer CA, Bhakta RK, Houk RJT. Luminescent metal-organic frameworks. Chemical Society Reviews. 2009;38(5):1330-52.

110. Chen B, Wang L, Zapata F, Qian G, Lobkovsky EB. A Luminescent Microporous Metal- Organic Framework for the Recognition and Sensing of Anions. Journal of the American Chemical Society. 2008;130(21):6718-9.

111. Chen B, Yang Y, Zapata F, Lin G, Qian G, Lobkovsky EB. Luminescent Open Metal Sites within a Metal–Organic Framework for Sensing Small Molecules. Advanced Materials. 2007;19(13):1693-6.

112. Achmann S. Metal-organic frameworks for sensing applications in the gas phase. Sensors. 2009;9(3):1574.

113. Lu G, Hupp JT. Metal−Organic Frameworks as Sensors: A ZIF-8 Based Fabry−Pérot Device as a Selective Sensor for Chemical Vapors and Gases. Journal of the American Chemical Society. 2010;132(23):7832-3.

114. Huxford RC, Della Rocca J, Lin W. Metal-organic frameworks as potential drug carriers. Current Opinion in Chemical Biology. 2010;14(2):262-8.

115. Horcajada P, Chalati T, Serre C, Gillet B, Sebrie C, Baati T, et al. Porous metal-organic-framework nanoscale carriers as a potential platform for drug delivery and imaging. Nat Mater. 2010;9(2):172-8.

116. Keskin S, Kızılel S. Biomedical Applications of Metal Organic Frameworks. Industrial & Engineering Chemistry Research. 2011;50(4):1799-812.

117. Herzog H. Capturing greenhouse gases. Scientific American. 2000;282(2):72.

118. Pearman GI. Greenhouse: planning for climate change. Environment. 1989;31(5):25.

119. Casper JK. Global Warming : Greenhouse Gases : Worldwide Impacts2009.

120. Resnik KP. Aqua ammonia process for simultaneous removal of CO_2, SO_2 and NO_x. Int J Environmental Technology and Management. 2004;4(1/2). Epub 104.

121. Bai H, Yeh AC. Removal of CO2 Greenhouse Gas by Ammonia Scrubbing. Industrial & Engineering Chemistry Research. 1997;36(6):2490-3.

122. Yeh AC, Bai H. Comparison of ammonia and monoethanolamine solvents to reduce CO2 greenhouse gas emissions. Science of The Total Environment. 1999;228(2-3):121-33.

123. Plaza MG, Pevida C, Arenillas A, Rubiera F, Pis JJ. CO2 capture by adsorption with nitrogen enriched carbons. Fuel. 2007;86(14):2204-12.

124. Cazorla-Amoros D, Alcaniz-Monge J, de la Casa-Lillo MA, Linares-Solano A. CO_2 As an Adsorptive To Characterize Carbon Molecular Sieves and Activated Carbons. Langmuir. 1998;14(16):4589-96.

125. Siriwardane RV, Shen M-S, Fisher EP, Poston JA. Adsorption of CO2 on Molecular Sieves and Activated Carbon. Energy & Fuels. 2001;15(2):279-84.

126. Motoyuki S. Activated carbon fiber: Fundamentals and applications. Carbon. 1994;32(4):577-86.

127. Cazorla-Amoros D, Alcaniz-Monge J, Linares-Solano A. Characterization of Activated Carbon Fibers by CO2 Adsorption. Langmuir. 1996;12(11):2820-4.

128. Moon S-H, Shim J-W. A novel process for CO2/CH4 gas separation on activated carbon fibers- electric swing adsorption. Journal of Colloid and Interface Science. 2006;298(2):523-8.

129. Shao X, Feng Z, Xue R, Ma C, Wang W, Peng X, et al. Adsorption of CO2, CH4, CO2/N2 and CO2/CH4 in novel activated carbon beads: Preparation, measurements and simulation. AIChE Journal. 2011;57(11):3042-51.

130. Jadhav PD, Chatti RV, Biniwale RB, Labhsetwar NK, Devotta S, Rayalu SS. Monoethanol Amine Modified Zeolite 13X for CO2 Adsorption at Different Temperatures. Energy & Fuels. 2007;21(6):3555-9.

131. Siriwardane RV, Shen M-S, Fisher EP, Losch J. Adsorption of CO2 on Zeolites at Moderate Temperatures. Energy & Fuels. 2005;19(3):1153-9.

132. Lee J-S, Kim J-H, Kim J-T, Suh J-K, Lee J-M, Lee C-H. Adsorption Equilibria of CO2 on Zeolite 13X and Zeolite X/Activated Carbon Composite. Journal of Chemical & Engineering Data. 2002;47(5):1237-42.

133. Gao W, Butler D, Tomasko DL. High-Pressure Adsorption of CO_2 on NaY Zeolite and Model Prediction of Adsorption Isotherms. Langmuir. 2004;20(19):8083-9.

134. Siriwardane RV, Shen MS, Fisher EP. Adsorption of CO_2, N_2, and O_2 on Natural Zeolites. Energy Fuels. 2003;17(3):571-6.

135. Su F, Lu C, Kuo S-C, Zeng W. Adsorption of CO_2 on Amine-Functionalized Y-Type Zeolites. Energy & Fuels. 2010;24(2):1441-8.

136. Danielle B, Mourad K, Patrick N, Murielle M, Robert H. Advances in principal factors influencing carbon dioxide adsorption on zeolites. Science and Technology of Advanced Materials. 2008;9(1):013007.

137. Ishibashi M, Ota H, Akutsu N, Umeda S, Tajika M, Izumi J, et al. Technology for removing carbon dioxide from power plant flue gas by the physical adsorption method. Energy Conversion and Management. 1996;37(6-8):929-33.

138. Yang H, Xu Z, Fan M, Gupta R, Slimane RB, Bland AE, et al. Progress in carbon dioxide separation and capture: A review. Journal of Environmental Sciences. 2008;20(1):14-27.

139. Wolsky AM, Daniels EJ, Jody BJ. CO2 Capture from the flue gas of conventional fossil-fuel-fired power plants. Environmental Progress. 1994;13(3):214-9.

140. Furukawa H, Ko N, Go YB, Aratani N, Choi SB, Choi E, et al. Ultrahigh Porosity in Metal-Organic Frameworks. Science. 2010;329(5990):424-8.

141. Eric P, Anne D. Thermodynamics of hydrogen adsorption in MOF-177 at low temperatures: measurements and modelling. Nanotechnology. 2009;20(20):204006.

142. Chae HK, Siberio-Perez DY, Kim J, Go Y, Eddaoudi M, Matzger AJ, et al. A route to high surface area, porosity and inclusion of large molecules in crystals. Nature. 2004;427(6974):523-7.

143. Millward AR, Yaghi OM. Metal-Organic Frameworks with Exceptionally High Capacity for Storage of Carbon Dioxide at Room Temperature. Journal of the American Chemical Society. 2005;127(51):17998-9.

144. Farha OK, Özgür Yazaydın A, Eryazici I, Malliakas CD, Hauser BG, Kanatzidis MG, et al. De novo synthesis of a metal- organic framework material featuring ultrahigh surface area and gas storage capacities. Nat Chem. 2010;2(11):944-8.

145. Koh K, Wong-Foy AG, Matzger AJ. A Porous Coordination Copolymer with over 5000 m^2/g BET Surface Area. Journal of the American Chemical Society. 2009;131(12):4184-5.

146. Ferey G, Mellot-Draznieks C, Serre C, Millange F, Dutour J, Surblé S, et al. A Chromium Terephthalate-Based Solid with Unusually Large Pore Volumes and Surface Area. Science. 2005;309(5743):2040-2.

147. Yan Y, Lin X, Yang S, Blake AJ, Dailly A, Champness NR, et al. Exceptionally high H_2 storage by a metal-organic polyhedral framework. Chemical Communications. 2009(9):1025-7.

148. Holst JR, Cooper AI. Ultrahigh Surface Area in Porous Solids. Advanced Materials. 2010;22(45):5212-6.

149. Figueroa JD, Fout T, Plasynski S, McIlvried H, Srivastava RD. Advances in CO2 capture technology- The U.S. Department of Energy's Carbon Sequestration Program. International Journal of Greenhouse Gas Control. 2008;2(1):9-20.

150. Llewellyn PL, Bourrelly S, Serre C, Vimont A, Daturi M, Hamon L, et al. High Uptakes of CO_2 and CH_4 in Mesoporous Metal—‚Organic Frameworks MIL-100 and MIL-101. Langmuir. 2008;24(14):7245-50.

151. Peng X, Cheng X, Cao D. Computer simulations for the adsorption and separation of $CO_2/CH_4/H_2/N_2$ gases by UMCM-1 and UMCM-2 metal organic frameworks. Journal of Materials Chemistry. 2011;21(30):11259-70.

152. Mu B, Schoenecker PM, Walton KS. Gas Adsorption Study on Mesoporous Metal- Organic Framework UMCM-1. The Journal of Physical Chemistry C. 2010;114(14):6464-71.

153. Li H, Eddaoudi M, O'Keeffe M, Yaghi OM. Design and synthesis of an exceptionally stable and highly porous metal-organic framework. Nature. 1999;402(6759):276-9.

154. Duren T, Millange F, Ferey G, Walton KS, Snurr RQ. Calculating Geometric Surface Areas as a Characterization Tool for Metal- Organic Frameworks. The Journal of Physical Chemistry C. 2007;111(42):15350-6.

155. Yoo Y, Jeong H-K. Generation of covalently functionalized hierarchical IRMOF-3 by post-synthetic modification. Chemical Engineering Journal. 2011(0).

156. Gascon J, Aktay U, Hernandez-Alonso MD, van Klink GPM, Kapteijn F. Amino-based metal-organic frameworks as stable, highly active basic catalysts. Journal of Catalysis. 2009;261(1):75-87.

157. Do X-D, Hoang V-T, Kaliaguine S. MIL-53(Al) mesostructured metal-organic frameworks. Microporous and Mesoporous Materials. 2011;141(1-3):135-9.

158. Surblé S, Millange F, Serre C, Düren T, Latroche M, Bourrelly S, et al. Synthesis of MIL-102, a Chromium Carboxylate Metal- Organic Framework, with Gas Sorption Analysis. Journal of the American Chemical Society. 2006;128(46):14889-96.

159. Britt D, Furukawa H, Wang B, Glover TG, Yaghi OM. Highly efficient separation of carbon dioxide by a metal-organic framework replete with open metal sites. Proceedings of the National Academy of Sciences. 2009;106(49):20637-40.

160. Bao Z, Yu L, Ren Q, Lu X, Deng S. Adsorption of CO2 and CH4 on a magnesium-based metal organic framework. Journal of Colloid and Interface Science. 2009;353(2):549-56.

161. Caskey SR, Wong-Foy AG, Matzger AJ. Dramatic Tuning of Carbon Dioxide Uptake via Metal Substitution in a Coordination Polymer with Cylindrical Pores. Journal of the American Chemical Society. 2008;130(33):10870-1.

162. An J, Geib SJ, Rosi NL. High and Selective CO2 Uptake in a Cobalt Adeninate Metal−Organic Framework Exhibiting Pyrimidine- and Amino-Decorated Pores. Journal of the American Chemical Society. 2009;132(1):38-9.

163. Dietzel PDC, Panella B, Hirscher M, Blom R, Fjellvag H. Hydrogen adsorption in a nickel based coordination polymer with open metal sites in the cylindrical cavities of the desolvated framework. Chemical Communications. 2006(9):959-61.

164. Panda T, Pachfule P, Chen Y, Jiang J, Banerjee R. Amino functionalized zeolitic tetrazolate framework (ZTF) with high capacity for storage of carbon dioxide. Chemical Communications. 2011;47(7):2011-3.

165. Debatin F, Thomas A, Kelling A, Hedin N, Bacsik Z, Senkovska I, et al. In Situ Synthesis of an Imidazolate-4-amide-5-imidate Ligand and Formation of a Microporous Zinc–Organic Framework with H2-and CO2-Storage Ability. Angewandte Chemie International Edition. 2010;49(7):1258-62.

166. An J, Rosi NL. Tuning MOF CO2 Adsorption Properties via Cation Exchange. Journal of the American Chemical Society. 2010;132(16):5578-9.

167. Smaldone RA, Forgan RS, Furukawa H, Gassensmith JJ, Slawin AMZ, Yaghi OM, et al. Metal–Organic Frameworks from Edible Natural Products. Angewandte Chemie International Edition. 2010;49(46):8630-4.

168. Gassensmith JJ, Furukawa H, Smaldone RA, Forgan RS, Botros YY, Yaghi OM, et al. Strong and Reversible Binding of Carbon Dioxide in a Green Metalâ€“Organic Framework. Journal of the American Chemical Society. 2011;133(39):15312-5.

169. Pachfule P, Banerjee R. Porous Nitrogen Rich Cadmium-Tetrazolate Based Metal Organic Framework (MOF) for H2 and CO2 Uptake. Crystal Growth & Design. 2011.

170. Banerjee R, Furukawa H, Britt D, Knobler C, O'Keeffe M, Yaghi OM. Control of Pore Size and Functionality in Isoreticular Zeolitic Imidazolate Frameworks and their Carbon Dioxide Selective Capture Properties. Journal of the American Chemical Society. 2009;131(11):3875-7.

171. Kim TK, Suh MP. Selective CO_2 adsorption in a flexible non-interpenetrated metal-organic framework. Chemical Communications. 2011;47(14):4258-60.

172. Rallapalli P, Prasanth K, Patil D, Somani R, Jasra R, Bajaj H. Sorption studies of CO_2, CH4, N_2, CO, O_2 and Ar on nanoporous aluminum terephthalate [MIL-53(Al)]]. Journal of Porous Materials. 2011;18(2):205-10.

173. Shultz AM, Farha OK, Hupp JT, Nguyen ST. A Catalytically Active, Permanently Microporous MOF with Metalloporphyrin Struts. Journal of the American Chemical Society. 2009;131(12):4204-+.

174. Zhao Z, Li Z, Lin YS. Adsorption and Diffusion of Carbon Dioxide on Metalâ''Organic Framework (MOF-5). Industrial & Engineering Chemistry Research. 2009;48(22):10015-20.

175. Chen Z, Xiang S, Zhao D, Chen B. Reversible Two-Dimensionalâ''Three Dimensional Framework Transformation within a Prototype Metalâ''Organic Framework. Crystal Growth & Design. 2009;9(12):5293-6.

176. Dybtsev DN, Chun H, Kim K. Rigid and Flexible: A Highly Porous Metal–Organic Framework with Unusual Guest-Dependent Dynamic Behavior. Angewandte Chemie International Edition. 2004;43(38):5033-6.

177. Wu HH, Reali RS, Smith DA, Trachtenberg MC, Li J. Highly Selective CO2 Capture by a Flexible Microporous Metal-Organic Framework (MMOF) Material. Chemistry-a European Journal. 2010;16(47):13951-4.

178. Saha D, Wei Z, Deng S. Equilibrium, kinetics and enthalpy of hydrogen adsorption in MOF-177. International Journal of Hydrogen Energy. 2008;33(24):7479-88.

179. Saha D, Bao Z, Jia F, Deng S. Adsorption of CO2, CH4, N2O, and N2 on MOF-5, MOF-177, and Zeolite 5A. Environmental Science & Technology. 2010;44(5):1820-6.

180. Thallapally PK, Tian J, Kishan MR, Fernandez CA, Dalgarno SJ, McGrail PB, et al. Flexible (Breathing) Interpenetrated Metal-Organic Frameworks for CO2 Separation Applications. Journal of the American Chemical Society. 2008;130(50):16842-3.

181. Park HJ, Suh MP. Mixed-Ligand Metal–Organic Frameworks with Large Pores: Gas Sorption Properties and Single-Crystal-to-Single-Crystal Transformation on Guest Exchange. Chemistry – A European Journal. 2008;14(29):8812-21.

182. Antonio T, Caroline M-D, Robert GB. Impact of ligands on CO[sub 2] adsorption in metal-organic frameworks: First principles study of the interaction of CO[sub 2] with functionalized benzenes. II. Effect of polar and acidic substituents. The Journal of Chemical Physics. 2010;132(4):044705.

183. Kanoo P, Ghosh AC, Cyriac ST, Maji TK. A Metal–Organic Framework with Highly Polar Pore Surfaces: Selective CO2 Adsorption and Guest-Dependent On/Off Emission Properties. Chemistry – A European Journal. 2011:n/a-n/a.

184. Zheng B, Bai J, Duan J, Wojtas L, Zaworotko MJ. Enhanced CO2 Binding Affinity of a High-Uptake rht-Type Metal- Organic Framework Decorated with Acylamide Groups. Journal of the American Chemical Society. 2011;133(4):748-51.

185. Yazaydın OA, Benin AI, Faheem SA, Jakubczak P, Low JJ, Willis RR, et al. Enhanced CO2 Adsorption in Metal-Organic Frameworks via Occupation of Open-Metal Sites by Coordinated Water Molecules. Chemistry of Materials. 2009;21(8):1425-30.

186. Rowsell JLC, Spencer EC, Eckert J, Howard JAK, Yaghi OM. Gas Adsorption Sites in a Large-Pore Metal-Organic Framework. Science. 2005;309(5739):1350-4.

187. Karra JR, Walton KS. Effect of Open Metal Sites on Adsorption of Polar and Nonpolar Molecules in Metalâ˜’Organic Framework Cu-BTC. Langmuir. 2008;24(16):8620-6.

188. Chowdhury P, Mekala S, Dreisbach F, Gumma S. Adsorption of CO, CO2 and CH4 on Cu-BTC and MIL-101 metal organic frameworks: Effect of open metal sites and adsorbate polarity. Microporous and Mesoporous Materials. 2011(0).

189. Surblé S, Millange F, Serre C, Duren T, Latroche M, Bourrelly S, et al. Synthesis of MIL-102, a Chromium Carboxylate Metal- Organic Framework, with Gas Sorption Analysis. Journal of the American Chemical Society. 2006;128(46):14889-96.

190. Barman S, Furukawa H, Blacque O, Venkatesan K, Yaghi OM, Jin G-X, et al. Incorporation of active metal sites in MOFs via in situ generated ligand deficient metal-linker complexes. Chemical Communications. 2011;47(43):11882-4.

191. Nelson AP, Farha OK, Mulfort KL, Hupp JT. Supercritical Processing as a Route to High Internal Surface Areas and Permanent Microporosity in Metal-Organic Framework Materials. Journal of the American Chemical Society. 2008;131(2):458-60.

192. Yang Q, Xu Q, Liu B, Zhong C, Berend S. Molecular Simulation of CO2/H2 Mixture Separation in Metal-organic Frameworks: Effect of Catenation and Electrostatic Interactions. Chinese Journal of Chemical Engineering. 2009;17(5):781-90.

193. Ramsahye NA, Maurin G, Bourrelly S, Llewellyn PL, Serre C, Loiseau T, et al. Probing the Adsorption Sites for CO2 in Metal Organic Frameworks Materials MIL-53 (Al, Cr) and MIL-47 (V) by Density Functional Theory. The Journal of Physical Chemistry C. 2007;112(2):514-20.

194. Lee WR, Ryu DW, Lee JW, Yoon JH, Koh EK, Hong CS. Microporous Lanthanide-Organic Frameworks with Open Metal Sites: Unexpected Sorption Propensity and Multifunctional Properties. Inorganic Chemistry. 2010;49(11):4723-5.

195. Wu D, Xu Q, Liu D, Zhong C. Exceptional CO2 Capture Capability and Molecular-Level Segregation in a Li-Modified Metalâ˜’Organic Framework. The Journal of Physical Chemistry C. 2010;114(39):16611-7.

196. Ma S, Zhou H-C. Gas storage in porous metal-organic frameworks for clean energy applications. Chemical Communications. 2010;46(1):44-53.

197. Steele BCH. Fuel-cell technology: Running on natural gas. Nature. 1999;400(6745):619-21.

198. Menon VC, Komarneni S. Porous Adsorbents for Vehicular Natural Gas Storage: A Review. Journal of Porous Materials. 1998;5(1):43-58.

199. Zhou W. Methane storage in porous metal−organic frameworks: current records and future perspectives. The Chemical Record. 2010;10(3):200-4.

200. Duren T, Sarkisov L, Yaghi OM, Snurr RQ. Design of New Materials for Methane Storage. Langmuir. 2004;20(7):2683-9.

201. Ma S, Sun D, Simmons JM, Collier CD, Yuan D, Zhou H-C. Metal-Organic Framework from an Anthracene Derivative Containing Nanoscopic Cages Exhibiting High Methane Uptake. Journal of the American Chemical Society. 2007;130(3):1012-6.

202. Senkovska I, Kaskel S. High pressure methane adsorption in the metal-organic frameworks $Cu_3(btc)_2$, $Zn_2(bdc)_2dabco$, and $Cr_3F(H_2O)_2O(bdc)_3$. Microporous and Mesoporous Materials. 2008;112(1-3):108-15.

203. Guo Z, Wu H, Srinivas G, Zhou Y, Xiang S, Chen Z, et al. A Metal–Organic Framework with Optimized Open Metal Sites and Pore Spaces for High Methane Storage at Room Temperature. Angewandte Chemie International Edition. 2011;50(14):3178-81.

204. Mendoza-Cortés JL, Han SS, Furukawa H, Yaghi OM, Goddard WA. Adsorption Mechanism and Uptake of Methane in Covalent Organic Frameworks: Theory and Experiment. The Journal of Physical Chemistry A. 2010;114(40):10824-33.

205. Getzschmann J, Senkovska I, Wallacher D, Tovar M, Fairen-Jimenez D, Duren T, et al. Methane storage mechanism in the metal-organic framework Cu3(btc)2: An in situ neutron diffraction study. Microporous and Mesoporous Materials. 2010;136(1-3):50-8.

206. Wu H, Simmons JM, Liu Y, Brown CM, Wang X-S, Ma S, et al. Metal–Organic Frameworks with Exceptionally High Methane Uptake: Where and How is Methane Stored? Chemistry – A European Journal. 2010;16(17):5205-14.

207. Andreas Zt. Materials for hydrogen storage. Materials Today. 2003;6(9):24-33.

208. K. Mark T. Hydrogen adsorption and storage on porous materials. Catalysis Today. 2007;120(3-4):389-98.

209. Zhao XB, Xiao B, Fletcher AJ, Thomas KM. Hydrogen Adsorption on Functionalized Nanoporous Activated Carbons. The Journal of Physical Chemistry B. 2005;109(18):8880-8.

210. Pang J. Hydrogen adsorption in mesoporous carbons. Applied Physics Letters. 2004;85(21):4887.

211. Nijkamp MG, Raaymakers JEMJ, van Dillen AJ, de Jong KP. Hydrogen storage using physisorption – materials demands. Applied Physics A: Materials Science & Processing. 2001;72(5):619-23.

212. Murray LJ, Dinca M, Long JR. Hydrogen storage in metal-organic frameworks. Chemical Society Reviews. 2009;38(5):1294-314.

213. Furukawa H, Miller MA, Yaghi OM. Independent verification of the saturation hydrogen uptake in MOF-177 and establishment of a benchmark for hydrogen adsorption in metal-organic frameworks. Journal of Materials Chemistry. 2007;17(30):3197-204.

214. Latroche M, Surblé S, Serre C, Mellot-Draznieks C, Llewellyn PL, Lee J-H, et al. Hydrogen Storage in the Giant-Pore Metal–Organic Frameworks MIL-100 and MIL-101. Angewandte Chemie International Edition. 2006;45(48):8227-31.

215. Fang Q-R, Zhu G-S, Jin Z, Ji Y-Y, Ye J-W, Xue M, et al. Mesoporous Metal–Organic Framework with Rare etb Topology for Hydrogen Storage and Dye Assembly. Angewandte Chemie International Edition. 2007;46(35):6638-42.

216. Kesanli B, Cui Y, Smith MR, Bittner EW, Bockrath BC, Lin W. Highly Interpenetrated Metal–Organic Frameworks for Hydrogen Storage. Angewandte Chemie International Edition. 2005;44(1):72-5.

217. Rowsell JLC, Yaghi OM. Strategies for Hydrogen Storage in Metal–Organic Frameworks. Angewandte Chemie International Edition. 2005;44(30):4670-9.

218. Dybtsev DN, Chun H, Yoon SH, Kim D, Kim K. Microporous Manganese Formate: A Simple Metal- Organic Porous Material with High Framework Stability and Highly Selective Gas Sorption Properties. Journal of the American Chemical Society. 2003;126(1):32-3.

219. Wang X-S, Ma S, Rauch K, Simmons JM, Yuan D, Wang X, et al. Metal-Organic Frameworks Based on Double-Bond-Coupled Di-Isophthalate Linkers with High Hydrogen and Methane Uptakes. Chemistry of Materials. 2008;20(9):3145-52.

220. Hirscher M. Hydrogen Storage by Cryoadsorption in Ultrahigh-Porosity Metal–Organic Frameworks. Angewandte Chemie International Edition. 2011;50(3):581-2.

221. Furukawa H, Ko N, Go YB, Aratani N, Choi SB, Choi E, et al. Ultrahigh Porosity in Metal-Organic Frameworks. Science. 2010;329(5990):424-8.

222. Herm ZR, Krishna R, Long JR. CO2/CH4, CH4/H2 and CO2/CH4/H2 separations at high pressures using Mg_2(dobdc). Microporous and Mesoporous Materials. 2012;151(0):481-7.

223. Li J-R, Kuppler RJ, Zhou H-C. Selective gas adsorption and separation in metal-organic frameworks. Chemical Society Reviews. 2009;38(5):1477-504.

224. Xu X, Zhao X, Sun L, Liu X. Adsorption separation of carbon dioxide, methane, and nitrogen on Hβ and Na-exchanged β-zeolite. Journal of Natural Gas Chemistry. 2008;17(4):391-6.

225. Keskin S. High CO_2 Selectivity of A Microporous Metal- Imidazolate Framework: A Molecular Simulation Study. Industrial & Engineering Chemistry Research. 2011;50(13):8230-6.

226. Mu B, Li F, Walton KS. A novel metal-organic coordination polymer for selective adsorption of CO_2 over CH_4. Chemical Communications. 2009(18):2493-5.

227. Demessence A, D'Alessandro DM, Foo ML, Long JR. Strong CO_2 Binding in a Water-Stable, Triazolate-Bridged Metal- Organic Framework Functionalized with Ethylenediamine. Journal of the American Chemical Society. 2009;131(25):8784-6.

228. Couck S, Denayer JFM, Baron GV, Remy T, Gascon J, Kapteijn F. An Amine-Functionalized MIL-53 Metal- Organic Framework with Large Separation Power for CO_2 and CH_4. Journal of the American Chemical Society. 2009;131(18):6326-7.

229. Bao Z, Yu L, Ren Q, Lu X, Deng S. Adsorption of CO2 and CH4 on a magnesium-based metal organic framework. Journal of Colloid and Interface Science. 2011;353(2):549-56.

230. Hamon L, Llewellyn PL, Devic T, Ghoufi A, Clet G, Guillerm V, et al. Co-adsorption and Separation of CO2- CH4 Mixtures in the Highly Flexible MIL-53(Cr) MOF. Journal of the American Chemical Society. 2009;131(47):17490-9.

231. Phan A, Doonan CJ, Uribe-Romo FJ, Knobler CB, O'Keeffe M, Yaghi OM. Synthesis, Structure, and Carbon Dioxide Capture Properties of Zeolitic Imidazolate Frameworks. Accounts of Chemical Research. 2009;43(1):58-67.

232. Finsy V, Ma L, Alaerts L, De Vos DE, Baron GV, Denayer JFM. Separation of CO2/CH4 mixtures with the MIL-53(Al) metal- organic framework. Microporous and Mesoporous Materials. 2009;120(3):221-7.

3

Chapter 3: Adsorption of Carbon Dioxide on Modified Zr-MOF

3

Adsorption of Carbon Dioxide on Modified Zr-MOF

Abstract

This chapter will report synthesis of Zr-MOF using a modified procedure, characterizations of the crystalline structure of this material including FTIR spectra and XRD pattern. Also, this chapter includes carbon dioxide adsorption on Zr-MOF at different temperatures and at low and high pressure. A white nanoparticle of Zr-metal organic framework (Zr-MOF, UiO-66) with a uniformed particle size around 100 nm was synthesized solvothermally and activated with solvent exchange using chloroform and methanol. The activation process with an exchangeable guest solvent using chloroform produced the Zr-MOF with high surface area; BET surface area was 1434 m^2/g while methanol activated sample has a BET surface area same as that reported before.

The Zr-MOF showed high thermal stability up to 753 K and the structure was destroyed at 828K. In addition, this material has a good resistance against the humidity content; its strucrure maintained after 18 months in atmospheric conditions. The chloroform activated Zr-MOF exhibited adsorption capacity of 79 and 45 cc (CO_2) g^{-1} at 1 atm, 273 and 302 K, respectively, while the heat of CO_2 adsorption was calculated to be around 28 kJ mol^{-1}. On the other hand, methanol activated sample presented lower values (62 and 36.5 ccg^{-1} at 273 and 297K, respectively) and higher heat of adsorption (31 kJ/mol). Chloroform modified sample exhibited higher CO_2 adsorption at high pressure. However, methanol activated Zr-MOF exposed higher selectivity of CO_2 over CH_4, showing 3.7 at 59 kPa and 237K.

3.1 Introduction

Recently, metal organic frameworks (MOFs) have been increasingly used as favourable materials in separation (1), gas storage (2), and catalysis (3). Traditional separation techniques have been employed broadly in industries but with some limitations (4-6).

Coordination polymers are promising materials due to their controllable porous structure and higher specific surface areas. They are constructed by organic ligands and metal clusters linked with coordination bonds (7-9).

Carbon dioxide as a major greenhouse gas has been believed to be the cause of global warming. Storage of CO_2 in a cost effective way has attracted a worldwide interest in research and industry. Previous investigations have shown that carbon dioxide could be efficiently adsorbed on metal organic frameworks with high surface areas at different temperatures (10). Most of the work was focused on carbon dioxide adsorption at a higher pressure up to 34 atm (11, 12). The adsorption at a relative low pressure($\leq$ 1 bar) and high temperature is still low and inapplicable in industrial processes (13, 14). In addition, many MOFs suffer from low thermal stability, which makes them unsuitable as adsorbents at high temperatures, in particular for CO_2 separation from flue gas.

Zr-MOF (UiO-66) was recently synthesized with a good thermal stability at 773 K and this material demonstrated tough chemical resistance against many solvents such as water, DMF, acetone and benzene. The building unit of Zr-MOF is a $Zr_6O_4(OH)_4(CO_2)_{12}$ with 12 coordinated sites which represent the coordination of metal atoms. The extension structure of Zr-MOF is cubic close packed structure. This MOF has high symmetrical structure as shown in Figure 3.1 (15, 16).

Also, other experimental and modelling studies have been done in parallel with our study; the UiO-66 was a very reliable material for both of CO_2 and CH_4 adsorption with an acceptable separator factor (17).

Recently, UiO-66 and UiO-67 were tested for hydrogen adsorption at high pressure and 77 K where UiO-67 with longer linker showed higher capacity for hydrogen storage due to reduced density, increased Langmuir surface area, and enhanced micropore volume (18). Some investigations have been reported for its functionalization (19, 20) and application in catalysis (21, 22).

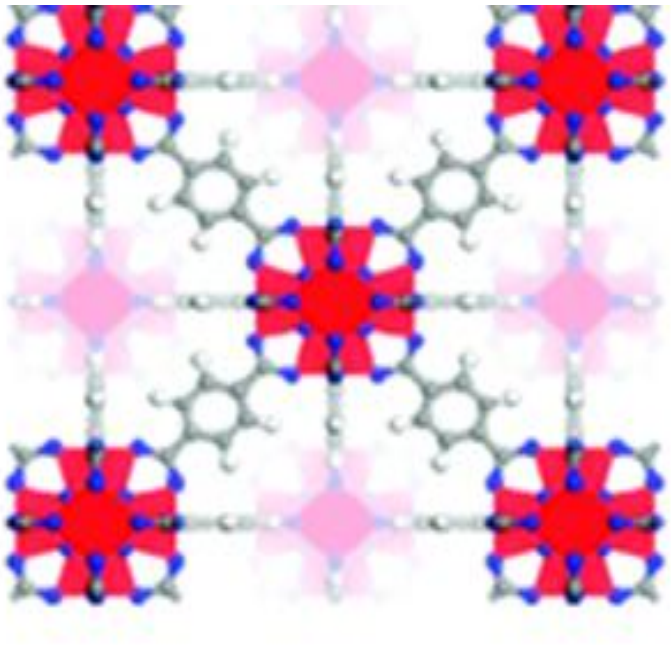

Figure: 3.1 UiO-66 structure (Zirconium, oxygen, carbon, and hydrogen atoms are red, blue, gray, and white, respectively) (15).

In this chapter, we report a modified procedure for synthesis of nanosize Zr-MOF. The synthesized Zr-MOF was activated by a solvent-exchange process to enhance its surface area. Sample characterizations were carried out. Its application for carbon dioxide adsorption was achieved at different temperatures and at atmospheric pressure. In addition, CO_2 and CH_4 adsorption capacities were obtained at high pressure, subsequently, the selectivity was calculated.

3.2 Experimental Work

3.2.1 Chemicals

The chemicals used in the synthesis process include DMF (Dimethylformamide) (99%), BDC (Terephthalic acid,98.9%) and $ZrCl_4$ (99%), which were obtained from Sigma-Aldrich, Thermo Fisher Scientific and Perth Scientific, respectively. Chloroform (99%) and methanol (analysis grade) were obtained from Sigma-Aldrich. The chemicals were used without further purification.

3.2.2 Synthesis and activation processes

Zr-MOF was synthesized by scaling-up the earlier procedure(15) with some changes. Typically, 2.27 mmol of $ZrCl_4$, 2.27 mmol 1, 4-benzenedicarboxylic acid (BDC) were mixed in 405.38 mmol of N, N-dimethylformamide (DMF). The mixed solution was placed inside an autoclave of 45 mL. Next, the sealed autoclave was positioned in a preheated oven at 393 K for 24 h. Then, the collected solid samples were filtered and dried by vacuum filtration. Finally, white powders were produced.

Activation process was done by using a solvent exchange method. Two solvents were used separately to activate modified-Zr-MOF. First, chloroform was used as solvent in this process. More specifically, about 0.3 g as-synthesized Zr-MOF was immersed inside 80 mL of chloroform for 5 days. Then, it was filtered and dried under vacuum; finally the dried material was heated under vacuum at 473 K for 2 days.

Second, methonal was used as solvent to exchange coordinated DMF and uncoordinated BDC by solvothermal treatment for dried sample. More specifically, 0.3 g of Zr-MOF was suspended into 25 mL of methanol then poured in an autoclave. The autoclave was tightly locked and heated in an oven at 373K for 24 hrs. After that, crystalline product was filtered and dried. Finally, dried sample was heated again under vacuum at 473K for 2 days.

3.2.3 Characterizations

X-ray powder diffraction patterns were obtained by a X-ray diffractometer (D8 Advance- Bruker aXS) using Cu *K*α radiation (λ = 1.5406 Å), with accelerating voltage and current of 40 kV and 40 mA, respectively, 2θ was ranged from 5 to 70° .

SEM analysis (Zeiss NEON 40 EsB CrossBeam) was used to capture and determine the morphologies of the crystalline Zr-MOF.

FTIR spectra (Spectrum 100-FT-IR Spectrometer-Perkin Elmer) were used to check the functional groups on the organic ligands as well as solvent molecules and non-reacted chemicals. The spectrum was scanned from 650 - 4000 cm^{-1} with a resolution of 4 cm^{-1} by using an attenuated total reflectance (ATR) technique. Material was tested directly as pressed powder.

A Quantachrome instrument (Autosorb-1) was used to determine the isotherms as well as the pore size and surface area of Zr-MOF; pore size(average pore size can be

used over the whole range of pressure at adsorption and desorption while the micropore size can be determined by DA method), pore volume(Total pore volume when the pore is completely filled thehighest relative pressure, BET surface area and micropore area(V-t method) were calculated by AS1Win software. An activated sample at 0.02 g was evacuated at 473K for 4 h prior to the adsorption measurements under high vacuum. Then nitrogen adsorption was done at 77K using net weight after degassing.

Thermal stability of Zr-MOFs and performance of activation process were checked by a thermogravimetric analysis (TGA) instrument (TGA/DSC1 STAR^e system-METTLER TOLEDO). Zr-MOF samples were loaded into an alumina pan which was automatically and in sequence moved on the balance and heated to 1173K at a rate of 5 K/min. An air flow rate was maintained at 10 mL/min.

3.2.4 Adsorption Study

3.2.4.1 Adsorption at 1 atm

First of all, 99.995% of CO_2 gas was supplied to adsorption instrument. CO_2 adsorption was determined using a Gemini I-2360 instrument at different temperatures and 1 atm. In more details, in Vacprep 061 instrument, 0.25 g of Zr-MOF was loaded in the known weight tube, and then degassed by heating at 473 K under vacuum overnight.

The sample was obtained after degassing to be used in the analysis on Gemini I-2360. It was focused in carbon dioxide adsorption at 273 K which can be provided by crushed ice slurry and room temperature.

3.2.4.2 Adsorption at high pressure

Adsorption isotherms of carbon dioxide (99.995%) and methane (99.995%) were investigated at high pressure up to 1000 kPa, 273 K by a micromeritics-ASAP2050. The powdered sample should be prepared before using in gas adsorption analysis by a suitable procedure to ensure full removal of impurities.

More specifically, a weighed sample was degassed on the same instrument by increasing the temperature at a heating rate of 10 K/min till 373 K to be continued at this temperature for 2 h then increasing the temperature again at the same heating

rate to 473K under vacuum (up to 0.4 kPa) to hold at these conditions for 8 h. Finally, an obtained net weight after degassing was used in the analysis at 273 K.

3.3 Results and Discussion

3.3.1 Structural Stability

XRD patterns of Zr-MOF-(old procedure of Cavka, et al (15)) and activated samples of Zr-MOF(modified procedure) showed that the positions of all peaks are the same (Figure 3.2). That means all samples have the same structure as UiO-66(old procedure) but they have different crystallinities as the intensities were changed. Choloroform activated Zr-MOF shows the highest crystallinity while methanol activated Zr-MOF is the lowest, that can refer to that choloroform is more reliable in activation process although methanol has higher effeciency for removal unreacted BDC and coordinated solvent as shown below in TGA profile. Modified-Zr-MOF demonstrated high stability against the water content by direct and indirect exposure. This material retained its structure the same when it was stored at ambient conditions for more than 18 months. Also, when this material was immersed in water for more than 6 hrs, the structure has not been changed as shown in Figure 3.3. Therefore, Zr-MOF can be used and stored for long time with slight impact on the crystalinity.

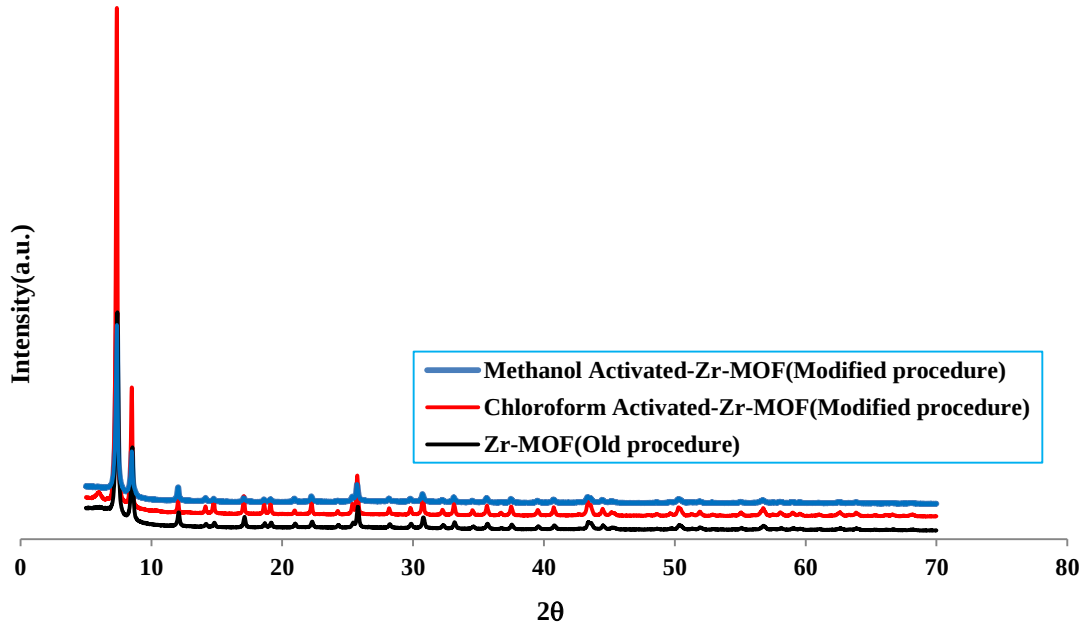

Figure: 3.2 XRD Patterns for Zr-MOF before and after activation compared with UiO-66(Published procedure(15))

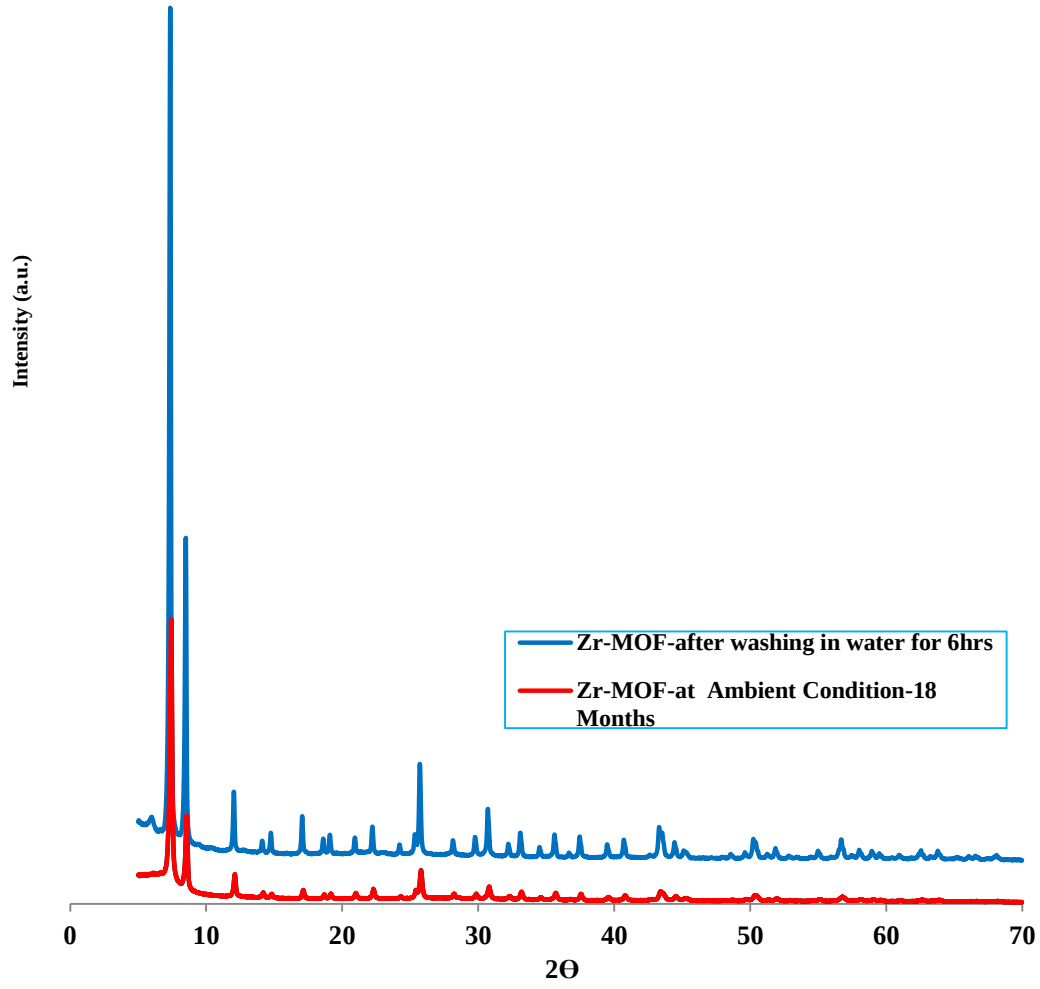

Figure: 3.3. XRD patterns for Zr-MOF under effect of water content

3.3.2 Morphological Description

SEM images show that homogeneous cubic particles of modified Zr-MOFs and Zr-MOF(old procedure) were obtained. The particle size is similar and around 100 nm in chloroform activated Zr-MOF while the crystal size of methanol-activated Zr-MOF is less than 100 nm (Figure 3.4). It seems that the morphological features of modified samples are similar while it is different from the morphology of Zr-MOF(UiO-66) which was published by Cavka et al. (15) because the modified samples were synthesized in different molar ratio.

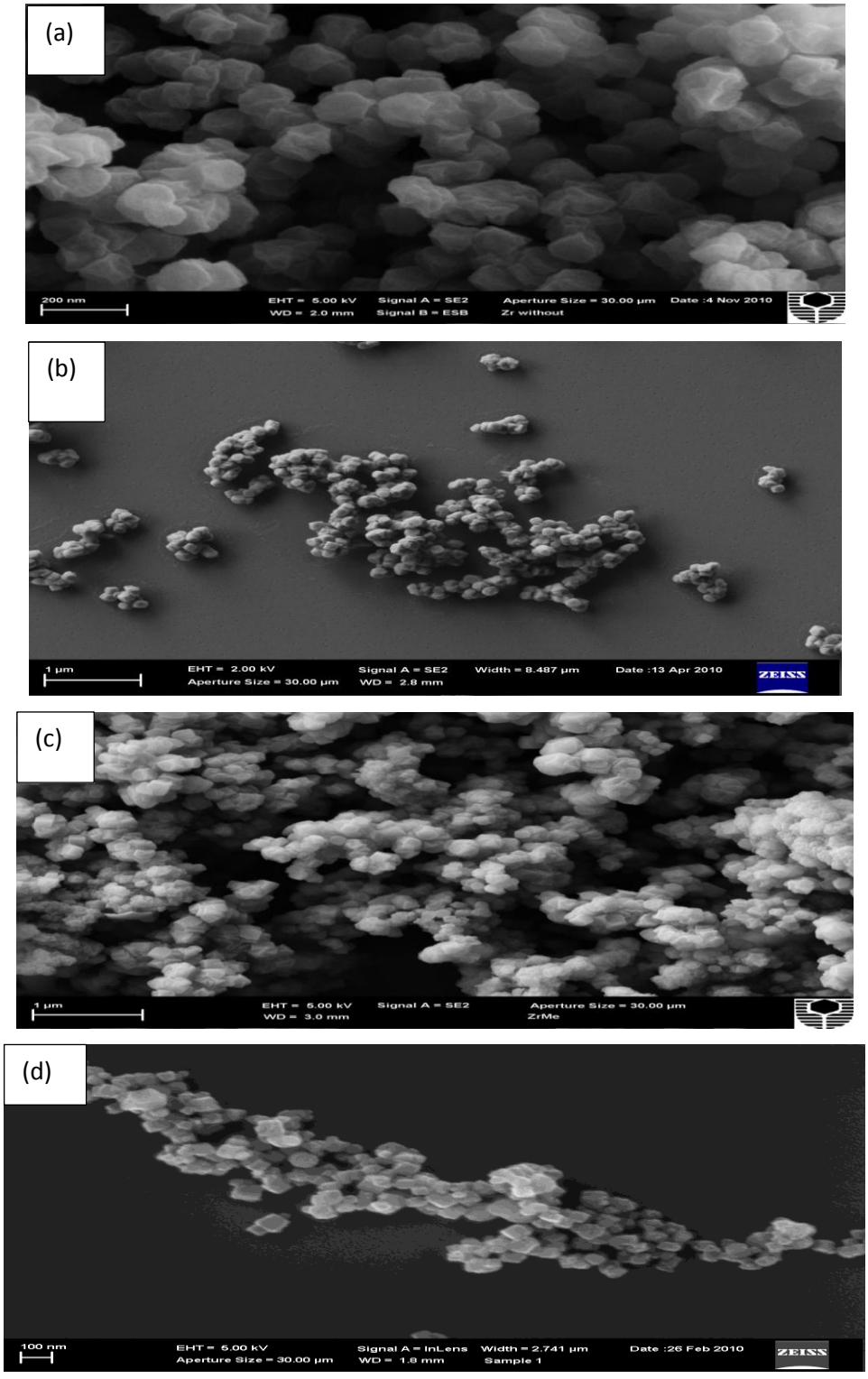

Figure: 3.4 SEM images of the Zr-MOF (a) and (b) Chloroform activated Zr-MOF in different dimentional scale, (c) Methanol activated Zr-MOF, and (d) UiO-66(old procedure)

3.3.3 Functional groups determination

Figure 3.5 shows FT-IR spectra of Zr-MOF as-synthesized and after activation by solvent exchange in chloroform and methanol. The peak at 1550 – 1630 cm^{-1} referred to C=O of carboxylates, which was coordinated with metal centres by O^- during the deprotonation process, could be observed on both spectra (23). This may be a main evidence for creating the coordination bonds in MOF.

However, the stretching variation band of C=O bond in carboxylic acid in the region of 1640 – 1670 cm^{-1} disappeared after activation by methanol and there is a bit of this peak remaining after activation by chloroform, suggesting that a good exchange of chloform and methanol to DMF and BDC which could be easily removed after heating. In each spectrum a weak peak in the region of 1450 – 1580 cm^{-1} belonging to the C=C in aromatic compound of organic linker occurred. The strong peak at around 1400 cm^{-1} was ascribed to C-O bond of C-OH group of carboxylic acid.

It can be seen from FTIR spectra, there is no extra-functional group added on the structure and the original groups are maintained except free carboxylic group which was removed when uncoordinated-BDC was discarded by activation process. However, the intensities of the functional groups of Zr-MOF which was activated by chloroform were higher than those of methanol activated Zr-MOF, which may refer to higher crystallinity and functionality at chloroform-activated Zr-MOF.

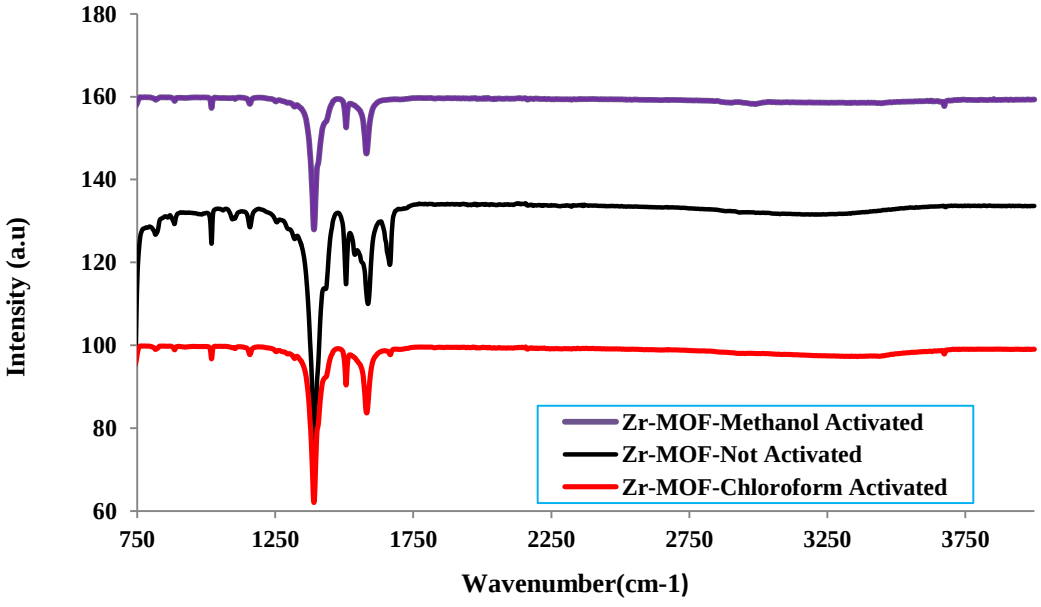

Figure: 3.5 FT-IR spectra of modified Zr-MOF

3.3.4 Nitrogen Isotherm and Pore Size Distribution

The porous structure of Zr-MOFs were tested by N_2 adsorption. Figure 3.6 (a) shows that the adsorption and desorption isotherms were overlapped in chloroform activated sample, this can refer to dominating micropore structure without a hysteresis whereas the adsorption/desorption isotherms of methanol activated sample shows obviously a hysteresis which indicates mesopore structure as well as the micropore structure.

Most textural parameters are presented in Table 3.1. The BET surface area of chloroform activated Zr-MOF is 1434 $m^2 g^{-1}$, while it is 1083 $m^2 g^{-1}$ for methanol activated sample, which is similar to the reported value before (12). Using chloroform in activation can effectively remove DMF and BDC residuals, resulting in higher crystanility and surface area. However, methanol can significantly remove the residuals, its surface area is lower as a result of lower crystallinity.

Table 3.1: Porous structure of Zr-MOF

Textural Properties	**Zr-MOF-Chloroform Activated**	**Zr-MOF-Methanol Activated**
Multi-point BET ($m^2 g^{-1}$)	1434	1083
$v-t$ method (micropore area %)	89.8%	76%
Average pore radius (Å)	9.1	11.4
Total pore volume ($cm^3 g^{-1}$)	0.654	0.619
Micropore Volume ($cm^3 g^{-1}$)	0.438	0.315

The micropore portion for chloroform activated-Zr-MOF is around 90% and the average pore size is 0.9 nm while they are 76% and 1.14 nm, respectively, for methanol activated Zr-MOF, suggesting the micropore was reduced and average pore size was increased with using methanol as an exchanging solvent. The pore size distributions from the BJH method show two major peaks centred at around 1.8 and 5 nm for methanol activated sample while they are 1.9 and 5 nm for chloroform activated sample (Figure 3.6(b)). However, the DA micropore distributions are presented in Figure 3.6(c) and illustrates that micropore size in methanol activated sample was lower than that of chloroform activated sample. The peaks are around 0.54 and 0.77 nm, for methanol activated and chloroform activated samples, respectively.

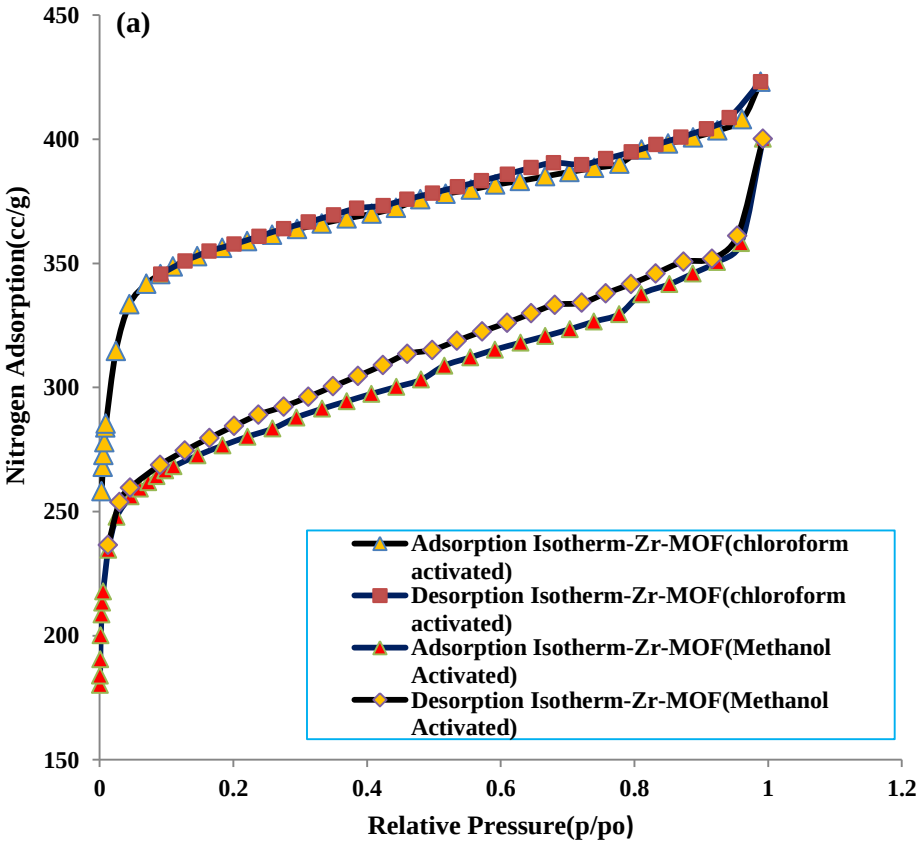

Figure: 3.6 (a) Nitrogen adsorption/desorption isotherms for activated Zr-MOFs

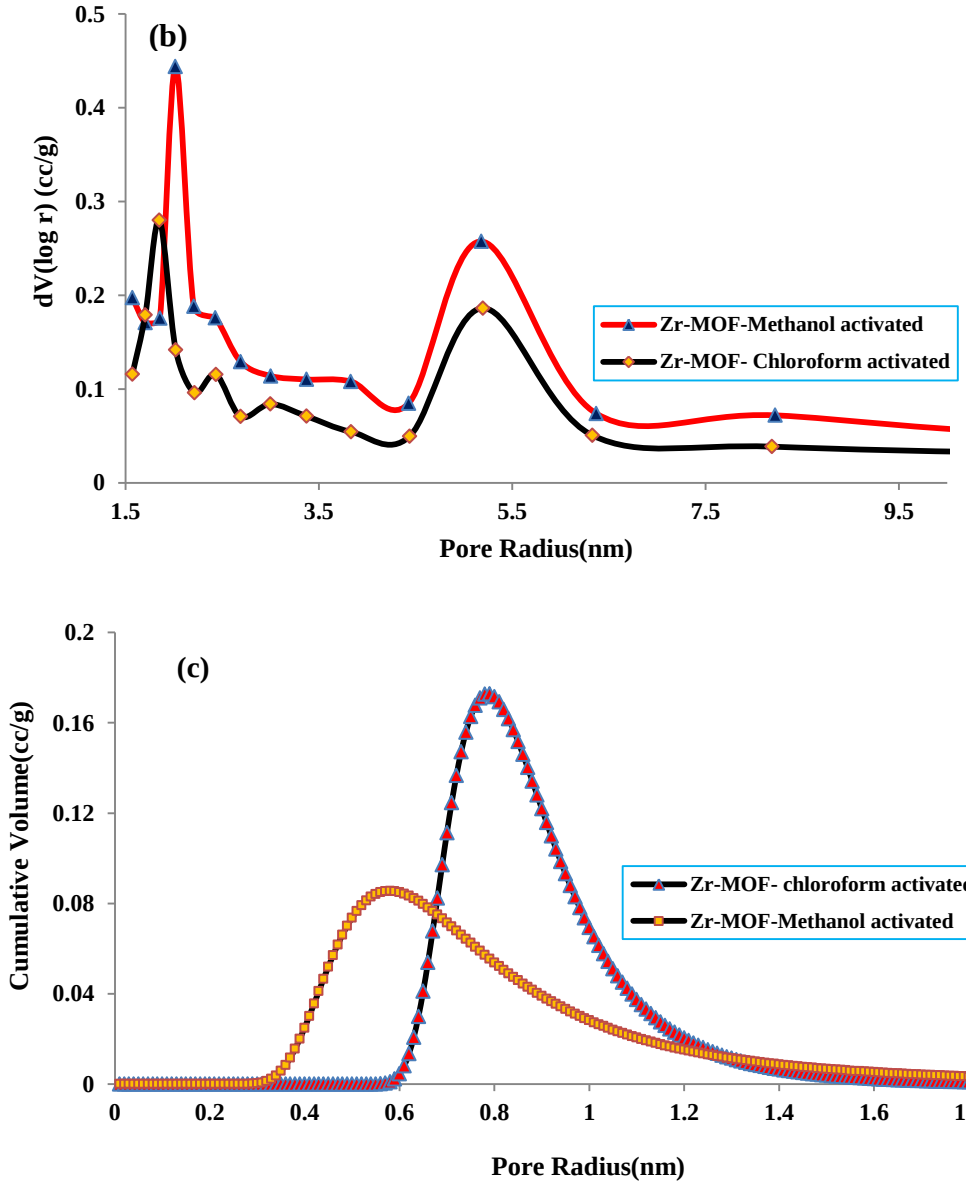

Figure: 3.6 (b) The BJH pore size distributions, and (c) DA micropore size distributions

3.3.5 Thermal Analysis

Weight loss profiles from thermogravimetric analysis (TGA) tests in Figure 3.7 show that before and after activation process, Zr-MOFs show loss of moisture and some of free solvent molecules consisting of 8% in chloroform activated sample and around 15% in methanol activated sample at temperature up to 393K. However, it is around

8% on unactivated sample. This amonut may be changed depending on the atmospheric conditions because Zr-MOF has extraordinary ability to adsorb moisture.

In Zr-MOF, before activation, weight loss of uncoordinated BDC and coordinated DMF molecules inside the pores is around 20% while in chloroform and methanol activated Zr-MOF, they are 3% and 0.5% respectively, which occurs up to 573 K. With increasing the temperature further up to 753 K, coordination bonds between the BDC molecules and metal centres were broken, this coordinated BDC in each sample had about 23% weight loss. Then, the whole structure is destroyed at 828 K.

Thermal analysis shows that thermal stability of Zr-MOF was not changed with changing the activation process. Methanol was more efficient to remove uncoordinated BDC but that may affect the pore structure. However, chloroform is more selective to enhace the micropore structure although there are resdual BDC and DMF .

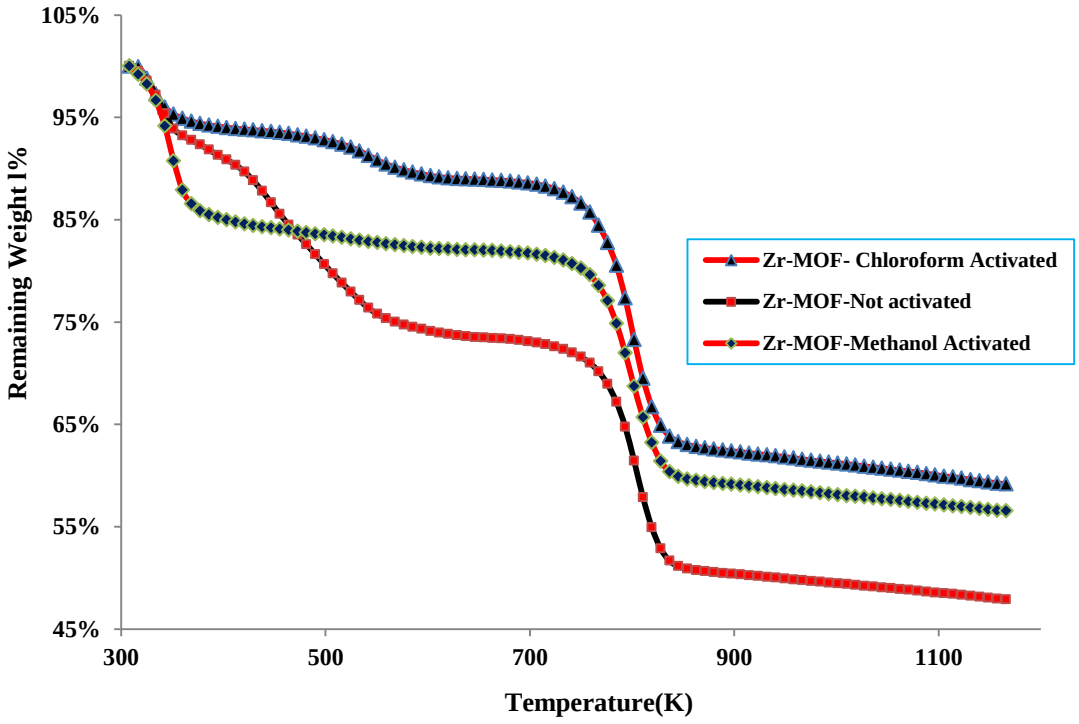

Figure: 3.7 TGA profiles of Zr-MOFs before and after activation

3.3.6 Carbon Dioxide Adsorption

3.3.6.1 Adsorption at 1 atm

Methanol activated sample (Figure 3.8) showed CO_2 adsorption capacity of 62 and 36.5 cc/g at 273 and 297K, respectively, at 1 atm while they were 79 at 273 and 45 cc/g at 302K on chloroform activated sample as shown in Figure 3.9. It is noted that the chloroform activation has improved the surface area of Zr-MOF and affinity of the structure to better adsorb CO_2 .

The adsorption capacities on chloroform activated sample are much higher than those the values previously reported on some MOFs, 22.5 cc g^{-1} (Zn-MOF, 1 atm, 298 K)(24), 26 cc g^{-1} (MMOF, 1 atm, 298 K)(13), 15.5 cc g^{-1} (Cu-SNU-6, 1 atm, 273 K)(10), 48 cc g^{-1} (ZnPO-MOF, 1 atm, 273 K)(25).

It has been reported that an inflection in CO_2 isotherm could occur on some MOFs, such as IRMOF-1, IRMOF-10, IRMOF-16(26), and MMOF (13). This inflection was attributed to the electrostatic attraction between molecules of CO_2 at lower pressure (26). However, in this investigation, the inflection was not observed on nanosize Zr-MOF similar to other MOFs, MOF-74 and ZnPO-MOF-24. We believe that the inflection is also related to the distribution of electrostatic charges inside the pores, which will be controlled by electrostatic nature of the pore surface or electronegatively property of metal centres.

Heat of adsorption for CO_2 was calculated based on the Clausius-Claperyron equation using coverage at diffreent pressure and temperatures.

$$\Delta H = -R\left[T_2T_1/(T_2 - T_1)\right]\ln\left[P_2/P_1\right] \qquad 3\text{-}1$$

Where P_1 and T_1 are the lower temperature and pressure while P_2, T_2 are the higher pressure and temperature, and R is the universal gas constant, 8.314 $J.mol^{-1}.K^{-1}$.

It was found that heat of adsorption would not change significantly and was 28.6 kJ mol^{-1} for chloroform activated sample and 31 kJ/mol for methanol activated sample. These values are less than that of MOF-74 (39 kJ mol^{-1}) (14), MIL-53-Cr (32 kJ mol^{-1}) (6), and MIL-53-Al (35 kJ mol^{-1})(6).

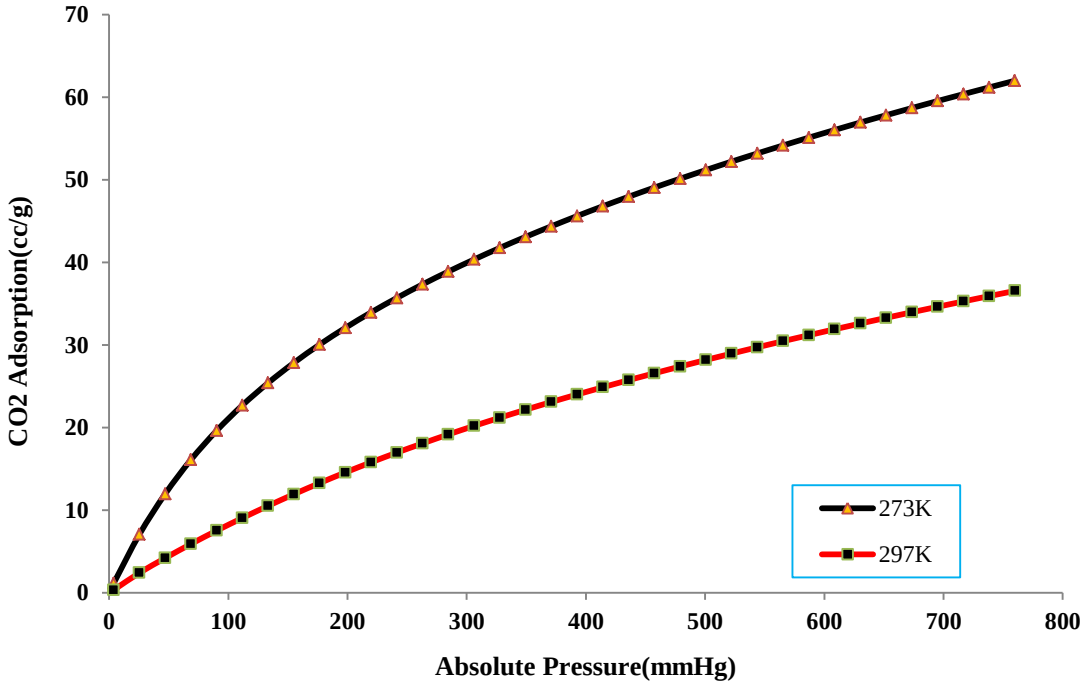

Figure: 3.8 CO_2 adsorption isotherms of methanol-activated Zr-MOF at 1atm and differenet temperatures

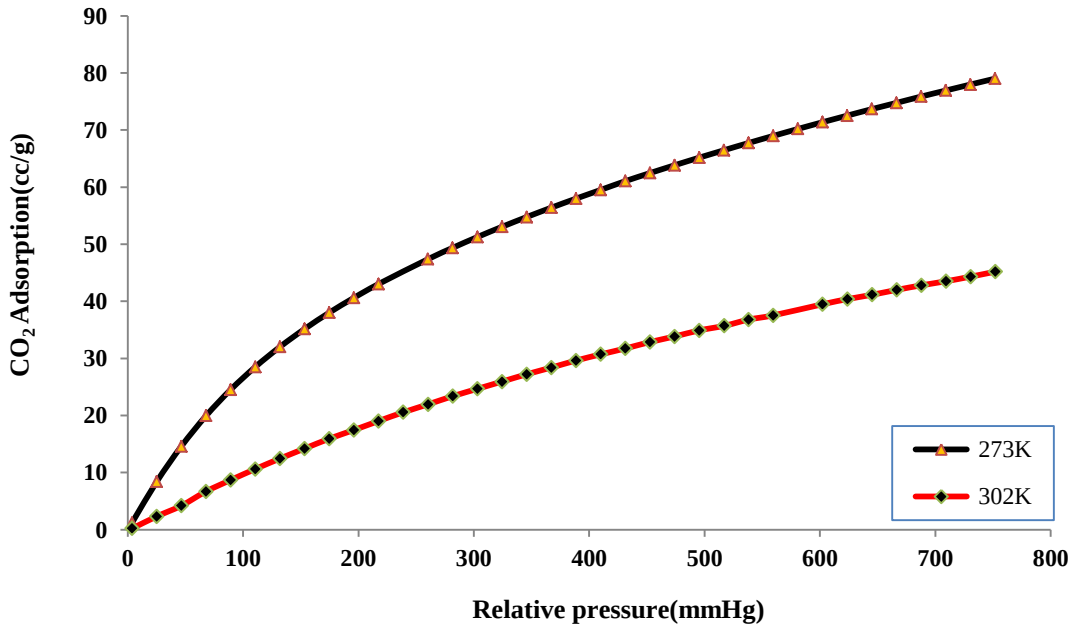

Figure: 3.9 CO_2 adsorption isotherms of chloroform activated Zr-MOF at 1atm and different temperatures

3.3.6.2 Adsorption at high pressure

3.3.6.2.1 CO_2 Adsorption

It was believed that the smallest pores are filled at the lowest pressures and that the larger pores can be gradually filled at higher pressures during CO_2 adsorption process (26). Figure 3.10 shows that chloroform activated Zr-MOF has more CO_2 adsorption than methanol activated sample; the adsorption was 8.1 and 7.31 mmol/g, respectively, at 273K and 988.6 kPa.

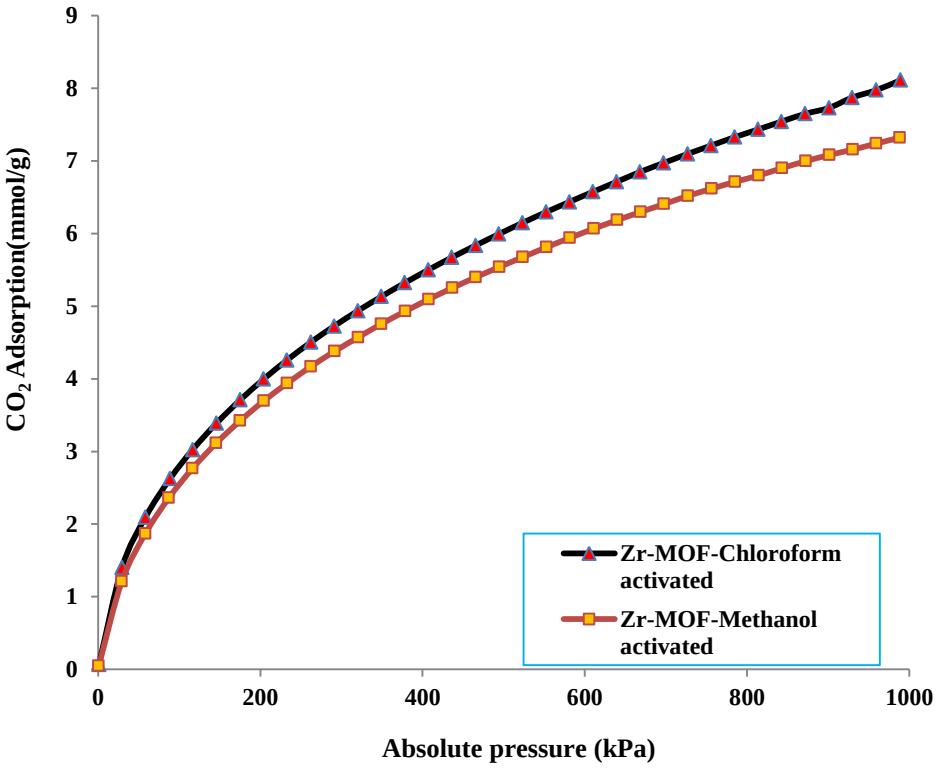

Figure: 3.10 CO_2 adsorption on modified Zr-MOFs at high pressure and 273K

3.3.6.2.2 CH_4 Adsorption and Selectivity

Figure 3.11 shows CH_4 adsorption on different samples activated by chloroform and methanol. It is much lower than CO_2 adsorption as a result of a difference in polarity between CO_2 and CH_4 molecules. Although both of them are not polar, CO_2 molecules have quadrupolar moment which can enhance the electrostatic forces (27) or hydrogen bonding formation (28). Furthermore, methane can be significantly

captured by activated Zr-MOF but chloroform activation is more affective to enhance CH_4 capture while methanol activation is lower. CH_4 adsorption capacity of 3.5 and 3.14 mmol/g were achieved on both samples respectively. Pure component was considered in calculation of selectivity according to the following equation;

$$Selectivity=V_{CO2}/V_{CH4} \quad 3\text{-}2$$

However, methanol activated Zr-MOF presented more selective to CO_2 at pressure less than 400 kPa, its selectivity is 3.7 at 59 kPa and 273K which is bigger than chlorofom activated Zr-MOF of 3.57 at the same conditions as displayed in Figure 3.12.

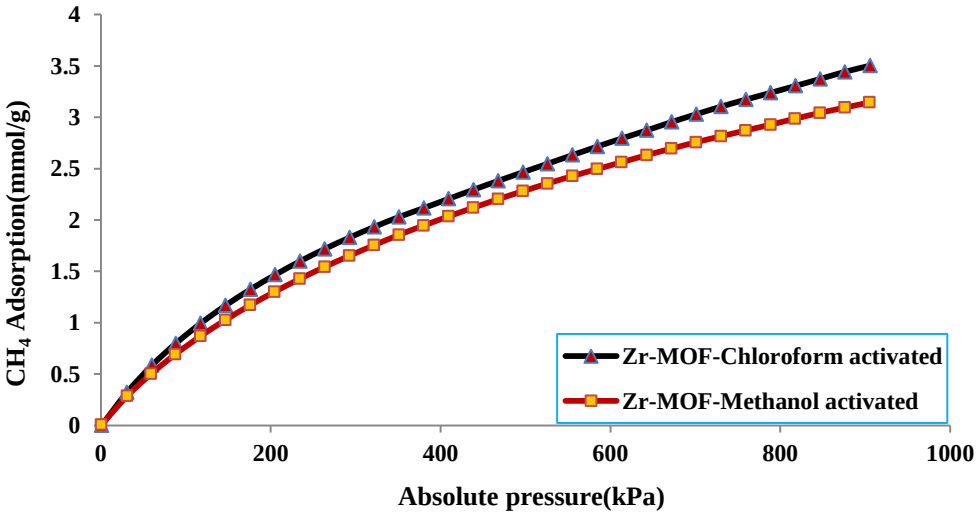

Figure: 3.11 CH_4 adsorption on midified Z-MOF at high pressure and 273K

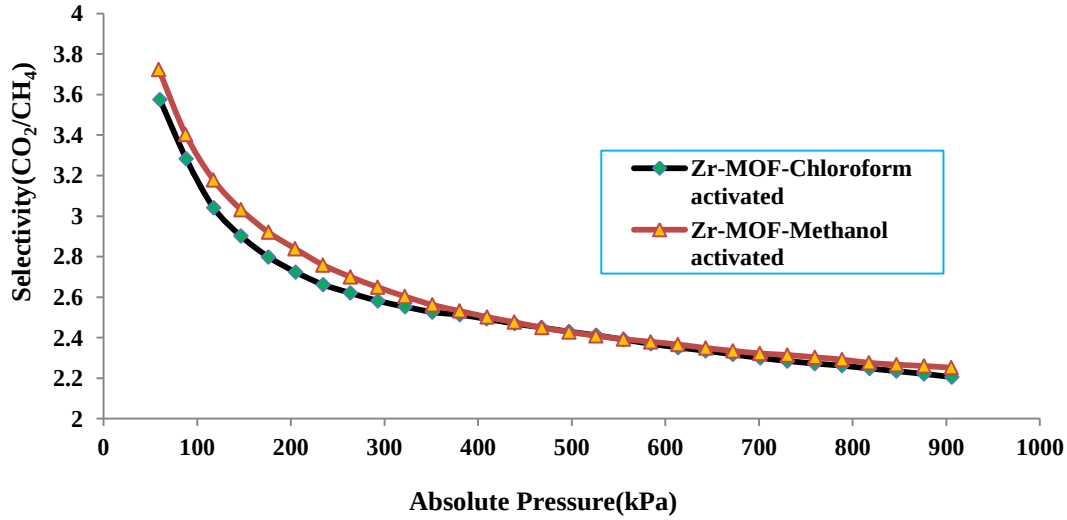

Figure: 3.12 Selectivity of CO_2 over CH_4 on Modified Zr-MOFs

3.3 Conclusion

Zr-MOFs were synthesized by a modified procedure and activated by different procedures. The crystalline structure was the same as UiO-66. Also, the morphology showed a cubic crystals in high geometry which seems different from the previous one.

The activation using chloroform or methanol as solvent exchange is efficient to remove molecules of DMF and unreacted BDC from the pores. Chloroform activation can enhance the porous structure and surface area more than methanol process. The thermal stability was very high and not changed with the activation process.

Zr-MOF exhibits an enhanced adsorption for carbon dioxide at varying temperatures, especially at chloroform activated Zr-MOF. Also, this material exposed very high stability in wetted atmosphere. It was found that, the heat of adsorption of carbon dioxide on methanol activated sample was higher than on chloroform activated sample but they are acceptable amongest other MOFs. These materials also demonstrated high adsorption capacity for carbon dioxide at high pressure.

Chloroform activated Zr-MOF exposed higher CO_2 and CH_4 adsorpyion at high pressure. However, methanol activated Zr-MOF was more selective to CO_2 at low pressure.

3.4 References

1. Couck S, Denayer JFM, Baron GV, Remy T, Gascon J, Kapteijn F. An Amine-Functionalized MIL-53 Metal-Organic Framework with Large Separation Power for CO2 and CH4. Journal of the American Chemical Society. 2009;131(18):6326-7.

2. Rowsell JLC, Millward AR, Park KS, Yaghi OM. Hydrogen sorption in functionalized metal-organic frameworks. Journal of the American Chemical Society. 2004;126(18):5666-7.

3. Xamena FXLI, Abad A, Corma A, Garcia H. MOFs as catalysts: Activity, reusability and shape-selectivity of a Pd-containing MOF. Journal of Catalysis. 2007;250(2):294-8.

4. Shukla P, Wang S, Sun H, Ang H-M, Tadé M. Adsorption and heterogeneous advanced oxidation of phenolic contaminants using Fe loaded mesoporous SBA-15 and H2O2. Chemical Engineering Journal. 2010;164(1):255-60.

5. Yong Z, Mata V, Rodrigues AE. Adsorption of carbon dioxide at high temperature - a review. Separation and Purification Technology. 2002;26(2-3):195-205.

6. Bourrelly S, Llewellyn PL, Serre C, Millange F, Loiseau T, Ferey G. Different adsorption behaviors of methane and carbon dioxide in the isotypic nanoporous metal terephthalates MIL-53 and MIL-47. Journal of the American Chemical Society. 2005;127(39):13519-21.

7. Llewellyn PL, Bourrelly S, Serre C, Filinchuk Y, Ferey G. How hydration drastically improves adsorption selectivity for CO2 over CH4 in the flexible chromium terephthalate MIL-53. Angewandte Chemie-International Edition. 2006;45(46):7751-4.

8. Férey G. Hybrid porous solids: past, present, future. Chemical Society Reviews. 2008;37(1):191.

9. Yaghi OM. Metal-organic Frameworks: A tale of two entanglements. Nat Mater. 2007;6(2):92-3.

10. Park HJ, Suh MP. Mixed-Ligand Metal-Organic Frameworks with Large Pores: Gas Sorption Properties and Single-Crystal-to-Single-Crystal Transformation on Guest Exchange. Chemistry-a European Journal. 2008;14(29):8812-21.

11. Ravikovitch PI, Vishnyakov A, Russo R, Neimark AV. Unified approach to pore size characterization of microporous carbonaceous materials from N-2, Ar, and CO_2 adsorption isotherms. Langmuir. 2000;16(5):2311-20.

12. Millward AR, Yaghi OM. Metal-organic frameworks with exceptionally high capacity for storage of carbon dioxide at room temperature. Journal of the American Chemical Society. 2005;127(51):17998-9.

13. Wu HH, Reali RS, Smith DA, Trachtenberg MC, Li J. Highly Selective CO_2 Capture by a Flexible Microporous Metal-Organic Framework (MMOF) Material. Chemistry-a European Journal. 2010;16(47):13951-4.

14. Britt D, Furukawa H, Wang B, Glover TG, Yaghi OM. Highly efficient separation of carbon dioxide by a metal-organic framework replete with open metal sites. Proceedings of the National Academy of Sciences of the United States of America. 2009;106(49):20637-40.

15. Cavka JH, Jakobsen S, Olsbye U, Guillou N, Lamberti C, Bordiga S, et al. A new zirconium inorganic building brick forming metal organic frameworks with exceptional stability. Journal of the American Chemical Society. 2008;130(42):13850-1.

16. Valenzano L, Civalleri B, Chavan S, Bordiga S, Nilsen MH, Jakobsen S, et al. Disclosing the Complex Structure of UiO-66 Metal Organic Framework: A Synergic Combination of Experiment and Theory. Chemistry of Materials. 2011;23(7):1700-18.

17. Yang Q, Wiersum AD, Jobic H, Guillerm V, Serre C, Llewellyn PL, et al. Understanding the Thermodynamic and Kinetic Behavior of the CO2/CH4 Gas Mixture within the Porous Zirconium Terephthalate UiO-66(Zr): A Joint Experimental and Modeling Approach. The Journal of Physical Chemistry C. 2011;115(28):13768-74.

18. Chavan S, Vitillo JG, Gianolio D, Zavorotynska O, Civalleri B, Jakobsen S, et al. H_2 storage in isostructural UiO-67 and UiO-66 MOFs. Physical Chemistry Chemical Physics. 2012.

19. Kandiah M, Nilsen MH, Usseglio S, Jakobsen S, Olsbye U, Tilset M, et al. Synthesis and Stability of Tagged UiO-66 Zr-MOFs. Chemistry of Materials. 2010;22(24):6632-40.

20. Chavan S, Vitillo JG, Uddin MJ, Bonino F, Lamberti C, Groppo E, et al. Functionalization of UiO-66 Metal-Organic Framework and Highly Cross-Linked Polystyrene with Cr(CO)(3): In Situ Formation, Stability, and Photoreactivity. Chemistry of Materials. 2010;22(16):4602-11.

21. Silva CG, Luz I, Llabres i Xamena FX, Corma A, Garcia H. Water Stable Zr-Benzenedicarboxylate Metal-Organic Frameworks as Photocatalysts for Hydrogen Generation. Chemistry-a European Journal. 2010;16(36):11133-8.

22. Vermoortele F, Ameloot R, Vimont A, Serre C, De Vos D. An amino-modified Zr-terephthalate metal-organic framework as an acid-base catalyst for cross-aldol condensation. Chemical Communications. 2011;47(5):1521-3.

23. Loiseau T, Serre C, Huguenard C, Fink G, Taulelle F, Henry M, et al. A rationale for the large breathing of the porous aluminum terephthalate (MIL-53) upon hydration. Chemistry-a European Journal. 2004;10(6):1373-82.

24. Thallapally PK, Tian J, Kishan MR, Fernandez CA, Dalgarno SJ, McGrail PB, et al. Flexible (Breathing) Interpenetrated Metal-Organic Frameworks for CO_2 Separation Applications. Journal of the American Chemical Society. 2008;130(50):16842-3.

25. Shultz AM, Farha OK, Hupp JT, Nguyen ST. A Catalytically Active, Permanently Microporous MOF with Metalloporphyrin Struts. Journal of the American Chemical Society. 2009;131(12):4204-+.

26. Walton KS, Millward AR, Dubbeldam D, Frost H, Low JJ, Yaghi OM, et al. Understanding inflections and steps in carbon dioxide adsorption isotherms in metal-organic frameworks. Journal of the American Chemical Society. 2008;130(2):406-+.

27. Culp JT, Goodman AL, Chirdon D, Sankar SG, Matranga C. Mechanism for the Dynamic Adsorption of CO_2 and CH_4 in a Flexible Linear Chain Coordination Polymer as Determined from In Situ Infrared Spectroscopy. The Journal of Physical Chemistry C. 2010;114(5):2184-91.

28. Bourrelly S, Llewellyn PL, Serre C, Millange F, Loiseau T, Férey G. Different Adsorption Behaviors of Methane and Carbon Dioxide in the Isotypic Nanoporous Metal Terephthalates MIL-53 and MIL-47. Journal of the American Chemical Society. 2005;127(39):13519-21.

4

Chapter Four: Effects of Ammonium Hydroxide Additives in Synthesis Process of Zr-MOF on the Characteristics and CO_2 Adsorption

4

Effects of ammonium hydroxide additives in synthesis process of Zr-MOF on the characteristics and CO_2 adsorption

Abstract

In this chapter, Zr-MOF synthesis procedure has been modified by adding ammonium hydroxide. The effects of ammonium hydroxide on porous structure, thermal stability and adsorption were investigated and enlarged pores were produced. It was found that using of ammonium hydroxide as additives in the synthesis process produced some effects on structure and characteristics of Zr-MOF. The pore size increased with raising the amount of additives and the maximum average pore size was found to be 2.72 nm in Zr-MOF-NH_4-2. However, the BET surface area of modified Zr-MOFs was found to be lower than Zr-MOF-(Parent). In addition, crystal size reduced with increasing the amount of additives. All samples with different amounts of NH_4OH present thermal stability the same as Zr-MOF-(Parent). At standard conditions the capacity of adsorption for carbon dioxide reduced with decreasing the micropore fractions of modified samples. It fell from 3.52 mmol/g on Zr-MOF to 2.11 mmol/g on Zr-MOF-NH_4-3. However, with this modification the material with the largest voids had the lowest heat of adsorption for carbon dioxide (22.9 kJ/mol). Also, the adsorption capacity for carbon dioxide increased at high pressure, especially for Zr-MOF-NH_4-2 at pressure more than 5 bars. It was about 8.63 mmol/g at 987 kPa, 273K. In addition, these materials were tested for methane adsorption. Zr-MOF (Parent) showed the highest methane adsorption; it was 3.62 mmol/g while Zr-MOF-NH_4-3 demonstrated the lowest methane adsorption at 2.43 mmol/g. However, the selectivity of CO_2/CH_4 on Zr-MOF-NH_4-1 and Zr-MOF-NH_4-3 had the best affinity to select CO_2 over CH_4.

4.1 Introduction

MOFs become aim of most industrial applications, especially in gas storage. These materials have a ultra-low density and high specific void volume (1). Most transition metals have been used increasingly in the synthesis of MOFs (2). One of noteworthy properties of MOFs is that these new materials can be easily modified and substituted to meet the specific requirements of applications by tailoring their properties (3), for example, the pore characteristics, which can be changed in size, shape (4) polarity (5) and cavities (6, 7).

Many studies attempted to modify and improve the characteristics of MOFs during the synthesis process (8-11), and others concentrated on post-synthesis of some MOFs to meet the required usage (12). MOFs were more suitable for adsorption applications with exceptionally high capacity to store carbon dioxide at the pressure up to saturation pressure at room temperature (13). High selectivity for capture carbon dioxide from gaseous mixtures was obtained on Mg-MOF-74 at low pressure (14). Moreover, enhancement of selective capture of CO_2 was gained by improving the pore or cavity chemistry toward more affinities for CO_2 (15, 16). On the other hand, many studies focused on ability of several MOFs to adsorb carbon dioxide and methane at low capacity (17, 18).

Recently, Zr-MOFs were reported with different organic linkers, 1,4-benzenedicarboxylate (UiO-66), 4,4′-biphenyldicarboxylate (UiO-67), and terphenyl-dicarboxylate (UiO-68) with the same topology (19, 20). Also amino-modified Zr-MOF (21) to make some changes in functionality and structure was performed, which can use Zr-MOF in different applications such as catalysts (22, 23).

In this chapter, the previous synthesis procedures of Zr-MOF and activation process were modified by using ammonium hydroxide as an additive in the synthesis process of Zr-MOF. The effects of the modification on structure change and carbon dioxide adsorption were investigated at low and high pressure.

4.2 Experimental work

4.2.1 Chemicals

All chemicals including DMF (99%), BDC (benzene-1, 4-dicarboxylic acid, 98.9%), ammonium hydroxide (NH_4OH, 24%), zirconium chloride ($ZrCl_4$, 99%) and chloroform ($CHCl_3$, 99%) were supplied by Sigma Aldrich, Thermo Fisher Scientific and Perth Scientific and used without further purification.

4.2.2 Synthesis

4.2.2.1 Zr-MOFs-(Parent)

Zr-MOF was synthesized by the previous procedure (19) with some amendments and activated by chloroform as discussed in section 3.2.2 in Chapter 3.

4.2.2.2 Zr-MOF-NH4

Zr-MOF-NH_4 was synthesized as below. In the synthesis of Zr-MOF-NH_4-1, the solvent (DMF) was divided into two parts. In the first, 202.69 mmol of DMF was mixed with BDC and stirred for 15 min, and then 0.2 ml of NH_4OH (2M) - was added in dropwisely under stirring. The second part of DMF was mixed with $ZrCl_4$ and stirred about 30 min. Then the two solutions were mixed together for around 20 min. The resulted solution was placed into a Parr PTFE-lined digestion vessel of 45 mL at 393 K for 24 hrs. The same procedure was repeated with adding 0.4 and 0.6 mL of NH_4OH to synthesize Zr-MOF-NH_4-2 and Zr-MOF-NH_4-3, respectively.

Activation of Zr-MOFs was carried out in the method as previously reported (24, 25). The crystalline materials were immersed inside chloroform solution for 5 days, and then the solids were filtered and dried under vacuum, finally, these materials were dried in an oven at 463 K overnight. The dried sample was heated under vacuum at 473 K for 2 days.

4.2.3 Characterizations

X-ray powder diffraction patterns were done by a XRD diffractometer (Diffractometer D8 Advance- BrukeraXS) with Cu Kα1 radiation (λ=1.5406 Å) to evaluate the stability of the crystalline structure.

The morphologies of the samples were determined by a SEM machine (Zeiss NEON 40 EsBCross Beam) to describe size and shape of crystals.

N_2 adsorption isotherms were measured by an Autosorb-1 (Quantachrome) to determine surface area by the BET and Langmuir models and pore size of mesopores by the BJH method. Average pore radius can be obtained for the whole range of pore size distribution (Mesopore, micropore, and Macropore) by average pore size method; in addition, micropore ratio can be measured by the t-plot method. Total pore volume was measured at relative pressure close to unity by total volume method. All these methods can be done by AS1Win software on the Autosorb-1. Firstly, around 10 mg of the sample were degassed at 473K under vacuum for 6 h. After that, the sample was ready to use in nitrogen adsorption measurement at 77 K by the same instrument.

FTIR spectra were obtained by a Perkin-Elmer 100-FT-IR Spectrometer to check the intensities of functional groups which may be related to the crystalline structure or other free chemicals inside the pores. Each spectrum was scanned from 650 to 4000 cm^{-1} with a resolution of 4 cm^{-1} using Universal ATR-Diamond/ZnSe as IR Accessory.

Thermal behavior of Zr-MOFs was determined by a TGA instrument (TGA/DSC1 $STAR^e$ system-METTLER TOLEDO). A sample of 20 mg was loaded into an alumina pan of 150 µL and placed automatically in the TGA furnace. The temperature was increased up to 1173 K in atmosphere of Argon and air mixture supplied with a flow rate of 20 ml/min.

4.2.4 Adsorption study

Static volumetric technique with an apparatus from Micromeritics (Gemini I- 2360) was used to measure the adsorption isotherm of pure CO_2 (99.995%) at 273 and 296 K at low pressure up to 100 kPa. About 0.25 g of each sample after drying was firstly weighed in

a tube and then activated by Vacprep 061 at 473 K under vacuum for two days. The sample after degassing process was used in analysis on Gemini I-2360. Carbon dioxide heat of adsorption was calculated from the Clausius-Claperyron equation (eq.3.1) replying on the isotherms measured at different temperatures by Gemini I-2360 at 100 kPa.

Micoromeritics- ASAP2050 was used to measure the adsorption isotherms of pure carbon dioxide (99.995%) and pure methane (99.995%) at pressure up to 1000 kPa. First of all, an activated sample was degassed by the same instrument with increasing the temperature at a ramp of 10 K/min till 373 K to exclude the moisture from the pores and hold at this temperature for 2 hrs, then increasing the temperature again at the same rate to 473 K under vacuum (up to 0.4 kPa) and hold at this condition for 8 hrs. Then the sample was used in the analysis at 273 K.

4.3 Results and Discussion

4.3.1 Structural Stability

All samples have the similar XRD patterns to that of Zr-MOF-(Parent), which was synthesized previously in Chapter 3 as shown in Figure 4.1 (a) and (b). However, the intensities were reduced with increasing the amount of additives (NH_4OH). The biggest change in intensity can be seen in the patterns of Zr-MOF-NH_4-3 and Zr-MOF-NH_4-2. These samples suffered from a decrease in the intensity of one main peak at $2\theta = 8.51°$.

The intensity of the peaks in the patterns of modified samples was reduced as a result of effect of ammonium additives on the crystalline structure formation. Also, it was found that, there is a relation between the peak intensities and peak widths together with crystal size, the crystal size decreases when the intensity decreases and width becomes wider. More significant modification in pore enlargement was Zr-MOF-NH_4-2, which had medium intensities amongst the samples. However, Sayari et al. claimed that the reduction in intensities means reducing the ordering of the structure which may be accompanied by shifting in the position of the peaks (26), and it was observed that Zr-MOF-NH_4-3 was wider than others.

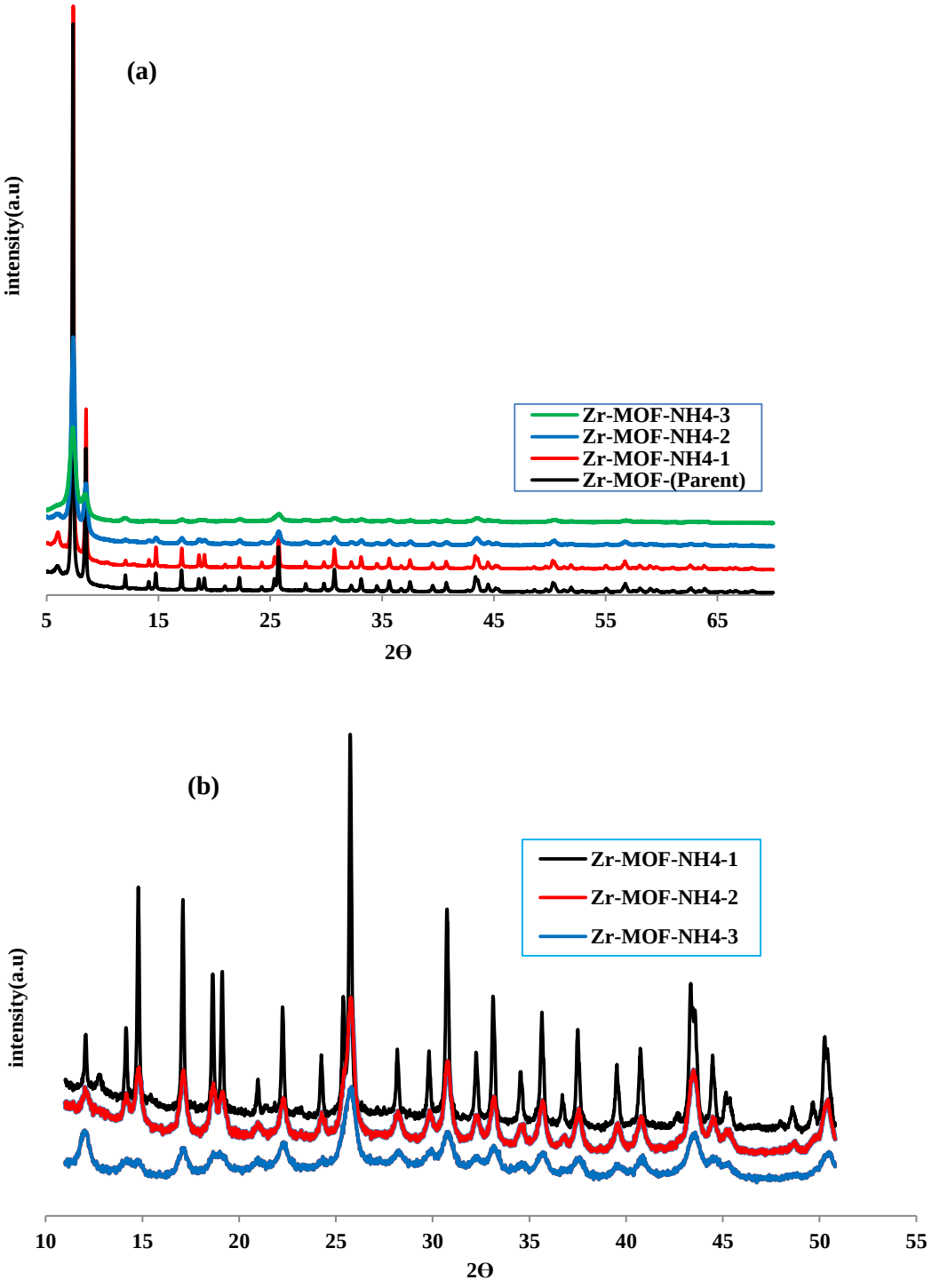

Figure: 4.1 (a) XRD patterns for Zr-MOF-(parent) and Zr-MOF-NH_4, (b) magnification scale of Zr-MOF-NH_4-1, Zr-MOF-NH_4-2 and Zr-MOF-NH_4-3 patterns

4.3.2 Morphological Description

SEM images (Figure 4.2) show clearly that crystal size of Zr-MOF-NH_4 decreased with increasing ammonium hydroxide additive in synthesis solution. It was believed that adding of ammonium hydroxide in synthesis solution will induce two effects**.** The pH has been increased and it will lead to increase in the solubility of the solute. With extra-addition, the solution becomes easy to be supersaturation and make small size crystal formation (27).

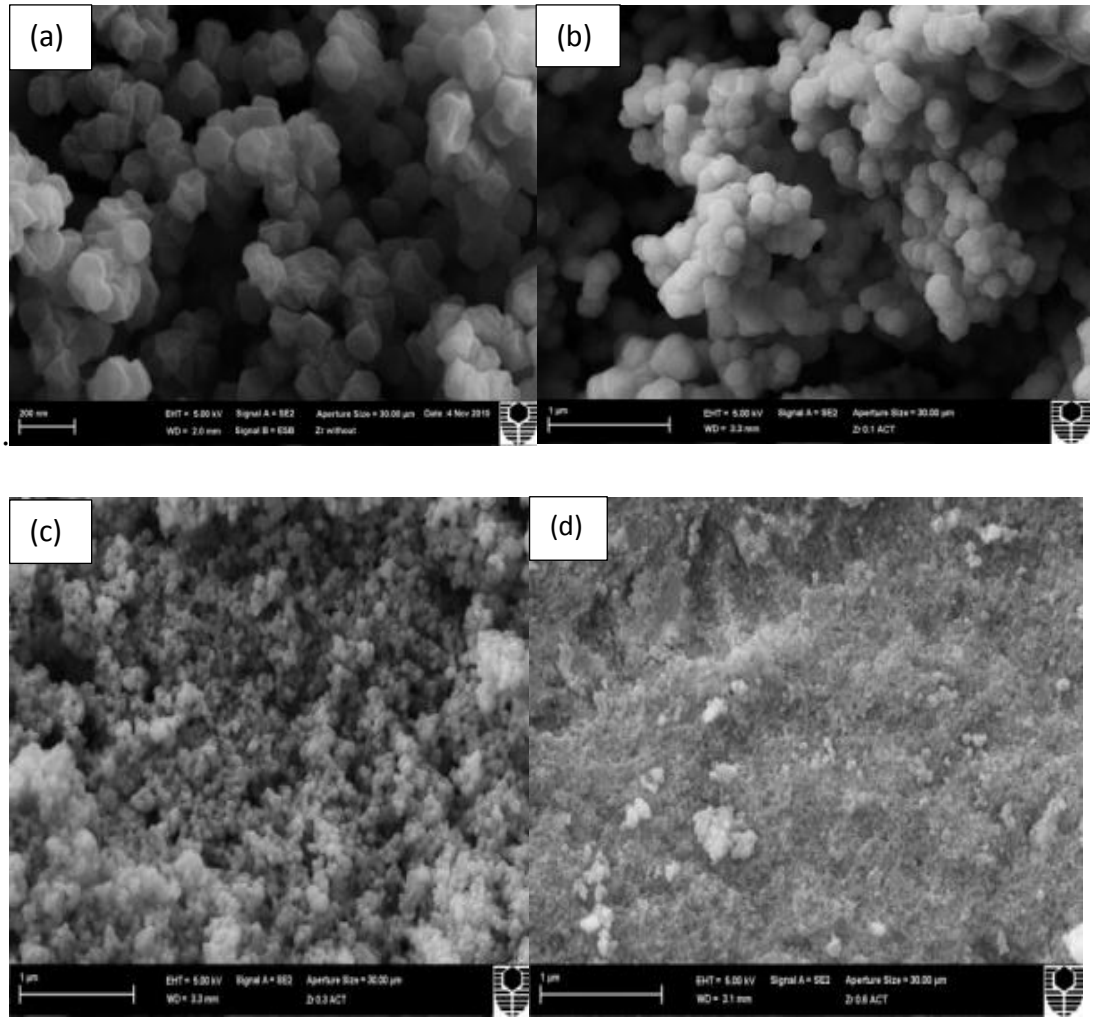

Figure: 4.2 SEM Images of Zr-MOFs, (a) Zr-MOF-without NH_4OH additives,(b) Zr-MOF-NH_4-1, (c) Zr-MOF-NH_4-2, (d) Zr-MOF-NH_4-3

4.3.3 Functional groups determination

FTIR spectra (Figure 4.3) and thermal analysis (Figure 4.6) for all samples proved that DMF molecules and un-reacted reactants (BDC molecules) were discarded, because, exchanging solvent activation method was more beneficial than a heating one, since a heating method may relatively affect the integrity of the structure. From a comparative study of FTIR spectra of activated and non-activated Zr-MOFs, it can be demonstrated that the stretching variation band of C=O bond in carboxylic acid in the region 1640-1670 cm^{-1} has been approximately disappeared in the activated samples. At the region of 1550-1630 cm^{-1}, C=O in carboxylates which were already coordinated with metal center by O^- after losing H^+ of OH group in carboxylic acid during the deprotonation process (28). Also all spectra have a weak peak in the region 1450-1580 cm^{-1} belonging to the C=C in aromatic compound of organic linker. In the region below of 1500 cm^{-1} all the peaks may indicate the variation inside the molecules, the band at 1250-1450 cm^{-1} indicated C-O bond of C-OH group of carboxylic acid.

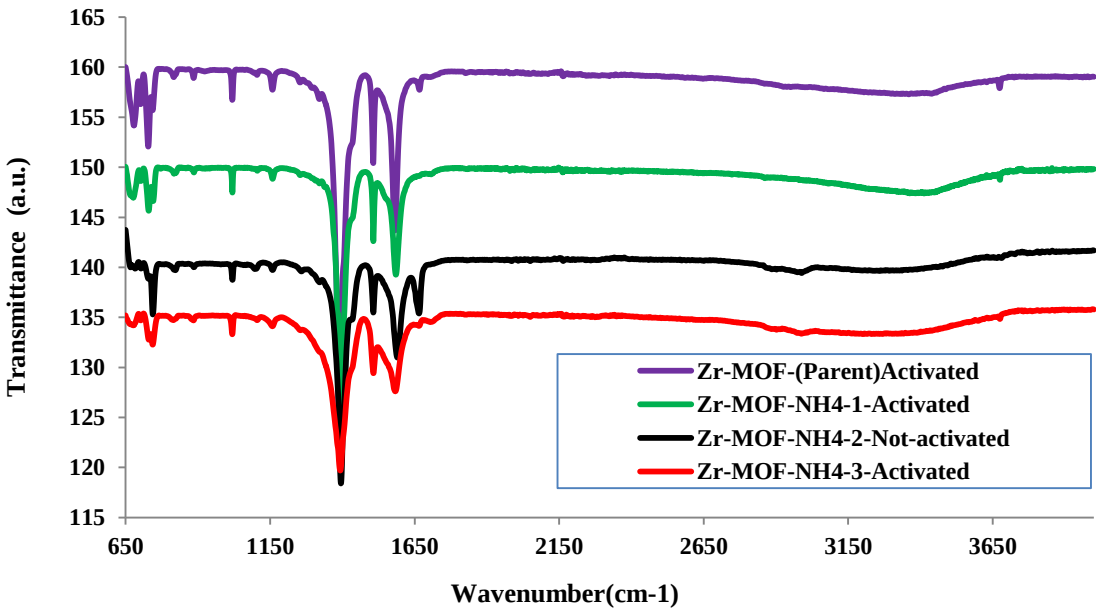

Figure: 4.3 FTIR spectra for Zr-MOFs with different amount of additive

The region of 3175-3600 cm^{-1} related to hydroxyl groups was found to be changed. Almost all spectra of all samples approximately have the same behavior. The main functional groups on organic linkers have been kept for all samples. In addition; the spectra of all the samples got the same peaks in fingerprint region from 1300 to 910 cm^{-1} with a slight difference in the intensities.

4.3.4 Nitrogen isotherm and pore size distribution

Table 4.1 shows that the total pore volume, average pore size increased whereas micropore volume deceased with raising the amount of ammonium hydroxide in the synthesis process. The total pore volume ranged from (0.65 cc/g) to (1.63 cc/g), and average pore size grew up from 0.91 to 2.72 nm with enhancing the amount of additives from 0 to 0.4 mL of additives.

Table 4.1: Pore size analysis as well as BET surface area of all sample of Zr-MOFs

MOF's Name	S_{BET} m^2/g	MP %	Average pore radius (Å)	Total pore volume (cm^3/g)	Micropore volume(cm^3/g)
Zr-MOF(Parent)	**1434**	**89.76%**	**9.1**	**0.65**	**0.562**
Zr-MOF-NH_4-1	**1320**	**82.0%**	**9.7**	**0.64**	**0.517**
Zr-MOF-NH_4-2	**1215**	**74.17%**	**27.2**	**1.63**	**0.475**
Zr-MOF-NH_4-3	**1202**	**65.32%**	**17.1**	**1.03**	**0.499**

Furthermore, Figure 4.4 (A) shows that Zr-MOF has two peaks centered at 1.8 and 5.0 nm, respectively. Zr-MOF-NH_4-1 shows a similar pore size profile with peaks shifted to lower size centered at 1.7 and 3.3 nm, respectively. Zr-MOF-NH_4-2 presents a smaller pore at 3.3 nm and many large pores greater than 20 nm. For Zr-MOF-NH_4-3, major pore size at about 10 nm is appearing. The above results indicate that addition of NH_4OH will create larger pore and increase average pore size and the maximum pore radius and pore volume were seen in Zr-MOF-NH_4-2 while they started to reduce again in Zr-MOF-NH_4-3.

The micropore percentage ranged from 89.76% to 65.32% when the amount of additives increases from 0 to 0.6 ml and micropore volume fell from 0.562 to 0.475 cc/g in Zr-MOF-2 then increased again in Zr-MOF-3 to be 0.499 cc/g. Moreover, the micropore radius was 0.8, 0.86, 0.86, 0.81 for Zr-MOF-(Parent), Zr-MOF-NH_4-1, Zr-MOF-NH_4-2, and Zr-MOF-NH_4-3, respectively, as shown in Figure 4.4 (B).

In addition, the BET surface area decreased in sequence from 1434 m^2/g in Zr-MOF-(Parent) to 1202 m^2/g in Zr-MOF-NH_4-3. The maximum BET surface area in Zr-MOF without any additives may be attributed to crystalinity of this material which was higher than Zr-MOF-NH_4 materials as it appears by comparison of intensities in XRD patterns of all samples (Figure 4.1) (18, 29).

Figure 4.5 shows N_2 adsorption/desorption isotherms of various Zr-MOFs samples. Zr-MOFs show some different profiles. In general, Zr-MOFs present microporous structure showing high adsorption at low pressure. There is a hysteresis loop at p/p_0=0.7-0.9 on isotherms of Zr-MOF-NH_4-2 and Zr-MOF-NH_4-3, indicating a large pore. Zr-MOF-NH_4-2 presents a sharp increase in adsorption at p/p_0=0.9, indicating the presence of macropores.

It seems that ammonium hydroxide seriously affect the pore structure as it was considered as a part of solvent in the synthesis process, and as a swelling factor for pore structure. As it was shown, less change occurred in the BET surface area. However, this enlargement in pore size may be accompanied with decrease in crystalinity of the structure (26).

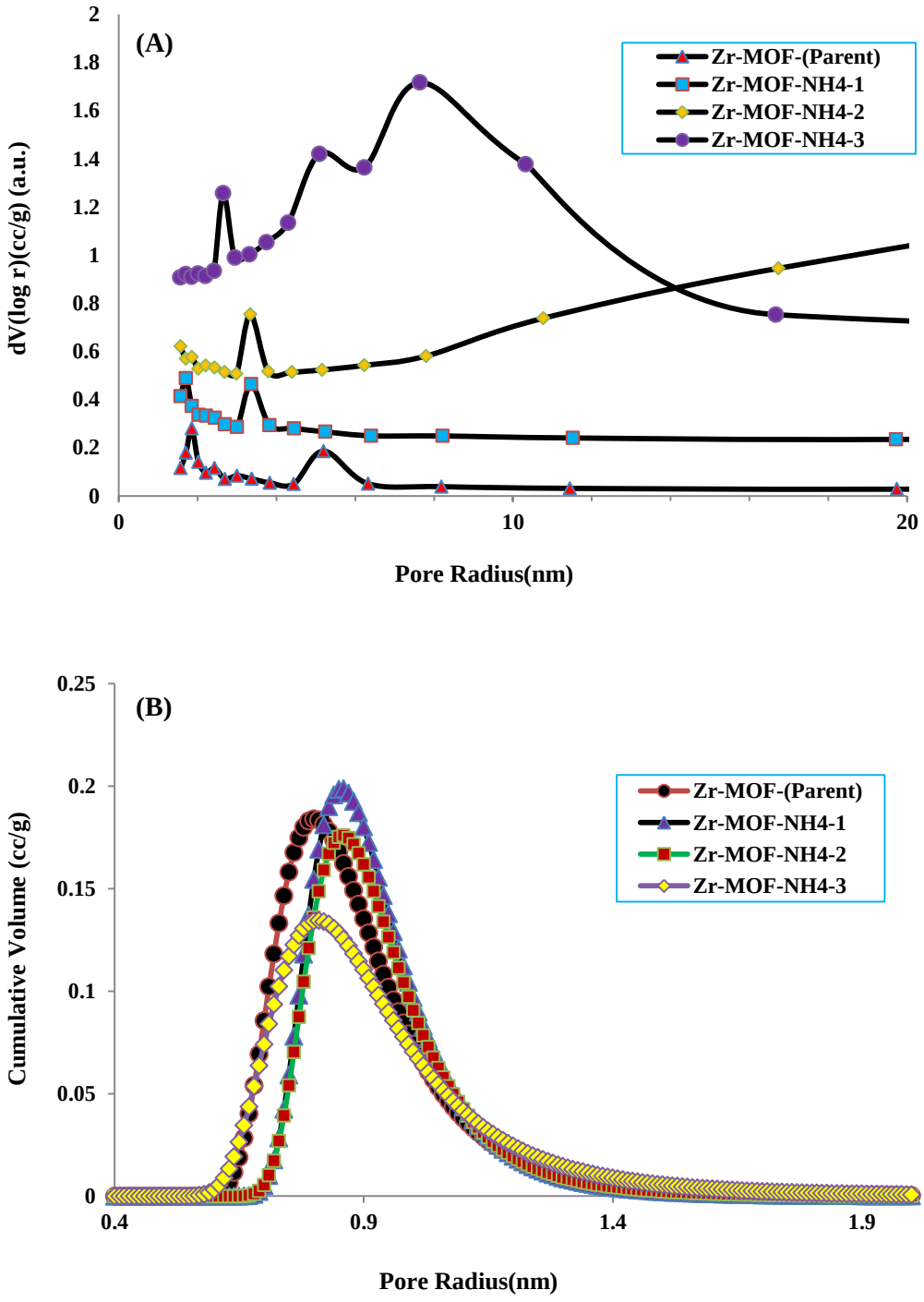

Figure: 4.4 Pore size distribution for Zr-MOFs (A) in Mesopore portion, and (B) in Micropore portion

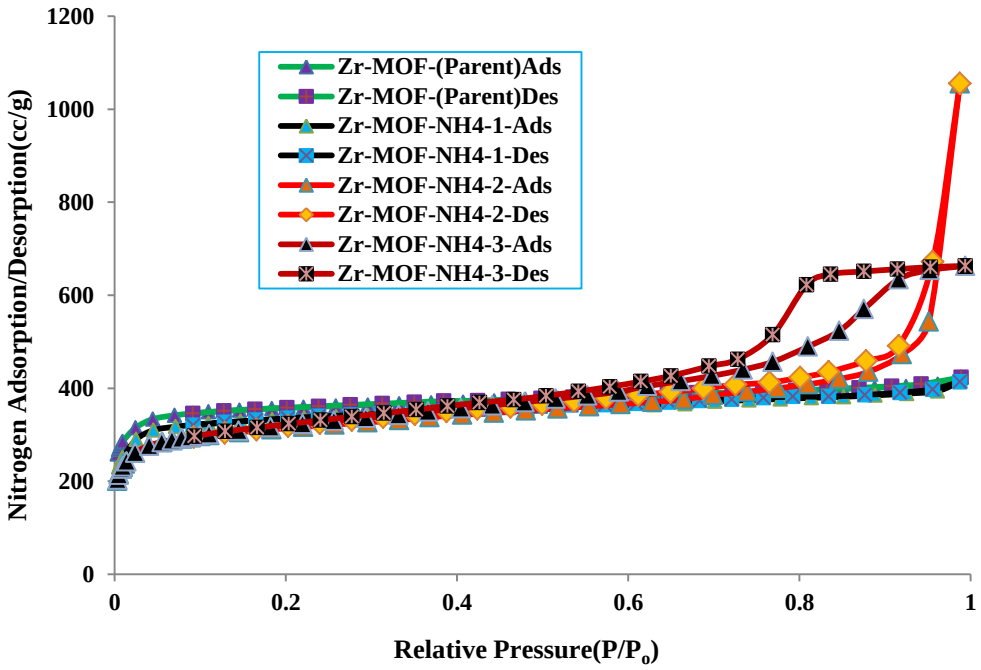

Figure: 4.5 Nitrogen adsorption/desorption isotherms at 77 K and 1 atm

4.3.5 Thermal Analysis

As it is shown in Figure 4.6, all as-synthesized samples have the following weight loss profiles; the moisture as well as free solvent (uncoordinated) ranged from 0.5 to 0.8 wt%, which can be removed at around 393 K. Uncoordinated BDC and coordinated solvent molecules have around 20 wt% that can be discarded at around 573 K. Coordinated BDC (1, 4-benzene dicarboxylate) has about 20 wt% which will be destroyed completely at 828 K except Zr-MOF-NH_4-2 at around 863K. In addition, the percentage of Zr_6O_6 is about 53%, 46.7%, 50% and 54% in Zr-MOF (Parent), Zr-MOF-NH_4-1, Zr-MOF-NH_4-2 and Zr-MOF-NH_4-3, respectively. These results suggest that all samples have approximately the same composition. Moreover, it can be seen from thermal analysis for activated samples (Figure 4.6). All samples had around 3 wt% of coordinated solvent remaining inside the pores. Additionally, all the samples present high thermal stability up to around 753 K which is the same as Zr-MOF (Parent) (Figure 3.7). Hence, the additives cannot affect the thermal stability of the modified materials; also, it was proved that no further connection has been found inside the pores as a result of using ammonium hydroxide in synthesis procedure.

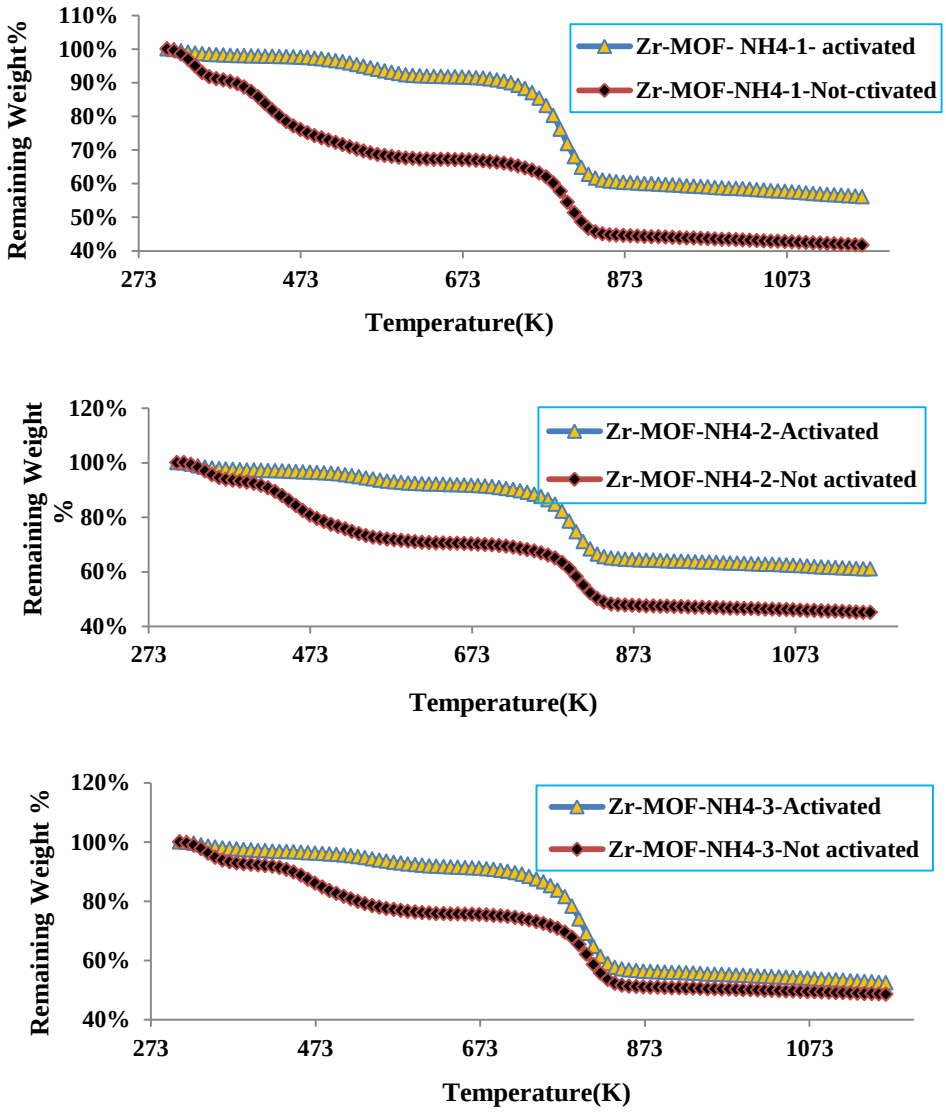

Figure: 4.6 Thermal analyses before and after activation for Zr-MOFs samples with different amount of ammonium hydroxide additives

4.3.6 CO_2 Adsorption

4.3.6.1 CO_2 adsorption at 1 atm

Carbon dioxide adsorption decreased with increasing the temperature and amount of NH_4-additives as shown in Figure 4.7 (a), (b), and (c); it was 63 and 30 cc/g at 273 and 307K, respectively on Zr-MOF-NH_4-1 while it was 47, 24.5 cc/g on Zr-MOF-NH_4-3.

These values are lower than the adsorption capacity on Zr-MOF-(Parent) which was discussed in Chapter 3. It suggests that with increasing the macropore and mesopore percentages in these materials, carbon dioxide adsorption capacity at atmospheric pressure decreased. On contrast, very high CO_2 uptake can be achieved at low temperature or at high pressure (17). The isotherm of carbon dioxide at pressure up to 1 atm cannot show adsorption for the pore larger than 1 nm (30).

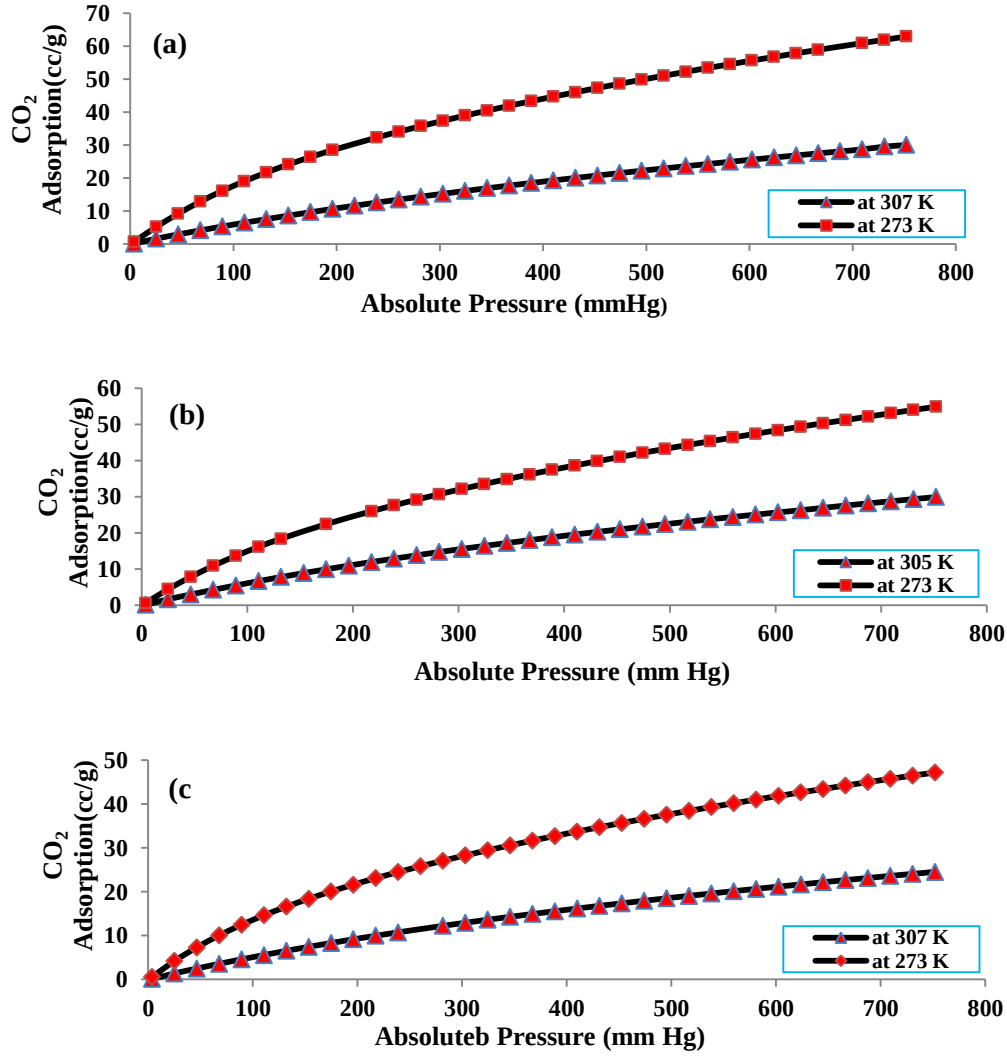

Figure: 4.7 CO_2 adsorption at different temperatures and 1atm on (a) Zr-MOF-NH_4-1, (b) Zr-MOF-NH_4-2, and (c) Zr-MOF-NH_4-3

The isosteric heat of adsorption calculated by the Clausius-Claperyron equation (Eq.3.1) reduced with increasing pore size of the modified samples. More specifically, the average heat adsorption on Zr-MOF-NH_4-2 was a 22.87 kJ/mol while it was a 28.65 kJ/mol on Zr-MOF-(Parent). It can be explained that large pore gives the opportunity to gas molecules to be adsorbed on the surface without any competing with similar molecules that have the same charges. Also the surface potentials may be less for large pores (30). Therefore the heat of adsorption showed the lowest value for the largest pore. Generally, the heat of adsorption slightly reduced with increasing coverage (Figure 4.8) Increasing the amount of adsorbed CO_2 can enhance the interaction between CO_2 molecules. The strong adsorption sites may be occupied at the first then the gas molecules may be interacted by weaker adsorption force (31, 32).

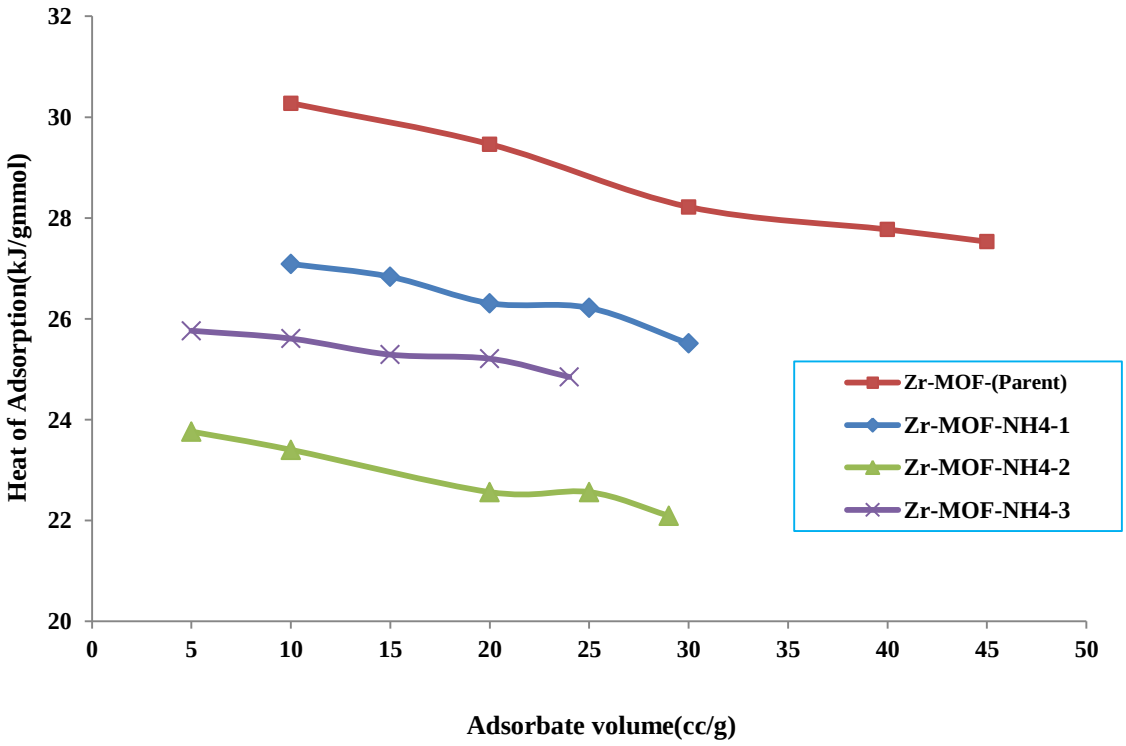

Figure: 4.8 Variation heat of adsorption for carbon dioxide on NH_4-modified Zr-MOFs as well as Zr-MOF-(Parent)

4.3.6.2 Adsorption at High Pressure

The adsorption at high pressure up to 1000 kPa on Zr-MOF-NH_4-2 showed high adsorption than Zr-MOF-(Parent) at the pressure more than 500 kPa (8.63 mmol/g at about 987 kPa) (Figure 4.9). This can be interpreted relying on the largest pore size which can be seen with Zr-MOF-NH_4-2. It agrees with that the smallest pores are filled by CO_2 at the lowest pressures, and then gradually, the large pores can be filled at higher pressure (30).

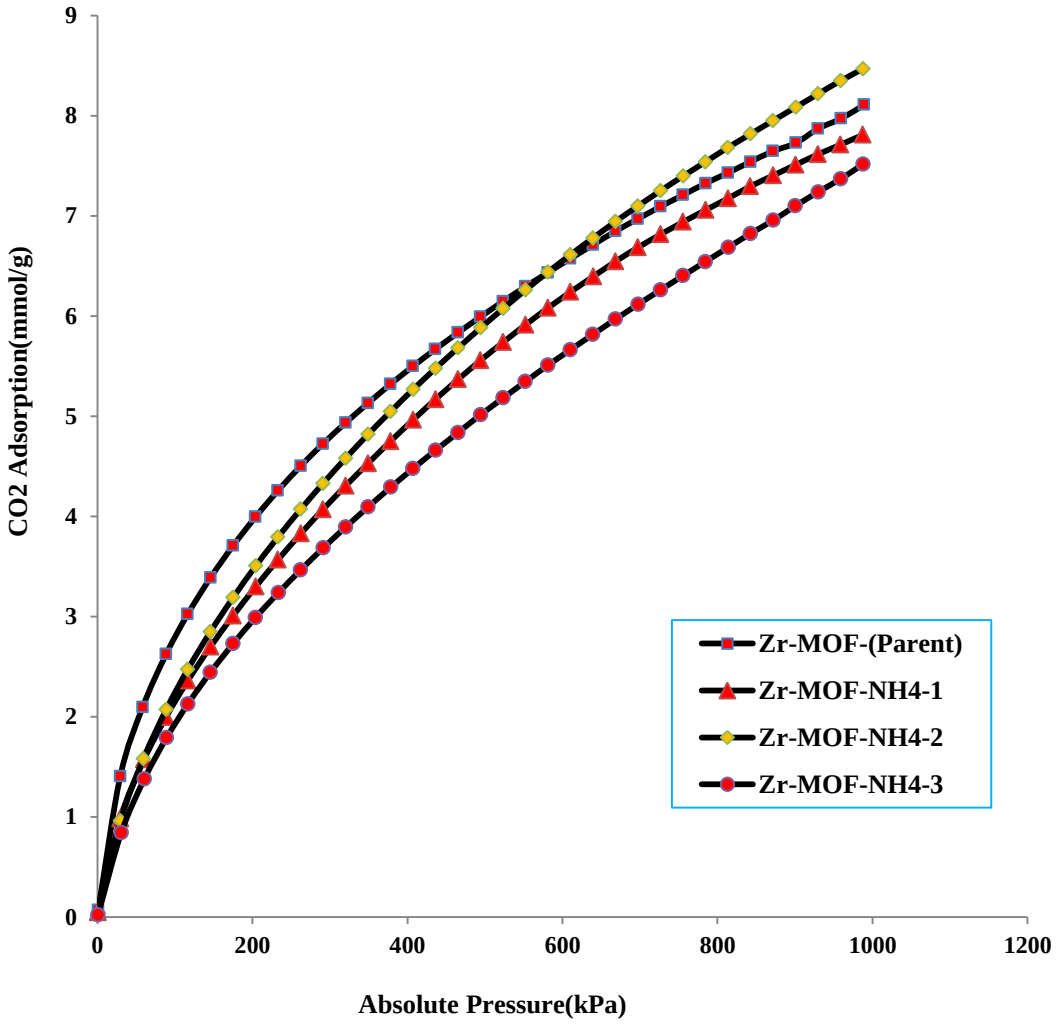

Figure: 4.9 CO_2 Adsorption at 273K and high pressure on Zr-MOFs

4.3.6.3 CH_4 Adsorption and Selectivity

Figure 4.10 shows that methane was adsorbed in different capacities on Zr-MOF-(Parent) and ammonium modified Zr-MOFs. Zr-MOF (Parent) exposed 3.44 mmol/g, and higher adsorption capacity than modified samples, while Zr-MOF-NH_4-2 displays the highest methane storage amongst the NH_4-modified samples. They are 3.09, 2.79, 2.43 mmol/g at 273K and 906 kPa for Zr-MOF-NH_4-2, Zr-MOF-NH_4-1 and Zr-MOF-NH_4-3. The selectivity of CO_2 over CH_4 by static adsorption at pressure ranging from 60 till 905 kPa is shown in Figure 4.11. It demonstrates that Zr-MOF-(Parent) has the lowest of separation power, whereas, Zr-MOF-NH_4-3 and Zr-MOF-NH_4-1 display the best separation factor for carbon dioxide over methane. It seems that CO_2 can separate significantly at pressure lower than 200 kPa. The high selectivity in the modified samples may be attributed to low abundance of small cages in these materials.

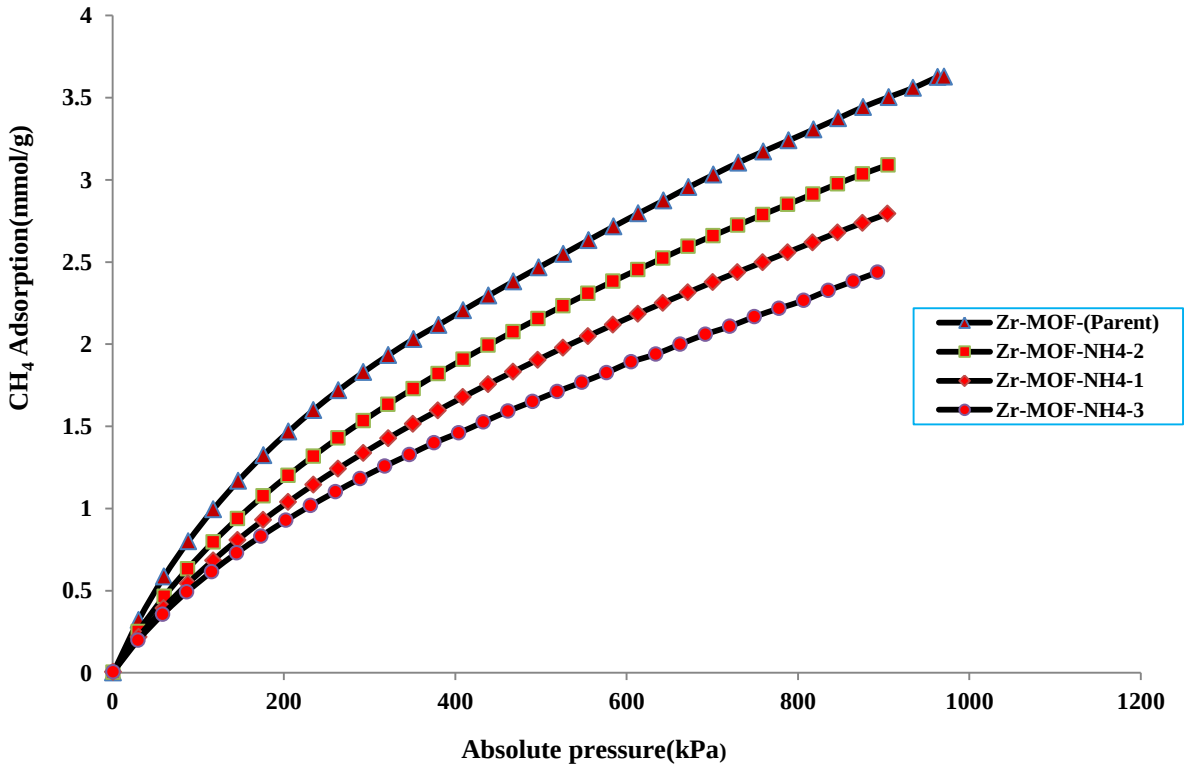

Figure: 4.10 Adsorption of CH_4 on Zr-MOFs at 273K and high pressure

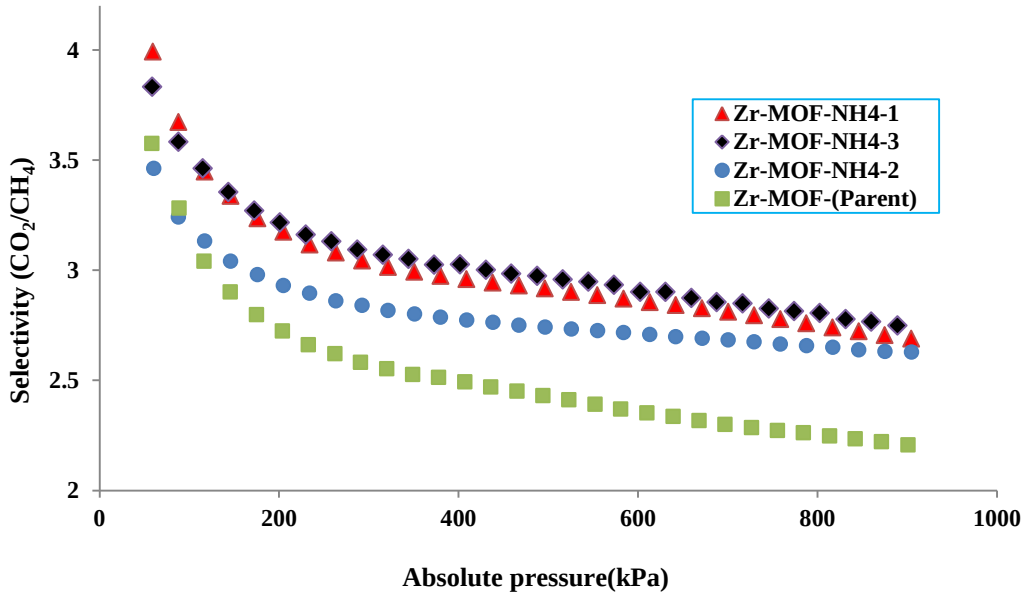

Figure: 4.11 Selectivity of CO_2/CH_4 on Zr-MOFs

4.4 Conclusion

In this chapter a new method to extend the pore volume in Zr-MOF was emerged by using ammonium hydroxide as an additive in the synthesis process. The characteristics of modified samples were changed depending on the amount of additive except the thermal stability which maintained the same as Zr-MOF. Although the BET surface area reduced in modified samples and the adsorption capacity was lower at STP, the adsorption capacity of carbon dioxide on Zr-MOF-NH_4-2 enhanced with increasing pressure over than 6 bars. Furthermore, the heat of adsorption reduced with increasing pore volume as represented by Zr-MOF-NH_4-2. These samples were tested for methane adsorption, Zr-MOF (Parent) displayed the highest methane adsorption and Zr-MOH-NH_4-3 was the lowest. However, because the selectivity of CO_2 over other gases depended on the characteristics of crystalline materials, the selectivity of CO_2 over CH_4 may be developed on modified samples. Hence, Zr-MOF-NH_4-1 and Or-MOF-NH_4-3 exposed the best selectivity.

4.5 References

1. Snurr RQ, Hupp JT, Nguyen ST. Prospects for nanoporous metal-organic materials in advanced separations processes. AIChE Journal. 2004;50(6):1090-5.

2. James SL. Metal-organic frameworks. Chemical Society Reviews. 2003;32(5):276-88.

3. Eddaoudi M, Li H, Yaghi OM. Highly Porous and Stable Metal−Organic Frameworks: Structure Design and Sorption Properties. Journal of the American Chemical Society. 2000;122(7):1391-7.

4. Millange F, Guillou N, Walton RI, Greneche J-M, Margiolaki I, Ferey G. Effect of the nature of the metal on the breathing steps in MOFs with dynamic frameworks. Chemical Communications. 2008(39):4732-4.

5. Preparation and characterization of ordered porous carbons for increasing hydrogen storage behaviors. Journal of Solid State Chemistry.

6. Eddaoudi M, Moler DB, Li H, Chen B, Reineke TM, O'Keeffe M, et al. Modular Chemistry: Secondary Building Units as a Basis for the Design of Highly Porous and Robust Metal−Organic Carboxylate Frameworks. Accounts of Chemical Research. 2001;34(4):319-30.

7. Eddaoudi M, Kim J, Rosi N, Vodak D, Wachter J, O'Keeffe M, et al. Systematic Design of Pore Size and Functionality in Isoreticular MOFs and Their Application in Methane Storage. Science. 2002;295(5554):469-72.

8. Gascon J, Aktay U, Hernandez-Alonso MD, van Klink GPM, Kapteijn F. Amino-based metal-organic frameworks as stable, highly active basic catalysts. Journal of Catalysis. 2009;261(1):75-87.

9. Vermoortele F, Ameloot R, Vimont A, Serre C, De Vos D. An amino-modified Zr-terephthalate metal-organic framework as an acid-base catalyst for cross-aldol condensation. Chemical Communications.47(5):1521-3.

10. Custelcean R, Gorbunova MG. A Metal- Organic Framework Functionalized with Free Carboxylic Acid Sites and Its Selective Binding of a Cl(H2O)4- Cluster. Journal of the American Chemical Society. 2005;127(47):16362-3.

11. Schaate A, Roy P, Godt A, Lippke J, Waltz F, Wiebcke M, et al. Modulated Synthesis of Zr-Based Metal–Organic Frameworks: From Nano to Single Crystals. Chemistry – A European Journal. 2011;17(24):6643-51.

12. Gadzikwa T, Farha OK, Mulfort KL, Hupp JT, Nguyen ST. A Zn-based, pillared paddlewheel MOF containing free carboxylic acids via covalent post-synthesis elaboration. Chemical Communications. 2009(25):3720-2.

13. Millward AR, Yaghi OM. Metal- Organic Frameworks with Exceptionally High Capacity for Storage of Carbon Dioxide at Room Temperature. Journal of the American Chemical Society. 2005;127(51):17998-9.

14. Britt D, Furukawa H, Wang B, Glover TG, Yaghi OM. Highly efficient separation of carbon dioxide by a metal-organic framework replete with open metal sites. Proceedings of the National Academy of Sciences. 2009;106(49):20637-40.

15. Bae Y-S, Farha OK, Hupp JT, Snurr RQ. Enhancement of CO2/N2 selectivity in a metal-organic framework by cavity modification. Journal of Materials Chemistry. 2009;19(15):2131-4.

16. An J, Rosi NL. Tuning MOF CO2 Adsorption Properties via Cation Exchange. Journal of the American Chemical Society. 2010;132(16):5578-9.

17. Wu H, Reali RS, Smith DA, Trachtenberg MC, Li J. Highly Selective CO2 Capture by a Flexible Microporous Metal–Organic Framework (MMOF) Material. Chemistry – A European Journal. 2010;16(47):13951-4.

18. Park HJ, Suh MP. Mixed-Ligand Metal–Organic Frameworks with Large Pores: Gas Sorption Properties and Single-Crystal-to-Single-Crystal Transformation on Guest Exchange. Chemistry – A European Journal. 2008;14(29):8812-21.

19. Cavka JH, Jakobsen S, Olsbye U, Guillou N, Lamberti C, Bordiga S, et al. A New Zirconium Inorganic Building Brick Forming Metal Organic Frameworks with Exceptional Stability. Journal of the American Chemical Society. 2008;130(42):13850-1.

20. Kandiah M, Usseglio S, Svelle S, Olsbye U, Lillerud KP, Tilset M. Post-synthetic modification of the metal-organic framework compound UiO-66. Journal of Materials Chemistry. 2010;20(44):9848-51.

21. Kandiah M, Nilsen MH, Usseglio S, Jakobsen Sr, Olsbye U, Tilset M, et al. Synthesis and Stability of Tagged UiO-66 Zr-MOFs. Chemistry of Materials. 2010;22(24):6632-40.

22. Gomes Silva C, Luz I, Llabrés i Xamena FX, Corma A, García H. Water Stable Zr–Benzenedicarboxylate Metal–Organic Frameworks as Photocatalysts for Hydrogen Generation. Chemistry – A European Journal. 2010;16(36):11133-8.

23. Vermoortele F, Ameloot R, Vimont A, Serre C, De Vos D. An amino-modified Zr-terephthalate metal-organic framework as an acid-base catalyst for cross-aldol condensation. Chemical Communications. 2011;47(5):1521-3.

24. Braun ME, Steffek CD, Kim J, Rasmussen PG, Yaghi OM. 1,4-Benzenedicarboxylate derivatives as links in the design of paddle-wheel units and metal-organic frameworks. Chemical Communications. 2001(24):2532-3.

25. Li H, Eddaoudi M, O'Keeffe M, Yaghi OM. Design and synthesis of an exceptionally stable and highly porous metal-organic framework. Nature. 1999;402(6759):276-9.

26. Sayari A, Yang Y, Kruk M, Jaroniec M. Expanding the Pore Size of MCM-41 Silicas: Use of Amines as Expanders in Direct Synthesis and Postsynthesis Procedures. The Journal of Physical Chemistry B. 1999;103(18):3651-8.

27. Wright PA. Microporous framework solids. Cambridge: Royal Society of Chemistry 2008.

28. Biemmi E, Bein T, Stock N. Synthesis and characterization of a new metal organic framework structure with a 2D porous system: $(H_2NEt_2)_2[Zn_3(BDC)_4]\cdot 3DEF$. Solid State Sciences. 2006;8(3-4):363-70.

29. Düren T, Millange F, Ferey Gr, Walton KS, Snurr RQ. Calculating Geometric Surface Areas as a Characterization Tool for Metalâˆ’Organic Frameworks. The Journal of Physical Chemistry C. 2007;111(42):15350-6.

30. Ravikovitch PI, Vishnyakov A, Russo R, Neimark AV. Unified Approach to Pore Size Characterization of Microporous Carbonaceous Materials from N2, Ar, and CO2 Adsorption Isotherms Langmuir. 2000;16(5):2311-20.

31. Himeno S. Characterization and selectivity for methane and carbon dioxide adsorption on the all-silica DD3R zeolite. Microporous and Mesoporous Materials. 2007;98(1-3):62.

32. Purewal JJ. Pore size distribution and supercritical hydrogen adsorption in activated carbon fibers. Nanotechnology. 2009;20(20):204012.

5

Chapter 5: Adsorption of CO2 on Amino-Zr-MOF

5

Adsorption of CO_2 on Amino-Zr-MOF

Abstract

In this chapter, we report amino functionalised Zr-MOF (amino-Zr-MOF) synthesis using 2-aminoterephthalic acid as an organic linker. This chapter aims to use amino-functional group on the structure to enhance the CO_2 adsorption capacity. This material was activated by methanol, which was very effective. However, this material was very sensitive to heating over 573 K. Experimentally, all physicochemical properties of the material were characterised by XRD, SEM, TGA, FTIR and N_2 adsorption to understand its crystalline structure, morphological description, thermal stability, and porous structure, respectively.

It was found that the topology of this material was similar to Zr-MOF while its morphology was different. However, it was thermally stable up to 623 K; lower than Zr-MOF (753 K). Furthermore, amino functional groups were detected by FTIR at 3394 and 3480 cm^{-1}. BET surface area was 1220 m^2/g.

Amino-Zr-MOF was tested for adsorption at standard and high pressure, CO_2 adsorption isotherm was achieved at 1 atm and different temperatures. The adsorption capacity was 100 (4.46) and 64 (2.86) cc/g (mmol/g) at 273 and 296 K, respectively. In addition, CO_2 and CH_4 adsorption at high pressure was also obtained to calculate the separation factor for carbon dioxide over methane of this material. CO_2 adsorption capacity on amino-Zr-MOF was 9 mmol/g at 988 kPa, 273K while CH_4 adsorption capacity was 3.7 mmol/g at 900 kPa and 273 K. The heat of CO_2 adsorption on amino-Zr-MOF was calculated to be 29.4 kJ/mol.

5.1 Introduction

Metal organic frameworks (MOFs) as new emerging porous materials have been investigated to be alternative adsorbents for various industrial and environmental applications (1, 2). The applications of MOFs have covered several areas including gas purification and separation (3), gas storage(4), drug delivery (5) and catalysis (6, 7) etc. Unprecedentedly, MOFs have many characteristics such as ability to be designed with required specifications, high rigidity and flexibility to be functionalised, and exceptional low density (8). The synthesis of MOFs can result in a robust extended framework with permanent porosity and these porosities may be fulfilled when the molecular building nets are connected by strong bonds (9, 10). Previously, some transition metals have been used in the synthesis of MOFs, but priority is given to Zn and Al (1, 11). These new materials can be functionalised via an organic linker, therefore, they can be modified for suitable applications by using functional groups (3, 12). It was noted that the presence of amino groups as functional groups in porous materials is very selective improvement to enhance their affinity to adsorb and separate CO_2. Hence, using of aminoterephthalates as linkers in MOF synthesis can enhance the performance of MOFs to capture carbon dioxide (13-15).

Particularly, amino-BDC has been used as a linker in IRMOF-3 to increase the ability to capture gases (16, 17). In addition, amino-MIL-53 was synthesised and used in different applications. It was proved that postsynthesis modification can succeed with the presence of an amino-functional group on the linker in direct synthesis (18, 19).

Zirconium oxide (ZrO_2) has stable properties and the nature of zirconium atom connection with oxygen (20) makes it attractive in synthesis of MOFs. Moreover, it was observed that the synthesis of organic ligand of this framework could be controlled to get several Zr-MOFs (UiO-66) (21). Modification and application of Zr-MOFs have been also reported. Recently, Kandish et al. (22) synthesised Zr-MOF (UiO-66) with different functional groups by using different linker ligands, H_2N-H_2BDC(Figure 5.1), O_2N-H_2BDC, and Br-H_2BDC. Silva et al. (23) used both UiO-66 and UiO-66-NH_2 as photocatalysts for hydrogen generation while Vermoortele et al.(24) selected amino-UiO-66 for the cross-aldol condensation.

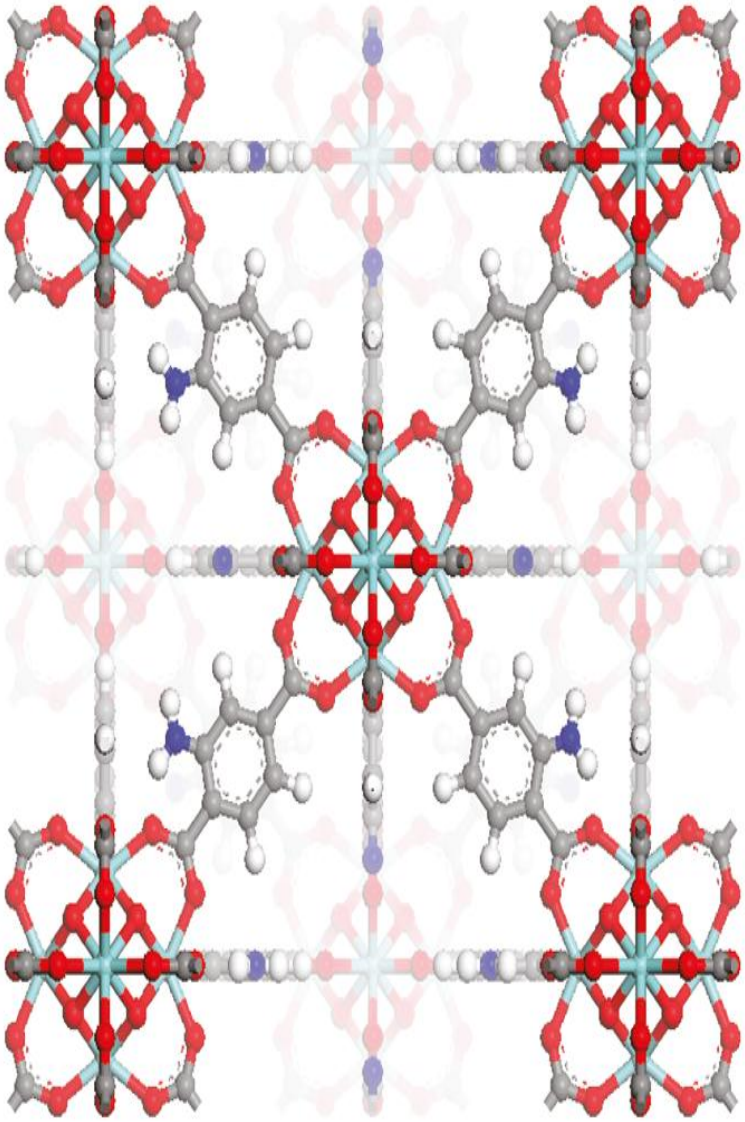

Figure: 5.1 Description of amino-Zr-MOF structure (22)

These researchers used different procedures and molar ratios in the synthesis of amino-modified Zr-MOF. However, few investigations have been reported in Zr-MOF application for CH_4 and CO_2 adsorption.

In this chapter, an amino-Zr-MOF was reported to be synthesised using a different precursor ratio and activation process. Characteristics of this material were obtained

and then tested for CO_2 adsorption at low and high pressure. Methane adsorption capacity was determined at high pressures to investigate the selectivity of CO_2 over methane.

5.2 Experimental

5.2.1 Chemicals

All chemicals including 2-amino-terephthalic acids (NH_2-BDC, 99%), zirconium chloride ($ZrCl_4$, 99.9%), dimethylformamide (DMF, 98%), methanol (CH_3OH, 99%) were supplied by Sigma-Aldrich and used without further purification.

5.2.2 Synthesis and activation

In a typical procedure to synthesise amino-Zr-MOF, 1.47 g (6.31 mmol) $ZrCl_4$ were dissolved in 15 mL DMF solution and stirring for around 20 min. Meanwhile, 1.06 g (5.85 mmol) NH_2-BDC were dissolved in 68 mL DMF solution and stirring for 30 min. Then, the two prepared solutions were mixed and placed in an autoclave of 125 mL. The sealed autoclave was then placed in an oven at 120 °C for 48 h. Finally, the greenish yellow crystalline product was extracted from the solution by vacuum filtration.

The crystalline product was activated by immersing in methanol for 5 d, and then it was filtered, dried and heated under vacuum at 473 or 573 K for 12 h.

5.2.3 Characterisations

X-ray powder diffraction patterns were recorded on a X-ray diffractometer (D8 Advanced BrukerAxs) with a transmission mode using Cu$K\alpha$ radiation (wavelength=1.54 Å) at low angle range of 2θ = 5-70° to evaluate the stability of the crystalline structure.

Morphology of materials including the shape and the size of crystals was determined by a SEM (Zeiss NEON 40 EsBCrossBeam) with high resolutions.

A Perkin-Elmer 100-FT-IR Spectrometer was used to investigate functional groups on a crystalline structure or inside the pores. Scan range was from 650 to 4000 cm^{-1} with resolution of 4 cm^{-1} using a Universal ATR-Diamond/ZnSe as IR Accessory.

N_2 physisorption measurements were done on a Quantachrome instrument (Autosorb-1) at 77K and standard pressure. The surface area was obtained by the BET method and pore size distribution was determined by the BJH, and DA methods. It is essential that, the degassing should be set very well at a suitable temperature. In more details, around 15 mg of the sample was degassed at 473K under vacuum for 6 h. After that, the pores were opened and the net weight was used in adsorption/desorption measurement at 77K in the analysis port on the same instrument.

Thermal stability of the crystalline structure was checked by a TGA instrument (TGA/DSC1 STAR^e system, METTLER-TOLEDO). Also, it can investigate performance of activation process. Practically, a sample of 10 mg was loaded into an alumina pan of 150 µL and placed automatically in the TGA furnace to heat at a heating rate of 10 K/min from 308 up to 1173K in an inert medium of 20 mL/min Argon gas.

5.2.4 Adsorption Study

A static volumetric technique with an apparatus of Micromeritics (Gemini I-2360) was used to determine adsorption isotherm of CO_2 (99.995%) at 273 and 296 K under pressure up to 100 kPa.

Firstly, about 0.3 g of amino-Zr-MOF was weighed in a tube and then degassed by Vacprep 061 overnight at 473 K under vacuum. The net weight of the sample after degassing process was used in analysis port of Gemini I-2360. Carbon dioxide heat of adsorption was calculated from the Clausius-Claperyron equation replying on the data of adsorption isotherms which were measured at different temperatures by Gemini I-2360 at 100 kPa.

A Micromeritics-ASAP2050 was used to measure the adsorption isotherms of carbon dioxide (99.995%) and methane (99.995%) at high pressure up to 1000 kPa.

First, a sample was degassed on the same instrument by increasing the temperature at a heating rate of 10 K/min till 373 K to hold at this temperature for 2 h then increasing the temperature again at the same heating rate to 473K under vacuum (up to 0.4 kPa) to hold at these conditions for 8 h.

Finally, an obtained net weight after degassing was used in the analysis at 273 K.

5.3 **Results and discussion**

5.3.1 Topology Description

XRD patterns of amino-Zr-MOFs are illustrated in Figure: 5.2. The profiles of the as-synthesised amino-Zr-MOF and amino-Zr-MOF activated at 473 K were the same, similar to Zr-MOF pattern. However, the XRD of sample after activation at 573K was totally different. The XRD profile presented a broad peak at 2θ =7.5°, and most peaks were disappeared suggesting amorphous structure due to the collapse of crystalline structure.

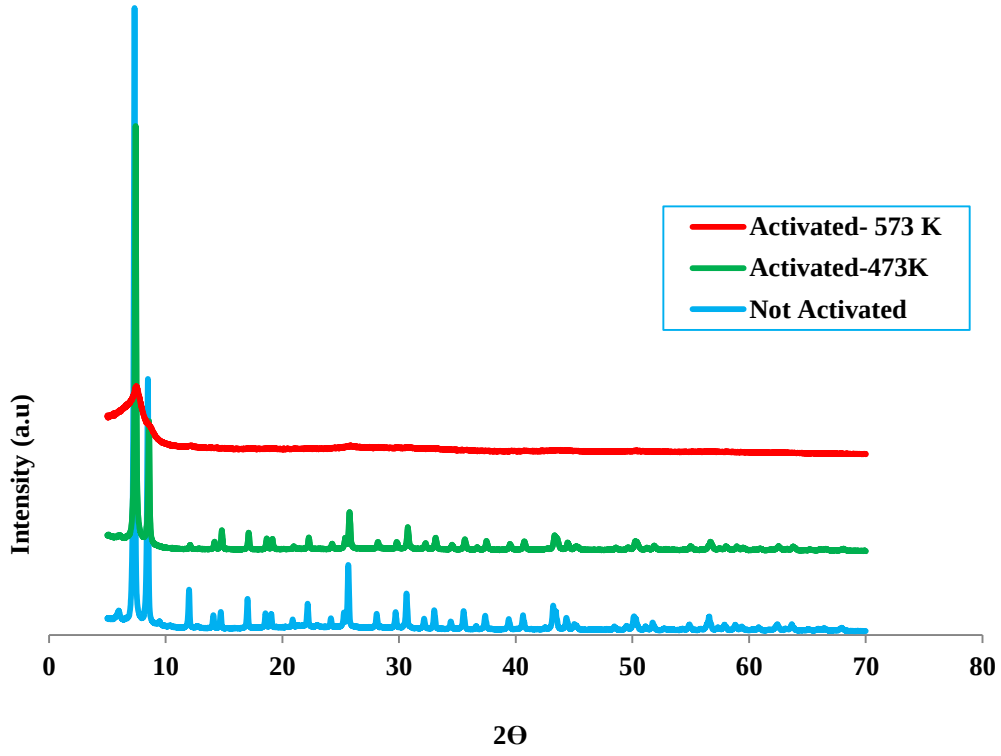

Figure: 5.2 XRD Patterns for Amino-Zr-MOF before and after activation

5.3.2 Morphological Description

Figure 5.3 shows SEM photo of amino-Zr-MOF. As seen, amino-Zr-MOF presented as symmetrical crystals with triangular base-pyramid shape.

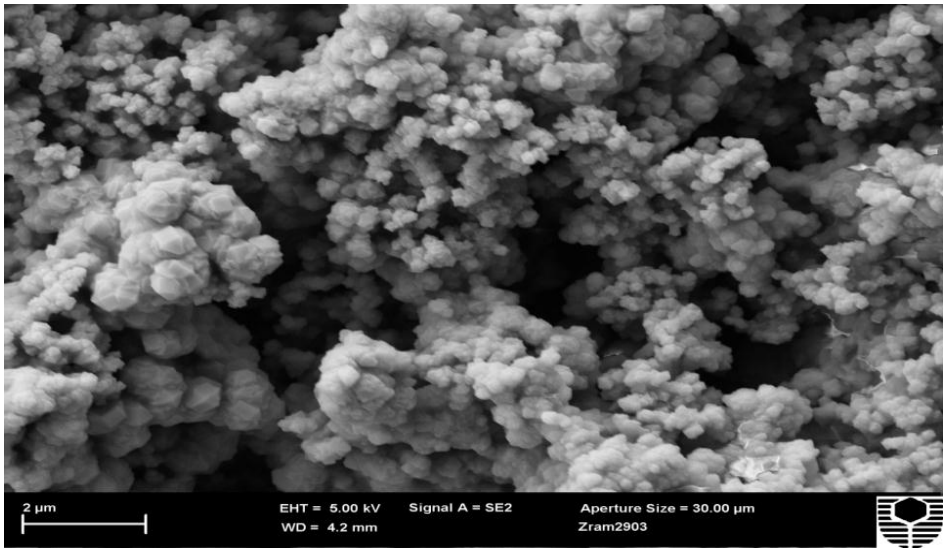

Figure: 5. 3 SEM Image for Amino-Zr-MOF, activated-473K

5.3.3 Functional group determination

FTIR spectra of amino-Zr-MOF as-synthesised and activated by methanol and heating at varying temperatures were found to have carboxyl functional group and amino functional group as well. It was shown in Figure 5.4-(a) some peaks within the bands of 1400-1767 cm^{-1} which were referred to carboxylic functional groups (25); On as-synthesised material spectrum, carboxyl group from free aromatic carboxylic acid was observed at 1656 cm^{-1}(26). It was removed after activation as shown on the spectra of materials after activation, which showed the removal of non-coordinated BDC and DMF molecules from the pores. It was observed, on the spectra of as-synthesized and activated at 473K in Figure 5.4(a), the bands of 1430-1533 cm^{-1} indicating the presence of amino-carboxylate compounds that were coordinated with zirconium metal centre by $–CO_2$ asymmetrical stretching at the peaks in 1497 cm^{-1} and 1564 cm^{-1} as well as $–CO_2$ symmetrical stretching at the peaks 1424 and 1385 cm^{-1}(25, 27, 28). The amino-groups can obviously be recognised on the spectrum after activation. More specifically, from magnification part of the spectrum of as-synthesized amino-Zr-MOF, Figure 5.4 (b), two peaks with much low intensities appearing at 3466 and 3377 cm^{-1} were related to primary amines- NH_2 on the organic linker. Low intensities of these peaks may be attributed

to the strong bonding between the amino groups on the coordinated acid with both of amino groups of free NH_2-BDC inside the pores and bridging OH group on the metal centre(19, 29). Whereas, after activation, primary amines, -NH_2 on the organic linker can be easily seen at 3394 and 3480 cm^{-1} while the bridging OH group can be seen at 3675 cm^{-1} (28) as shown in magnification part on spectrum of activated material (Figure 5.4 (b)). It was observed that a small shifting in the position of amino-groups stretching on the spectra before and after the activation process. Explanation of this phenomenon may be that, amino group of organic linker was affected by moisture content from the surroundings and other functional groups inside the pores before activation.

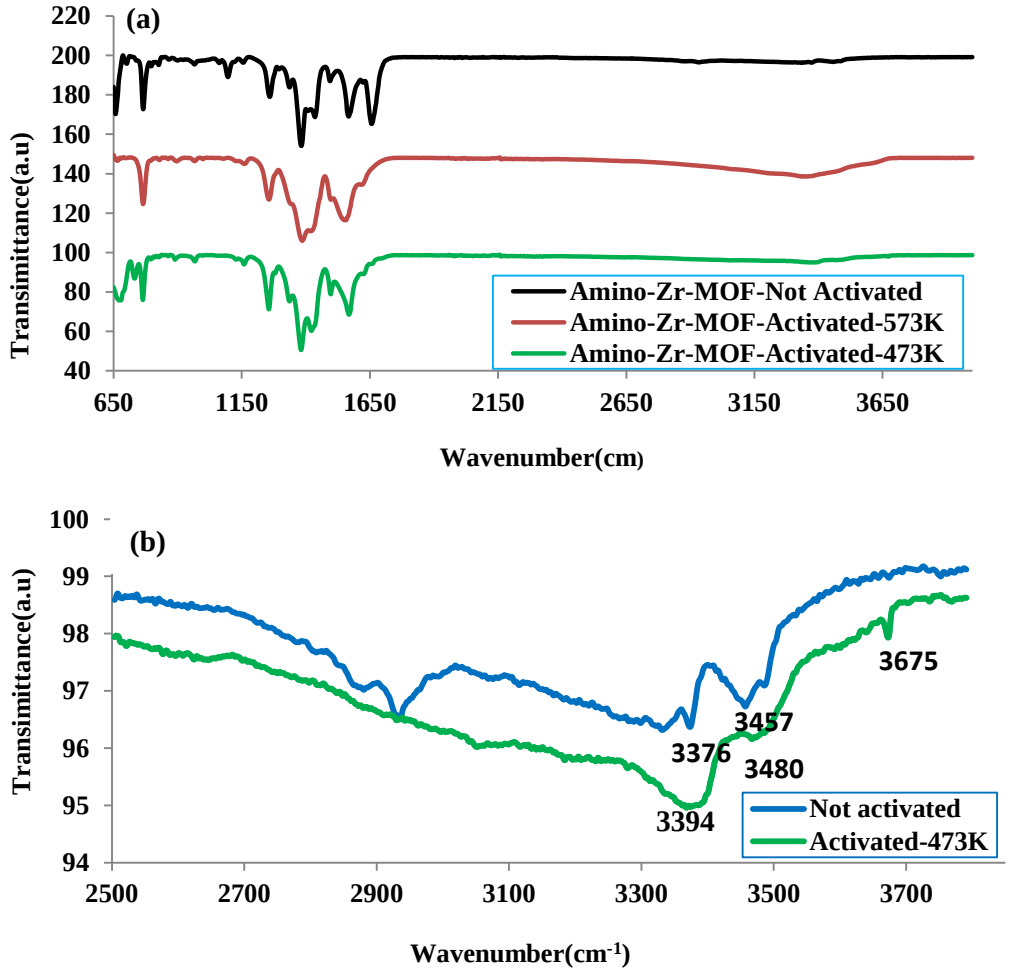

Figure: 5.4(a) - FTIR spectra for amino-Zr-MOF before and after activation (b)- magnification parts for amino-functional groups area in activated and unactivated amino-Zr-MOF

From the spectrum of amino-Zr-MOF after heating at 573 K, it was found that the intensities of peaks at 1564, 1497, 1424 and 1384 cm^{-1} were reduced. Also, the width of the band 1479-1785 cm^{-1} was reduced; this may be an indicator of the structure collapse because these peaks are related to coordinating of organic linkers with metal centres. It means this linkage was broken if heating over 573 K.

5.3.4 Nitrogen Isotherm and Pore Size Distribution

The nitrogen isotherms of activated amino-Zr-MOFs displays the difference in surface area and pore size distributions as presented in Figure 5.5 and Figure 5.6 (a,b) respectively. It can be seen that amino-Zr-MOF activated at 473 K presented a highly developed microporous structure with much higher N_2 adsorption than the sample after heating treatment at 573 K. The hysteresis in the isotherm was very distinct in the latter sample which may indicate the merge of small pores to large pores (mesopore) because in mesoporous materials, the movement of gas molecules can affect strongly by capillary condensation as well as attractive interaction between the gas molecules themselves(30). Also this hysteresis may be one of evidence to form random pore structure which can be enriched with many cavities to confine gas molecules and enhance the hysteresis (31).

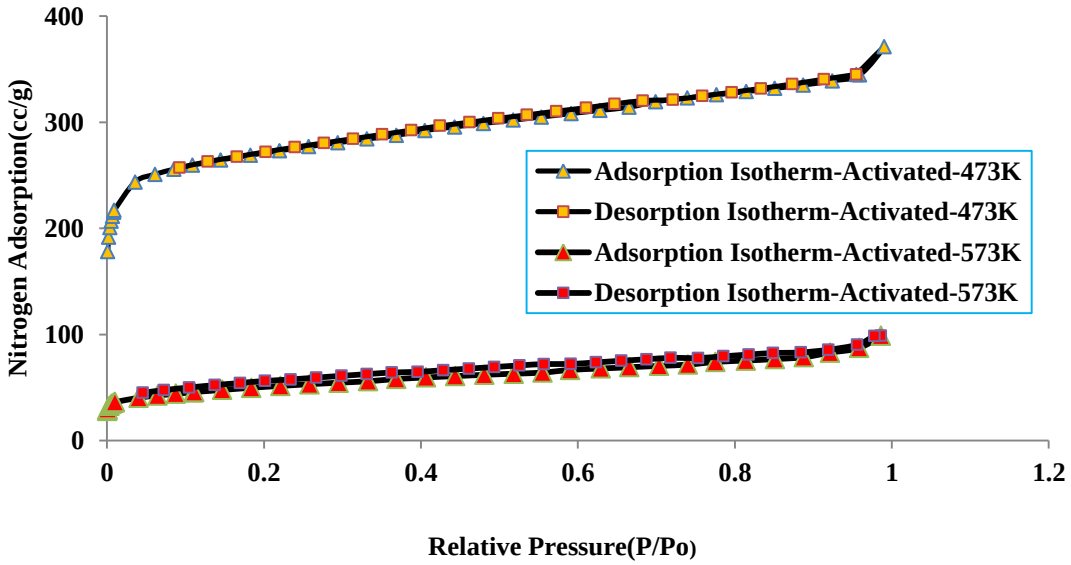

Figure: 5.5 Nitrogen adsorption/desorption for activated Amino-Zr-MOF at 473K and 573K respectively

The mesopore size distribution of amino-Zr-MOF activated at 473 K showed two peaks centred at 1.5 and 3.3 nm, respectively. However, amino-Zr-MOF activated at 573 K showed a shift of pore size to larger pore range. The two peaks were changed to 2.4 and 4.4 nm, respectively as shown in Figure 5.6 (a), while micropore was very limited with a very low volume as shown in Figure 5.6 (b) compared with activated material at 473 K.

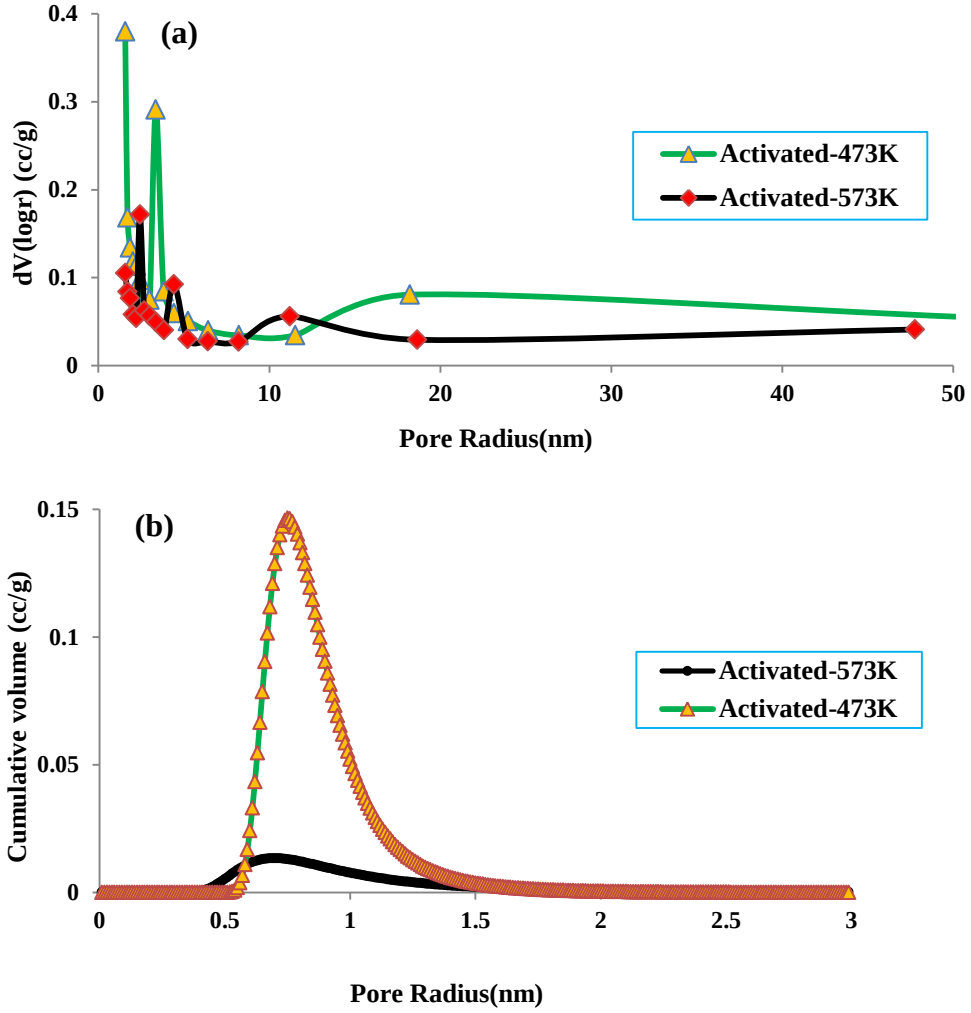

Figure: 5.6 Pore size distribution in (a) Mesopore and (b) Micropore structures

The BET surface area of amino-Zr-MOF activated at 473 K was 1220 m^2/g while the Langmuir surface area was 1395 m^2/g. The average pore radius was 0.99 nm and the total pore volume was 0.611 cm^3/g. The surface area of this sample is similar to the

result reported by Zlotea et al. (32). However, the BET surface area of the sample activated at 573 K was significantly reduced to 180 m^2/g, which reflects the destruction of porous structure. A comparison of amino-Zr-MOF with other MOFs shows that amino-Zr-MOF still has high porosity (Table 5.1). The above results suggested that activation of as-synthesised amino-Zr-MOF could be only done below 573 K. It was found that above 573 K, the crystalline structure of amino-Zr-MOF could be destroyed to produce amorphous phase.

Table 5.1: BET surface area of different amino functionalized metal organic frameworks.

Sample	**$S_{BET}(m^2/g)$**	**Reference**
MIL-125(Ti)	1130	(32)
UiO-66(Zr)-NH_2	1206(1280)	(32)
IRMOF-3 DEF	3683	(12)
Amino-MIL-53(Al)	675	(12)
Amino-MIL-101(Al)	2100	(33)
Amino-Zr-MOF	1220	This work

5.3. 5 Thermal analyses

TGA profiles of amino-Zr-MOF can confirm that the structure of amino-Zr-MOF collapsed at heating higher than 573K, which means it has lower thermal stability than Zr-MOF as demonstrated in Figure 5.7. From Figure 5.8, there is a weight loss occurred at around 623 K on amino-Zr-MOF curve, which was not displayed on the Zr-MOF. This loss belongs to the presence of NH_2 as functional groups inside the pores making new connection between the functional groups and oxygen of metal centre inside the pores. Meanwhile, the weight loss profile of amino-Zr-MOF treated at 473K showed two weight loss processes at 623 K – 823 K, suggesting the presence of the interconnection binding. By breaking this interconnection, the whole structure of amino-Zr-MOF collapsed and most pores were blocked. In a previous report, such a weight loss was not found (22), which may be due to using a different activation process. In more details, it seems that non-coordinated BDC and DMF molecules consist of about 22 wt% while the coordinated and interconnected BDC represents by about 19 wt%. On the same figure, thermal analysis curve for the sample activated at 473 K shows the whole amount of non-coordinated materials was discarded from the pores at 550 K. On the other hand, the interconnection was impossible to be broken with the structure intact even it was observed from the curve for activated at 573 K that the coordinated BDC molecules are still linked.

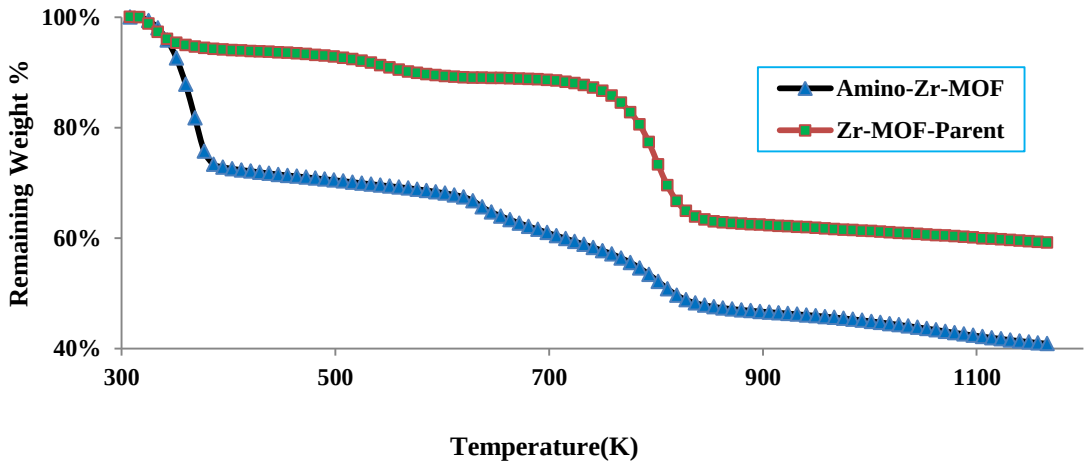

Figure: 5.7 Comparative view for thermal behaviour between amino-Zr-MOF and Zr-MOF after activation

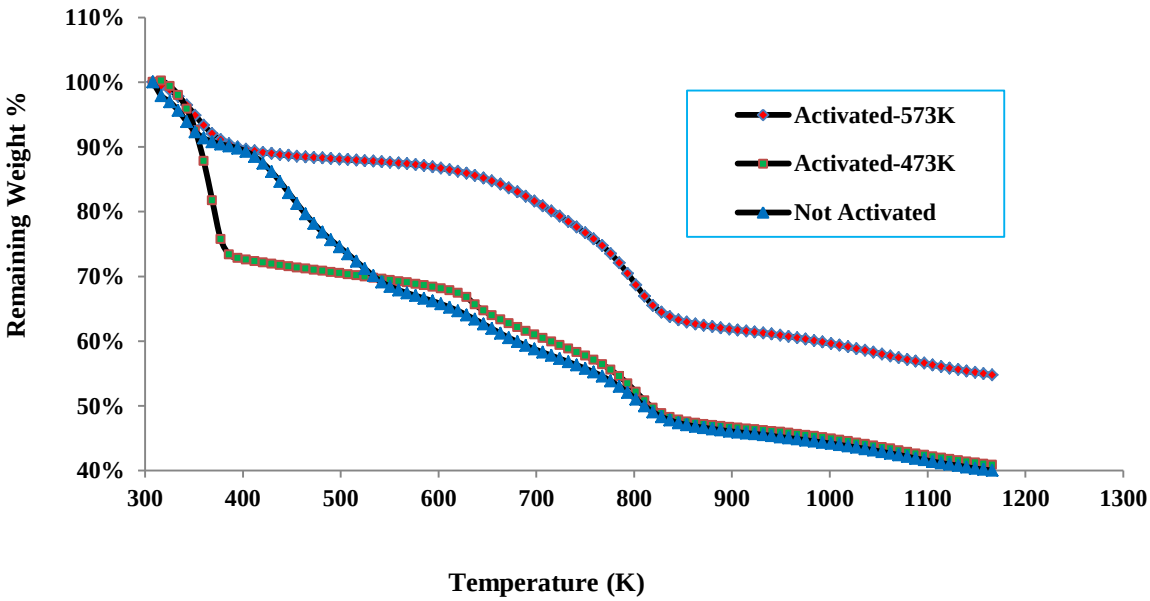

Figure: 5.8 Thermal analysis for amino-Zr-MOF

5.3.6 CO_2 Adsorption

5.3.6.1 Adsorption at 1 atm

Figure 5.9 displays CO_2 adsorption isotherms on amino-Zr-MOF at 273 K and 296 K. Amino-Zr-MOF showed good adsorption of CO_2 and the capacity depended on temperature. At 1 atm, 273 K, CO_2 adsorption could reach 4.46 mmol/g, which is higher than that on Zr-MOF. This could be attributed to the presence of basic amino groups in porous structure. In addition, the adsorption of CO_2 at 296 K was reduced and the capacity was determined as 2.85 mmol/g. Heat of adsorption was calculated using the Clausius-Clapeyron equation (Eq.3.1) and an average value from different CO_2 coverage on amino-Zr-MOF was obtained as 29.4 kJ/mol. Table 5.2 presents the heat of CO_2 adsorption on various amino-functionalised MOFs. The value of amino-Zr-MOF is reasonable in comparison with other amino-functionalised MOFs (18). The relatively higher values of the heat of CO_2 adsorption is due to amino groups which could create an electric field inside the pores against more polarisable adsorbates (34).

Table 5.2: Heat of CO_2 adsorption on different amino-functionalised MOFs

Sample	CO_2 Heat of adsorption(kJ/mol)	Reference
IRMOF-3 DEF	20	(12)
Amino-MIL-53(Al)	38	(12)
Amino-MIL-101(Al)	28	(33)
Amino-Zr-MOF	29.3	This work

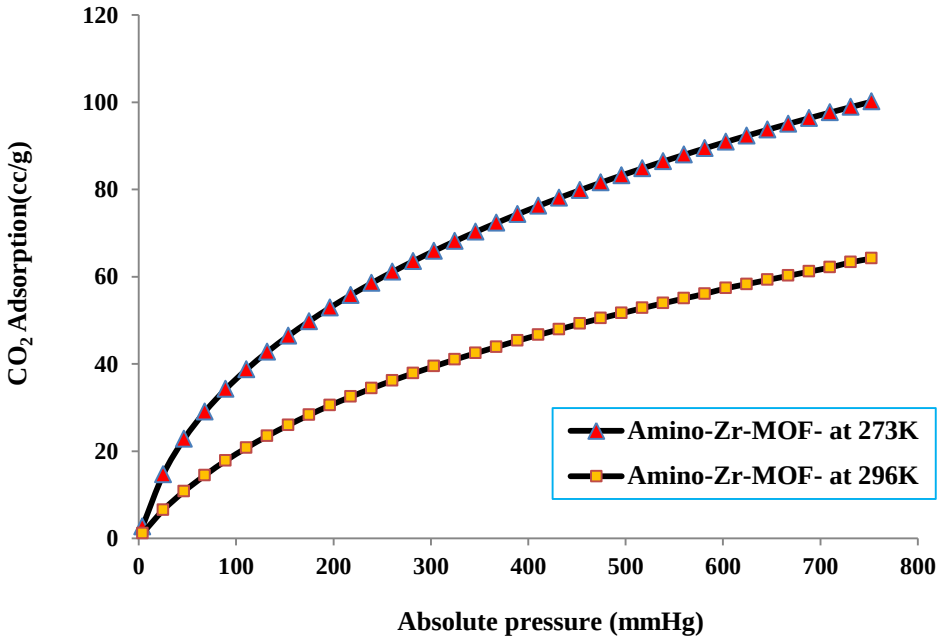

Figure: 5.9 Adsorption of CO_2 on Amino-Zr-MOF at different temperatures

5.3.6.2 Adsorption at High Pressure and Selectivity

It was known that the real capacity of adsorption on MOF cannot be gained at STP therefore adsorption capacity for CO_2 on amino-Zr-MOF was obtained at high pressure up to 980 kPa at 273 K as shown in Figure 5.10. Furthermore, CH_4 adsorption isotherm was also presented in Figure 5.11. As seen, CH_4 and CO_2 adsorption increased with increasing pressure but CO_2 adsorption was higher than CH_4, especially at low pressure less than 200 kPa. The adsorption values were 9.04 and 3.73 mmol/g for CO_2 (980 kPa, 273 K) and CH_4 (900 kPa, 273 K), respectively. This may be attributed to polar nature of gas molecules; CO_2 has quadrupolar moment (-1.4×10^{-35} C m^2) (35). In addition, amino-functional groups inside the pores creat basic environment with high affinity to adsorb acidic molecules such as CO_2. Whereas, CH_4 molecules are non-polar (36) and known as a weak acid.

The difference in adsorption capacities for CO_2 and CH_4 is very desirable in industrial application to increase the separation factor of CO_2 over CH_4. The selectivity of CO_2 to CH_4 was obtained based on the ratio of the equilibrium adsorption at varying pressures and is shown in Figure 5.12. It is seen that the selectivity of CO_2/CH_4 on amino-Zr-MOF decreased with increasing pressure and it ranged from 4.5 to 2.35 over the range of pressure between 0.3 and 9 atm, 273K. This material may be selected as very good separator at pressure lower than 200 kPa.

\

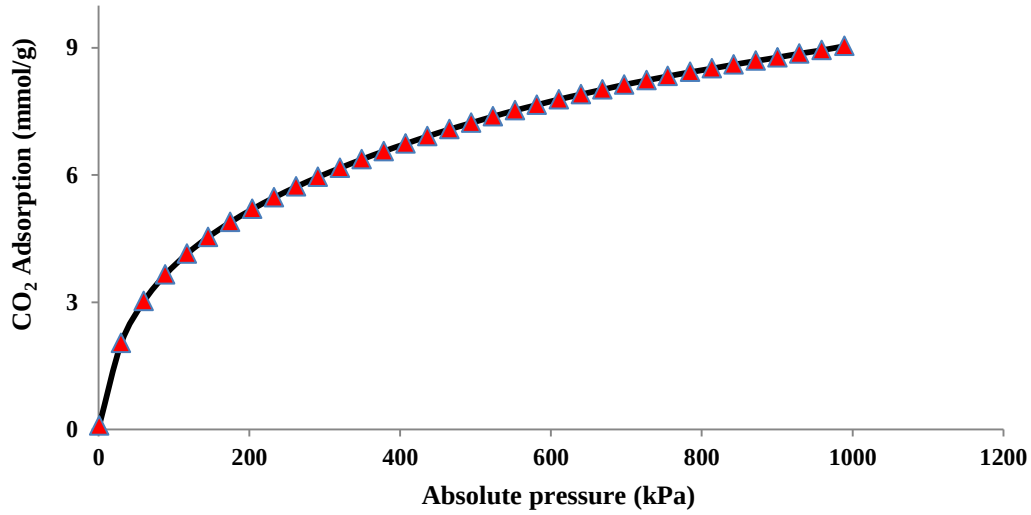

Figure: 5.10 Adsorption of CO_2 at high pressure

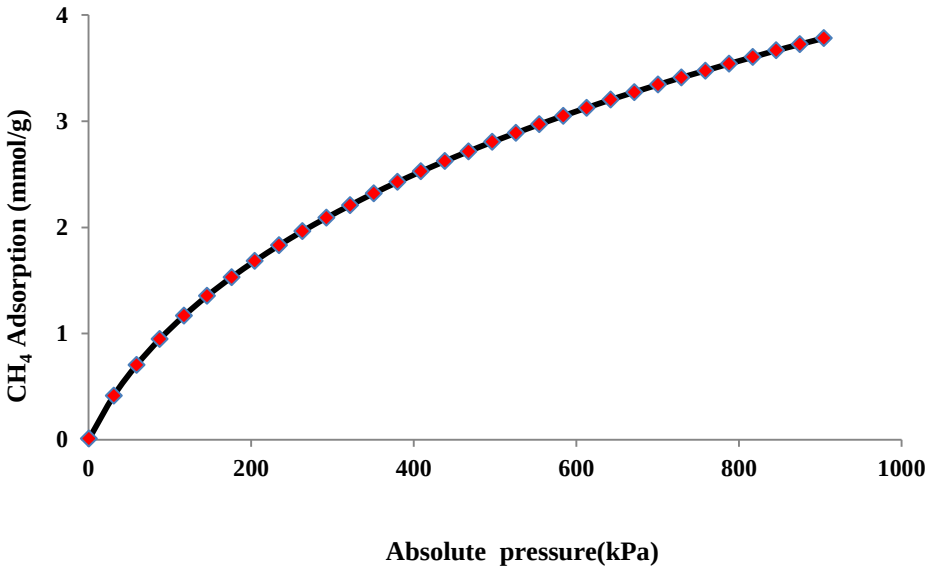

Figure: 5.11 Adsorption of CH_4 on Amino-Zr-MOF at high pressure

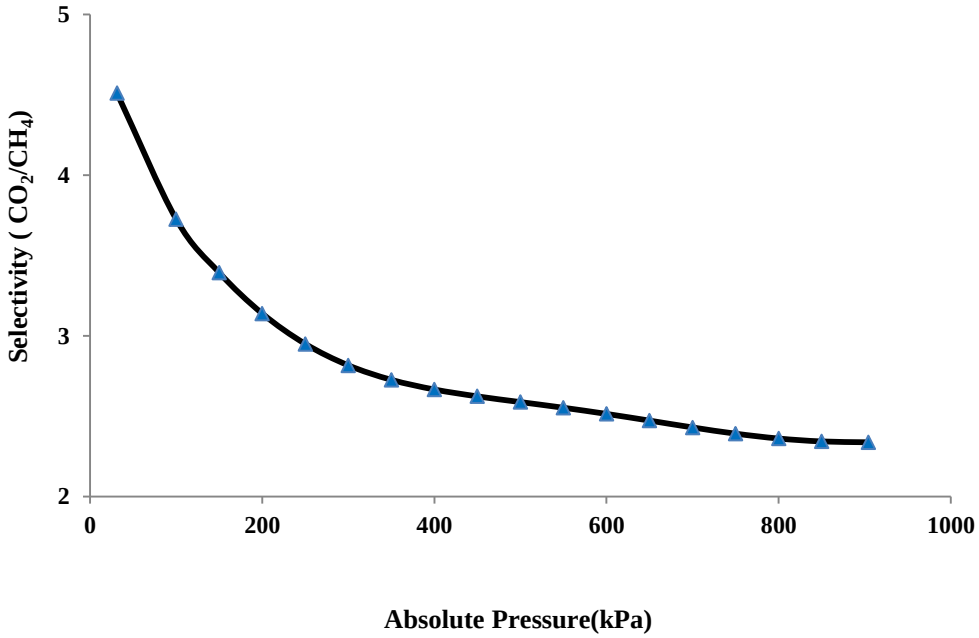

Figure: 5.12 Selectivity of CO_2 over CH_4 for static adsorption

5.4 Conclusion

This chapter shows modified synthesis procedure of amino-Zr-MOF and activation process by methanol treatment. The characterizations of this material were obtained and adsorption capacities at different temperature and pressure were measured as well. It was found that methanol is very affective solvent which can be used to enhance the surface area. Temperature is very important factor in activation procedure. Hence, porous structure of amino-Zr-MOF may be damaged with increasing temperature up to 573 K or more. Moreover, the whole structure was collapsed at 623 K; thermal stability lower than that of Zr-MOF.

CO_2 adsorption was investigated at STP and it was higher than that of Zr-MOF. CO_2 and CH_4 adsorption capacities were acquired at high pressure and 273 K, showing affinity of this material to adsorb CO_2 gas was stronger than CH_4, therefore, this material can be selected as a screener to select CO_2 over CH_4 gas. The CO_2/CH_4 selectivity decreased with increasing pressure.

5.5 References

1. Férey G, Mellot-Draznieks C, Serre C, Millange F. Crystallized Frameworks with Giant Pores: Are There Limits to the Possible? Accounts of Chemical Research. 2005;38(4):217-25.

2. Wolsky AM, Daniels EJ, Jody BJ. CO2 Capture from the flue gas of conventional fossil-fuel-fired power plants. Environmental Progress. 1994;13(3):214-9.

3. Mueller U, Schubert M, Teich F, Puetter H, Schierle-Arndt K, Pastre J. Metal-organic frameworks-prospective industrial applications. Journal of Materials Chemistry. 2006;16(7).

4. Gallo M, Glossman-Mitnik D. Fuel Gas Storage and Separations by Metal−Organic Frameworks: Simulated Adsorption Isotherms for H2 and CH4 and Their Equimolar Mixture. The Journal of Physical Chemistry C. 2009;113(16):6634-42.

5. Horcajada P, Serre C, Maurin G, Ramsahye NA, Balas F, Vallet-Regí Ma, et al. Flexible Porous Metal-Organic Frameworks for a Controlled Drug Delivery. Journal of the American Chemical Society. 2008;130(21):6774-80.

6. Chen B, Yang Y, Zapata F, Lin G, Qian G, Lobkovsky EB. Luminescent Open Metal Sites within a Metal–Organic Framework for Sensing Small Molecules. Advanced Materials. 2007;19(13):1693-6.

7. Rowsell JLC, Spencer EC, Eckert J, Howard JAK, Yaghi OM. Gas Adsorption Sites in a Large-Pore Metal-Organic Framework. Science. 2005;309(5739):1350-4.

8. Snurr RQ, Hupp JT, Nguyen ST. Prospects for nanoporous metal-organic materials in advanced separations processes. AIChE Journal. 2004;50(6):1090-5.

9. Wu C-D, Hu A, Zhang L, Lin W. A Homochiral Porous Metal−Organic Framework for Highly Enantioselective Heterogeneous Asymmetric Catalysis. Journal of the American Chemical Society. 2005;127(25):8940-1.

10. James SL. Metal-organic frameworks. Chemical Society Reviews. 2003;32(5).

11. Yaghi OM, O'Keeffe M, Ockwig NW, Chae HK, Eddaoudi M, Kim J. Reticular synthesis and the design of new materials. Nature. 2003;423(6941):705-14.

12. Gascon J, Aktay U, Hernandez-Alonso MD, van Klink GPM, Kapteijn F. Amino-based metal-organic frameworks as stable, highly active basic catalysts. Journal of Catalysis. 2009;261(1):75-87.

13. Vitillo JG, Savonnet M, Ricchiardi G, Bordiga S. Tailoring Metal–Organic Frameworks for CO2 Capture: The Amino Effect. ChemSusChem. 2011;4(9):1281-90.

14. Vogiatzis KD, Mavrandonakis A, Klopper W, Froudakis GE. Ab initio Study of the Interactions between CO2 and N-Containing Organic Heterocycles. ChemPhysChem. 2009;10(2):374-83.

15. Arstad B, Fjellvåg H, Kongshaug K, Swang O, Blom R. Amine functionalised metal organic frameworks (MOFs) as adsorbents for carbon dioxide. Adsorption. 2008;14(6):755-62.

16. Rowsell JLC, Yaghi OM. Effects of Functionalization, Catenation, and Variation of the Metal Oxide and Organic Linking Units on the Low-Pressure Hydrogen Adsorption Properties of Metal−Organic Frameworks. Journal of the American Chemical Society. 2006;128(4):1304-15.

17. Britt D, Tranchemontagne D, Yaghi OM. Metal-organic frameworks with high capacity and selectivity for harmful gases. Proceedings of the National Academy of Sciences. 2008;105(33):11623-7.

18. Couck S, Denayer JFM, Baron GV, Rémy T, Gascon J, Kapteijn F. An Amine-Functionalized MIL-53 Metal−Organic Framework with Large Separation Power for CO2 and CH4. Journal of the American Chemical Society. 2009;131(18):6326-7.

19. Ahnfeldt T, Gunzelmann D, Loiseau T, Hirsemann D, Senker Jr, Férey G, et al. Synthesis and Modification of a Functionalized 3D Open-Framework Structure with MIL-53 Topology. Inorganic Chemistry. 2009;48(7):3057-64.

20. Nawrocki J, Rigney M, McCormick A, Carr PW. Chemistry of zirconia and its use in chromatography. Journal of Chromatography A. 1993;657(2):229-82.

21. Cavka JH, Jakobsen S, Olsbye U, Guillou N, Lamberti C, Bordiga S, et al. A New Zirconium Inorganic Building Brick Forming Metal Organic Frameworks with Exceptional Stability. Journal of the American Chemical Society. 2008;130(42):13850-1.

22. Kandiah M, Nilsen MH, Usseglio S, Jakobsen S, Olsbye U, Tilset M, et al. Synthesis and Stability of Tagged UiO-66 Zr-MOFs. Chemistry of Materials. 2010;22(24):6632-40.

23. Gomes Silva C, Luz I, Llabrés i Xamena FX, Corma A, García H. Water Stable Zr–Benzenedicarboxylate Metal–Organic Frameworks as Photocatalysts for Hydrogen Generation. Chemistry – A European Journal. 2010;16(36):11133-8.

24. Vermoortele F, Ameloot R, Vimont A, Serre C, De Vos D. An amino-modified Zr-terephthalate metal-organic framework as an acid-base catalyst for cross-aldol condensation. Chemical Communications. 2011;47(5).

25. Loiseau T, Serre C, Huguenard C, Fink G, Taulelle F, Henry M, et al. A Rationale for the Large Breathing of the Porous Aluminum Terephthalate (MIL-53) Upon Hydration. Chemistry – A European Journal. 2004;10(6):1373-82.

26. Biemmi E, Bein T, Stock N. Synthesis and characterization of a new metal organic framework structure with a 2D porous system: (H2NEt2)2[Zn3(BDC)4]·3DEF. Solid State Sciences. 2006;8(3–4):363-70.

27. Bauer S, Serre C, Devic T, Horcajada P, Marrot Jrm, Férey Gr, et al. High-Throughput Assisted Rationalization of the Formation of Metal Organic Frameworks in the Iron(III) Aminoterephthalate Solvothermal System. Inorganic Chemistry. 2008;47(17):7568-76.

28. Grzesiak AL, Uribe FJ, Ockwig NW, Yaghi OM, Matzger AJ. Polymer-Induced Heteronucleation for the Discovery of New Extended Solids. Angewandte Chemie International Edition. 2006;45(16):2553-6.

29. Stavitski E, Pidko EA, Couck S, Remy T, Hensen EJM, Weckhuysen BM, et al. Complexity behind CO2 Capture on NH2-MIL-53(Al). Langmuir. 2011;27(7):3970-6.

30. K. Sing DE, R. Haul, L. Moscou, R. Pierotti, J. Rou-, querol aTS. REPORTING PHYSISORPTION DATA FOR GAS/SOLID SYSTEMS with Special Reference to the Determination of Surface Area and Porosity. Pure Appl Chem. 1985;57(4):603-19.

31. Geoffrey M. The effect of pore space connectivity on the hysteresis of capillary condensation in adsorption—desorption isotherms. Journal of Colloid and Interface Science. 1982;88(1):36-46.

32. Zlotea C, Phanon D, Mazaj M, Heurtaux D, Guillerm V, Serre C, et al. Effect of NH2 and CF3 functionalization on the hydrogen sorption properties of MOFs. Dalton Transactions. 2011;40(18).

33. Serra-Crespo P, Ramos-Fernandez EV, Gascon J, Kapteijn F. Synthesis and Characterization of an Amino Functionalized MIL-101(Al): Separation and Catalytic Properties. Chemistry of Materials. 2011;23(10):2565-72.

34. Farrusseng D, Daniel Cc, Gaudillère C, Ravon U, Schuurman Y, Mirodatos C, et al. Heats of Adsorption for Seven Gases in Three Metal−Organic Frameworks: Systematic Comparison of Experiment and Simulation. Langmuir. 2009;25(13):7383-8.

35. Bourrelly S, Llewellyn PL, Serre C, Millange F, Loiseau T, Férey G. Different Adsorption Behaviors of Methane and Carbon Dioxide in the Isotypic Nanoporous Metal Terephthalates MIL-53 and MIL-47. Journal of the American Chemical Society. 2005;127(39):13519-21.

36. Ferey G. Hybrid porous solids: past, present, future. Chemical Society Reviews. 2008;37(1).

6

Chapter Six: Effect of HNO_3 Additives in the Synthesis of Zr-MOFs on Their Structure and Capacities of Carbon Dioxide Adsorption

6

Effect of HNO_3 additives in the synthesis of Zr-MOFs on their structure and capacities of carbon dioxide adsorption

Abstract

In this chapter, we report synthesis of Zr-MOF with nitric acid as an additive in synthesis procedure. The modifications aimed to enhance the pore size by effects of nitric acid additive; also to check the functionality of product and compare them with NO_2-Zr-MOF. The crystalline products were compared with Zr-MOF and Zr-MOF-NO_2. It was found that all the XRD patterns of the materials were similar. Thermal analysis showed all samples with nitric acid additive started to decompose at temperature 773 K, same as Zr-MOF while Zr-MOF-NO_2 was stable up to about 623 K. FTIR spectra showed no functional groups were formed as a result of adding nitric acid whereas nitro-functional group appeared on Zr-MOF-NO_2 spectrum. The BET surface area decreased with increased amount of additives and with existence of NO_2 group. The pore size distribution was dramatically changed toward macropore in Zr-MOF-NO_3-2 while the average pore size in NO_3-modified samples and Zr-MOF-NO_2 was higher than Zr-MOF. However, the crystal size reduced with increasing the amount of nitric acid additive. CO_2 adsorption capacity at STP conditions decreased from 61.39 cc/g on Zr-MOF-NO_3-1 to 57.90 cc/g on Zr-MOF-NO_3-2, which was lower than that on Zr-MOF (79 cc/g). However, Zr-MOF-NO_2 exposed acceptable adsorption capacity at the same conditions; it was 74.7 cc/g. Heat adsorption of carbon dioxide on Zr-MOF-NO_3-1 and Zr-MOF-NO_3-2 were 27 and 17.8 kJ/mol, respectively, while it was 37 kJ/mol on Zr-MOF-NO_2. Zr-MOF-NO_3-2 and Zr-MOF-NO_3-1 exposed higher CO_2 adsorption at high pressure whereas Zr-MOF-NO_2 demonstrated a lower value; it was 8, 7.8, and 6 mmol g^{-1} at 849.6 kPa, respectively. Also, the selectivity of CO_2 over CH_4 was the biggest at Zr-MOF-NO_3-2; it ranged from 4.4 at low pressure (59 kPa) to 3.1 at 626 kPa.

6.1 Introduction

Metal - containing nodes have been successfully exploited to determine the properties of final product (1). In addition, using multicarboxylate ligands was helpful to predict the extended networks (2). Therefore, metal organic frameworks have been increasingly used in different applications, such as separation (3), hydrogen storage (4), catalysts (5) and others (6).

These materials can easily be developed to fit a selective application by understanding a mechanism of crystal growth via the synthesis process. This may help to controlling the characteristics of final product such as morphology, size, structure, and composition. Also presence and creation of crystal defects can be investigated and controlled. Process parameters have a prime role to determine the performance of crystallisation process, therefore, choice of the reagents should importantly be taken into account in the synthesis process (7). In addition, it was found that the solvent composition can have a great influence on the crystallisation kinetics in the synthesis process for many MOFs, this effect can enhance the solvation operation via the synthesis process (8). Furthermore, it was claimed in formation of zinc paddle wheel SBUs that the additives can affect the secondary building unit structure and consequently, the topology of MOF may be changed.

Some additives can change the pH of reaction medium, the low pH can lead to form MOF linked through a single metal ion whereas the high pH can result in MOFs assembled via PW-4-zinc cluster(9). The MOF can be synthesised in a manner, strongly depended on the real reaction conditions, such as reaction time, temperature, solvent, co-solvent and basic additives (10). Some additives such as triethylamine (TEA) and H_2O_2 in limited concentration were used to improve the characteristics of MOF-5 to adsorb hydrogen gas. The H_2O_2 additive participated to enhance both of surface area and pore volume, resulting in higher hydrogen storage capacity (11). Furthermore, nitric acid was used as an additive in a synthesis process of new zinc terephthalate metal organic frameworks including H_2NEt_2 ions occupied inside the pores as a result of additives (12).

Separation and purification have been researched; CO_2 and CH_4 were the most common gases selected. Zr-MOF (UiO-66) was synthesized (13, 14), modified and used in some applications as catalysts (15, 16). Recently, it was taken into account the effect of acetic acid, benzoic acid, and water on the synthesis of Zr-MOFs to enhance their crystal sizes (17). In this chapter, Zr-MOF was prepared in two direct modification methods, the first was by increasing the synthesis medium acidity via using nitric acid as an additive and the second was by using a NO_2-functionalised –organic linker. Most characteristics of the crystalline products were investigated. In addition, these materials were tested for carbon dioxide adsorption by a static volumetric method. Heat of adsorption for carbon dioxide was calculated.

6.2 Experimental works

6.2.1 Chemicals

Zirconium chloride ($ZrCl_4$, 99%), 1, 4-Benzenedicarboxylic acid (BDC, 98.9%), 2-Nitro-1, 4-Benzenedicarboxylic acid (NO_2- BDC, ≥ 99%), Dimethylformamide (DMF, 99%), Nitric Acid (96%), Chloroform (Analysis grade, 99%) and Methanol (Analysis grade, 99%) were supplied from Sigma Aldrich, Scientific Perth and Thermo Fisher Scientific and used without further purification

6.2.2 Synthesis and Activation Procedure

6.2.2. 1 Zr-MOF-NO_3-1 and -2

Zr-MOF-NO_3 was synthesized by the same procedure mentioned in Chapter 3 but with some modifications. Generally, 2.27 mmol of $ZrCl_4$ was dissolved in 202.69 mmol of DMF and 2.27 mmol of BDC was dissolved in 202.69 mmol of DMF separately, then 1.5 mmol of HNO_3 (3 M) was added to the BDC solution was and mixed very well. After that, the two solutions were mixed together in a Parr PTFE-lined digestion vessel of 45 mL for around 30 min. Then, the autoclave

was tightly sealed and placed in a preheating oven at 393 K for 24 h. Finally, nano-scaled crystals were produced after vacuum filtration of the ending solution.

To synthesize Zr-MOF-NO_3-2, the same above procedure can be repeated by adding 4.2 mmol of HNO_3 (3 M) in the BDC solution in the synthesis procedure.

Zr-MOF-NO_3-1 and 2 were activated by immersing about 0.5 g from each of them separately inside 50 mL of chloroform for 5 d and then the product solution was filtered and dried under vacuum. Eventually, the white crystalline powder was heated at 463 K overnight. The dried product was heated again under vacuum at 473 K for 48 h.

6.2.2. 2 Zr-MOF-NO_2

The Zr-MOF-NO_2 was solvothermally synthesized at 393 K for 24 h according to the above procedure, but was modified and scaled up in a 125 mL Teflon-lined steel autoclave under autogenously pressure. More specifically, 6.26 mmol of $ZrCl_4$ was mixed with 5.778 mmol of NO_2-BDC in 1110.7 mmol (86 mL) of DMF, and then the starting solution was placed in an autoclave. The autoclave should be tightly closed and placed in the preheating oven at 393 K for one day. After that, the autoclave should be cooled enough till room temperature. Finally, very uniform crystals were produced by using vacuum filtration.

Zr-MOF-NO_2 was activated by immersing about 0.5 g of Zr-MOF-NO_2 in 60 mL of methanol for 4 d, and then the solution was filtered and dried under vacuum. Finally the white crystalline powder was heated at 423K overnight. The dried powder was reheated under vacuum at 473K for 48 h.

6.2.3 Characterizations

X-ray powder diffraction patterns were achieved by a XRD diffractometer (Diffractometer D8 Advance- Bruker aXS) with Cu Kα radiation (λ=1.5406 Å) to determine the topology and check the stability of the crystalline structure at low angle range of 2θ = 5-70° with accelerating voltage and current of 40 kV and 40 mA, respectively.

The morphological description of crystals and crystal size were done by A SEM instrument (Zeiss NEON 40 EsB CrossBeam) with maximum magnification power of 100 nm.

Functional groups on a crystalline structure or inside the pores were scanned and investigated by a Perkin-Elmer 100-FT-IR Spectrometer. Scans were done in the range from 650 to 4000 cm^{-1} with resolution of 4 cm^{-1} using Universal ATR-Diamond/ZnSe as IR Accessory.

The surface area, total pore volume, micropore area, average pore size, and pore size distribution can be measured and calculated on an Autosorb 1 (Quantachrome) by A1Win software. Also, N_2 adsorption/desorption isotherms at 77 K can be determined. In more specifically, firstly, around 15 mg of the sample was degassed at 473 K under vacuum for 8 h. After that, the net weight was loaded into analysis port to measure nitrogen adsorption/desorption isotherm at 77 K (Liquid Nitrogen).

Thermal stability was tested by a TGA instrument (TGA/DSC1 STAR^e system-METTLER TOLEDO). In more detail, an alumina pan of 150 µL was filled by a sample of 16 mg, placed on sample disc and automatically transferred to settle on the sensitive balance. Then, in an atmosphere of 100% Argon (20 mL/min) it was heated at a rate of 10 K/min from 308 K to 1173 K.

6.2.4 Adsorption study

6.2.4.1 CO_2 Adsorption at 1 atm

A static volumetric method with an instrument from Micromeritics- (Gemini I-2360) was used to measure the specific adsorbed volume of pure CO_2 (99.995%) at 273 and 296 K at atmospheric pressure. The temperature was controlled to maintain the isothermal condition.

Firstly, about 0.25 g of dried sample was weighed in the weighed tube and then degassed by heating in Vacprep 061 at 473 K under vacuum for 48 h. After

degassing, the net weight of the sample was recorded and the sample tube was moved to analysis port of Gemmini I-2360.

The Clausius-Claperyron equation (Eq.3.1) was used to determine heat of adsorption for carbon dioxide by using CO_2 adsorption isotherm data at different temperatures.

6.2.4.2 Adsorption at High Pressure

The adsorption isotherms of pure carbon dioxide (99.995%) and pure methane (99.995%) at high pressure were measured by Micoromeritics- ASAP2050. The samples were degassed by increasing the temperature at a ramp of 10 K/min till 373 K to hold at this temperature for 2 hrs then increasing the temperature again at the same rate to 473K under vacuum (up to 0.4 kPa) to hold at this condition for 8 hrs. Then an obtained net weigh was used in the analysis. All analyses were achieved at 273 K.

6.3 Results and discussion

6.3.1. Structural stability

From XRD patterns in Figure 6.1(a) it was observed that reflection intensity reduced with increasing nitric acid additives. That means the structural ordering of the NO_3- modified materials decreases as the intensity decreases. However, the intensities of Zr-MOF-NO_2 pattern were the lowest.

All the peaks seem to be overlapped for all samples; it is a good indication of maintaining the structure of Zr-MOF-NO_3 and Zr-MOF-NO_2 as the same as Zr-MOF (Parent) even after adding different amounts of HNO_3 in the synthesis process of Zr-MOF-NO_3.

Crystal sizes of all samples have been calculated based on the Scherrer equation(18). The crystal size decreased with increasing amount of additives. They are 508, 449.0, and 298.2 Å for Zr-MOF-Parent, Zr-MOF-NO_3-1 and Zr-MOF-NO_3-2, respectively, while it is 378.0 Å for Zr-MOF-NO_2.

In addition, it was claimed that the pore size can be modified by some additives in direct synthesis and can be estimated from the atomic plane spacing (d) when it

is wider. The pore size is larger accompanying with disordered structure(19). Figure 6.1 (b) demonstrates atomic plane spacing of Zr-MOF-NO_3, Zr-MOF-NO_2 in a comparative view with Zr-MOF-(Parent).

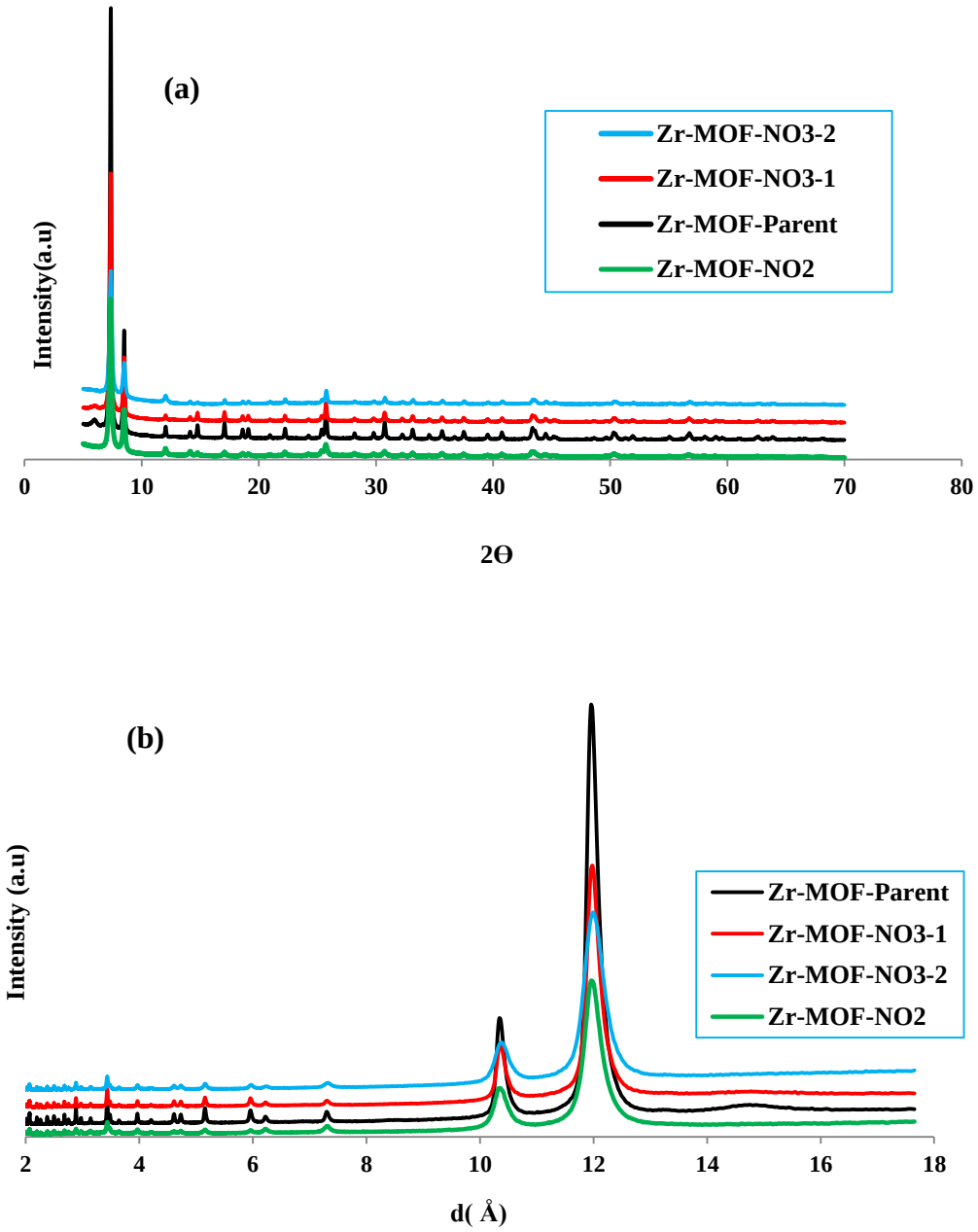

Figure: 6.1 PXRD patterns for NO3-modified Zr-MOF samples 1, 2 and Zr-MOF-NO2 compared with Zr-MOF-Parent (a) 2Θ versus reflection intensity and (b) d-spacing versus reflection intensity

6.3.2 Morphological Description

The morphological descriptions in Figure 6.2 (a) and (b) show obviously the difference in the crystal size in Zr-MOF-NO_3 images, which reduced with increasing HNO_3 additives in the direct synthesis process. In addition, the crystal shape seems to be cubic for both samples of Zr-MOF-NO_3 which is similar to that of Zr-MOF while it seems triangular base-pyramid shape for Zr-MOF-NO_2 as shown in Figure6.2(c).

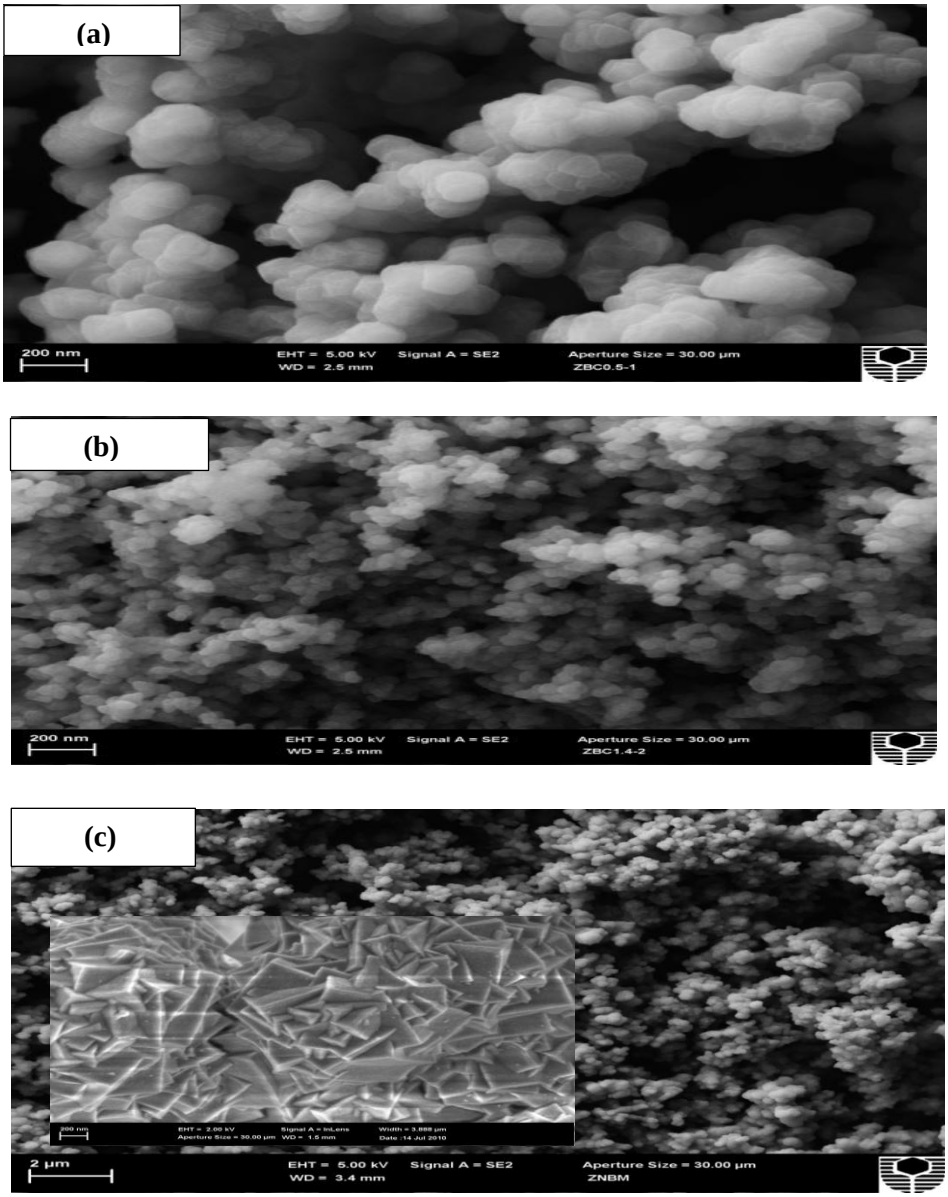

Figure: 6.2 SEM Images (a) Zr-MOF-NO_3-1, (b) Zr-MOF-NO_3-2, and (c) Zr-MOF-NO_2

6.3.3 Functional groups determination

FTIR spectra in Figure 6.3 show that the free carboxylic acid (O═COH functional group) can be seen at band 1640-1670 cm^{-1} with a peak at 1656 cm^{-1} (20, 21) on non-activated samples of Zr-MOF-NO_3-2 and Zr-MOF-NO_2. This band was removed after activation process on all the samples. Also, all the spectra of Zr-MOF-NO_3 did not show nitro-functional group on the structure.

However, asymmetrical stretching vibration of functional group of NO_2 at the peak of 1537 cm^{-1} and symmetrical stretching vibration of NO_2 at 1391 cm^{-1} appeared on Zr-MOF-NO_2 (22-24).

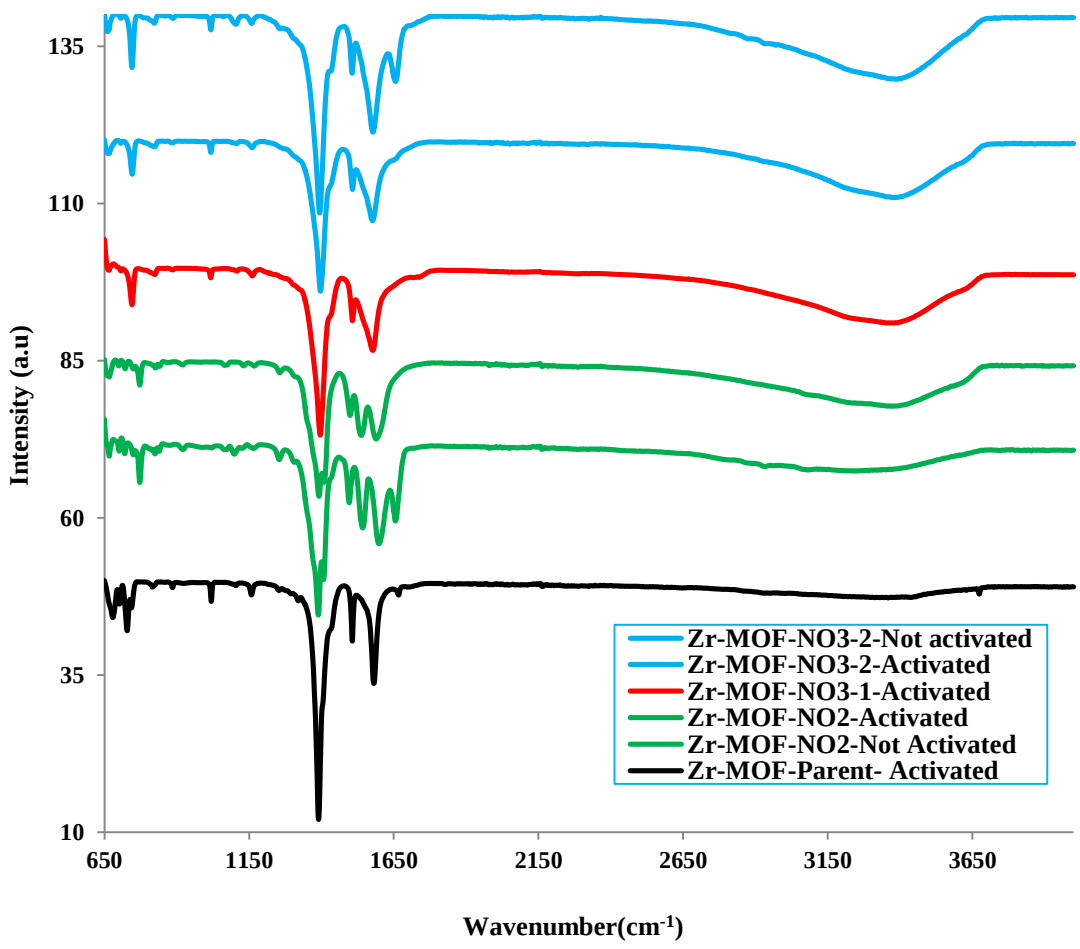

Figure: 6.3 FTIR spectra for Zr-MOF-NO_3-1 and 2 as well as Zr-MOF-NO_2

6.3.4 Nitrogen Adsorption and Pore Size Distribution

Figure 6.4 shows nitrogen adsorption/desorption isotherms at 77 K on Zr-MOF-NO_3-1, Zr-MOF-NO_3-2, and Zr-MOF-NO_2. It was noted that both Zr-MOF-NO_3 isotherms and Zr-MOF-NO_2 have a hysteresis. In contrast with Zr-MOF-Parent, adsorption and desorption isotherms were completely overlapped. This may prove the change in width of pores during modifications. Therefore, these samples had different behaviours to adsorb nitrogen gas depending on the ratio of micropores to mesopores.

In addition, at low relative pressure (<0.05) in Figure 6.4 vertical parts in adsorption isotherm represent evidence to amount of micropore which increases with increasing the length of vertical lines. In this range only micropores might be filled and with increasing pressure higher mesopore might be filled as shown with low slope line in relative pressure range from 0.05 till around 0.95. At relative pressure around unity the vertical line represents macropore region and this may be obviously seen just with Zr-MOF-NO_3-2.

Table 6.1 shows the micropore percentage (MP%) was reduced from 89.8% for Zr-MOF-Parent to 65.7% for Zr-MOF-NO_2 and the total pore volume increased to reach the highest value of 1.077 cc/g on Zr-MOF-NO_3-2 and it was higher than Zr-MOF-Parent (0.654 cc/g) and Zr-MOF-NO_2 (0.489 cc/g). Both Zr-MOF-NO_3-1 and Zr-MOF-NO_3-2 have the highest pore size, 18.94 and 18.73 Å, respectively, while Figure 6.5 (A) shows that the micropore size was the lowest for Zr-MOF-NO_3-2 and Zr-MOF-NO_2, 6.2 Å and 7.1 Å respectively.

Mesopore distribution for all samples was shown in Figure 6.5 (B). More specifically, mesopore size distribution has a different range depending on the geometry of the pores; it was ranged from 3.18 nm in Zr-MOF-NO_3-1 to 2.6 nm in Zr-MOF-NO_3-2 with an indication of presence of macropore size as the accumulative volume increased on a wide range of pore radius more than 30 nm. Also, mesopore is in the range from 1.78 to 16.3 nm in Zr-MOF-NO_2.

The BET and Langmuir surface areas were calculated and the highest BET and Langmuir surface area were 1248 and 1407 m^2/g for NO_3-modified samples, respectively, which are lower than the surface areas of Zr-MOF-(Parent). However, Zr-MOF-NO_2 had a smaller BET and Langmuir surface area; they are 819, and 906 m^2/g respectively.

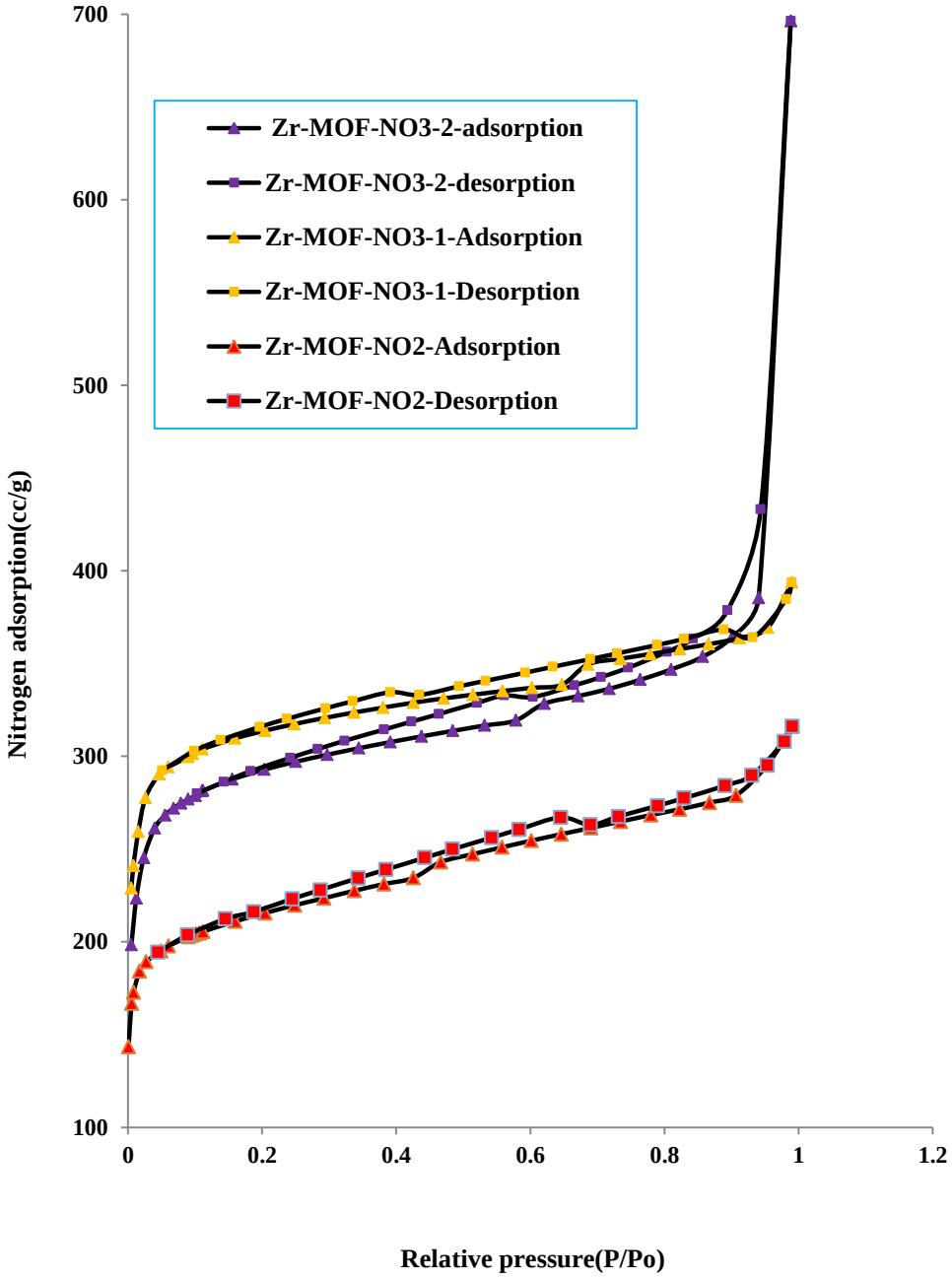

Figure: 6.4 Nitrogen Adsorption-Desorption isotherms

It can be believed that the lowest surface area in Zr-MOF-NO_2 may be attributed to the presence of functional groups inside the pores, which can pull the structure toward centre of the pores because of their interaction with other functional group inside the pores. As a matter of the fact, the relation between the -NO_2 functional (acidic group) groups and bridging -OH (basic group) group is strong enough to make bulky permanent interaction inside the pores (25).

Table 6.1: BET, Langmuir surface area and pore size distribution for Zr-MOFs

Zr-MOF Type	BET Surface Area (m^2/g)	Langmuir Surface Area(m^2/g)	Average Pore Radius(Å)	Total Pore Volume (cm^3/g)	M P (%)
Zr-MOF-Parent	1434	1563	9.1	0.654	89.8%
Zr-MOF-NO_3- 1	1248	1407	18.9	0.609	79%
Zr-MOF-NO_3-2	1149	1275	18.7	1.08	75%
Zr-MOF-NO_2	819	906	11.8	0.489	65.7%

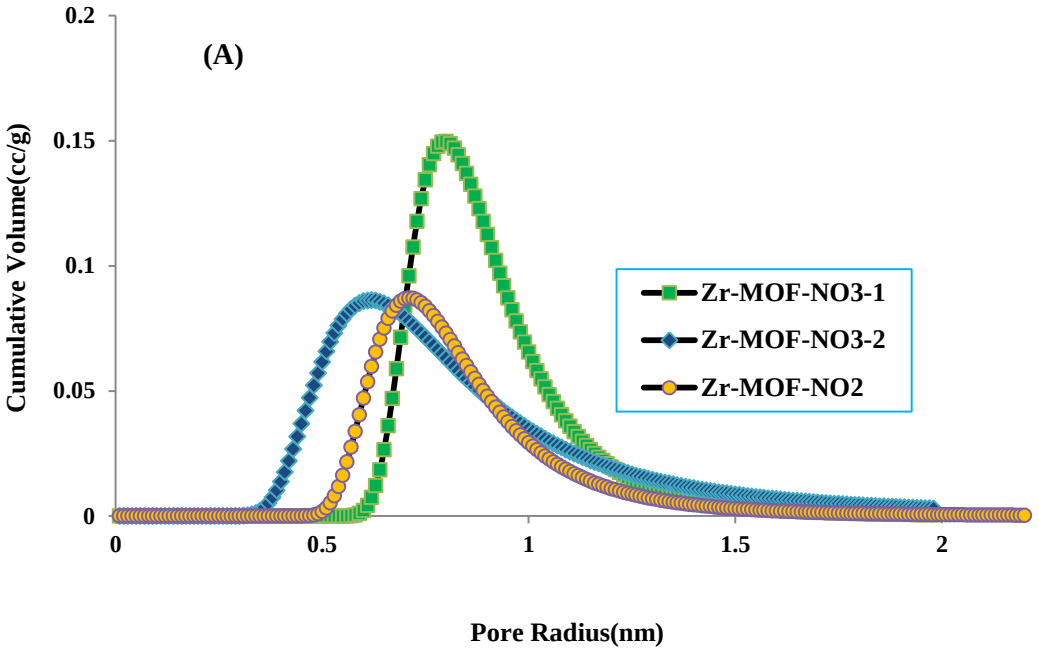

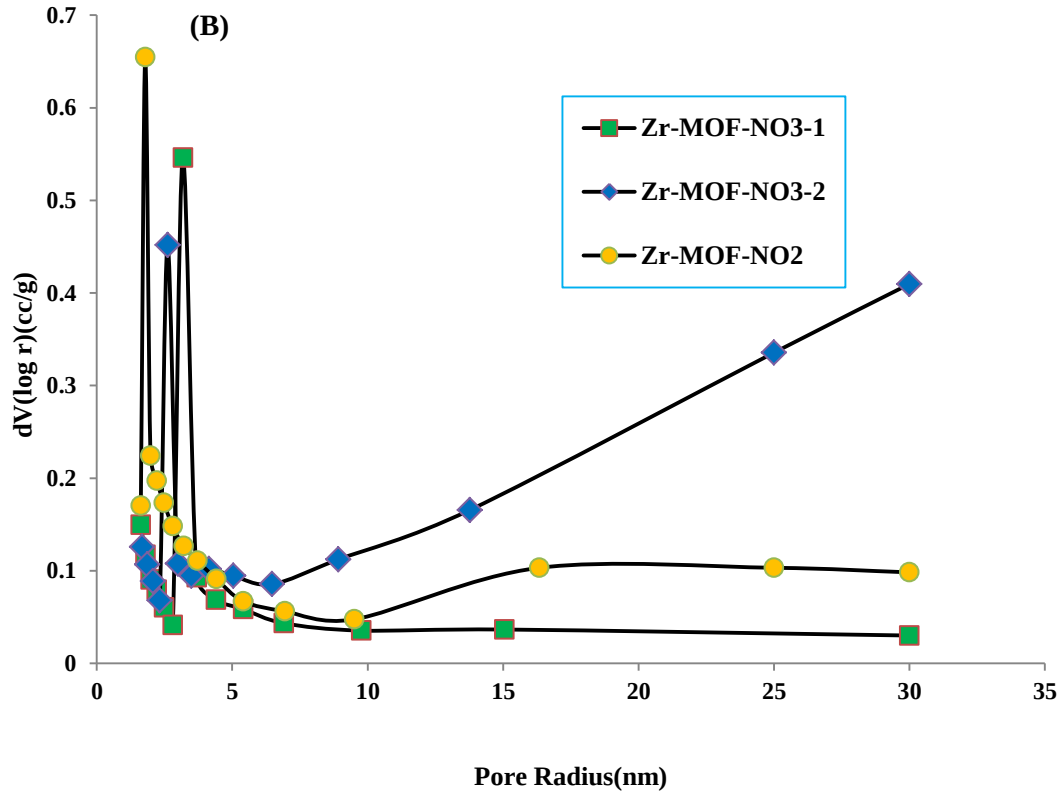

Figure: 6.5 A- Micropore size distribution, B- Mesopore size distribution

6.3.5 Thermal Stability

From Figure 6.6, it was found that Zr-MOF-NO_3-1 and -2 behaved in a similar way to Zr-MOF-Parent under heating up to 900 ^{0}C. It was observed that the amount of BDC and free DMF was 15% (Zr-MOF-NO_3-1), 20% (Zr-MOF-NO_3-2), and 20% (Zr-MOF-NO_2), which were interacted inside the pores by hydrogen bond and Van Der Waals forces depending on the conditions of a synthesis procedure. These amounts were reduced to 2%, 5%, and 0.5% for activated Zr-MOF-NO_3-1, Zr-MOF-NO_3-2, and Zr-MOF-NO_2, respectively and efficiency of discarding relying on the performance of activation process.

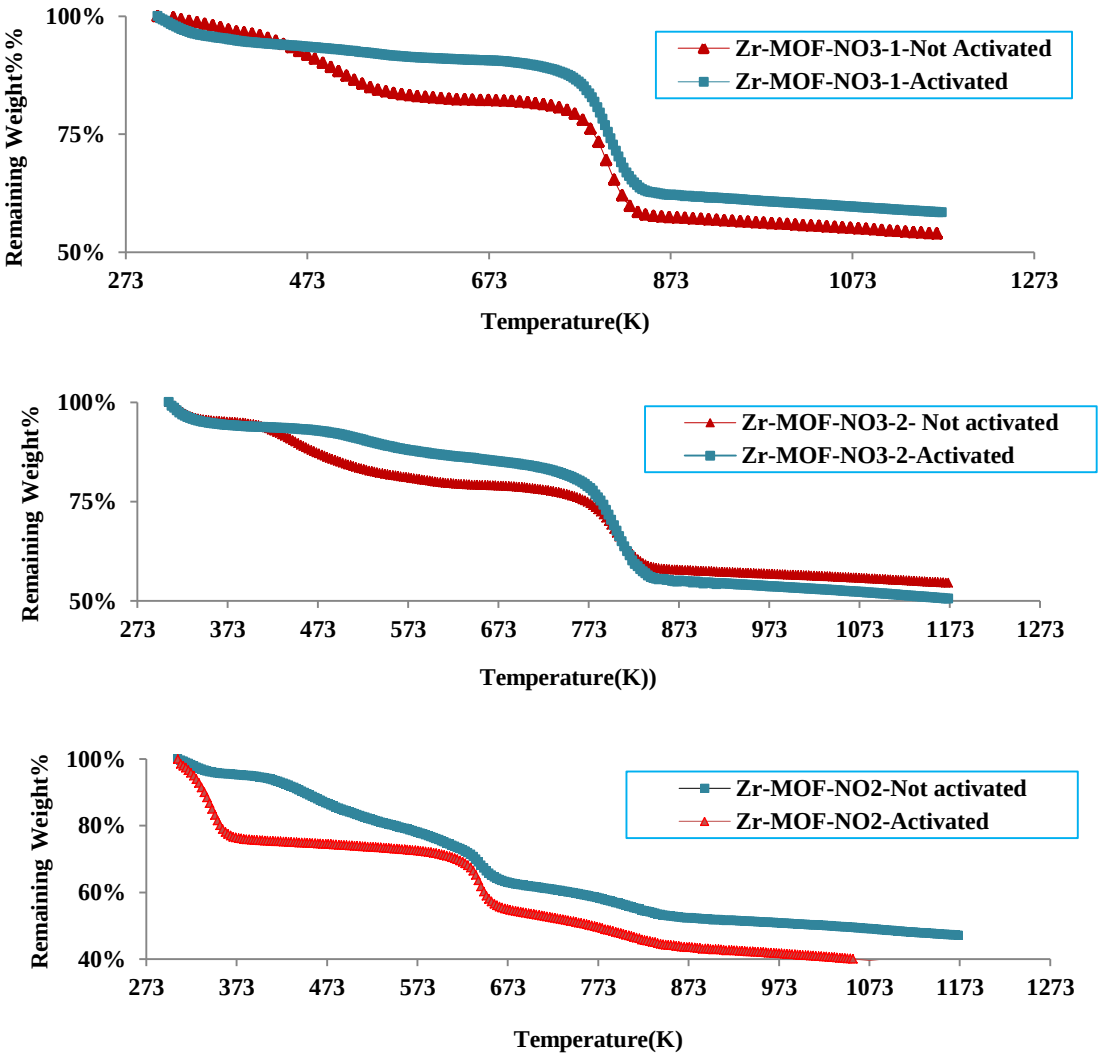

Figure: 6. 6 Thermal analysis for activated and not activated samples

According to TGA experiments the coordinated BDC or NO_2-BDC percentages in activated samples (in above sequence) were calculated as about 26%, 26%, and 27% while the percentages of Zr_6O_6 were 57%, 55% and 44%. These percentages may be affected by the amount of moisture which usually can be adsorbed on the surface of materials.

All Zr- MOF-NO_3 started to decompose at around 753 K similar to Zr-MOF (13), it means the HNO_3 additives within this range did not affect the thermal stability of Zr-MOF-NO_3 and the structure was destroyed as a result of disconnecting BDC-linkers from the structure by increasing the temperature up to 823 K. However, Zr-MOF-NO_2 was thermally stable till 593 K when interconnection was broken; the whole structure may collapse at about 823K.

6.3. 6 Adsorption Study

6.3.6.1 Carbon Dioxide Adsorption at STP

Figure 6.7 shows CO_2 adsorption capacity at 1 atm and different temperatures on (a) Zr-MOF-NO_3-1, (b) Zr-MOF-NO_3-2 and (c) Zr-MOF-NO_2. The adsorption capacities reduced when the temperature was increased. Also, it was found that affinity of carbon dioxide to adsorb on NO_3-modified materials was reduced with increasing the amount of additives.

On the other hand, Zr-MOF-NO_2 displayed an acceptable adsorption capacity compared with Zr-MOF-Parent. Volumetric amount of carbon dioxide adsorption on Zr-MOF-NO_2 was 74.7 cc/g while Zr-MOF-NO_3-1 and Zr-MOF-NO_3-2 had 61.3 and 57.9 cc/g, respectively. Furthermore, the decreasing carbon dioxide adsorption with increasing the amount of additives may be related to the change of pore geometrical properties, and reduced surface area. It was proved that the smallest micropore might be filled at STP while the mesopore and macropore might be filled at high pressure (26), therefore the adsorption capacity of Zr-MOF-NO_3-1 was higher than Zr-MOF-NO_3-2 at STP.

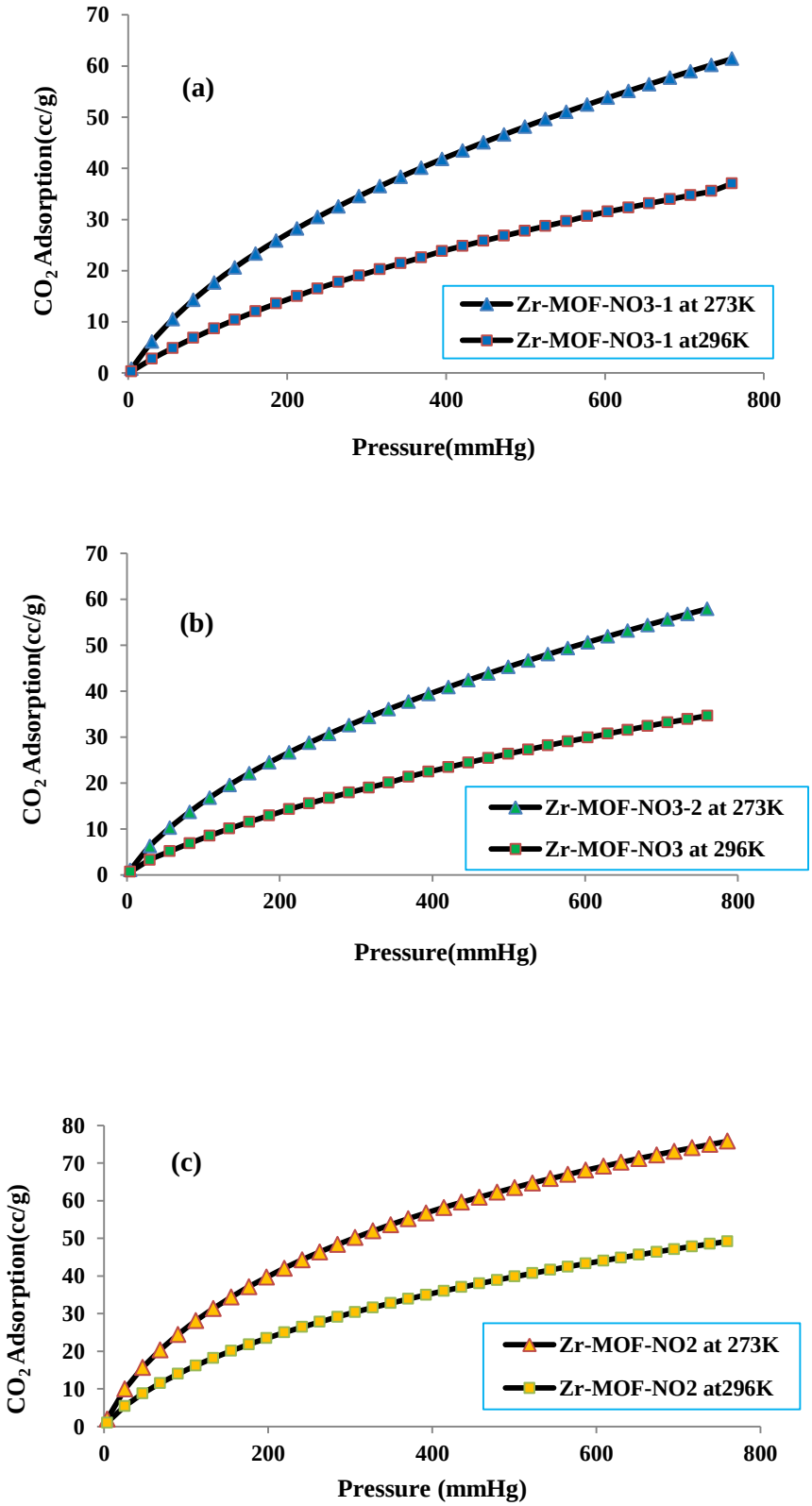

Figure: 6.7 Carbon dioxide adsorption on (a)Zr-MOF-NO_3-1,(b) Zr-MOF-NO_3-2, and (c) Zr-MOF-NO_2 at 1atm and different temperatures

It is worthy to mention, the affinity of Zr-MOF-NO_2 toward carbon dioxide capture at STP was approximately similar to Zr-MOF-Parent with slight differences in adsorption capacity, although surface area of Zr-MOF-NO_2 was smaller. That may be caused by the presence of NO_2-functional group (acidic group) which is not reliable to be a major binding group on the structure directly interacting with CO_2. The effect of NO_2 functional group inside the pores can be explained; availability of NO_2-functional group on organic linkers in metal organic frameworks may lead to increase in the polarity of the organic linker by changing the charge distribution and that may enhance CO_2 adsorption (27, 28).

Isosteric heat of adsorption of CO_2 in Figure 6.8 was calculated by the Clausius-Claperyron equation (Eq.3.1) from isotherms that measured at 273 and 296K for Zr-MOF-NO_3-1, Zr-MOF-NO_3-2, and Zr-MOf-NO_2 as shown in Figure 6.7.

The heat of adsorption was lower for Zr-MOF-NO_3-1 and Zr-MOF-NO_3-2 than Zr-MOF-NO_2; it was 27, 17.8, and 37 kJ/mol, respectively. The heat adsorption of CO_2 on Zr-MOF-NO_3-2 is the lowest amongst Zr-MOFs. That may be attributed to its largest pore volume as explained in Chapter 4. On the other hand, it is the largest on Zr-MOF-NO_2 which may be because of influence of NO_2-functional group.

From Figure 6.8, it can be obviously noted on Zr-MOF-NO_2 that the first layer of coverage on uniform surface was made first at low pressure when the heat of adsorption reaches a maximum value then other layers were created with low heat of adsorption.

In addition, the variation in the heat of adsorption with increasing the surface coverage was very small in all the samples and it was the smallest in the case of Zr-MOF-NO_3-2 and the largest in Zr-MOF-NO_2.

That may indicate a very good evidence for a low heterogeneity of adsorption system (29) for all samples and specially in NO_3-modified Zr-MOF. That can contribute to facile regeneration process in approximately uniform rate.

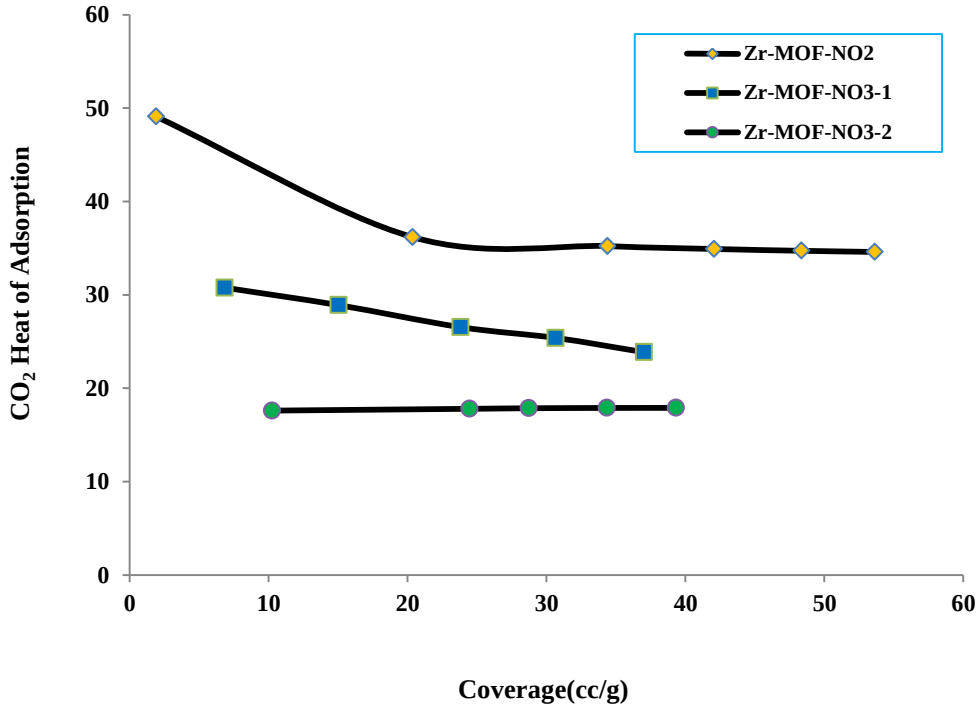

Figure: 6.8 Variation of isosteric heat of adsorption with carbon dioxide coverage

6.3.6.2 Adsorption at High Pressure

6.3.6.2.1 CO_2 Adsorption

Figure 6.9 shows that the adsorption behaviours of NO_3 and NO_2 modified Zr-MOFs are different at high pressure from that at 1atm. CO_2 adsorption on Zr-MOF-NO_3-2 was the highest and the one on Zr-MOF-NO_2 was the lowest at pressure up to 849 kPa; they are 7.82 and 6 mmol g^{-1}, respectively. In addition, it seems that the enlargement of pore can affect the adsorption capacity at higher pressure as discussed in Chapter four, therefore the adsorption of CO_2 on Zr-MOF-NO_3-1 increased above that on Zr-MOF-(Parent) when the pressure increased over 224.5 kPa. Also, CO_2 adsorption on Zr-MOF-NO_3-2 was higher than Zr-MOF-(Parent) as the pressure jumped over 358.5 kPa. In Zr-MOF-NO_3-2 and Zr-MOF-NO_3-1, the maximum values

were 8 and 7.8 mmol g^{-1} at 849.6 kPa respectively while it was 7.5 mmol g^{-1} at 842.3 kPa.

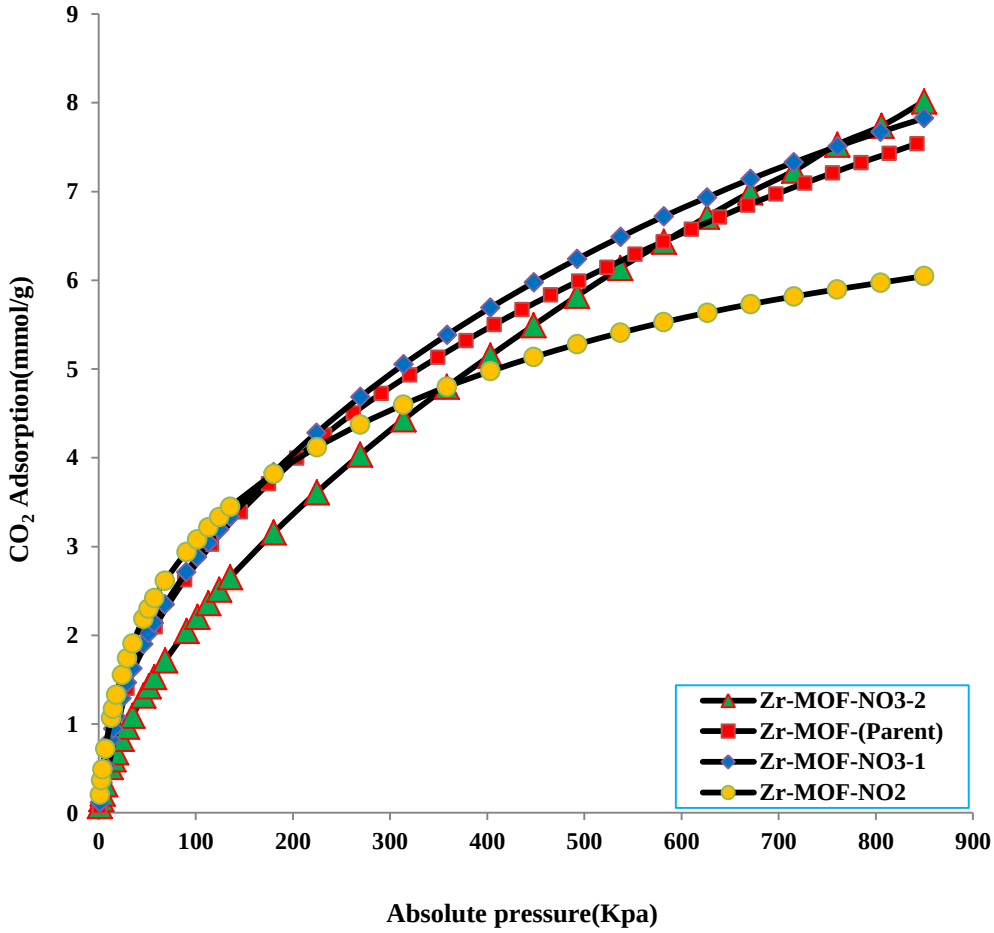

Figure 6.9 Adsorption of CO_2 at high pressure and 273K on Various Zr-MOFs.

6.3.6.2.2 CH_4 Adsorption and Selectivity

CH_4 adsorption was reduced when the amount of HNO_3-additives increased as shown in Figure 6.10. It was obviously seen that Zr-MOF-NO_3-1 and Zr-MOF-NO_3-2 exposed adsorption capacity of 3.45, and 3 mmol g^{-1} respectively. Zr-MOF-NO_2 displayed higher CH_4 adsorption capacity at pressure up to 271 kPa. When the pressure increased higher, the adsorption was less than Zr-MOF-NO_3-1 but it was higher than Zr-MOF-NO_3-2. The maximum CH_4 adsorption at Zr-MOF-NO_2 was 2.83 mmol g^{-1}.

Consequently, the enlargement in pore and surface area was not important factor in CH_4 adsorption which may decrease with increasing the amount of additives.

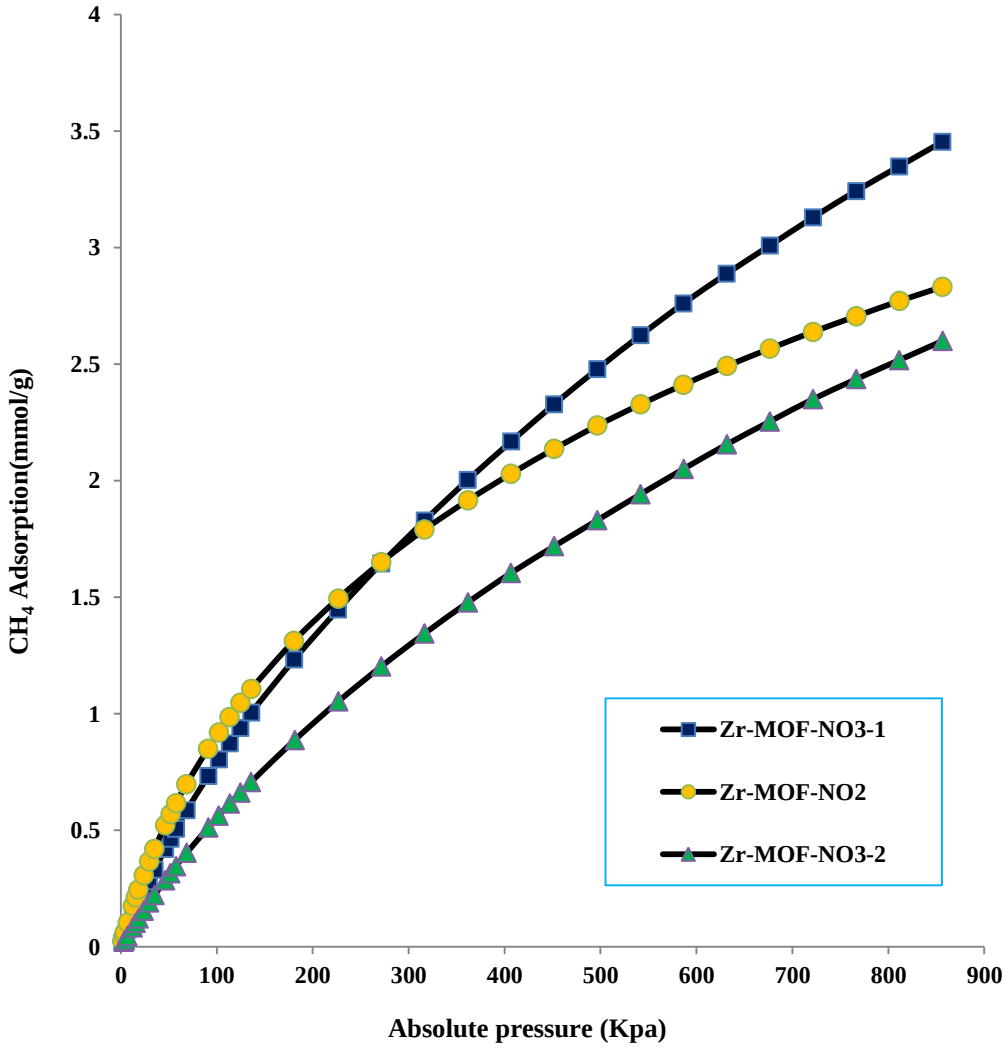

Figure 6.10 Adsorption of CH_4 on Zr-MOF-NO_2 and NO_3-modified Zr-MOFs at high pressure and 273K

The selectivity of CO_2 from its mixture with CH_4 is improved, better than Zr-MOF-(Parent) in all samples, especially, in HNO_3-modified samples. As shown in Figure 6.11, the superiority in separation was owned for Zr-MOF-NO_3-2 which was higher than Zr-MOF-NO_3-1, and Zr-MOF-NO_2; the CO_2

selectivity was 4.4, 4.2, and 4 respectively at 57kPa. It is worthy to notice that, the selectivity of Zr-MOF-NO_3-2 is the highest over the wide range of pressure; it is 3.11 at 626 kPa while it is 2.4 and 2.26 at Zr-MOF-NO_3-1 and Zr-MOF-NO_2, respectively.

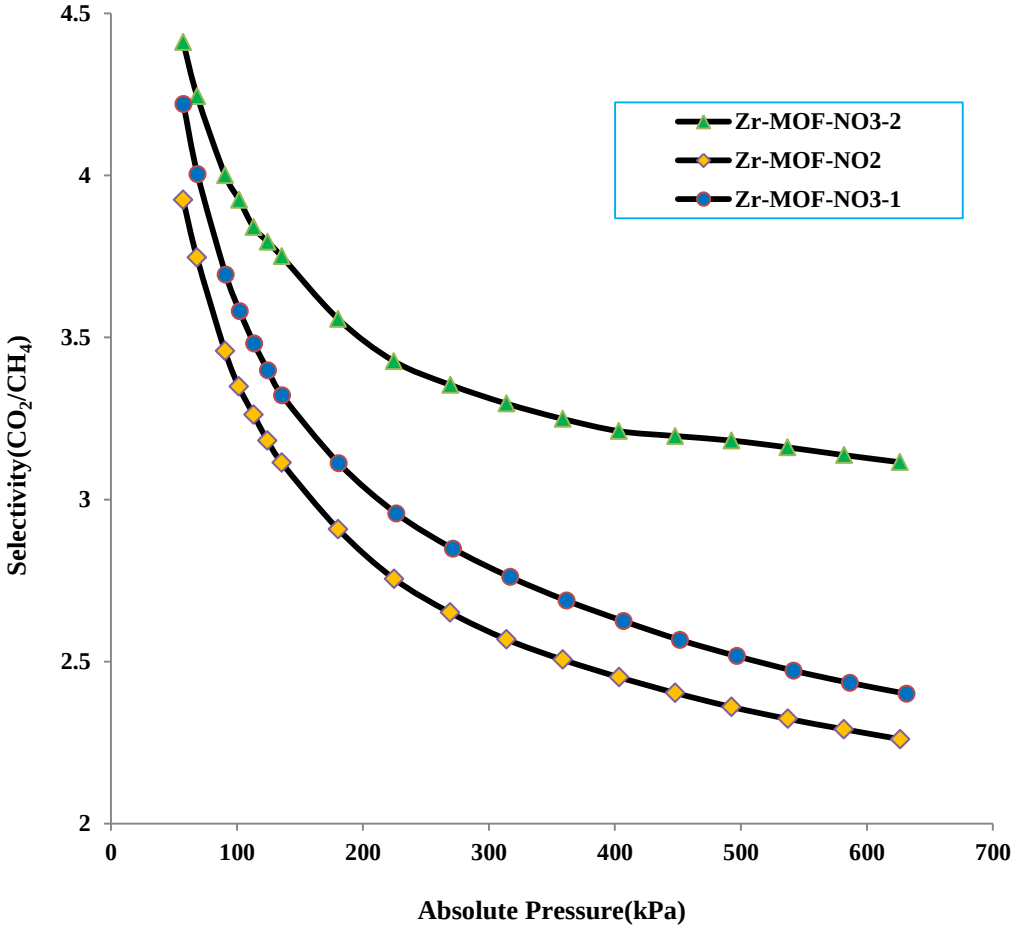

Figure 6.11 Selectivity of CO_2 over CH_4 on various Zr-MOFs.

6.4 Conclusion

This chapter focused on the effect of direct modification of Zr-MOF within the synthesis process on textural characteristics, CH_4, and carbon dioxide adsorption. This modification was achieved in two paths; the first was by using NO_2- functionalised organic linker in the synthesis while the second

was by adding HNO_3 as an additive in the synthesis process. All the synthesized samples had the same topology as that of Zr-MOF-Parent. Zr-MOF-NO_2 had NO_2- functional group inside the pores and none of NO_3-modified samples had extra functional group. In addition, they had the similar thermal stability. However, Zr-MOF-NO_2 had lower thermal stability than others. This modification made a change in the pore size distribution as well as crystal size. Specifically, crystal size reduced with increasing the amount of additives.

The CO_2 adsorption capacity for HNO_3-modified samples (Zr-MOF-NO_3-1 and Zr-MOF-NO_3-2) reduced with increasing the additives which was lower than that of Zr-MOF-Parent. The CO_2 adsorption capacity on Zr-MOF-NO_2 was acceptable. However, the heat of CO_2 adsorption decreased in HNO_3-modified samples, lower than Zr-MOF-Parent and increased in NO_2-functionalised sample. The relation between the carbon dioxide coverage and heat of adsorption referred to homogeneity of adsorption system. The CO_2 adsorption at high pressure was affected by pore size in HNO_3-modified samples, Zr-MOF-NO_3-2 and Zr-MOF-NO_3-1 had the highest values. However, Zr-MOF-NO_2 exposed lower CO_2 adsorption. The largest selectivity of CO_2 over CH_4 was shown for Zr-MOF-NO_3 samples.

6. 5 References

1. Wright PA. Microporous framework solids. Cambridge: Royal Society of Chemistry 2008.

2. Li H, Eddaoudi M, O'Keeffe M, Yaghi OM. Design and synthesis of an exceptionally stable and highly porous metal-organic framework. Nature. 1999;402(6759):276-9.

3. Couck S, Denayer JFM, Baron GV, Remy T, Gascon J, Kapteijn F. An Amine-Functionalized MIL-53 Metal- Organic Framework with Large Separation

Power for CO2 and CH4. Journal of the American Chemical Society. 2009;131(18):6326-7.

4. Rowsell JLC, Millward AR, Park KS, Yaghi OM. Hydrogen Sorption in Functionalized Metal- Organic Frameworks. Journal of the American Chemical Society. 2004;126(18):5666-7.

5. Llabrés i Xamena FeX, Abad A, Corma A, Garcia H. MOFs as catalysts: Activity, reusability and shape-selectivity of a Pd-containing MOF. Journal of Catalysis. 2007;250(2):294-8.

6. Horcajada P, Serre C, Maurin G, Ramsahye NA, Balas F, Vallet-Regí Ma, et al. Flexible Porous Metal-Organic Frameworks for a Controlled Drug Delivery. Journal of the American Chemical Society. 2008;130(21):6774-80.

7. Kawano M, Haneda T, Hashizume D, Izumi F, Fujita M. A Selective Instant Synthesis of a Coordination Network and Its Ab Initio Powder Structure Determination. Angewandte Chemie International Edition. 2008;47(7):1269-71.

8. Ameloot R, Gobechiya E, Uji-i H, Martens JA, Hofkens J, Alaerts L, et al. Direct Patterning of Oriented Metal–Organic Framework Crystals via Control over Crystallization Kinetics in Clear Precursor Solutions. Advanced Materials. 2010;22(24):2685-8.

9. Wang X-L, Qin C, Wang E-B, Su Z-M. Metal Nuclearity Modulated Four-, Six-, and Eight-Connected Entangled Frameworks Based on Mono-, Bi-, and Trimetallic Cores as Nodes. Chemistry – A European Journal. 2006;12(10):2680-91.

10. Vagin S, Ott AK, Rieger B. Paddle-Wheel Zinc Carboxylate Clusters as Building Units for Metal-Organic Frameworks. Chemie Ingenieur Technik. 2007;79(6):767-80.

11. Cheng S, Liu S, Zhao Q, Li J. Improved synthesis and hydrogen storage of a microporous metal–organic framework material. Energy Conversion and Management. 2009;50(5):1314-7.

12. Biemmi E, Bein T, Stock N. Synthesis and characterization of a new metal organic framework structure with a 2D porous system: $(H_2NEt_2)_2[Zn_3(BDC)_4]\cdot 3DEF$. Solid State Sciences. 2006;8(3–4):363-70.

13. Cavka JH, Jakobsen S, Olsbye U, Guillou N, Lamberti C, Bordiga S, et al. A New Zirconium Inorganic Building Brick Forming Metal Organic Frameworks

with Exceptional Stability. Journal of the American Chemical Society. 2008;130(42):13850-1.

14. Kandiah M, Nilsen MH, Usseglio S, Jakobsen Sr, Olsbye U, Tilset M, et al. Synthesis and Stability of Tagged UiO-66 Zr-MOFs. Chemistry of Materials.22(24):6632-40.

15. Gomes Silva C, Luz I, Llabrés i Xamena FX, Corma A, García H. Water Stable Zr–Benzenedicarboxylate Metal–Organic Frameworks as Photocatalysts for Hydrogen Generation. Chemistry – A European Journal. 2010;16(36):11133-8.

16. Vermoortele F, Ameloot R, Vimont A, Serre C, De Vos D. An amino-modified Zr-terephthalate metal-organic framework as an acid-base catalyst for cross-aldol condensation. Chemical Communications. 2011;47(5):1521-3.

17. Schaate A, Roy P, Godt A, Lippke J, Waltz F, Wiebcke M, et al. Modulated Synthesis of Zr-Based Metal–Organic Frameworks: From Nano to Single Crystals. Chemistry – A European Journal. 2011;17(24):6643-51.

18. Jaboyedoff M, Kubler B, Thelin P. An empirical Scherrer equation for weakly swelling mixed-layer minerals, especially illite-smectite. Clay Minerals. 1999;34(4):601-17.

19. Sayari A, Kruk M, Jaroniec M, Moudrakovski IL. New Approaches to Pore Size Engineering of Mesoporous Silicates. Advanced Materials. 1998;10(16):1376-9.

20. Devic T, Horcajada P, Serre C, Salles F, Maurin G, Moulin Ba, et al. Functionalization in Flexible Porous Solids: Effects on the Pore Opening and the Host−Guest Interactions. Journal of the American Chemical Society. 2009;132(3):1127-36.

21. Biswas S, Ahnfeldt T, Stock N. New Functionalized Flexible Al-MIL-53-X (X = -Cl, -Br, -CH_3, -NO_2, -$(OH)_2$) Solids: Syntheses, Characterization, Sorption, and Breathing Behavior. Inorganic Chemistry. 2011;50(19):9518-26.

22. Muckenhuber H, Grothe H. The heterogeneous reaction between soot and NO2 at elevated temperature. Carbon. 2006;44(3):546-59.

23. Boyd SA, Sheng G, Teppen BJ, Johnston CT. Mechanisms for the Adsorption of Substituted Nitrobenzenes by Smectite Clays. Environmental Science & Technology. 2001;35(21):4227-34.

24. Bernt S, Guillerm V, Serre C, Stock N. Direct covalent post-synthetic chemical modification of Cr-MIL-101 using nitrating acid. Chemical Communications. 2011;47(10):2838-40.

25. Horcajada P, Salles F, Wuttke S, Devic T, Heurtaux D, Maurin G, et al. How Linker's Modification Controls Swelling Properties of Highly Flexible Iron(III) Dicarboxylates MIL-88. Journal of the American Chemical Society. 2011;133(44):17839-47.

26. Hu X, Radosz M, Cychosz KA, Thommes M. CO_2-Filling Capacity and Selectivity of Carbon Nanopores: Synthesis, Texture, and Pore-Size Distribution from Quenched-Solid Density Functional Theory (QSDFT). Environmental Science & Technology. 2011;45(16):7068-74.

27. Li B, Wei S, Chen L. Molecular simulation of CO_2, N_2 and CH_4 adsorption and separation in ZIF-78 and ZIF-79. Molecular Simulation. 2011;37(13):1131-42.

28. Banerjee R, Furukawa H, Britt D, Knobler C, O'Keeffe M, Yaghi OM. Control of Pore Size and Functionality in Isoreticular Zeolitic Imidazolate Frameworks and their Carbon Dioxide Selective Capture Properties. Journal of the American Chemical Society. 2009;131(11):3875-7.

29. Himeno S, Tomita T, Suzuki K, Yoshida S. Characterization and selectivity for methane and carbon dioxide adsorption on the all-silica DD3R zeolite. Microporous and Mesoporous Materials. 2007;98(1-3):62-9.

7

Chapter 7: CO_2 Adsorption on MIL-53, MIL-96, and Amino-MIL-53 MOFs

7

CO_2 adsorption on MIL-53, MIL-96, and amino-MIL-53 MOFs

Abstract

In this chapter, MIL-53, MIL-96 and amino-MIL-53 were prepared, characterized and tested in CO_2 adsorption. These MOFs exposed different characteristics but MIL-53 and amino-MIL-53 have the same topology. BET surface areas were 1519, 687, and 262 m^2/g for MIL-53, MIL-96, and amino-MIL-53, respectively. Also they expose different thermal stability; MIL-53 has the highest stability which decomposed at 773 K. However, amino-MIL-53 and MIL-96 show the lower thermal stability, decomposing after heating up to 650 and 570 K, respectively.

MIL-53 shows CO_2 adsorption capacity at 56 and 64 cc/g at 296 and 273K, respectively. CO_2 heat of adsorption on MIL-53 was found to be 39 kJ/mol. MIL-96 exhibits CO_2 adsorption capacity of 124 cc/g at standard conditions while the heat of adsorption is 28.6 kJ/mol. Amino-MIL-53 has CO_2 adsorption capacity at standard conditions of 48 cc/g, while the heat of adsorption is 28 kJ/mol.

Dynamic adsorption (working capacity) presents the biggest value on MIL-53, giving 169 cc/g at 1 bar and room temperature (304 K). Amino-MIL-53 shows dynamic adsorption capacity of 128 cc/g at the same conditions. However, MIL-96 demonstrates dynamic adsorption of 89 cc/g at 1 bar and 298K. On the other hand, some of Zr-MOFs, Zr-MOF, Zr-MOF-NH_2, and Zr-MOF-NO_2 which were used at 1 bar as comparative samples displays of 48, 86, and 128 cc/g, at 304, 304, and 291K, respectively. It seems that MIL-53, Zr-MOF-NO_2, and amino-MIL-53 present higher working capacity, due to their larger pore size.

7.1 Introduction

There is a strong relationship between the adsorption of CO_2 and structure or chemical composition of metal organic frameworks. Several metal salts were used to synthesize many MOFs and their isoreticular such as Zn^{+2}(1), Zr^{+4}(2) and Al^{+3}. Trivalent metals M^{+3}(Al^{3+}, Cr^{+3}, Fe^{+3}, V^{+3}) have been used in preparation MIL-n, which was built from infinite chain of corner sharing $M_4(OH)_2$ octahedra. These may be classified to different structures relying on the type of linkers or metals such as MIL-53 (3-5), MIL-96 (6), MIL-100 (7), MIL-101 and MIL-47 (8).

MIL-53 intrinsically has suffered from a reversible structural transition from open to close when the temperature is changed, without the assistance of the guest molecules. As a result, this material has demonstrated unprecedented large temperature hysteresis (9). It was claimed that using of benzenetricarboxylic acid, it is possible to synthesize non-interpenetrating Zn-MOFs with enhanced thermal stability and rigidity, which belongs to the properties of BTC such as triple–bidentate functionality(10). However, Al-BTC metal organic framework (MIL-96) has lower thermal stability than MIL-53 (6).

The breathing phenomenon of MIL-53 may happen with changing the pressure. More specifically, the pores of this material can expand and open with increased pressure and can close with reduced pressure of a gas (11). Also this phenomenon can be seen upon dehydration when water is rapidly removed upon heating to give a structure with the more open porosity (12, 13).

There are two types of adsorption process (14); the first is static adsorption which can occurred under static conditions, that can be obtained from adsorption/desorption isotherms (15, 16), the second is dynamic adsorption which is usually used in industrial applications and it can be achieved by breakthrough experiment through a fixed bed column (17).

Fixed bed dynamic adsorption is a current gas separation facility which may use selective adsorbents (18) such as zeolites (19) and activated carbon (20) for capture of carbon dioxide. Metal organic frameworks recently emerge with incredible characteristics including high surface area, pore volume and high capacity for CO_2 (21).

The choice of a suitable adsorbent is very important which should be considered in designing an adsorption process because the capture of carbon dioxide by this process is primly depended on the affinity of this gas with an adsorbent (22). Two mechanisms can achieve this adsorptive separation in PSA; the first is equilibrium effect which can be obtained from various affinity of gases with the adsorbent and the second is kinetic effect which can be produced as a result of presence of different diffusion rates for gases in the mixture (23). Moreover, adsorption-based separation methods are influenced by the variance in adsorption equilibrium, diffusion rates of diverse molecules or size segregation of components depending on adsorbent pore sizes, therefore the preeminent adsorbent for the application is specified by its capacity or by changes in inter-particle diffusivities in the working temperature and pressure range (24, 25).

MIL-53(Al) has been used as an adsorbent for separating CO_2 from methane (CH_4), depending on the strong relationship between CO_2 molecules and oxygen of the corner sharing hydroxyl groups of the MIL-53(3). Amino-group was expected to enhance carbon dioxide adsorption on amino functionalized zeolites (26), however, CO_2 adsorption on amino-MIL-53 was reduced but this material has gained a high ability to separate carbon dioxide from a gas mixture including carbon dioxide, methane and nitrogen at high pressure (27, 28). In this chapter, MIL-53, MIL-96, and amino-MIL-53 were synthesized and characterized. Also, adsorption capacities were obtained at standard pressure and different temperatures. Breakthrough experiments were done in comparison with Zr-MOFs materials which were discussed in previous chapters such Zr-MOF, amino-Zr-MOF and nitro-Zr-MOF.

7.2 Experimental Work

7.2.1 Chemicals

All chemicals including benzene-1, 3, 5-tricarboxylic acid (BTC, 98.9%), aminoterephthalicacid (amino-BDC, 99%), benzene-1, 4-dicarboxylic acid (BDC, 98%), dimethylformamide (DMF), and aluminium nitrate nonahydrate ($Al(NO_3)_3.9H_2O$, 98%) were purchased from Sigma-Aldrich and used without further

purification. Deionized water was prepared by Ibis-Technology-Ultrapure water device at Curtin University.

7.2.2 Synthesis Process

7.2.2.1 Amino-MIL-53 Synthesis

Amino-MIL-53 was synthesized according to a previously reported procedure (29) by scaling up around three times. Typically, 5.82 mmol of $Al(NO_3)_3.9H_2O$ were dissolved in 41.5 mL of DMF, and 8.66 mmol of amino-BDC were dissolved in 41.5 mL of DMF. After very well mixing the two parts were mixed together inside a Teflon container, and then, placed in an autoclave of 125 mL. The sealed autoclave was placed in a preheating oven at 423 K for three days. After that, the autoclave was left to cool down to room temperature, then the product solution was filtered under vacuum to collect a yellow solid of amino-MIL-53, which was crushed to get a fine yellow powder.

Amino-MIL-53 was activated by immersing in methanol for 5 days then heated at 473K under vacuum for 3 days to remove non-coordinated reactants and solvents.

7.2.2.2 MIL-53(Al)

MIL-53 (-Al) was synthesized under hydrothermal conditions using one of previous procedures(12), however, at a scale-up of 5.5 times. 19.69 mmol of Al $(NO_3)_3.9H_2O$, 9.42 mmol of BDC and 29.93 mL of deionised water were mixed together inside a Teflon container and then placed into an autoclave which was tightly sealed. The autoclave was heated at 493K into a preheating oven for three days. Finally, the white powder was obtained after vacuum filtration.

MIL-53(Al) was activated by a solvothermal treatment using DMF (30); 0.5 g of MIL-53 was suspended in 12 mL of DMF and then placed inside an autoclave of 23 mL. The tightly closed autoclave was heated at 423 K for one day. Eventually, the product was filtered, dried and heated under vacuum at 473 K for 4 days.

7.2.2.3 MIL-96(Al)

MIL-96(Al) was synthesized according to the following typical procedure; 19.83 mmol of $Al(NO_3)_3.9H_2O$, 4.23 mmol of benzene-1,3,5-tricarboxylic acid (BTC) and 26.93 mL of deionised water were mixed altogether inside a 125 mL Teflon container for around 40 min, and then placed into an autoclave. The tightly sealed autoclave was heated at 493 K in a preheating oven for 2 days. After vacuum filtration, a greenish white crystalline product was collected and washed several times with deionized water and further dried at 373 K.

MIL-96(Al) was activated by immersing the dried product into methanol for 5 days and then solvothermally treated with methanol 48 hrs at 403 K. Then, the final product was dried under vacuum at room temperature and then heated under vacuum at 493 K for 6 days. The procedures of synthesis and activation of MIL-96 were not used before.

7.2.3 Characterizations

XRD patterns of materials were determined by the PXRD instrument (Diffractometer-D8-Advance BrukeraXS) using Cu Kα1 radiation (λ=1.5406A) over the range of 2θ from 5 to 70°.

Morphologies of the crystals were described by SEM with high resolution (Zeiss NEON 40 EsBCrossBeam) and high magnification power.

FTIR spectra were investigated by a Perkin-Elmer instrument (100-FT-IR-Spectrometer) over the range of wavenumber from 650 till 4000 cm^{-1}.

BET, Langmuir surface areas, pore size distribution and pore volume were measured by nitrogen adsorption/desorption isotherms, in liquid nitrogen (77 K) on a Quantachrome instrument /Autosorb-1 using AS1Win software.

Thermal stability of these MOFs was checked by TGA experiments in Argon atmosphere with a heating rate of 10 $^{\circ}C$/min using a TGA/DSC1 STARe system (METTLER-TOLEDO). A sample of 15 mg was loaded in an alumina pan, and then placed in sample disc to be automatically moved inside TGA and settled on a sensitive balance. Finally, the weight loss was measured in the temperature range from 308K till 1173K.

7.*2.4 Adsorption Study*

7.2.4.1 Static adsorption

A static volumetric technique with an apparatus from Micromeritics(Gemini I-2360) was used to measure the adsorption isotherm of pure CO_2 (99.995%) at different temperatures at low pressure up to 760 mmHg. About 0.15 g of a sample was firstly loaded in a sample tube and then degassed by Vacprep 061 at 473 K under vacuum for 6 hrs.

After degassing process, analysis was carried out on the Gemini I-2360. The above procedure was applied for all activated samples (Amino-MIL-53, MIL-53(Al), and MIL-96(Al)).

A heat of CO_2 adsorption was calculated using the Clausius-Claperyron equation (Eq.3.1) based on isotherm data measured at different temperatures.

7.2.4.2 Dynamic Adsorption

Breakthrough experiments were done in a set up as described in Fig.7.1. A stainless steel column of 4 mm (ID) and 15 cm (length) was packed by powders of a material to fill around 14 cm of the column. Quartz wool was used as stopper at the ends of the tube to avoid suspending of packed material inside the tube.

The total flow rate of gases (N_2 (99%), CO_2 (99%) passing during the column was 20 mL/min at 20% of CO_2. The flow rate was controlled by calibrated mass flow controllers (GFC-CO_2 and GFC-N_2, AALBORG). A long tube before the column was twisted in a spring shape to achieve perfect mixing.

A heating tape (Heating Tape HT95502 Earthed 25mm Wide 60cm Long 100W-230V A.C) was turned around the packed bed to dehydrate and regenerated a material before running an experiment.

A gas chromatograph instrument (GC-17A, Shimadzu) uses a TCD detector to analyse the gases in effluent after flowing via the column or during the bypass line.

More specifically, MIL-96(0.57 g), MIL-53(0.572 g), amino-MIL-53 (0.593 g), Zr-MOF (0.62 g), Zr-MOF-NO_2 (0.565 g) and Zr-MOF-NH_2 (0.7 g) were packed into the adsorption column separately, and then dried by heating at 423 K overnight. Next, N_2 and CO_2 gas mixture was passing through the packed column then through calibrated GC to investigate CO_2 content in effluent.

The breakthrough of MIL-53, amino-MIL-53, Zr-MOF, and Zr-MOF-NO_2 was done at 304 K while of Zr-MOF-NH_2 and MIL-96 was achieved at 291 and 298K respectively. The gas was pressurized to the system at 100kPa.

Zr-MOFs were synthesized, characterized and tested for static adsorption in previous chapters and used in this chapter as comparative samples in dynamic adsorption.

Working capacity can be calculated by using breakthrough data. Breakthrough time can be determined by numerically integrating for experimental breakthrough data according to the following equation (31);

$$t_{t=\int_0^\infty (1-\frac{c}{c_0})dt} \qquad 7\text{-}1$$

Carbon dioxide capacity (loading) was calculated depending on the dynamic mass balance during the column bed which can be represented by the following equation (32);

$$q = \frac{\frac{y_{co2}*Q_f*t_t*P_s}{R*T_s} - \frac{y_{co2}*\epsilon_T*V_b*P_b}{R*T_b}}{m_c} \qquad 7\text{-}2$$

Where the porosity (ϵ_T) can be estimated by the following equation;

$\epsilon_T=1-(\rho_b/\rho_p)$ 7-3

ρ_b; Bulk density(which can easily be measured)

ρ_p; Average particle density (2.65gcc^{-1}) (33)

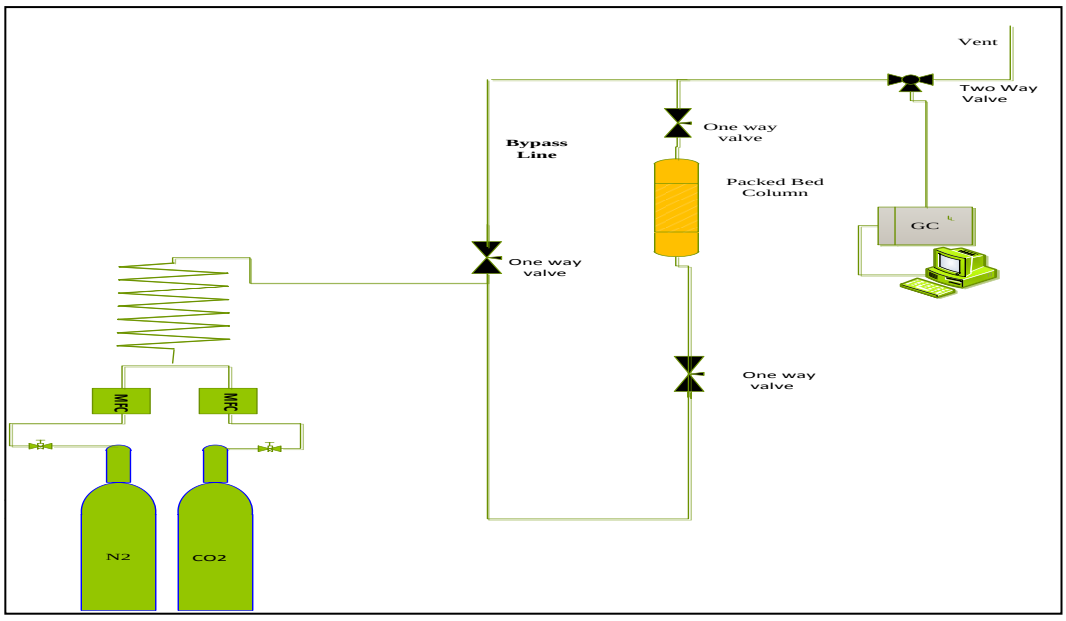

Figure: 7.1 Schematic diagram of fixed-bed adsorption experiments

7.3 Results and Discussion

7.3.1 Structural Stability

XRD patterns of Al-MOFs are presented in Figure7.2. It seems that the pattern of amino-MIL-53 is similar to that of MIL-53 with a reduction in intensity of the peaks. Also, it can be observed that there are two very small peaks on the pattern of amino-MIL-53(2θ=10,15.3), which are not displayed on the pattern of MIL-53. It can be attributed to the presence few amount of free amino-BDC inside the pores which may lead to the small shifting in the peaks of amino-MIL-53.

The pattern of MIL-96 has a different structure than MIL-53 compounds with owing the narrowest peaks whereas amino-MIL-53 has the broadest peaks. That can be a prime sign to different crystal sizes where amino-MIL-53 had the smallest crystals and MIL-96 had the biggest crystals.

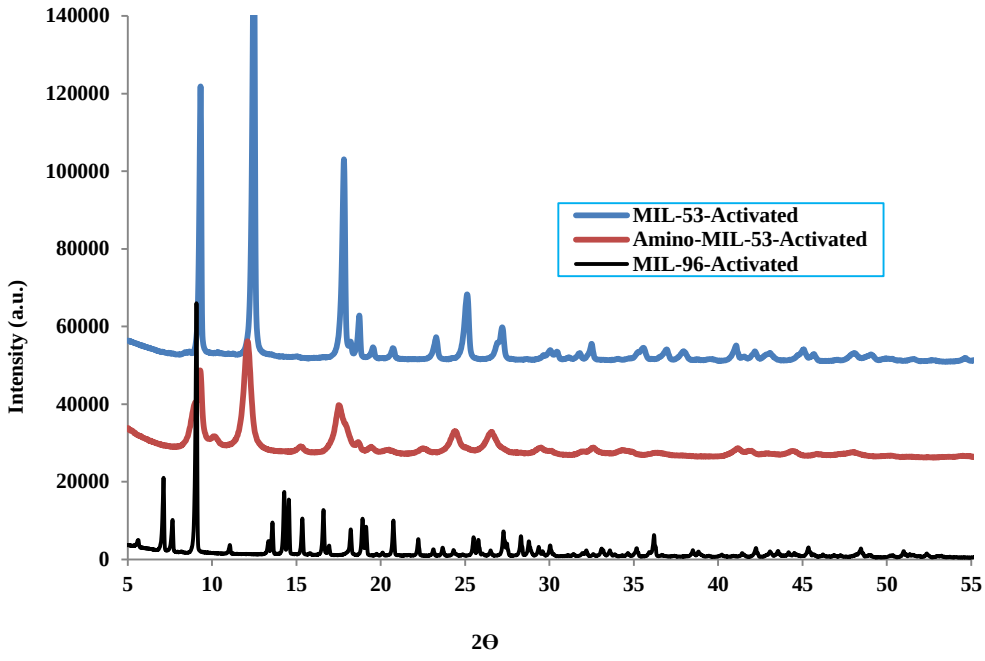

Figure: 7.2 XRD pattern of activated samples of MIL-53(Al), MIL-96(Al), and amino-MIL-53(Al)

7.3.2 Morphological Description

Morphological images of these materials are described in Figure 7.3. The average size of MIL-53, MIL-96 and amino-MIL-53 was 4, 5 and 0.35 µm, respectively.

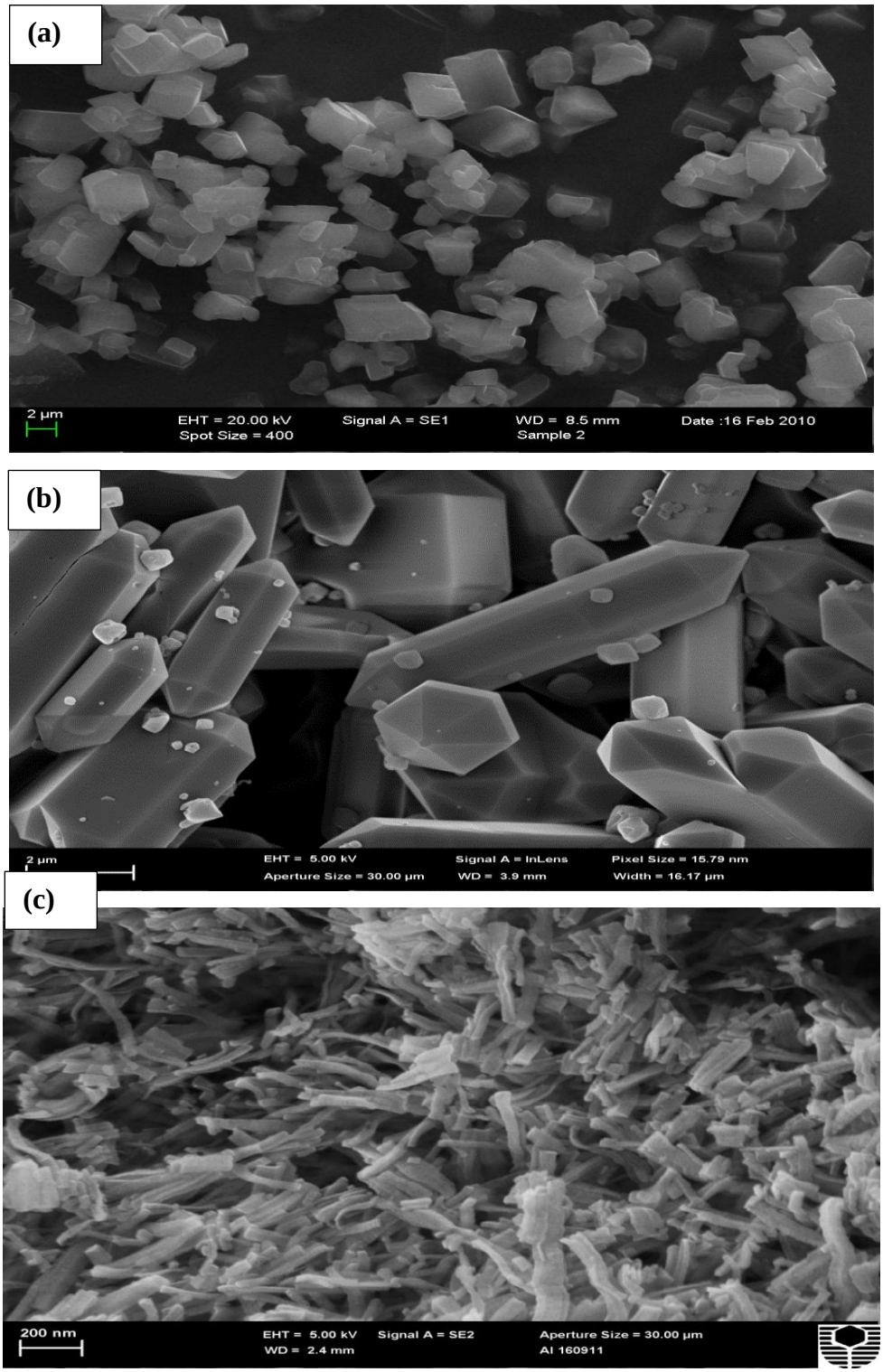

Figure: 7.3 SEM Images of (a) MIL-53, (b) MIL-96, and (c) Amino-MIL-53

7.3.3 Functional Groups Determination

These materials show different infrared spectra as seen in Figure 7.4. Activated MIL-53 spectrum demonstrates very good evidences for coordination of BDC linkers with Al-metal centres when -CO_2 asymmetric stretching appears at 1574 and 1505 cm^{-1}

while -CO_2 symmetrical stretching at 1443 and 1397 cm^{-1}(34). Also, -CO_2 stretching at the band of 1730-1650 cm^{-1} relating to free BDC inside the pores is completely disappeared after activation as proved by TGA. A bridging hydroxyl group was displayed at 1630 (12) and 3607 cm^{-1} as well.

Spectrum of amino-MIL-53 in Fig.7.4 demonstrates primary amino groups at 3387 and 3497 cm^{-1}. The perfect coordination process is demonstrated by the existence of -CO_2 asymmetric stretching at 1565 and 1494 cm^{-1}, in addition, -CO_2 symmetric stretching is observed at 1440 and 1389 cm^{-1}. Moreover, bridging hydroxyl groups are appearing at 1619 and 3631 cm^{-1}. Also, it is observed the peak of 1688 cm^{-1} showing that the activation of this material by immersing in methanol cannot discard all molecules of free BDC from the pores because a few amount of BDC was encapsulated and it is impossible to be removed by activation process.

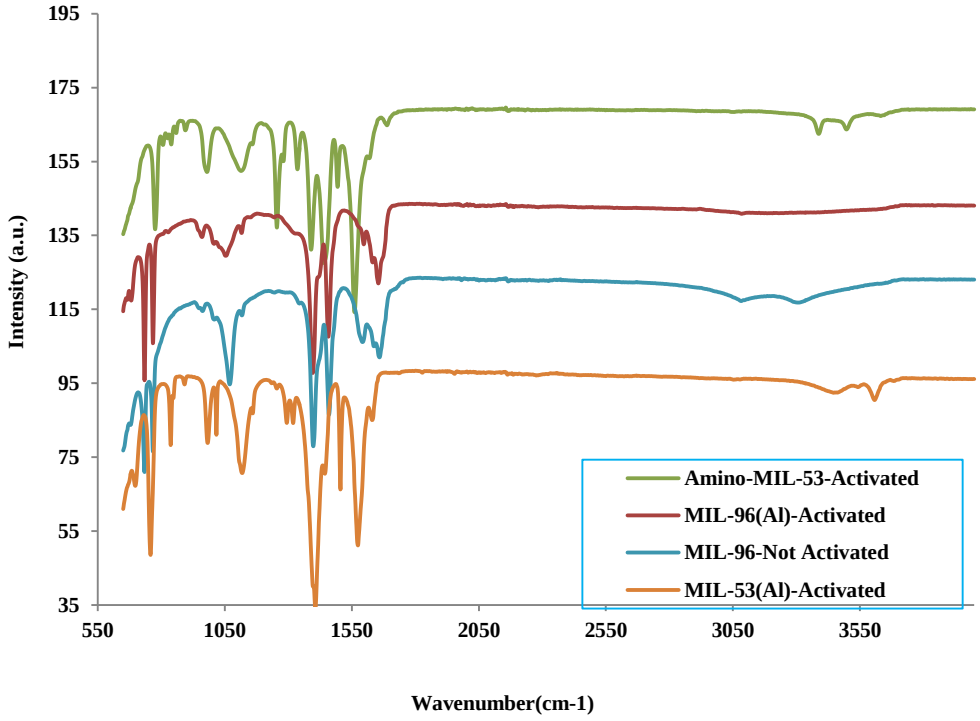

Figure: 7.4 FTIR spectra of amino-MIL-53, MIL-96(Al), and MIL-53(Al)

Spectrum of MIL-96 in Figure 7.4 shows some differences. The spectra of this material before and after activation demonstrated that the free acid (BTC) inside the pores was not removed by activation process as displayed in the peak of 1654 cm^{-1} in spectrum of before activation, which was wider than the peak after activation. As explained in TGA for this material, the free BTC was present inside the pores. It was

claimed that the spectrum of MIL-96 was deprotonated completely (100%); therefore, the peak of free acid was absent. However, we believe, the reduction in the width of this peak was an indicator of the presence of these molecules inside the pores. Spectrum of MIL-96 after activation shows the coordination process is perfect as proved by the presence of –CO2 asymmetrical stretching at 1597 cm^{-1} while –CO2 symmetrical stretching was shown at 1457 and 1396 cm^{-1}. Bridging hydroxyl group is observed at 1632 cm^{-1}.

7.3. 4 Nitrogen Adsorption and pore size distribution

The BET and Langmuir surface areas of MIL-53(Al) were 1519 and 1863 m^2/g, respectively, higher than the previously published values (12). Figure 7.5 (a) shows that the adsorption and desorption curves seem almost in overlapping , consequently, this material has a majority in micropore and the micropore radius is estimated at 0.46 nm as displayed in Figure 7.5 (b). Also, the mesopore is available and it can be filled at relative high pressure. Furthermore, mesopores are distributed in multiple pore size from 1.5 to 4.5 nm as pore radius but the most dominated pore radius is 3.2 and 1.6 nm as shown in Figure 7.5 (c). The total pore volume and the average pore size are 0.778 cc/g and 1.02 nm, respectively.

MIL-96 has the BET and Langmuir surface areas of 687 and 800 m^2/g, respectively; lower than the values of MIL-53. Figure 7.6 (a) demonstrates that the adsorption and desorption isotherms are not completely overlapped. Hence, both micropore and mesopore structures are present in this material. Also it seems that desorption isotherm has positive deviation with deceasing the relative pressure at two locations at relative pressure 0.508- 0.549 and 0.78- 0.824, which may indicate the presence further captured gas molecules inside the pores more than usual at these specified pressure ranges. The measured value of pore radius in micropore structure is 0.46 nm as shown in Figure 7.6 (b); it is similar to MIL-53. The MIL-96(Al) has a limited hysteresis which is a consequent of mesopore structure by capillary condensation. Mesopore distribution is shown in Figure 7.6(c) giving pore radius of 1.6 and 2.7 nm. The total pore volume and average pore radius are 0.335 cc/g and 0.97 nm, respectively.

Fig.7.7 shows N_2 adsorption isotherms and pore size distributions of amino-MIL-53. The BET and Langmuir surface areas are 262 and 591 m^2/g, respectively. They are lower than the values previously reported (30). Figure 7.7 (a) displays the adsorption

and desorption isotherm with a high hysteresis. Also, it is seen that, the micropore line approached to zero, that means the micropore structure was approximately absent in this material as displayed in Figure 7.7 (b) where the smallest pore radius is 1.2 nm. Fig.7.7 (c) shows that mesopores distribute in a wide range including 1.8, 3.5, 4.7, 9.9 nm and increase toward the macropore range while the dominated radius is 1.8 nm. The average pore size over the whole pore size distribution is 9.9 nm while the total pore volume is 1.31 cc/g. The bulk density of each sample in this chapter was measured in the laboratory; it was 0.45, 0.4, 0.5, 0.6, 0.55, 0.5 g cc^{-1} for MIL-53, amino-MIL-53, MIL-96, Zr-MOF, amino-Zr-MOF, and nitro-Zr-MOF respectively.

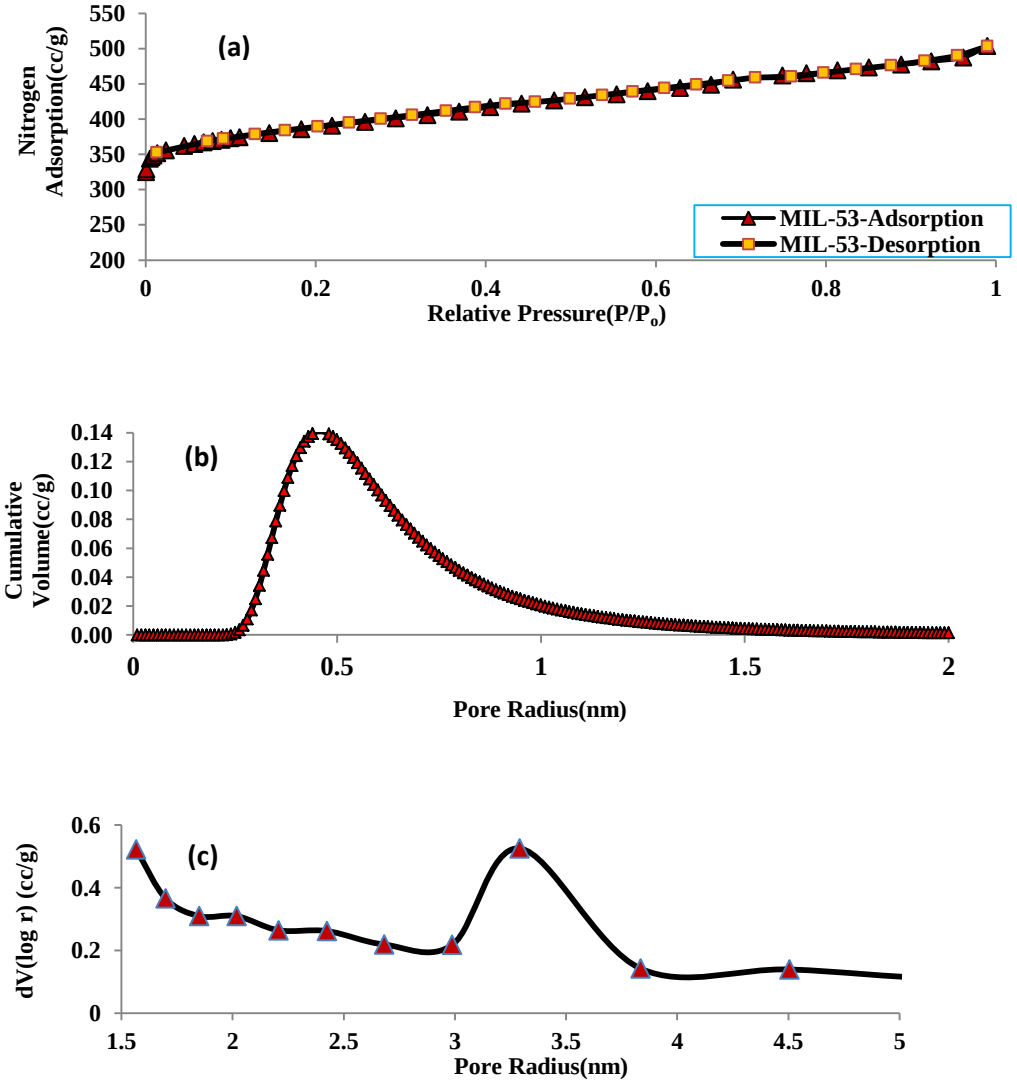

Figure: 7.5 (a) Adsorption/Desorption Nitrogen isotherms (b) Micropore distribution and (c) Mesopore distribution in MIL-53(Al)

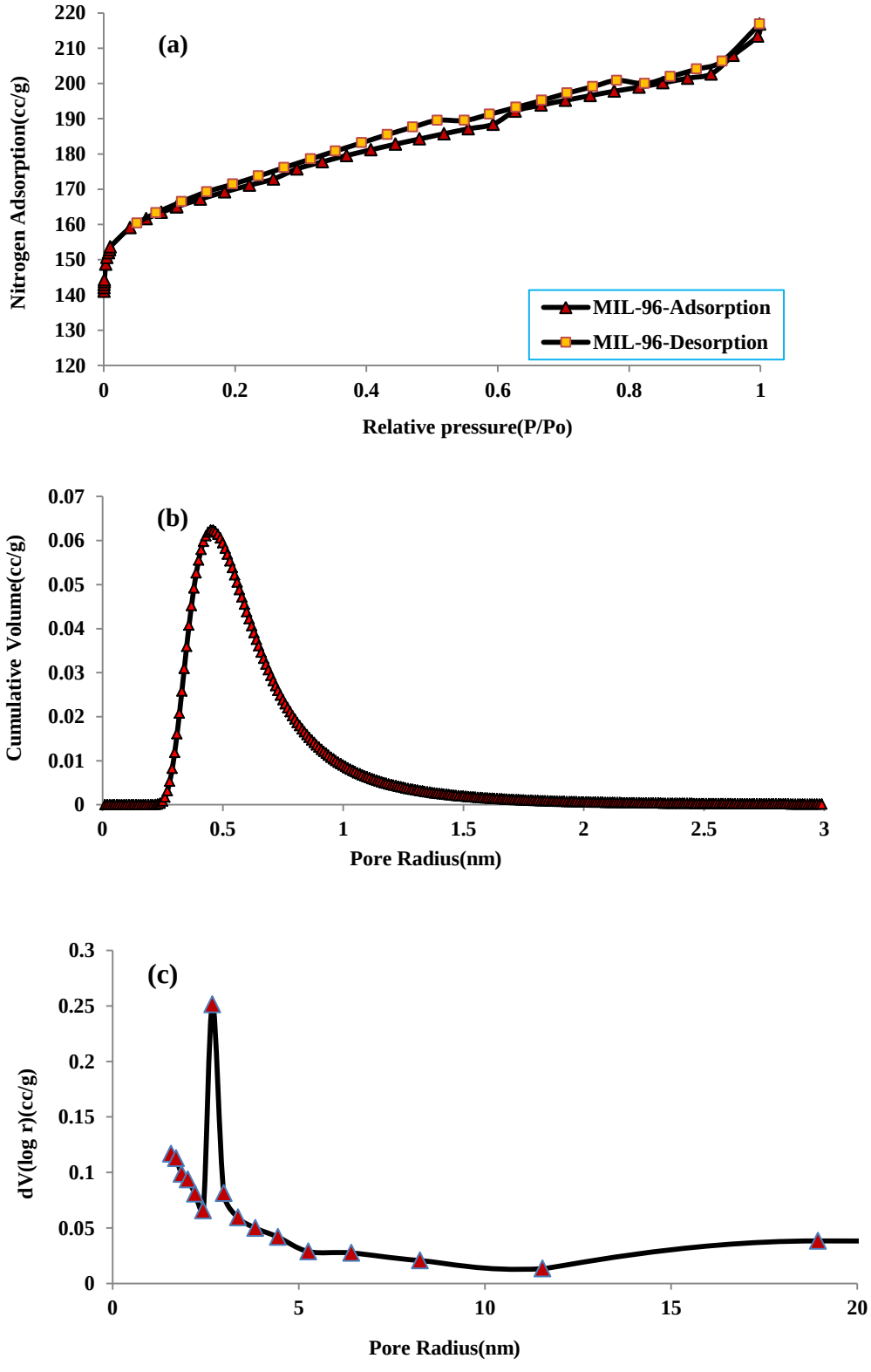

Figure: 7. 6 (a) Adsorption/Desorption Nitrogen isotherms, (b) Micropore distribution and (c) mesopore distribution in MIL-96(Al)

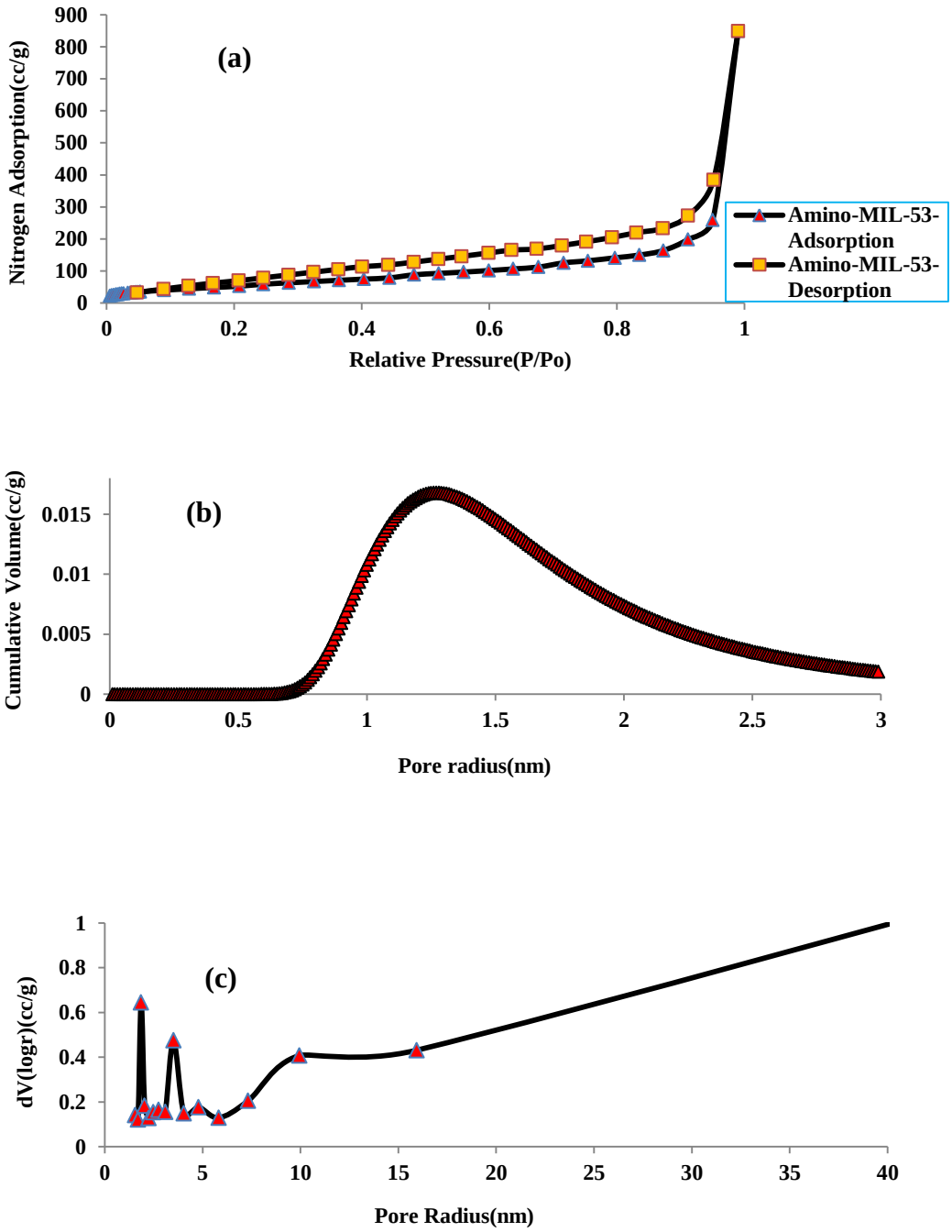

Figure: 7.7 (a) Adsorption/Desorption Nitrogen isotherms, (b) Micropore distribution and (c) mesopore distribution in Amino-MIL-53

7.3.5 Thermal Analysis

In TGA profiles (Figure 7.8, (a), (b), (c)), it seems from (a) that MIL-53 is thermally stable up to 773 K and its structure may be damaged under heating at the temperature higher than 773 K, while the whole structure is collapsed at 900 K. It seems from profile (a), the pores of MIL-53 can be produced from DMF, BDC molecules and

free from any interconnection. TGA profile(a) (Figure 7.8) is similar to what was previously published (12).

TGA profile (Figure 7.8 (b)) of MIL-96 shows MIL-96 starts to decompose when the temperature upsurges over 570 K and it may completely decompose at about 920 K. It is seen from this profile that this material has some interconnection inside the pores because of presence of three hydroxyl groups on non-coordinated benzene-1, 3, 5-tricarboxylic acid inside the pores. It can be believed that if these functional groups interact by hydrogen bond with other groups in three directions they may produce stiff bulk inside the pores. Hence, MIL-96 may collapse as this bulk is removed.

TGA profile in Figure 7.8(c) shows that amino-MIL-53 begins to decompose at around 650K and the whole structure may transfer to amorphous form of aluminium oxide at around 880K.

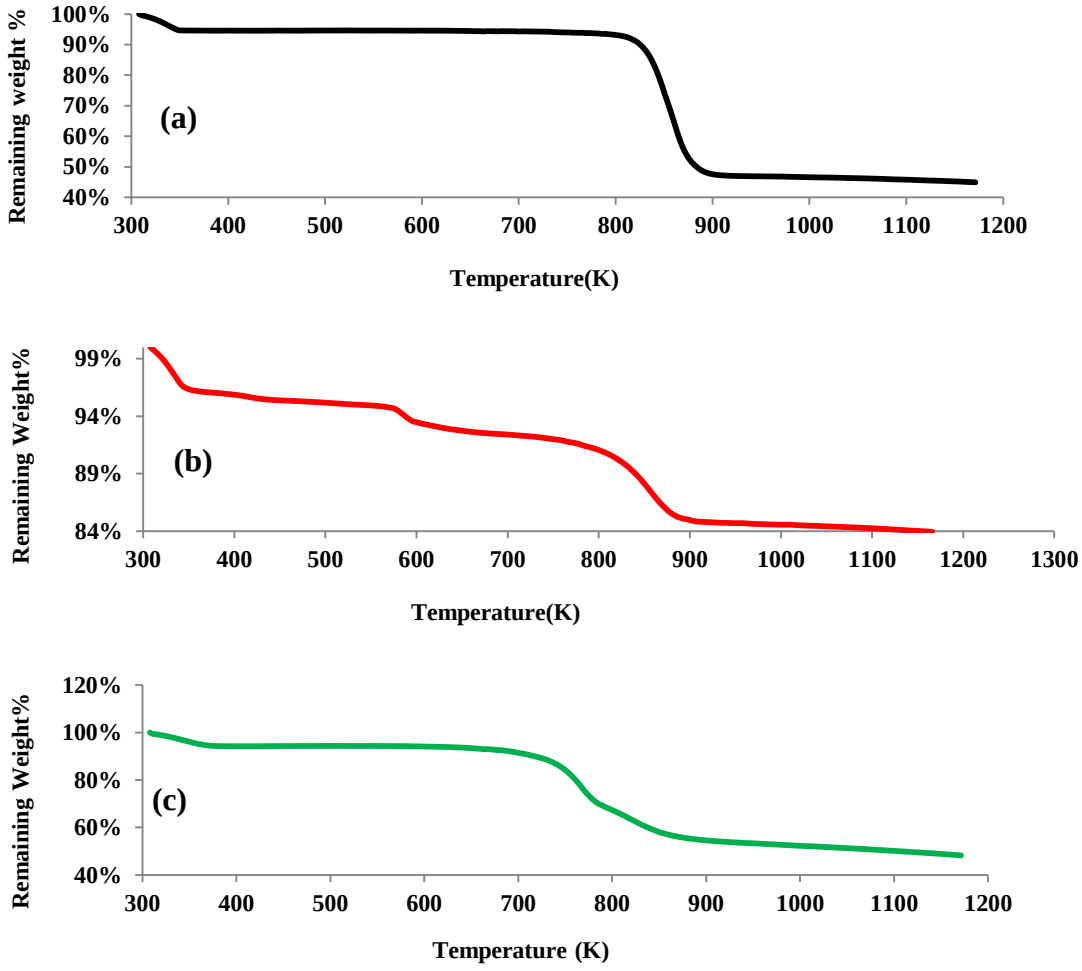

Figure: 7.8 Thermal analysis of (a) MIL-53, (b) MIL-96, and (c) Amino-MIL-53

7.3.6 CO_2 Adsorption

7.3.6.1 Static adsorption

Figure 7.9 (a) shows that around 64 and 56 cc/g of CO_2 are captured on MIL-53(Al) at 273 and 296K, respectively. Also, this material presents an inflection in the isotherm at low pressure and this inflection is clearly viewed as a wide step at 296K while it was very narrow step at 273 K. This inflection on this material was reported at pressure less than 6 bar, which was explained as a strong interaction between CO_2 molecules and the framework structure at pressure up to 6 bar, consequently, the structure was shrinkage (35). CO_2 heat of adsorption is around 39 kJ/mol, which is in a good agreement with a published value (36).

Figure 7.9 (b) shows the adsorption capacities of CO_2 on MIL-96 as 124 and 96.5 cc/g at 273 and 296 K, respectively. These values are higher than those on MIL-53 although MIL-96 has a small surface area. This can be attributed to the presence of three bridging hydroxyl groups per each linker (BTC) (6, 37), which can enhance the basicity inside pores.

MIL-96 has heat of adsorption for CO_2 around 28.6 kJ/mol, which is significantly lower than that obtained on MIL-53 and also lower than the value of MIL-96 previously published(6).

Figure 7.9 (c) demonstrates that the adsorption capacities of CO_2 on amino-MIL-53 are the lowest amongst prepared MIL- materials, giving 48 and 42 cc/g at 273 and 296 K respectively, even though primary amino-groups are present inside the structure. It was found that the synthesis and activation of this material had some difficulties (28) which may be related to the presence of amino-group on the linker and to very fine crystalline product. Therefore using methanol to exchange the guest material was not efficient to remove all of free amino-terephthalic acid from the pores of this material.

However, the heat of adsorption for CO_2 on amino-MIL-53 was 28 kJ/mol, which is the lowest amongst prepared-MIL- materials in this chapter and lower than published values(27). This may be owing to large pore size in amino-MIL-53 after activation.

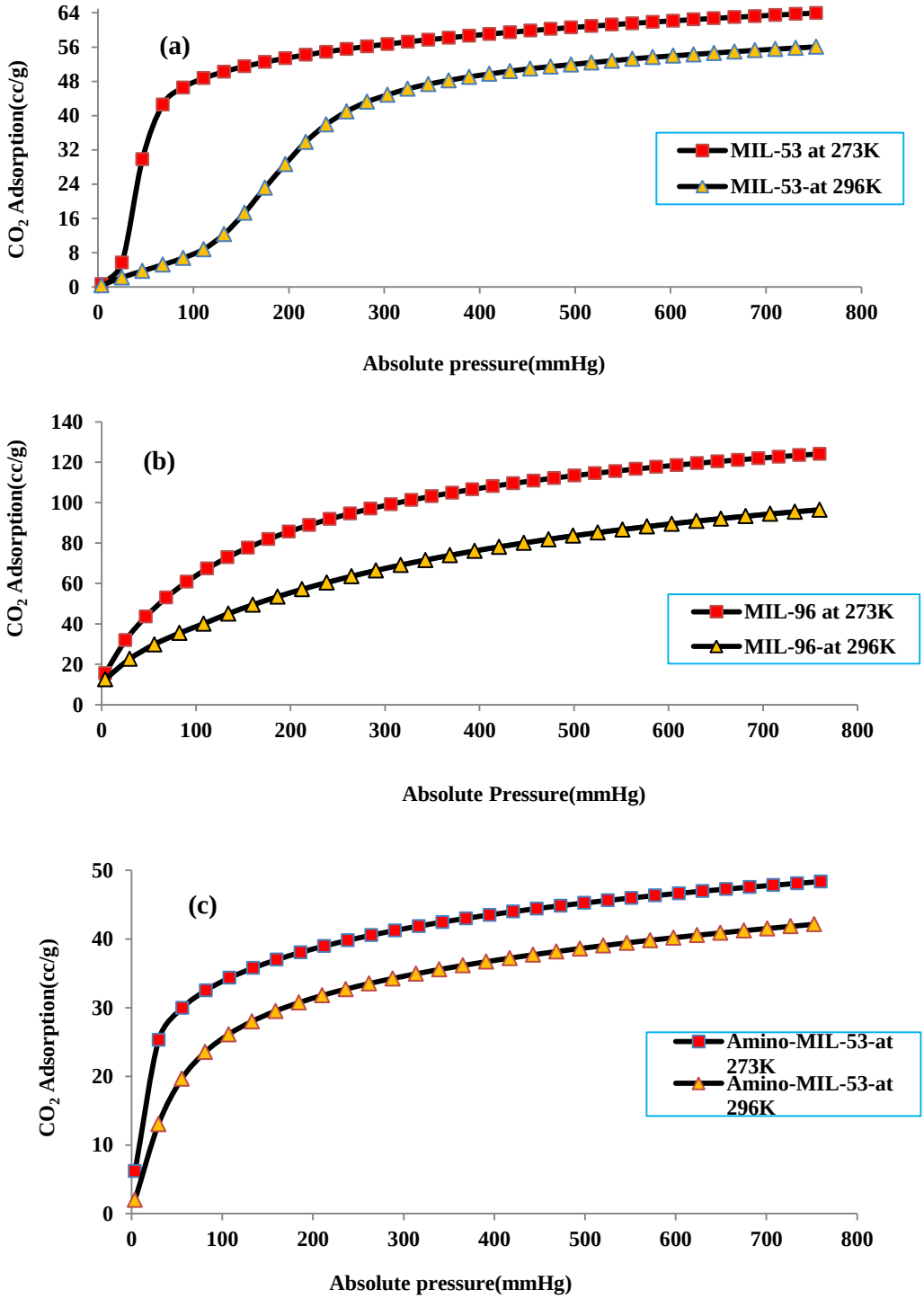

Figure: 7.9 CO2 adsorption at 1atm and different temperatures

7.3.6.2 Dynamic adsorption

Capturing carbon dioxide from a mixture of gases in a packed bed was also investigated. It can be seen from Figure 7.10, CO_2 breakthrough on MIL-53 occurred at time of 26 minutes while it occurred at 21 and 14 minutes on amino-MIL-53 and

MIL-96, respectively. The working capacities were calculated to evaluate capturing potential of each adsorbent under the conditions similar to real conditions. It is obtained that the performance of MIL-53 to capture carbon dioxide within a whole adsorption/desorption cycle is significantly higher than amino-MIL-53(Al) and MIL-96(Al). Their working capacities are 169, 128, and 89 cc/g, respectively. These results are different from adsorption capacities in static volumetric adsorption at standard conditions. More significantly, although dynamic adsorption was achieved at risen temperature, MIL-53 compounds have much higher capacity than that at static adsorption at STP. This may attribute to variety in pore size. It was proved that the wide pore size distribution can have a broad breakthrough curve (38) that can be interpreted; the material with pore diameter larger than the kinetic diameter of CO_2 (0.39 nm) may have a higher working capacity in breakthrough experiments. The high pore size is available in amino-MIL-53 following by MIL-53 and MIL-96. However, MIL-53 may have more expansion upon adsorption of CO_2 which makes the pore larger. Also, it was investigated that the pressure drop has been increased during the packed column, it was 220, 230, 210, 250, 240, 230kPa for MIL-53, MIL-96, amino-MIL-53, Zr-MOF, Zr-MOF- NH_2, and Zr-MOF-NO_2 respectively which can participate enhancement dynamic adsorption at MIL-53 with large pore volume as large volume in micro-pores can develop supermicropores (39).

Also, it may be believed that passing the nitrogen during the adsorbent prior to passing CO_2 gas may contribute to open the pores of the material to be ready to capture carbon dioxide with absence the blockage of the pores at low pressure. Moreover, N_2 in pre-treatment process can temporarily adsorb inside the pores, and then has to be exchanged and displaced with CO_2. Also, it can be observed that the breakthrough time of amino-MIL-53 is higher than that of MIL-53.

Other breakthrough curves of CO_2 through some porous materials of Zr-MOFs are shown in Figure 7.11. It seems that the high breakthrough time is occurring on nitro-Zr-MOF 20 minutes while the time is 17 and 9.25 minutes for amino-Zr-MOF and Zr-MOF (Parent), respectively.

Long-time of breakthrough may be attributed to dynamic exchange in the locations between N_2 in pre-treatment process and CO_2 as explained above. In addition, the working capacities were calculated to be 128, 86 and 48 cc/g for nitro-Zr-MOF, amino-Zr-MOF and Zr-MOF (Parent), respectively. As it was discussed, the pore radius and N_2 pre-treatment have prime roles in determining the working capacity.

Therefore, nitro-Zr-MOF had the larger working capacity than others as its average pore radius was bigger. It was reported in pervious chapters that the pore radius was 1.8, 0.99, and 0.91 nm for nitro-Zr-MOF, amino-Zr-MOF and Zr-MOF (Parent).

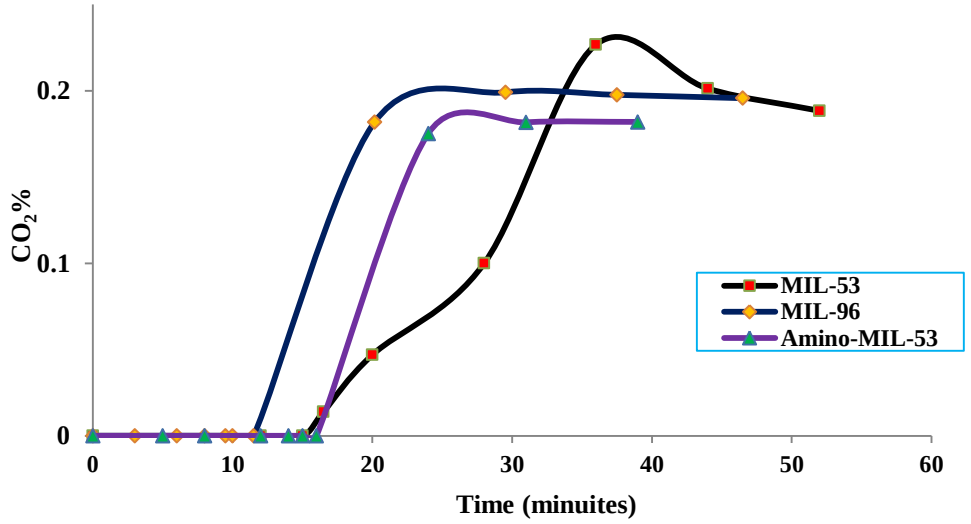

Figure: 7.10 Breakthrough curves through Al-MOFs

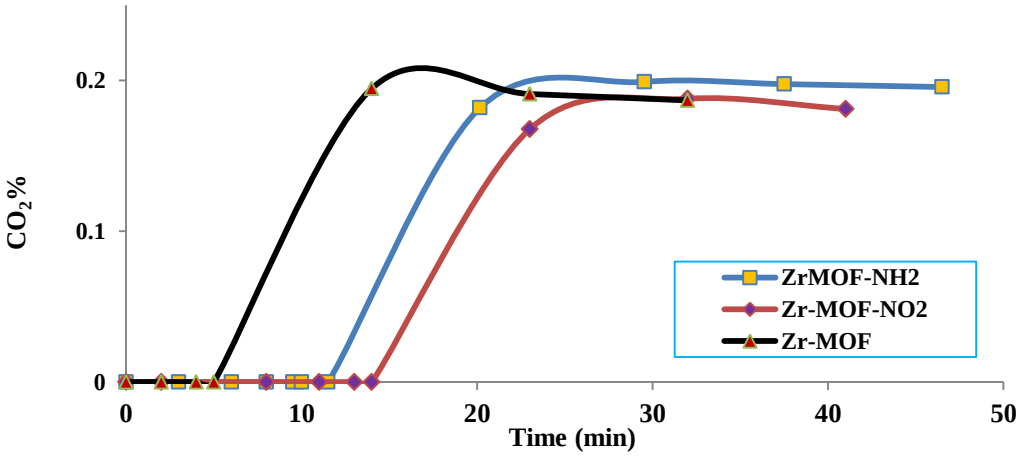

Figure: 7.11 Breakthrough curves through Zr-MOFs

7.4 Conclusion

MIL-53, MIL-96 and amino-MIL-53 were synthesized, characterized and tested for CO_2 adsorption by static and dynamic methods. It was found that, MIL-53(Al) had the highest thermal stability and the highest surface area (BET and Langmuir). The

CO_2 adsorption capacity on this material at 1 bar was acceptable with a high heat of adsorption whereas it got exceptionally the highest working capacity amongst the MOFs in this study.

MIL-96 showed the lowest thermal stability with an acceptable surface area. This material had the highest adsorption capacity for CO_2 at STP. On the other hand, it had reasonable heat of adsorption and working capacity.

Amino-MIL-53 emerged realistic thermal stability with very low surface area compared with other MOFs. It had low CO_2 adsorption capacity at STP, with low heat of adsorption; however, it had large working capacity.

7.5 References

1. Millward AR, Yaghi OM. Metal−Organic Frameworks with Exceptionally High Capacity for Storage of Carbon Dioxide at Room Temperature. Journal of the American Chemical Society. 2005;127(51):17998-9.
2. Cavka JH, Jakobsen S, Olsbye U, Guillou N, Lamberti C, Bordiga S, et al. A New Zirconium Inorganic Building Brick Forming Metal Organic Frameworks with Exceptional Stability. Journal of the American Chemical Society. 2008;130(42):13850-1.
3. Arstad B, Fjellvåg H, Kongshaug K, Swang O, Blom R. Amine functionalised metal organic frameworks (MOFs) as adsorbents for carbon dioxide. Adsorption. 2008;14(6):755-62.
4. Kolokolov DI, Jobic H, Stepanov AG, Guillerm V, Devic T, Serre C, et al. Dynamics of Benzene Rings in MIL-53(Cr) and MIL-47(V) Frameworks Studied by 2H NMR Spectroscopy. Angewandte Chemie International Edition. 2010;49(28):4791-4.
5. Millange F, Férey G, Morcrette M, Serre C, Doublet ML, Grenèche JM, et al. Towards the reactivity of MIL-53 or FeIII(OH)0.8F0.2[O2C-C6H4-CO2]versus lithium. In: Ruren Xu ZGJC, Wenfu Y, editors. Studies in Surface Science and Catalysis: Elsevier; 2007. p. 2037-41.
6. Loiseau T, Lecroq L, Volkringer C, Marrot J, Férey G, Haouas M, et al. MIL-96, a Porous Aluminum Trimesate 3D Structure Constructed from a Hexagonal Network of 18-Membered Rings and μ3-Oxo-Centered Trinuclear Units. Journal of the American Chemical Society. 2006;128(31):10223-30.

7. Horcajada P, Surble S, Serre C, Hong D-Y, Seo Y-K, Chang J-S, et al. Synthesis and catalytic properties of MIL-100(Fe), an iron(iii) carboxylate with large pores. Chemical Communications. 2007(27):2820-2.

8. Hamon L, Serre C, Devic T, Loiseau T, Millange F, Férey Gr, et al. Comparative Study of Hydrogen Sulfide Adsorption in the MIL-53(Al, Cr, Fe), MIL-47(V), MIL-100(Cr), and MIL-101(Cr) Metal−Organic Frameworks at Room Temperature. Journal of the American Chemical Society. 2009;131(25):8775-7.

9. Liu Y, Her J-H, Dailly A, Ramirez-Cuesta AJ, Neumann DA, Brown CM. Reversible Structural Transition in MIL-53 with Large Temperature Hysteresis. Journal of the American Chemical Society. 2008;130(35):11813-8.

10. Yaghi OM, Davis CE, Li G, Li H. Selective Guest Binding by Tailored Channels in a 3-D Porous Zinc(II)−Benzenetricarboxylate Network. Journal of the American Chemical Society. 1997;119(12):2861-8.

11. Ramsahye NA, Maurin G, Bourrelly S, Llewellyn PL, Loiseau T, Serre C, et al. On the breathing effect of a metal-organic framework upon CO2 adsorption: Monte Carlo compared to microcalorimetry experiments. Chemical Communications. 2007(31).

12. Loiseau T, Serre C, Huguenard C, Fink G, Taulelle F, Henry M, et al. A Rationale for the Large Breathing of the Porous Aluminum Terephthalate (MIL-53) Upon Hydration. Chemistry – A European Journal. 2004;10(6):1373-82.

13. Llewellyn PL, Bourrelly S, Serre C, Filinchuk Y, Férey G. How Hydration Drastically Improves Adsorption Selectivity for CO2 over CH4 in the Flexible Chromium Terephthalate MIL-53. Angewandte Chemie International Edition. 2006;45(46):7751-4.

14. Álvarez-Merino MA, López-Ramón V, Moreno-Castilla C. A study of the static and dynamic adsorption of Zn(II) ions on carbon materials from aqueous solutions. Journal of Colloid and Interface Science. 2005;288(2):335-41.

15. Chien AC, Chuang SSC. Static and dynamic hydrogen adsorption on Pt/AC and MOF-5. International Journal of Hydrogen Energy. 2011;36(10):6022-30.

16. Preparation and characterization of ordered porous carbons for increasing hydrogen storage behaviors. Journal of Solid State Chemistry.

17. Cheng Y, Huang Q, Eić M, Balcom BJ. CO2 Dynamic Adsorption/Desorption on Zeolite 5A Studied by 13C Magnetic Resonance Imaging. Langmuir. 2005;21(10):4376-81.

18. Hayashi H, Taniuchi J, Furuyashiki N, Sugiyama S, Hirano S, Shigemoto N, et al. Efficient Recovery of Carbon Dioxide from Flue Gases of Coal-Fired Power Plants by Cyclic Fixed-Bed Operations over K2CO3-on-Carbon. Industrial & Engineering Chemistry Research. 1998;37(1):185-91.

19. Mérel J, Clausse M, Meunier F. Carbon dioxide capture by indirect thermal swing adsorption using 13X zeolite. Environmental Progress. 2006;25(4):327-33.

20. Siriwardane RV, Shen M-S, Fisher EP, Poston JA. Adsorption of CO2 on Molecular Sieves and Activated Carbon. Energy & Fuels. 2001;15(2):279-84.

21. Yazaydın AOzr, Snurr RQ, Park T-H, Koh K, Liu J, LeVan MD, et al. Screening of Metal−Organic Frameworks for Carbon Dioxide Capture from Flue Gas Using a Combined Experimental and Modeling Approach. Journal of the American Chemical Society. 2009;131(51):18198-9.

22. Dantas TLP, Luna FMT, Silva Jr IJ, Torres AEB, de Azevedo DCS, Rodrigues AE, et al. Modeling of the fixed - bed adsorption of carbon dioxide and a carbon dioxide - nitrogen mixture on zeolite 13X. Brazilian Journal of Chemical Engineering. 2011;28:533-44.

23. Delgado JA, Uguina MA, Sotelo JL, Ruíz B, Rosário M. Carbon Dioxide/Methane Separation by Adsorption on Sepiolite. Journal of Natural Gas Chemistry. 2007;16(3):235-43.

24. Walton KS, LeVan MD. A Novel Adsorption Cycle for CO2 Recovery: Experimental and Theoretical Investigations of a Temperature Swing Compression Process. Separation Science and Technology. 2006;41(3):485-500.

25. Ruthven DM. Principles of adsorption and adsorption processes. New York: Wiley; 1984.

26. Su F, Lu C, Kuo S-C, Zeng W. Adsorption of CO2 on Amine-Functionalized Y-Type Zeolites. Energy & Fuels. 2010;24(2):1441-8.

27. Couck S, Denayer JFM, Baron GV, Rémy T, Gascon J, Kapteijn F. An Amine-Functionalized MIL-53 Metal−Organic Framework with Large Separation Power for CO2 and CH4. Journal of the American Chemical Society. 2009;131(18):6326-7.

28. Ahnfeldt T, Gunzelmann D, Loiseau T, Hirsemann D, Senker Jr, Férey G, et al. Synthesis and Modification of a Functionalized 3D Open-Framework Structure with MIL-53 Topology. Inorganic Chemistry. 2009;48(7):3057-64.

29. Stavitski E, Pidko EA, Couck S, Remy T, Hensen EJM, Weckhuysen BM, et al. Complexity behind CO_2 Capture on NH_2-MIL-53(Al). Langmuir. 2011;27(7):3970-6.

30. Gascon J, Aktay U, Hernandez-Alonso MD, van Klink GPM, Kapteijn F. Amino-based metal-organic frameworks as stable, highly active basic catalysts. Journal of Catalysis. 2009;261(1):75-87.

31. James M. Becnel CEH, James McIntyre, Michael A. Matthews and James A. Ritter. Fundamentals of Fixed Bed Adsorption Process: Analysis of Adsorption Breakthrough and Desorption Elution Curves. Proceedings of the American Society for Engineering Education Annual Conference and Exposition; Montreal, Quebec, Canada.June 19 –23, 2002.

32. Paulo Cruz AM, Fernao D. Magalhaes. Usin In-Bed Temperature Profiles for Visualizing the Concentration-Front Movement. Chem Engr Edu. 2001;35(2). Epub 139.

33. Fonteno WC. PROBLEMS & CONSIDERATIONS IN DETERMINING PHYSICAL PROPERTIES OF HORTICULTURAL SUBSTRATES. Acta Horticulture. 1993;342. Epub 204.

34. Yaghi OM, Li H, Groy TL. Construction of Porous Solids from Hydrogen-Bonded Metal Complexes of 1,3,5-Benzenetricarboxylic Acid. Journal of the American Chemical Society. 1996;118(38):9096-101.

35. Bourrelly S, Llewellyn PL, Serre C, Millange F, Loiseau T, Férey G. Different Adsorption Behaviors of Methane and Carbon Dioxide in the Isotypic Nanoporous Metal Terephthalates MIL-53 and MIL-47. Journal of the American Chemical Society. 2005;127(39):13519-21.

36. Boutin A, Coudert Fo-X, Springuel-Huet M-A, Neimark AV, Férey Gr, Fuchs AH. The Behavior of Flexible MIL-53(Al) upon CH4 and CO2 Adsorption. The Journal of Physical Chemistry C. 2010;114(50):22237-44.

37. Lieder C, Opelt S, Dyballa M, Henning H, Klemm E, Hunger M. Adsorbate Effect on AlO4(OH)2 Centers in the Metal−Organic Framework MIL-53 Investigated by Solid-State NMR Spectroscopy. The Journal of Physical Chemistry C. 2010;114(39):16596-602.

38. Liu H-C, Fried JR. Breakthrough of lysozyme through an affinity membrane of cellulose-cibacron blue. AIChE Journal. 1994;40(1):40-9.

39. Branton. Use of Classical Adsorption Theory to Understand the Dynamic Filtration of. Adsorption science & technology. 2011;29(2):117-38.

8

Chapter Eight: Conclusions and Recommendations for Future Work

8.1 Conclusions

To meet the objectives of this thesis, several metal organic frameworks such as Zr-MOF, Zr-MOF-NH_4, Zr-MOF-NH_2, Zr-MOF-NO_3, Zr-MOF-NO_2, AlBDC-MOF (MIL-53), AlBTC-MOF (MIL-96), and amino-MIL-53 were synthesized and activated by modified methods. All these MOFs were tested for carbon dioxide adsorption. From the investigations presented in this thesis, the following important conclusions can be made.

1- Zr-MOFs were synthesized according to a modified procedure and the activation process can employ solvent exchange methods. Some of Zr-MOFs such as Zr-MOF, Zr-MOF-NH_4 and Zr-MOF-NO_3 could be activated by chloroform with heating at mild temperature rather than methanol, which was efficient to remove molecules of dimethylformamide (DMF) and non-reacted benzene dicarboxylic acid (BDC) from the pores enhancing porous structure and surface area. However, it was found that Zr-MOF-NH_2 and Zr-MOF-NO_2 cannot be activated by chloroform but they were successfully activated by methanol. AlBDC-MOF (MIL-53) was synthesized by a solvothermal activation in dimethylformamide (DMF), which was a better way to remove water and free terephthalic acid molecules from the pores. AlBTC-MOF (MIL-96) was synthesized by a new procedure and activated in two steps; first by immersing in methanol, then by solvothermal treatment in methanol. This method was more effective to activate this material. Amino-MIL-53 was synthesized by one of the previous procedures while it was activated by methanol as a new method to remove non-coordinated terephthalic acid from the pores.

2- Zr-MOF-(Parent) has high surface area, high thermal stability and well developed microporous structure. It was found that the pore size and crystal size could be modified by using NH_4OH and HNO_3 as additives in the direct

synthesis procedure. As a result, Zr-MOF-NH_4 and Zr-NOF-NO_3 were produced. The crystal size of the materials reduced while the pore size increased when the amount of the additives were increased. The surface area of the modified samples was reduced but thermal stability was maintained. FTIR analysis proved no functional group was added to the structure. Zr-MOF-NH_2 and Zr-MOF-NO_2 presented the same structure as Zr-MOF, Zr-MOF-NH_4, and Zr-MOF-NO_3, however, their thermal stability was very low. The surface area of these materials were lower than that of Zr-MOF(Parent). Morphology of these materials was different from that of Zr-MOF and Zr-MOF-NH_4. MIL-53 provided higher surface area than those reported before with high thermal stability. MIL-96 exposed low surface area and low thermal stability while morphological description provided a good crystal shape and crystal size with uniform hexagonal shape. Amino-MIL-53 demonstrated lower surface area than reported value while the thermal stability was the same.

3- Zr-MOF-(Parent) exhibited a good adsorption capacity for CO_2 at varying temperatures. Modification in the direct synthesis process of Zr-MOF by using ammonium hydroxide and nitric acid additives was a good method to enlarge the pore size and regeneration of the adsorbents at low energy. Although the BET surface area reduced in the modified samples and the adsorption capacity was lower at STP, the adsorption capacity was higher than Zr-MOF-(Parent) at high pressure on Zr-MOF-NH_4-2, and the selectivity of CO_2/CH_4 was enhanced on Zr-MOF-NH_4-1 and Zr-MOF-NH_4-3. Moreover, Zr-MOF-NH_2 presented the highest CO_2 adsorption amongst Zr-MOFs. The selectivity of CO_2 over CH_4 was acceptable.

Furthermore, Zr-MOF-NO_2 had CO_2 adsorption capacity higher than Zr-MOF-NO_3 at 1 atm, however, it exposed lower CO_2 adsorption at high pressure. The selectivity of CO_2 over CH_4 on Zr-MOF-NO_3-2 was the highest amongst Zr-MOFs in this thesis.

4- AlBTC-MOF (MIL-96) exhibits a very good carbon dioxide capacity at STP. It is higher than all MOFs used in this study while AlBDC-MOF(MIL-53) achieved a capacity half of that of MIL-96 and amino-MIL-53 showed the lowest adsorption capacity at the same conditions. Breakthrough experiments for MOFs in this thesis demonstrated a variety in the breakthrough time and amount of adsorbed CO_2. Dynamic adsorption of carbon dioxide on MIL-96, Zr-MOF and Zr-MOF-NH_2 was approximately similar to the values which were obtained in static adsorption. While MIL-53, Zr-MOF-NO_2, and amino-MIL-53 showed adsorption capacities much higher than the values of static adsorption. Furthermore, MIL-53(Al) was investigated as the highest whereas the dynamic adsorption on Zr-MOF (Parent) was the lowest. In addition, the dynamic adsorption on Zr-MOF-NO_2 and amino-MIL-53 ranked in the second and third following MIL-53. It was observed that capacity of dynamic adsorption was improved when the pore size was increased and expanded. Also, pre-treatment of the adsorbent bed by nitrogen gas was crucial for open the pores before injecting CO_2 gas mixture.

8.2 Recommendations for Future Work

1- We used BDC, NH_2-BDC, BTC and NO_2-BDC as organic linkers in this thesis, other aromatic carboxylic acid linkers with different functional groups could be used in synthesis of Zr-MOF. Also, one type of metal ion (Zr^{+4} or Al^{+3}) to synthesize MOFs was tested, it can be recommended to use mixed metal ions such as Zr^{+4} and Al^{+3} together in the synthesis process and different organic ligands to check new possibility to synthesize new metal organic frameworks. In addition, it will be very interesting to use mixed organic linkers together in the synthesis process with one metal ion or use mixed metals with mixed ligand altogether. All new MOFs produced can be checked for gas storage, separation, catalysts, sensing, or drug delivery under different pressures and temperatures.

2- According to our results in this research, it was found that Zr-MOFs are promising materials for capture of carbon dioxide with high chemical and

thermal stability, which can be used in industrial applications. We strongly recommend post-synthesis modifications for this type of material toward enhancing carbon dioxide adsorption at STP. We believe Zr-MOF-NH_3 and Zr-MOF-NO_2 can be modified easily by finding some organic compounds which have the ability to interact with their functional groups and at the same time they can enhance carbon dioxide adsorption capacity or the selectivity of carbon dioxide over other gases.

3- Adsorption isotherm for Zr-MOF at 10 bars was done in this thesis therefore adsorption study at high pressure up to 35 bars should be achieved to get the whole capacity of adsorption for carbon dioxide.

4- According to the stability of the structure in water which was exposed in this thesis by Zr-MOF, studying the effect of the moisture content in gas mixture on the dynamic adsorption capacity of carbon dioxide should be achieved to determine the acceptable limit of moisture content.

5- In this study, static selectivity was done to measure the separating factor of CO_2 /CH_4; therefore we recommend measuring the kinetic selectivity in the future to get the optimum ratio of the gases to achieve the best selectivity.

6- In this thesis we checked effectiveness of methanol on the activation process; therefore we recommend using other solvents in activation process for a comparative study.

7- According to characterizations of Zr-MOF, it will be essential to make simulation study to predict the change in the characteristics under the influence of different additives such as NH_4OH, HNO_3, HCl and others. Also, a simulation study to check the effect of moisture content or ammonium content on the CO_2 capacity should be carried out.

8- MOF-96 was synthesized in a new procedure in this thesis, which shows enhanced adsorption capacity of CO_2 at standard conditions, therefore it will be noteworthy to check the selectivity of CO_2 over CH_4 on this material. Also, the modification of the synthesis procedure as well as activation procedure will be recommended toward enhancement in the surface area of this MOF. It will be necessary to synthesize AlBTC-MOF by adding different amount of additives to check the stability of the structures as well as the possibility to make changes in morphology and surface area.

9- It will be very interesting to carry out the breakthrough experiments at different temperatures, and to simulate the dynamic adsorption mathematically.